Research and Development in

Breast Ultrasound

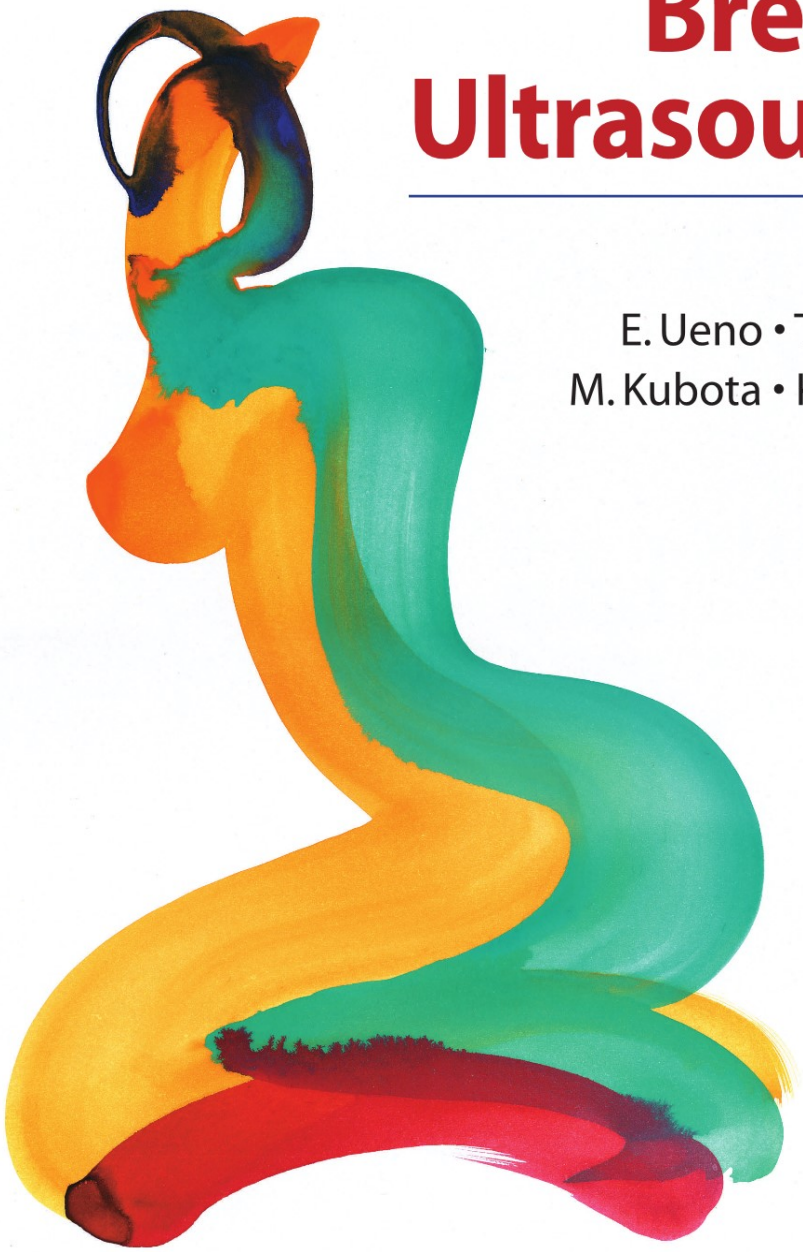

E. Ueno • T. Shiina
M. Kubota • K. Sawai
(Eds.)

Springer

E. Ueno, T. Shiina, M. Kubota, K. Sawai (Eds.)
Research and Development in Breast Ultrasound

E. Ueno, T. Shiina
M. Kubota, K. Sawai (Eds.)

Research and Development in Breast Ultrasound

With 150 Figures, Including 37 in Color

Ei Ueno, M.D., Ph.D.
Associate Professor, Department of Breast-Thyroid-Endocrine Surgery
Institute of Clinical Medicine, University of Tsukuba
1-1-1 Tennodai, Tsukuba, Ibaraki 304-8573, Japan

Tsuyoshi Shiina, Ph.D.
Professor, Institute of Information Sciences and Electronics, University of Tsukuba
1-1-1 Tennodai, Tsukuba, Ibaraki 304-8573, Japan

Mitsuhiro Kubota, M.D.
Director of Yamachika Memorial Hospital
3-19-14 Koyawata, Odawara, Kanagawa 256-0815, Japan

Kiyoshi Sawai, M.D.
Associate Professor, Department of Endocrine & Breast Surgery
Kyoto Prefectural University of Medicine
465 Kajii-cho, Kawaramachi-Hirokoji, Kamigyo-ku, Kyoto 602-0841, Japan

Cover Illustration: Madoka Momota

Library of Congress Control Number: 2004116202

ISBN 4-431-40277-2 Springer-Verlag Tokyo Berlin Heidelberg New York

Springer is a part of Springer Science+Business Media
springeronline.com

Printed in Japan

Typesetting: SNP Best-set Typesetter Ltd., Hong Kong
Printing and binding: Shinano, Inc., Japan

Printed on acid-free paper

Preface

Ultrasonic examination of the breast has been a valuable diagnostic tool for more than half a century since J.J. Wild, T. Wagai, and others first used it in 1950. The first International Congress on the Ultrasonic Examination of the Breast (ICUEB) was convened in Philadelphia in 1979 by Goldberg (United States), Wells (United Kingdom), Wagai (Japan), Kobayashi (Japan), and Kossoff (Australia). Further congresses in the series have taken place every other year to discuss related theoretical and clinical discoveries. These meetings led to the founding of the International Association for Breast Ultrasound (IABU) in 1991, and have contributed to improving ultrasonic examination techniques and the associated medical benefits.

The 13th ICUEB was held in Kyoto, Japan, in April 2003. International events at that time—the military operations in Iraq and the SARS outbreaks in several countries—threatened attendance; however, only one oral presentation and one poster presentation had to be canceled, and an impressive 98% of our schedule proceeded as planned. Over the three days of the congress, participants made significant contributions through presentations and discussions, and we moved closer to a global mutual understanding.

From the many oral presentations and posters we selected the best for publication in this volume, entitled *Research and Development in Breast Ultrasound*. The book covers a variety of engaging topics, including discovery of the piezoelectric phenomenon, DCIS diagnosis, interventional ultrasound, screening by ultrasound, and diagnostic criteria. It also includes an original paper by Dr. Kujiraoka, "Incident Angle of the Plunging Artery of Breast Tumors," which won first prize at the poster session. We are sure the next ICUEB will build on these strong foundations.

Finally, special heartfelt thanks go to Professor Ki Keun Oh from Korea, Dr. Yi-Hong Chou from Taiwan, and Dr. Jack Jellins from IBAS.

Ei Ueno, M.D.
Chairman, 13th ICUEB
Chief Editor

Contributors

The following organizations and individuals provided financial support for the 13th International Congress on the Ultrasonic Examination of the Breast (ICUEB).

Public Organizations:

Commemorative Organization for the Japan World Exposition '70
Japan National Tourist Organization
The Pharmaceutical Manufacturers Association of Tokyo
Oosaka Pharmaceutical Manufacturers Association
The Japan Labor Cultural Association
Ibaraki Health Service Association

Pharmaceutial Companies:

Amgen Ltd.
Asahi Chemical Industry Co., Ltd.
AstraZeneca
Aventis Pharma Ltd.
Azwell Inc.
Banyu Pharmaceutical Co., Ltd.
Bayer AG
Bristol Myers K.K.
Chugai Pharmaceutical Co., Ltd.
Daiichi Pharmaceutical Co., Ltd.
Dainippon Pharmaceutical Co., Ltd.
Eiken Chemical Co., Ltd.
Eisai Co., Ltd.
Elmed Eisai Co., Ltd.
Fujisawa Pharmaceutical Co., Ltd.
Fuso Pharmaceutical Industries, Ltd.
Graxo Smith Kline K.K.
Grelan Pharmaceutical Co., Ltd.
Japan Tobacco Inc.
Kaken Pharmaceutical Co., Ltd.
Kakenshoyaku Co., Ltd.
Kanebo, Ltd.
Kirin Brewery Co., Ltd.
Kissei Pharmaceutical Co., Ltd.
Kowa Company, Ltd.
Kyorin Pharmaceutical Co., Ltd.
Kyowa Hakko Kogyo Co., Ltd.
Maruho Co., Ltd.
Maruishi Pharmaceutical Co., Ltd.
Meiji Milk Products Co., Ltd.
Meiji Seika Kaisha Ltd.
Merck Hoei Ltd.
Mikasa Seiyaku Co., Ltd.
Minophagen Pharmaceutical Co., Ltd.
Mitsubishi Pharma Corporation
Mochida Pharmaceutical Co., Ltd.
Morinaga Milk Industry Co., Ltd.
Nihon Pharmaceutical Co., Ltd.
Nihon Schering K.K.
Nikken Chemicals Co., Ltd.

Nippon Boehringer Ingelheim Co., Ltd.
Nippon Chemiphar Co., Ltd.
Nippon Kayaku Co., Ltd.
Nippon Shinyaku Co., Ltd.
Nippon Zoki Pharmaceutical Co., Ltd.
Nipro Pharma Corporation
Novartis Pharma K.K.
Ono Pharmaceutical Co., Ltd.
Otsuka Pharmaceutical Co., Ltd.
Pfizer Japan Inc.
Rohto Pharmaceutical Co., Ltd.
Sankyo Co., Ltd.
Santen Pharmaceutical Co., Ltd.
Sanwa Kagaku Kenkyusho Co., Ltd.
Sato Pharmaceutical Co., Ltd.
Sawai Pharmaceutical Co., Ltd.
Schering-Plough K.K.
Shionogi & Co., Ltd.
Snow Brand Milk Products Co., Ltd.
SSP Co., Ltd.
Sumitomo Pharmaceutical Co., Ltd.
Taiho Pharmaceutical Co., Ltd.
Taisho Pharmaceutical Co., Ltd.
Takeda Chemical Industries, Ltd.
Tanabe Seiyaku Co., Ltd.
Teijin Ltd.
Teikoku Hormone Mfg. Co., Ltd.
Terumo Corporation, Japan
Toa Eiyo Ltd.
Torii Pharmaceutical Co., Ltd.
Towa Pharmaceutical Co., Ltd.
Toyama Chemical Co., Ltd.
Tsumura & Co.
Wakamoto Pharmaceutical Co., Ltd.
Wyeth Lederle Japan, Ltd.
Yakult Co., Ltd.
Yamanouchi Pharmaceutical Co., Ltd.

Others:

Mr. Hiroaki Aoki
Asazen
Breast Clinic Kodama Surgery
Chikatsu Clinic
Hayashi Clinic
Ibarakiken Medical Center
Ide Clinic
Mr. Seiji Inagawa
Mr. Mikio Kakinuma
Kogure Clinic
Kokonomi-kai Shimazaki Clinic
Ms. Tomiko Kuriyama
Medison Co., Ltd.
Miyamae Clinic
Ms. Itsuko Ogura
Ohtashiro Clinic
Dr. Noriko Ohtashiro
Ryuin-kai Ushio Hospital
Saitoh Clinic
Suzuki ENT Clinic
Takezono Skin Clinic
Ms. Utako Tayama
Ms. Fumi Tsuritani
Ueno Surgical Clinic
Mr. Haruyuki Yamada
Zensen-kai

Contents

Discovery of the Piezoelectric Phenomenon: Curie and Langevin

Dominique Amy

In 1880, the brothers Pierre and Jacques Curie predicted and demonstrated piezoelectricity. They showed that crystals of tourmaline, quartz, cane sugar, and Rochelle salt generate electrical polarization from mechanical stress; quartz and Rochelle salt exhibited the most piezoelectricity. Twenty natural crystal classes exhibit direct piezoelectricity. Converse piezoelectricity was mathematically deduced from fundamental thermodynamic principles by Lippmann in 1881. The Curies immediately confirmed the "converse effect" and proved the complete reversity of electroelastomechanical deformations in piezoelectric crystals: development of charge on a crystal is proportional to an applied mechanical stress. The converse effect: the geometric strain of a crystal is proportional to an applied voltage.

The major contributions of Pierre Curie are discovery of piezoelectricity, invention of the piezoelectric quartz, formulation of the principle of symmetry, invention of the Curie scale, establishing Curie's law, and establishing the theoretical relationship between crystallography and physics. To assist in his experiments, Curie constructed several delicate pieces of apparatus, such as balances, electrometers, and piezoelectric crystals. Quartz piezoelectric transducers consist of thin slabs or plates cut in a precise orientation to the crystal axes depending on the application.

Paul Langevin was born in Paris on January 23, 1872. He had been supervised by Pierre Curie during his laboratory classes at the ESPCI school (Ecole Supérieure Physique Chimie Industrielles) in Paris (1898–1902). Later, he became Professor of Physics at the College de France and director of the ESPCI and was elected to the Academy of Sciences in 1934. A contemporary of Marie Curie, Albert Einstein, and Hendrik Lorenz, he was noted for his work on the molecular structure of gas and his theory of magnetism and was very active in spreading relativity theory in France. During World War I, he was inventor of the underwater sonar for submarine detection, with very important work on piezoelectricity and on piezoceramics. He created the first quartz sandwich transducer in 1915. The experiment has a watch in which the quartz dilatation is proportional to the applied tension:

$$A = \&U$$

21 avenue Victor Hugo, Aix-en-Provence, 13100, France

where A = centimetric dilatation, U = potential difference in volts, and & = $2.16 \cdot 10^{-10}$.

If U corresponds to 10 000 volts, A will be 0.02 μm. This piezoelectric phenomenon is thus very small and it would be necessary to apply very high electric tension to have sufficient ultrasonic power. If the quartz is covered with two steel blades (Langevin), all the unit has to vibrate only one block. There will be a quartz thickness reduction because it is the triplet thickness, which must be equal to the half-length wave. Moreover, the triplet amplification will be multiplied by a factor of 25 and the necessary tension is reduced 30 fold. The quartz sandwich transducer is thus the ideal electroacoustic transformer. This transducer has been upgraded by the use of mosaic of small identical quartzs (easier to obtain), then with piezoelectric ceramics transmitters (barium titanate) presenting an piezoelectric coefficient 300 times superior to quartz. During reception, the Langevin triplet behaves like a radio antenna and the ultrasonic wave will cause a difference in potential appearance. It should be noted that during the reception it would be possible to detect ultrasound whose amplitude is a million times smaller than at the emission. By calculating the exact crystal frequency resonance, by using harmonics, and new ceramics, great progress could be carried out.

The history of piezoelectricity could have been somewhat different if Pierre Curie had not died accidentally early in April 1906 (after his Nobel Prize award in 1903). His wife, Marie Curie, continued her work on radioactivity and the discovery of polonium and radium. But the year 1911 must have been for her a terrible year (in spite of the fact she was awarded the Nobel Prize in Chemistry) because she was rejected by the Academy of Sciences; also, she was involved in the "Langevin affair," a love triangular affair with Mrs. Langevin.

> "I believe that there is no connection between my scientific work and the facts of private life . . . I cannot accept the idea in principle that the appreciation of the value of scientific work should be influenced by libel and slander concerning private life." (Marie Curie, 1911)

The list of applications of piezoelectric instrumentation continues to grow and now includes ultrasound in medicine, phonograph pickups, air transducer microphone remote controls, underwater transducers and sonars, aerospace, ballistics, biomechanics, engine testing, engineering, and industrial and factory applications.

A Review of Theoretical and Experimental Aspects of Imaging the Elastic Attributes of Tissue In Vivo

Jonathan Ophir

The literature describing the gross mechanical properties of tissues is primarily concerned with muscle (skeletal and cardiac) as well as with blood vessel walls [1]. Relatively little has been written about the mechanical properties of other normal and pathological tissues. Pathological changes are generally correlated with changes in tissue elastic modulus; in fact, the standard medical practice of soft tissue palpation is based on qualitative, low-resolution assessment of the static elastic modulus of tissue. Many cancers, such as scirrhous carcinoma of the breast, appear as extremely hard nodules [2]. In quite a few cases, despite the difference in elastic modulus, the small size of a pathological lesion and/or its location deep in the body precludes its detection and evaluation by palpation. In general, the lesion may or may not possess echogenic properties that could make it ultrasonically detectable. For example, tumors of the prostate or the breast could be invisible in standard ultrasound examinations, yet be much harder than the embedding tissue.

Diffuse diseases such as cirrhosis of the liver are known to significantly reduce the elastic modulus of the liver tissue as a whole [2], yet they may appear normal in conventional ultrasound examination. Because the ultrasonic echogenicity and the elasticity of tissue are generally uncorrelated, it is expected that imaging tissue elastic modulus will provide new information that is related to tissue structure and/or pathology (Fig. 1).

Biological tissues can be considered as approximating homogeneous gels [3]. Different modes of elastic wave propagation in such media are determined primarily by their bulk (K) and shear (G) elastic moduli. In biological soft tissues, the value of K far exceeds that of G. The bulk properties (and hence the ultrasonic properties) are determined by the molecular composition of the tissue [1], whereas the shear properties are determined by the higher level of tissue organization [3]. Because deformable soft tissues are essentially volume incompressible (i.e., Poisson ratio, ~0.5), their shear moduli are proportional to their longitudinal (Young's) moduli [4]. It follows that estimation and imaging of the Young's moduli of tissue should in principle convey information about their shear properties, and hence about the higher level of tissue organization.

Ultrasonics Laboratory, Department of Radiology, University of Texas Medical School, 6431 Fannin Street, Houston, TX 77030, USA

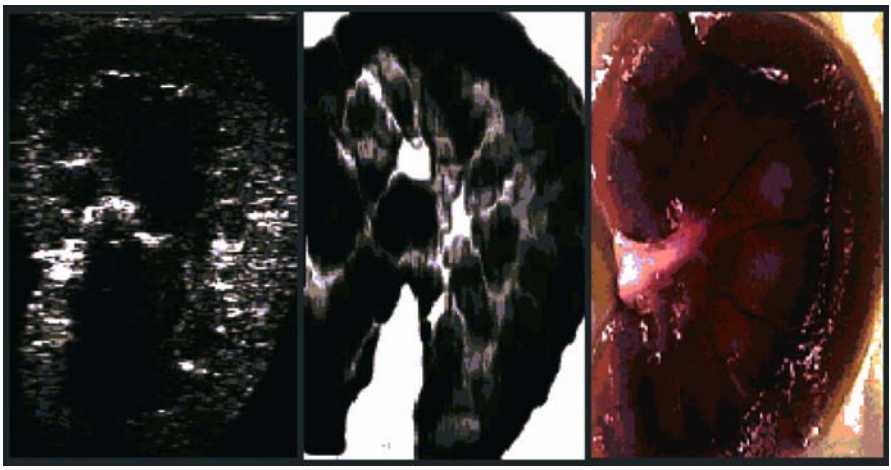

FIG. 1. A sonogram, elastogram, and gross pathology slide showing the longitudinal appearance of an ovine kidney in vitro. Note the distinct appearance of the pyramids in the elastogram and the contrast in stiffness between the cortex and the medulla on the elastogram (*black*, stiff; *white*, soft)

No known modality is capable of imaging these important elastic properties of tissue directly. It is therefore necessary to apply an external mechanical stimulus to the tissue system and to observe the tissue response in terms of local internal deformations. In principle, any high-resolution imaging modality may be used for such observations. The use of ultrasound for this purpose, however, has several important advantages that include real-time imaging capabilities, very high resolution in motion estimation (~1 μm), simplicity, noninvasiveness, and relative low cost.

Ultrasonic methods for deriving information related to the elastic properties of soft tissues have been described in the literature in the past 10 years. These techniques rely on one of the following procedures: Doppler tissue velocity measurements [5–7], decorrelation techniques to quantify motions in tissues [8–11], and visual inspection of M-mode and B-mode image. Internal mechanical excitation (motion of cardiac structures, arterial pulsation) or external vibrational sources of motion are used to produce displacement of the tissues under investigation. The displacements of different tissues are then analyzed by one of these techniques.

Elastography is performed by obtaining a set of ultrasonic echo signals from a target, subjecting the target to a small axial deformation, and obtaining a second set of echo signals. Time-delay estimations along the direction of the applied load are computed by performing piecewise cross-correlation analysis on congruent pairs of signal segments. Using the gradient operator, the time-shift estimates are then converted to longitudinal strain information, which could be displayed in the form of a two-dimensional strain image named elastograms. We have demonstrated that the

strain distributions in tissues are correlated to the distribution of tissue elastic moduli under certain conditions. Furthermore, general inverse methods for calculating elastic modulus images from elastograms have been described by Skovoroda et al. and by Sumi et al. [12]. In addition to axial strain elastograms, it is also possible to obtain lateral strain elastograms and Poisson's ratio elastograms, which convey additional tissue mechanical information.

We have constructed an elastography device based on an Philips/ATL HDI-1000 imaging system, which was designed to produce sonograms and corresponding elastograms of the breast in vivo. This device is able to acquire elastograms at a rate of up to 15/s. We have also been working on elastographic imaging of the prostate. Elastograms can produce good-quality images of tissue strain that easily demonstrate stiff yet ultrasonically occult, isoechoic lesions. The images in Fig. 1 demonstrates the different sonographic and elastographic appearance of an ovine kidney in vitro.

We have also developed a theoretical framework (called a strain filter or strain transfer function) that can predict the upper bound of imaging performance of elastography given the engineering system parameters. This tool is based on the Cramer–Rao lower bound for the variance of time-delay estimations and on the analysis of the decorrelation of shifted signals. Once the system bandwidth, center frequency, sonographic signal-to-noise ratio (SNR), and window size are specified, and the estimation algorithm known, the elastographic parameters of elasticity SNR, dynamic range, sensitivity, contrast-to-noise ratio, and resolution may be calculated. The strain filter may be derated by nonstationary effects such as transducer beam profiles and attenuation in the tissues.

Acknowledgment. The author is indebted to numerous contributions made to this work over the last 13 years by many investigators and students who will be acknowledged separately. Supported in part by National Cancer Institutes Program Project grant P01-CA64597.

References

1. Fung YC (1981) Biomechanical properties of living tissues. Springer, New York
2. Anderson WAD (1953) Pathology. Mosby, St. Louis
3. Sarvazyan AP (1993) Shear acoustic properties of soft biological tissues in medical diagnostics. J Acoust Soc Am Proc 125th meet 93(part 2):2329
4. Saada S (1983) Elasticity, theory and applications. Pergamon, New York
5. Lerner RM, Parker KJ (1987) Sono-elasticity in ultrasonic tissue characterization imaging. In: Thijssen JM (ed) Proceedings, 7th European Community workshop Nijmegen, The Netherlands
6. Krouskop TA, Dougherty DR, Levinson SF (1987) A pulsed Doppler ultrasonic system. J Rehabil Res Dev 24:1–8
7. Yamakoshi Y, Sato J, Sato T (1990) Ultrasonic imaging of internal vibration of soft tissue. IEEE Trans Ultrason Ferroelect Freq Control UFFC-17:45–53
8. Dickinson RJ, Hill CR (1982) Measurement of soft tissue motion using correlation between A-scans. Ultrasound Med Biol 8:263–271
9. Wilson LS, Robinson, DE (1982) Ultrasonic measurement of small displacements and deformations tissues. Ultrason Imag 4:71–82

10. Tristam M, Barbosa DC, Cosgrove DO, et al (1986) Ultrasonicstudy of in vivo kinetic characteristics. Ultrasound Med Biol 12:927–937
11. Tristam M, Barbosa DC, Cosgrove DO, et al (1988) Application of Fourier analysis in clinical study of patterns. Ultrasound Med Biol 14:695–797
12. Sumi C, Suzuki A, Nakayama K (1995) Estimation of shear modulus distribution in soft tissue from strain distribution. IEEE Trans BME 42(2):193–202

In Vivo Breast Examination by Real-Time Freehand Elasticity Imaging System

Tsuyoshi Shiina[1] and Ei Ueno[2]

Summary. Tissue elasticity imaging technology is expected to be a new modality for breast diagnosis, based on hardness as a tissue characteristic that is affected by tissue disease such as cancer. Different approaches of elasticity imaging have been investigated, and at present some are at the stage of developing a practical system. In clinical measurement, high-speed processing is required for real-time diagnosis, and freehand manipulation of the ultrasonic probe, such as in the usual ultrasonic diagnosis, is desirable for simple operation. Thus, we developed a tissue elasticity imaging system with freehand tissue compression based on a combined autocorrelation method. The method enables us to obtain tissue strain distribution as tissue elasticity with high speed and suppressing error due to lateral slip of the probe caused by freehand compression. The developed method was applied to breast disease measurements in vivo. Consequently, it is shown that the system can estimate the strain images in real time, and is effective not only in diagnosis of tissue hardness but also in determination of disease expansion area. It is also confirmed that the method is applicable to breast measurements in vivo.

Key words. Ultrasonic imaging, Tissue elasticity, Breast examination, Cancer diagnosis

Introduction

The hardness of tissue is closely related to the pathological state, and many diseased tissues such as in breast cancer, liver cirrhosis, and arteriosclerosis become hard with disease progress. In recent years, Krouskop et al. [1] measured the elasticity of some diseased tissue of breast and prostate in vitro and showed that the elasticity (Young's modulus) of most malignant tissues was larger than that of normal tissues. Therefore, by measuring tissue elasticity quantitatively, we can perform tissue diagnosis based on the mechanical properties of tissues. Thus, many investigations on imaging tissue

[1] Graduate School of Systems and Information Engineering, University of Tsukuba, 1-1-1 Tennodai, Tsukuba, Ibaraki 304-8573, Japan
[2] Institute of Clinical Medicine, University of Tsukuba, Tsukuba, Japan

elasticity by ultrasound have been done since the 1990s. Ophir et al. [2] began the study of imaging strain distribution under static tissue compression, and Yamakoshi et al. [3] proposed another means that images propagation velocity distribution of mechanical vibration under tissue vibration. Here, the measurements are based on the fact that hard tissue has a small strain and a high propagation speed.

However, owing to some merits such as high spatial resolution and easy implementation, methods with static tissue compression are now mainly investigated. In this method, first, the strain is produced inside a tissue by performing static tissue compression, and this strain distribution is obtained from ultrasonic echo signals before and after tissue deformation. Different approaches of static methods have been investigated, and at present some are at the stage of developing a practical system to be used clinically. Advantages of ultrasonic examination such real-time and simple (freehand) operation must be preserved in the elasticity imaging system. A high-speed algorithm for estimating strain distribution and processing with hardware are required for real-time measurement. Regarding simple operation, freehand manipulation of the ultrasonic probe as in the usual ultrasonic diagnosis is desirable. At the beginning, tissue compression for elasticity imaging was performed using a stepping motor attached to an ultrasonic probe for an accurate compression in the axial direction. However, this system becomes a large-scale setup, and it is difficult to move a probe to the measured position while monitoring the B-mode image. Consequently, application of this system is limited, and it also takes a long time for measurements. From this point of view, we have developed a high-speed tissue elasticity imaging system based on the combined autocorrelation method (CAM) [4–6], which can overcome the problem of lateral slip and apply freehand manipulation of the probe for tissue compression. Furthermore, we evaluated this system through clinical breast disease measurements in vivo.

Development of High-Speed Freehand Strain Imaging

Principle of the Imaging Method

For measuring a strain distribution, it is necessary to produce a strain inside a tissue by compressing or relaxing a tissue. In ultrasonic tissue elasticity measurement, tissue compression (relaxation) is performed using an ultrasonic probe. Moreover, ultrasonic echo signals from the inside of a tissue before and after deformation are also measured simultaneously with tissue compression. A displacement distribution, which shows where each point inside a tissue is moved, is estimated from these ultrasonic echo signals. Next, we differentiate a displacement distribution spatially for obtaining strain distribution and visualize a strain distribution as an elasticity image. Here, as a property of the ultrasonic system, strain estimation accuracy in the direction of an ultrasonic beam (axial direction) is better than that in the direction that is perpendicular to the axial direction (lateral direction). This condition is satisfied in compression with a stepping motor because the compression direction coincides with the axial direction. In freehand compression, however, it is necessary to suppress the influence of lateral slip. It is also necessary to have a large dynamic range of strain for stable measurement that does not depend on compression speed and quantity.

We previously developed a base algorithm of the combined autocorrelation method [4, 5], which can estimate strain distribution accurately and at high speed and has a large dynamic range of strain. However, this method does not overcome the problem of lateral slip. Therefore, we extended the method to overcome the problem of lateral slip [6]. The details of this method are shown next.

In tissue elasticity imaging, tissue deformation between two ultrasonic measurements is very small (the mean strain is a few percent). First of all, by using the two-dimensional (2-D) envelope correlation coefficient, we can conquer the problem of phase aliasing as well as the spatial correlation method. However, the feature of this method is to search only on the grid points of the half-wavelength interval in the axial direction and the interval of scan lines in the lateral direction (Fig. 1) because a 2-D envelope correlation coefficient is conducted for the purpose of selecting the zone where aliasing does not occur. Thus, an improvement in the processing speed is attained in this method. Here, the half-wavelength interval in the axial direction enables us to optimize computing efficiency without phase aliasing.

Therefore, we can estimate the strain stably in a large dynamic range. Next, at the zone without aliasing error, fine estimation of displacement is carried out by using phase detection as well as the autocorrelation method. Finally, if the axial displacement distribution can be estimated as already mentioned, the strain distribution can be found by differentiating it spatially. Furthermore, the CAM overcomes the problem of lateral slip by using the 2-D correlation.

The foregoing is processing of a strain distribution estimation by the CAM, and the features of this method are high precision and high speed, to support a large dynamic range of strain and lateral slip. So far, we have verified the ability of this method through simulations and phantom experiments. Consequently, it is shown that the processing speed of the CAM is about eight times as fast as that of the conventional spatial correlation method, and the accuracy of the CAM is twice as accurate as that of the spatial correlation method [5]. Furthermore, it is shown that the dynamic range of strain estimated by the CAM is 0.05% to 5.0% (the optimal dynamic range is 0.5%–2.0%), and this method can support lateral slip to about 4 mm. In addition, in this chapter, we use the 1.2 mm (axial) × 1.0 mm (lateral) correlation window and the

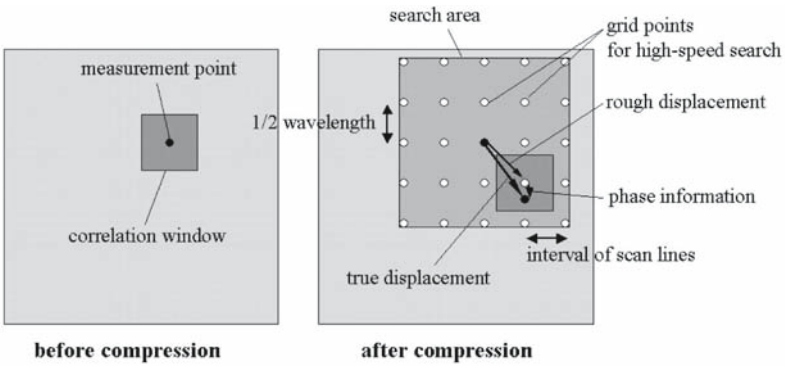

Fig. 1. Schematic diagram of the combined autocorrelation method (CAM)

3.2 mm (axial) × 2.2 mm (lateral) displacement search area. Such sizes are decided from results of the phantom experiment based on the condition for the fine strain image.

Simulation Analysis

A 60 mm × 60 mm tissue model is used and compressed by 3% in the axis direction, and lateral displacement is applied from 0.0 mm to 1.4 mm. We then simulate the RF signals before and after the deformation and estimate the strain distribution from these RF signals using three methods: the one-dimensional (1-D) CAM, which does not search the correlation window in the lateral direction, the CAM, and the correlation method. To simulate the RF signals, we use the following parameters. The center frequency of the ultrasonic probe is 5.0 MHz, the sampling frequency is 30 MHz, the beam width is 1.0 mm (full width at half maximum), and the A-line interval is 0.5 mm. Figure 2 shows the strain estimation accuracy of three methods with respect to lateral slip (lateral displacement). The result confirms that the error increases rapidly when the lateral displacement exceeds half the beam width in the 1-D CAM, but that strain can be estimated robustly regardless of the size of the lateral displacement in the CAM.

Next, we simulate the behavior of the tissue under compression with the three-dimensional (3-D) finite-element method (FEM), generate the RF signals before and after compression based on this FEM result, and estimate the strain distribution with three techniques. In this simulation, we use a 60 mm × 60 mm × 60 mm tissue model in which there is a 15-mm-diameter, 60-mm-long columnar hard inclusion. Here, we set the elastic modulus (Young's modulus) of the surrounding material to 10 kPa and set the elastic modulus of the inclusion to 30 kPa. We then compress this model in two ways. First, we apply a pressure of 200 Pa perpendicularly from the model surface. Second, we apply pressure (axial component, 200 Pa; lateral component, 30 Pa) in the diagonal direction from the model surface.

Figure 3 shows the strain distribution obtained on the central cross section of the tissue model estimation when a tissue model is compressed perpendicularly. In this case, because there is little lateral displacement, the 1-D CAM and the CAM yield the

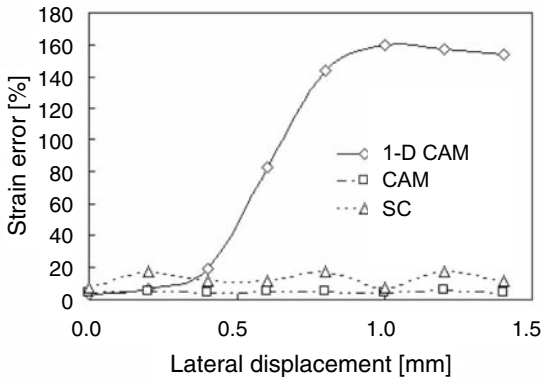

FIG. 2. Estimated strain error due to lateral displacement

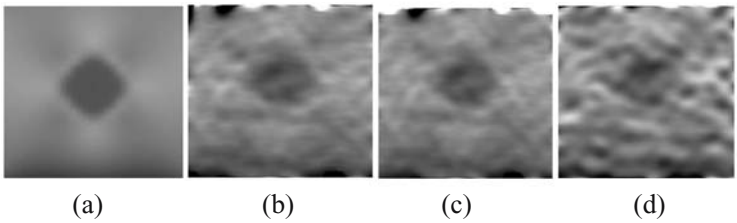

Fig. 3. Estimated strain distribution when compressing a tissue model perpendicularly (grayscale: 0.0%–3.5%). **a** Ideal strain distribution. **b** CAM. **c** 1-D CAM. **d** Spatial correlation method

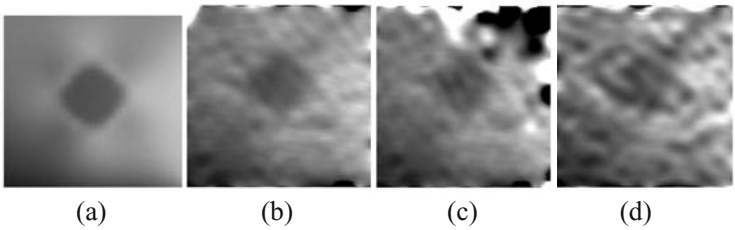

Fig. 4. Estimated strain distribution when compressing a tissue model diagonally (grayscale: 0.0%–3.5%). **a** Ideal strain distribution. **b** CAM. **c** 1-D CAM. **d** Spatial correlation method

same results. Figure 4 shows the result when a tissue model is compressed diagonally. In this case, the lateral displacement becomes large at the upper right part of the model. Therefore, the 1-D CAM produces some mistakes in the upper right. In contrast, the CAM produces a correct estimate. Also, the CAM generates a smaller error than the spatial correlation method.

Development of Real-Time System

System Constitution

We tried to develop a real-time tissue elasticity imaging system that can perform stable measurements with freehand tissue compression. Our system consists of an ultrasonic probe (7.5 MHz, liner array, interval of scan lines is about 0.3 mm), an ultrasonic scanner (sampling frequency, 30 MHz), and a personal computer (CPU: Intel Pentium IV 2.2 GHz × 2; memory: 1 GB). The small compression plate is attached to an ultrasonic probe so that stable tissue compression is attained and the stress field is transmitted more uniformly; consequently, a good strain image is obtained (Fig. 5). The ultrasonic scanner is remodeled so that IQ signals digitized at the rate of 30 MHz can be taken out. Combining the quadrature detector with hardware in the ultrasonic

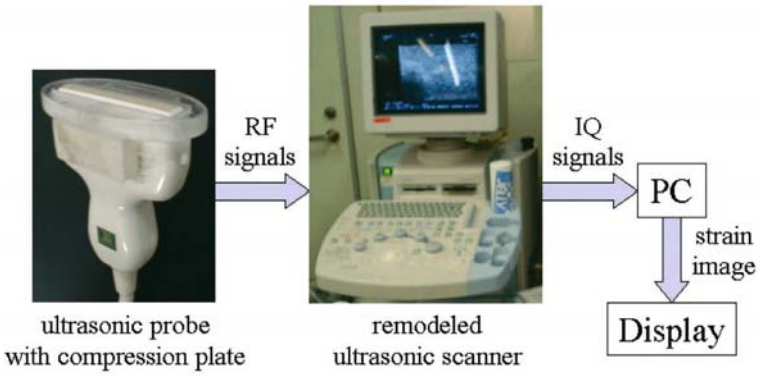

Fig. 5. Developed tissue elasticity imaging system

scanner and performing parallel processing with the dual CPU, the processing speed becomes fast. We also improve the processing speed by using the optimal compiler for Intel CPU and the high-speed image-processing library software. Here, the frame rate for the strain image depends on the strain measurement area and performance of the CPU. At present, the frame rate is about 5 frame/s (fps) at the 30 mm (axial) × 55 mm (lateral) strain measurement area. It will be possible to improve the processing speed further, that is, to the same frame rate of a B-mode image, by increasing the CPU performance or developing a hardware unit for signal processing.

The area and boundary of a tumor in a strain image and that in a B-mode image are not necessarily the same, and some tumors that are not observed in the B-mode image may be visualized in the strain image. For recognizing the corresponding portions between the strain image and the B-mode image, we adopted a way of displaying both images: a strain image is superimposed on the B-mode image with a translucent color scale, where red and blue indicate that tissues are soft and hard, respectively (Fig. 6). Using a translucent strain image, it becomes easy to recognize what part of the strain image corresponds to the region of tumor displayed in the B-mode image as the tissue structure.

In general, the level of the strain changes while freehand compressing or relaxing tissues; consequently, it is necessary to dynamically change the range for displaying the strain during tissue compression or relaxiation. Therefore, we calculate the mean of strain distribution within a region of interest (ROI), and we adaptively change the display range using this mean value. Thus, the maximum of the range is set to 2.5 times the mean value; the minimum of the range is always set to 0. Using this adaptive strain display range, the stable strain image can be obtained without depending on the level of compression.

In Vivo Breast Measurements

To verify the ability of our developed system by in vivo clinical measurements, we applied the system to breast disease measurements, which may be one of the most useful applications of tissue elasticity imaging. In clinical measurements, medical

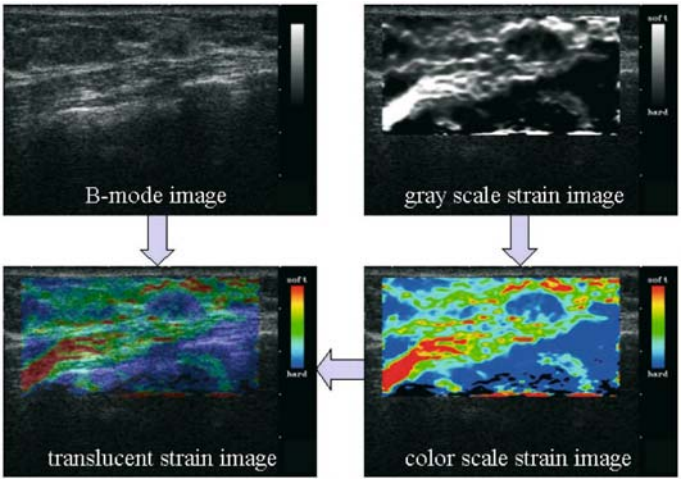

Fig. 6. Strain image display method. Because it is difficult to determine the position relation between a strain image and a B-mode image, we produce a color scale strain image, make it translucent, and overlay it on the B-mode image

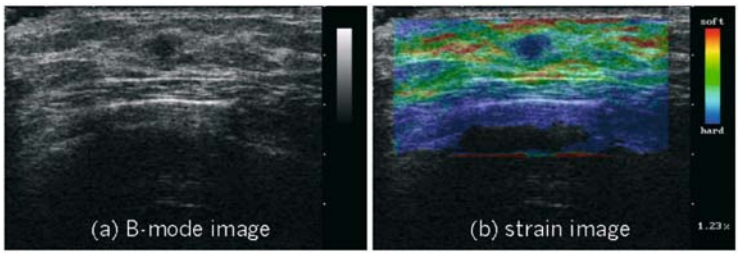

Fig. 7. In vivo measurement result from a 39-year-old woman with a noninvasive ductal carcinoma. There is a tumor, blue-colored, that represents a hard area, with a diameter of about 5 mm in the center of the figure. *The number shown in the lower right of strain image* is the mean strain

doctors operated the ultrasonic probe after obtaining a patient's consent. Figure 7 shows a case of an invasive ductal carcinoma (a 59-year-old woman). In the B-mode image, the existence of a tumor with a diameter of about 10 mm may be observed but its boundary is blurred. On the other hand, it is shown that the tumor is hard in the strain image (Fig. 7). The expansion area of a tumor is clear in this strain image, while it is not clear in the B-mode image. Therefore, it is expected that the strain image is useful not only for a diagnosis of tissue hardness but also for that of the expansion area of the cancer. In our system, although the B-mode image and strain image is obtained at the frame rate of 25 fps at present model. Figure 7 shows in vivo measurement result from a 39-year-old woman with a noninvasive ductal carcinoma. There

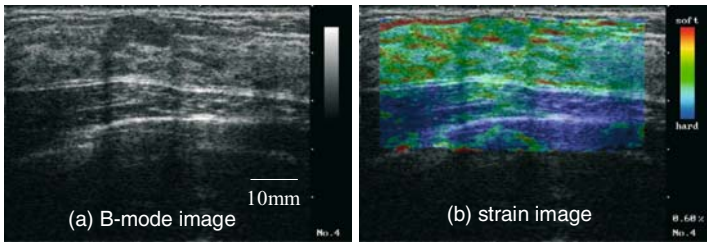

Fig. 8. In vivo measurement result from a 42-year-old woman with a fibroadenoma with a diameter of about 10 mm in the figure. Area of tumor is depicted as a softer region

is a blue-colored tumor that represents a hard area, with a diameter of about 5 mm in the center of the figure. The number shown in the lower right of strain image is the mean strain. Therefore, it indicates that our system also has a high spatial resolution in clinical measurement.

Figure 8 shows a case of a fibroadenoma with a diameter of about 10 mm in the figure. In the B-mode image, tumors are displayed as a hypoechoic region in both Fig. 7 and Fig. 8. In contrast, the colors at the tumor area are different between them, that is, fibroadenoma is depicted as a softer region compared with cancer. These results reveal that the system can provide us novel information on tissue characterization that is not obtained from the conventional images and is helpful for clinical diagnosis.

Discussion

The foregoing results for in vivo evaluation validated that the strain image provided by the developed system is effective in diagnosis of breast disease, not only detection of tumor but also discrimination between benign and malignant. In terms of frame rate, although the performance of initial system was 5 fps, the latest model released by Hitachi Medical Corporation attains 25 fps. According to results of preliminary phantom experiments, for obtaining a strain image, the range of strain to obtain a strain image is 0.05% to 5.0% (the optimal deformation is 0.5%–2.0%). This range admits in vivo breast measurements and a wide-enough range to be applied by free-hand compression.

The elasticity image can be basically obtained in any portion where a B-mode image is displayed. However, if an ultrasonic signal is not acquired, an error will be caused in a strain image. For example, in breast measurement, because an ultrasound does not propagate beyond the pectoral major muscle, the strain estimation error arises in the area beyond the pectoral major muscle. However, fortunately, the area of interest in breast measurement is above the pectoral major muscle. On the other hand, the elasticity image can be often obtained in the shadow of a B-mode image because the phase shift between two echoes is detectable even from relatively lower signals.

Conclusion

We developed a combined autocorrelation method (CAM) to estimate strain distribution in tissue. The advantages of the CAM are higher speed and accuracy than the conventional spatial correlation method because it is based on the Doppler method. Also, this method overcomes the problem of aliasing, a weakness of the Doppler method; consequently, the CAM can estimate strain over a wide dynamic range.

The CAM also overcomes the problem of lateral slip on the body surface in the clinical situation. Results of simulation analysis confirmed the ability of the CAM to be robust for lateral slip. These properties are suitable to measurement of the strain stably by freehand deformation and performing in vivo breast measurements using the system.

Consequently, it is confirmed that a stable strain image can be obtained also by deforming a tissue freehand in vivo. In our system, performing parallel processing based on the extended CAM and using the optimal compiler for CPU, the strain imaging frame rate can increase, and the latest model attains about 30 frame/s (fps). From the results of breast measurements, it is shown that our system is effective not only in assessment of tissue hardness but also in diagnosis of the expansion area of the tumor. In future work, we aim at quantitative elasticity measurement for pathological diagnosis and plan to apply our system to other parts of the body where it is considered that elasticity imaging is effective, such as the prostate, liver, kidney, and myocardium.

References

1. Krouskop TA, Wheeler TM, Kallel F, et al. (1998) Ultrason Imaging 20:260
2. Ophir J, Cespedes I, Ponnekanti H, et al. (1991) Ultrason Imaging 13:111
3. Yamakoshi Y, Sato J, Sato T (1990) IEEE Trans Ultrason Ferroelect Freq Contrib 37:45
4. Yamakawa M, Shiina T (2001) Jpn J Appl Phys 40:3872
5. Shiina T, Doyley MM, Bamber JC (1996) Proc IEEE Ultrason Symp p. 1331
6. Yamakawa M, Shiina T (1999) Jpn J Appl Phys 38:3393

Usefulness of Ultrasonic Strain Measurement-Based Mechanical Properties Imaging Technique: Toward Realization of Short-Time Diagnosis/Treatment

Chikayoshi Sumi[1], Mitsuhiro Kubota[2], Go Wakabayashi[3], and Minoru Tanabe[3]

Summary. For various soft tissues (e.g., liver, breast), we are developing the ultrasonic strain measurement-based mechanical properties (e.g., shear modulus, viscoshear modulus) reconstruction/imaging technique. To clarify the limitation of our quantitative reconstruction/imaging technique as a diagnostic tool for differentiating malignancies, together with improving the spatial resolution and dynamic range, we are collecting clinical reconstruction image data. Furthermore, we are applying our technique as a monitoring technique for the effectiveness of chemotherapy (anticancer drug, ethanol, etc.), thermal therapy (micro- and rf electromagnetic wave, HIFU, laser, etc.), and cryotherapy. Because soft tissues are deformed in 3-D space by externally situated quasistatic and/or low-frequency mechanical sources, multidimensional signal processing improves strain measurement accuracy and reduces inhomogeneity-dependent modulus reconstruction artifacts. These properties have been verified by us through simulations and phantom/human in vivo experiments. Briefly, here we discuss the limitations of low dimensional signal processing. Moreover, we exhibit the superiority on both differential diagnosis for these human in vivo malignancies and monitoring for these therapies of our quasi-real-time imaging (using conventional US equipment) to conventional B-mode imaging. Our technique is available as a clinical visualization technique both for diagnosis and treatment, and monitored mechanical properties data can also be effectively utilized as the measure for enhancing controlling therapy, such as the exposure energy, the foci, and the exposure interval. In the near future, suitable combination of various simple and low-invasive therapy techniques with our imaging technique will open up a new clinical style allowing diagnosis and subsequent immediate treatment. This approach should substantially reduce total medical expenses.

Key words. Cancer, Ultrasonic strain measurement-based mechanical properties reconstruction/imaging, Shear modulus, Viscoshear modulus, Differential diagnosis,

[1] Department of Electrical & Electronics, Faculty of Science & Technology, Sophia University, 7-1 Kioi-cho, Chiyoda-ku, Tokyo 102-8854, Japan
[2] Department of Surgery, Yamachika Memorial Hospital, 3-19-14 Koyahata, Odawara, Kanagawa 256-0815, Japan
[3] Department of Surgery, Keio University School of Medicine, 35 Shinanomachi, Shinjuku-ku, Tokyo 160-8582, Japan

Therapy, Monitoring of effectiveness of treatment, Short-time diagnosis/treatment, Combined diagnosis/treatment system

Introduction

It is well recognized that the pathological stage of living human soft tissues highly correlates with quasi-static and low-frequency mechanical properties, that is, shear modulus, viscoshear modulus, etc. With such a fact in mind, as the diagnosis tool for various in vivo superficial and deeply situated tissues (e.g., breast, liver), we are developing the ultrasonic strain measurement-based mechanical properties reconstruction/imaging technique [1–8, 21–23]. To clarify the limitation of our technique, together with improving the spatial resolution and dynamic range, we are collecting clinical reconstruction image data. Furthermore, as the mechanical properties reversibly or irreversibly change by chemotherapy (anticancer drug, ethanol, etc.), cryotherapy, and thermal therapy [micro- and radiofrequency (rf) electromagnetic wave, high-intensity focused ultrasound (HIFU), laser, etc.) [10–15], we are applying our technique as a monitoring technique for the effectiveness of these therapies [16–20].

Because soft tissues are deformed in three-dimensional (3-D) space by externally situated quasi-static and/or low-frequency mechanical sources, multidimensional signal processing improves strain measurement accuracy [5] and reduces inhomogeneity-dependent modulus reconstruction artifacts [8, 9]. These properties have been verified by us through simulations and phantom/human in vivo experiments. Briefly, we discuss here the limitations of low dimensional signal processing.

Moreover, we exhibit the superiority on both differential diagnosis for these human in vivo malignancies and monitoring for these therapies of our quasi-real-time imaging [using conventional ultrasonography (US) equipment, and a conventional workstation, specifically, Compaq XP 1000 Alpha 500 MHz] to conventional B-mode imaging. Recently, to treat human in vivo liver malignancies, several types of interstitial micro- and rf electromagnetic wave thermal applicator systems are widely utilized, in which, respectively, the mono-needle-type electrode and several paired needle electrodes/a plate electrode are employed. However, as we could confirm on the human breast in vivo that our technique has high potential as a practical tool for differentiating early-stage malignancies [e.g., 7], we first utilized the rf electromagnetic wave applicator using only needle electrodes [16–23]. Our imaging technique favorably visualized on the fresh calf liver in vitro the spatial and temporal changes of elasticity due to the rf electromagnetic wave heating, the extraheating, and cooling down. Here we present our high spatial resolution reconstruction/imaging on human liver carcinoma in vivo [21] as well as human breast malignancies in vivo (scirrhous carcinoma), after which, to verify the usefulness as a monitoring technique, we present our reconstructions/images obtained on the rf electromagnetic wave heating of the fresh calf liver in vitro [16–23] and obtained on microelectromagnetic wave heating of the human liver carcinoma in vivo [21].

Materials and Methods

Shear Modulus Reconstruction/Imaging Technique

In our developed reconstruction/imaging technique, the relative shear modulus distribution is reconstructed from ultrasonically measured strain tensor field data with respect to reference shear moduli provided in properly realized wide regions [1–4]. That is, the configurations of mechanical sources and reference regions should be realized so that the reference regions extend in a direction that crosses the dominant tissue deformation.

Displacement vector field generated by spontaneous heart motion and/or externally applied pressures or vibrations can be measured by applying our developed ultrasonic rf-echo phase-matching method [5, 6] to the successively acquired rf-echo data frames, or the paired rf-echo data frames, that is, those under predeformation and postdeformation. In this method, a displacement is determined by using the phase characteristics of the finite local echo data as the index to iteratively search for the corresponding local data. As the change of the local phase characteristics due to tissue deformation causes the accuracy of the determination to deteriorate, the local region size is made suitably smaller during the iterative phase matching. By performing this phase matching throughout the region of interest (ROI), an accurate displacement vector field data is obtained. The axial/lateral/elevational resolutions are respectively determined by the axial/lateral/elevational lengths of the final local region. Subsequently, the displacement field data is differentiated using a filter with a cutoff frequency [1, 3] to obtain the strain field data. The multidimensional phase matching improves the strain measurement accuracy [5, 8]. As the general measurement accuracy of displacement is accurately estimated in a beam direction, the beam could be transmitted in multiple directions. Although the measurement accuracy is degraded, various one-dimensional (1-D) measurement methods can also be utilized together, including the autocorrelation method [2].

To determine the globally relative shear modulus distribution with respect to the reference shear moduli, simultaneous partial differential equations (PDEs) having the strain tensor as the spatially inhomogeneous coefficients are used. However, as the inevitable strain measurement errors and unfortunately occurring improper configurations of mechanical sources and reference regions make the determination problem poorly handled, the robust numerical-based implicit integration approach [4] is used, which incorporates a computationally efficient regularization method using low-pass-filtered spectra derived from strain measurement data. The conjugate gradient method was utilized to realize the implicit integration. On 1-D reconstruction, calculated ratios of the measured strains can be used as the final estimates of the target globally relative shear modulus values [5, 7], substantially reducing the computational time of the implicit integration. By setting the reference regions passing through stress concentration regions, this 1-D reconstruction can reduce the artifacts occurring in the strain image in front of and behind the stiff region (estimated to be softer) [5]. Moreover, multidimensional reconstruction reduces 3-D inhomogeneity-dependent artifacts and consequently heightens the spatial resolution [8, 9]. Here, we show the artifact reduction through simulations (Fig. 1).

A simulated cube phantom (50.0-mm sides) was uniformly compressed in the axial direction (x-axis) with a displacement of 0.25 mm (boundary conditions of the

bottoms, displacement amount of 0 mm in the axial direction, and the others force free). The phantom includes a spherical inhomogeneous region at a depth $x = 25.0$ mm with 5-mm radius. The shear modulus value of the inhomogeneous region is set twice as high as that of the surrounding medium, i.e., 2.0×10^5 N/m^2 versus 1.0×10^5 N/m^2, and Poisson's ratio is uniformly set at 0.47. The resultant internal displacement vector field was calculated by the successive overrelaxation (SOR) method. A cubic ROI is used (30.0-mm sides) having an inhomogeneous region at the central part. Using the resultant strain tensor data from the ROI, 3-D reconstruction is performed under a 3-D stress distribution. The reference region is set at the upper surface of the ROI. 1-D reconstruction is also performed assuming 1-D stress distribution in every x–y plane, as are two-dimensional (2-D) reconstructions assuming a 2-D stress distribution and a 2-D strain distribution in every x–y plane.

Interstitial rf Electromagnetic Wave Applicator System [16–23]

In our developed interstitial rf electromagnetic wave applicator system, only paired needle electrodes are used to apply the electric currents (13.56 MHz). The change of the tissue electric impedance is automatically matched, and therefore constant currents can be applied with power less than 1 kW. Here, two paired electrodes were utilized with a diameter of 2 mm. Using our rf applicator system together with our reconstruction/imaging technique as the monitoring technique, the size and the state of the energy-induced thermal lesion can be controlled.

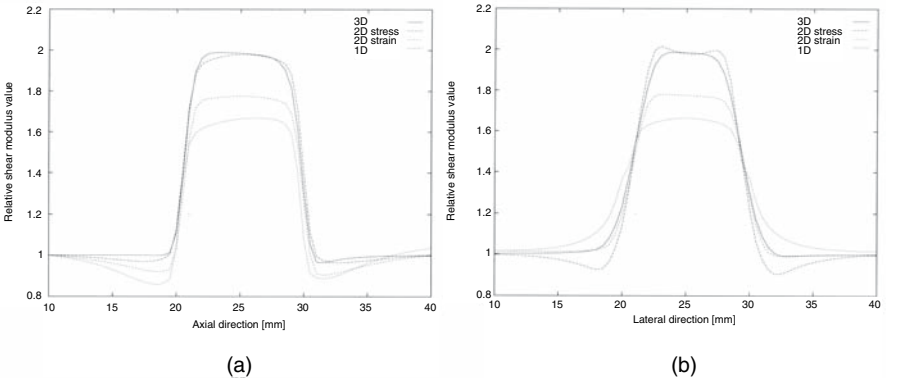

FIG. 1. Three-dimensional (3-D) inhomogeneity-dependent artifacts using a low dimensional reconstruction. Shear modulus reconstructions were obtained under the assumptions of 3-D (x, y, z) stress, 2-D (x, y) stress, 2-D (x, y) strain, and 1-D (x) stress distributions on a simulated cubic phantom of 50.0 mm × 50.0 mm × 50.0 mm including a twofold higher shear modulus spherical region at a depth $x = 25.0$ mm with 5-mm radius (2.0×10^5 N/m^2 versus 1.0×10^5 N/m^2). This phantom was compressed in the axial direction (x-axis) with a displacement of 0.25 mm. Cubic regions of interest (ROIs) (30.0 mm × 30.0 mm × 30.0 mm) are set at the central part of the inhomogeneous spherical region. The reference region is set at the upper surface of the ROI. **a** and **b** are, respectively, the axial x-profiles and lateral y-profiles of reconstructions passing through the center of the spherical inhomogeneous region

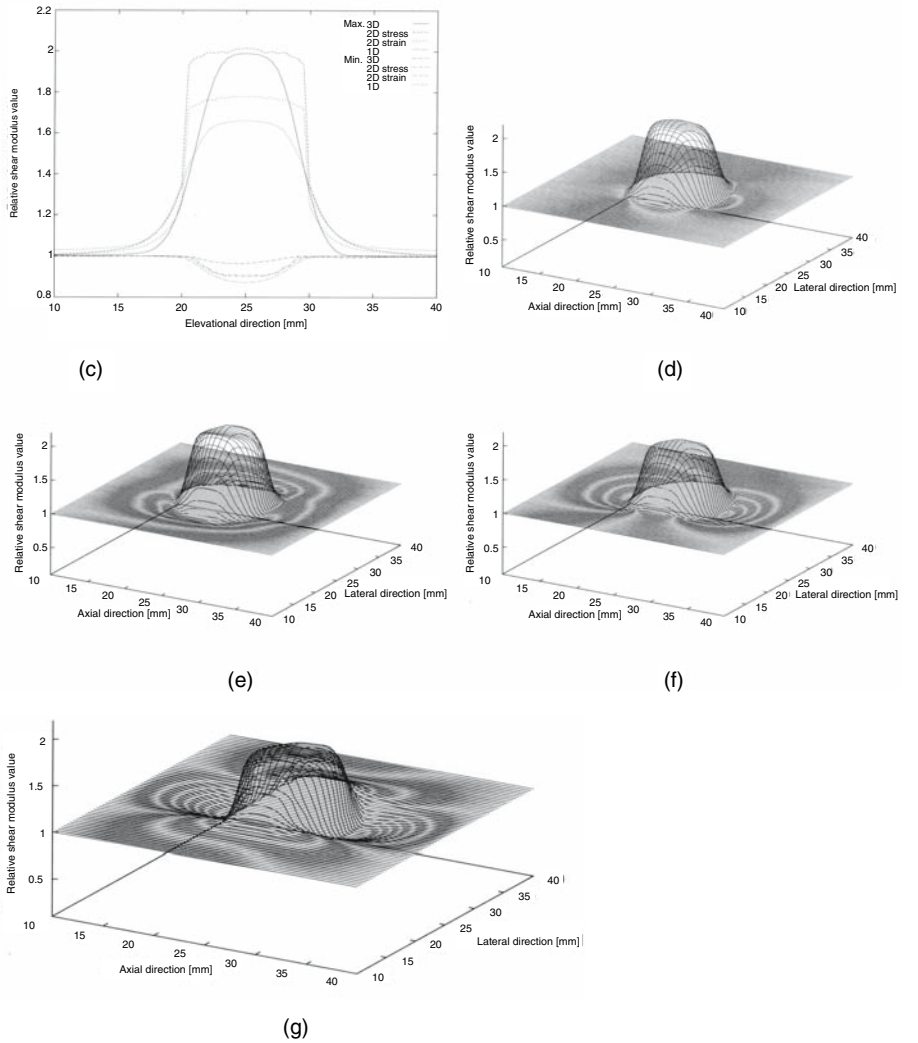

FIG. 1. *Continued*. **c** Maximum and minimum values of the reconstructions obtained at each x–y plane with elevational position z = 10.0 to 40.0 mm. **d**, **e**, **f**, and **g** are, respectively, the 3-D reconstruction, 2-D reconstructions (2-D stress and 2-D strain assumptions), and 1-D reconstruction with elevational position z = 25.0 mm. Low dimensional reconstructions are quantitatively degraded. In the low dimensional reconstructions, an artifact due to stress concentration is found in front of and behind the stiff region, apparently due to successive assumption of 1-D stress, 2-D strain, and 2-D stress. These results also cause a misleading diagnosis in that the lateral and elevational sizes of the stiff lesion are larger than that of the original. Overall, it is clear that low dimensional reconstructions are affected by 3-D inhomogeneity-dependent artifacts and spatial resolution is decreased

Interstitial Microwave Coagulation Therapy Equipment

The microwave coagulation therapy equipment utilized was Microtaze (2.45 GHz; Aswell, Osaka, Japan). The power was set at 70 W. A mononeedle electrode was used with a diameter of 1.6 mm (TMD-16CBL-10/250; Aswell).

Experiments on Human Breast and Liver In Vivo

Breast Scirrhous Carcinoma Case (Fig. 2)

The volunteer (69 years old) was supinely positioned, and the ROI was set at 48.0 mm $\times$ 44.6 mm spreading from the depth of 17.1 mm in her breast. A block of reference material of known shear modulus value was put between the ultrasound transducer

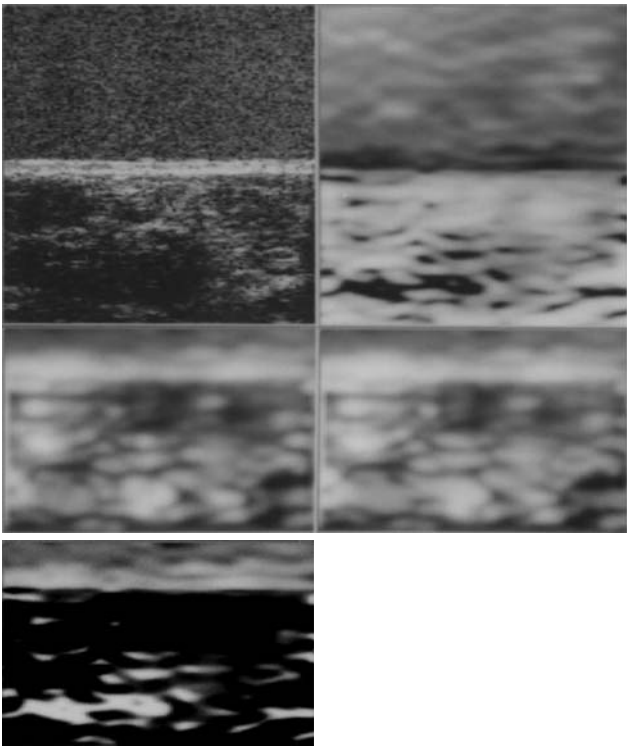

FIG. 2. In vivo human breast tissues. Scirrhous carcinoma case (59 years old; ROI size, 48 mm $\times$ 44.6 mm, depth from 17.1 mm): B-mode image and 2-D-regularized shear modulus reconstruction images (spatial resolution of 0.8 mm $\times$ 3.2 mm) with the measured stain ratio as the initial estimates (highest value, 2.35×10^7 N/m^2; *upper right*, DR, 65.4 dB, lowest value, 1.26×10^4 N/m^2; bright region, relatively low shear modulus value; *middle left* and *middle right*, DR, 54.9 dB, lowest value, 4.21×10^4 N/m^2; bright region, high shear modulus; *lower* is inversion of *upper right*)

and her breast, and her breast tissue was compressed by the transducer by hand such that the ROI could deform in the scanning plane. The pre- and postcompression rf echo data frames were respectively acquired. The nominal frequency of the interrogating ultrasound was 7.5 MHz, and the sampling rate was 30 MHz (12 bits). Figure 2 (upper left) shows the B-mode image of the ROI under precompression.

Normal Liver Case (Fig. 3)

The volunteer (male, 31 years old) was supinely positioned, and the ROI of 35.7 mm × 49.7 mm spreading from 35.1 mm was set. The tissue was compressed by the ultrasound transducer, and during compression echo data frames were successively acquired. The US frequency was 8.0 MHz and the sampling rate was 40 MHz (12 bits). Figure 3a shows the B-mode image of the ROI, in which a reference line is drawn, at depth of 49.8 mm, where blood vessels could not be detected. The reference value was set at 1.0.

Liver Carcinoma Case (Fig. 4)

Here we show reconstructions/images of the carcinoma (diameter, 18 mm) in segment 6 of the female patient (73 years old). The 4-min microwave treatment was carried out under ventrotomy. Under the treatment, and before/after the treatment (closed up), respectively set ROIs were compressed by the transducer by hand. During compression, echo data frames were successively acquired. The US frequency and the sampling rate were, respectively, 7.5 MHz (linear type) and 30 MHz (12 bits) during treatment, and 3.5 MHz (convex type) and 14 MHz (12 bits) before/after the treatment. The ROIs include the same region of the carcinoma, and the ROIs respectively range under treatment with respect to her liver surface from a depth of 3.8 mm to 33.4 mm, and before/after treatment with respect to her skin surface from a depth of 10.6 mm to 52.4 mm (skin depth, about 15 mm). The convex ROI angle is 57.4°; however, here the ROIs are a rectangle of 41.8 mm × 51.8 mm, whereas the linear ROI during treatment is 29.6 mm × 41.5 mm. The B-mode images before, during, and after the treatment are shown of the ROIs, respectively, in Fig. 4a, 4b, and 4c. The reference lines before, during, and after the treatment were respectively set at depths of 11.9, 3.7, and

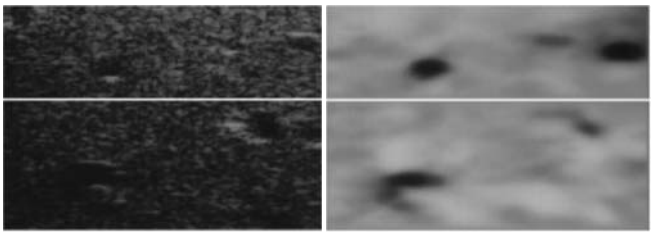

Fig. 3. In vivo human liver (31 years old; ROI size, 35.7 mm × 49.7 mm, depth from 35.1 mm to 70.8 mm). Reference line, 49.8 mm. **a** B-mode image; **b** reconstructed relative shear modulus image (DR, 70.2 dB)

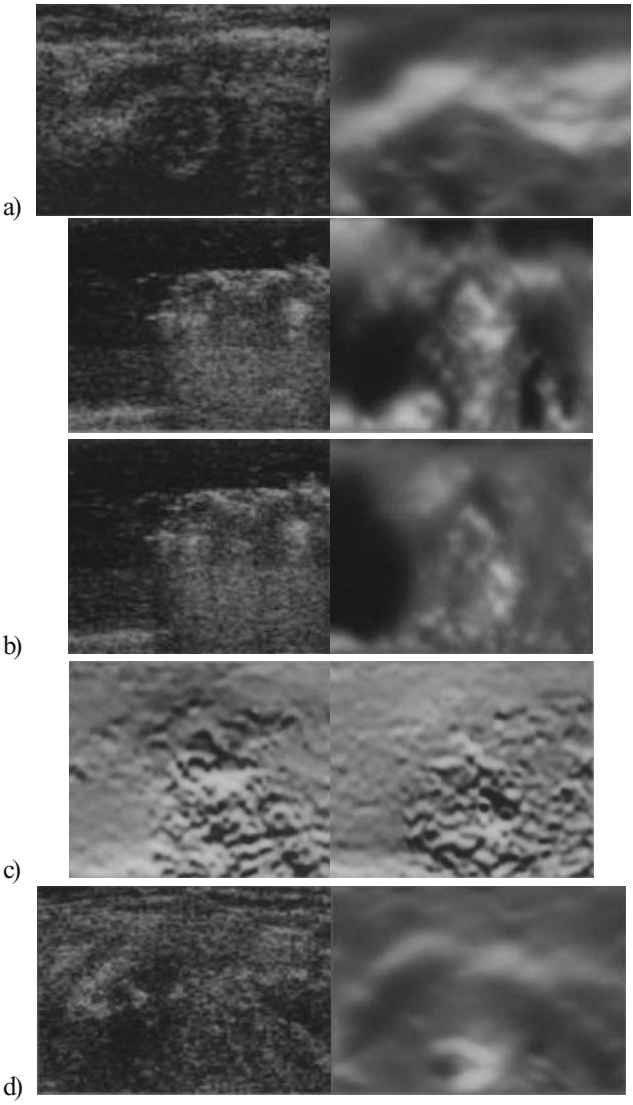

Fig. 4. In vivo human liver carcinoma (73 years old, female, segment 6): B-mode image (*left*) and 2-D-regularized shear modulus reconstruction image (*right*). Bright region has relatively low shear modulus value. **a** Before interstitial microwave treatment (2.45 GHz, 70 W, mononeedle electrode with 1.6 mm diameter). 3.5 MHz (convex type). ROI ranges with respect to her skin surface from the depth of 10.6 mm to 52.4 mm, and the convex ROI angle is 57.4°; however, the ROI is rectangular, 41.8 mm × 51.8 mm. DR, 18.7 dB. Spatial resolution of 1.7 mm × 1.9 mm. **b** During the treatment (for 4 min) under ventrotomy (two images). 7.5 MHz (linear type). ROI (29.6 mm × 41.5 mm) ranges with respect to her liver surface from the depth of 3.8 mm to 33.4 mm. DR, 38.7 dB (*upper*) and 34.7 dB (*lower*). Spatial resolution of 0.8 mm × 1.4 mm. **c** Strain images respective from which shear modulus reconstruction images (**b**) are obtained. **d** After the treatment (closed up). 3.5 MHz (convex). The same ROI and spatial resolution as those of **a**. DR, 27.8 dB

11.9 mm, where blood vessels could not be detected. The reference value was set at 1.0. Shear modulus reconstructions/images under and after treatment follow the next experiments on calf livers in vitro.

Experiments on Calf Liver In Vitro

As shown in the photograph (Fig. 5), the two paired needle electrodes were inserted at an angle of 45° in parallel into the calf liver specimen. The currents were constantly applied at 100 W.

Specimen 1 (Fig. 6)

The distance was 10 mm between the needle electrodes. This specimen was mechanically compressed such that acquisition was obtained of the precompression and postcompression echo data frames crossed with the paired electrodes. The US frequency was 7.5 MHz. In Fig. 6a,b, respectively, we show the B-mode images before and after heating of the ROI (23.3 mm × 19.6 mm, depth from 2.3 mm) under precompression. The reference line was set for shear modulus reconstruction at the upper borderline of the ROI, and the reference values were determined by calculating the ratios of the measured strains.

Specimen 2 (Fig. 7)

We monitored the spatiotemporal change of shear moduli. The distance between the needle electrodes was 20 mm, and current was applied twice for 5 min followed by a 10-min interval. Six points were observed: (1) before heating, (2) after 5 min of

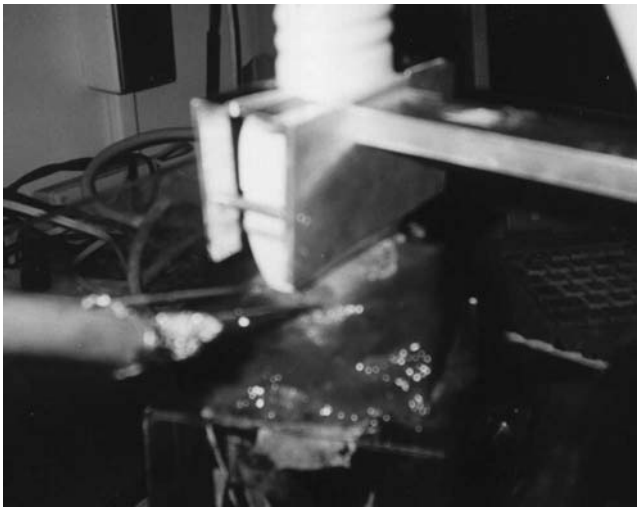

Fig. 5 Experimental setup of the in vitro calf liver specimen, a pair of two needle electrodes, and the ultrasound transducer

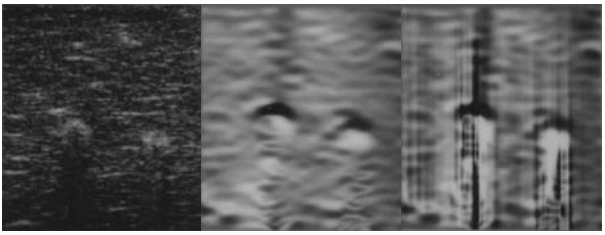

(a)

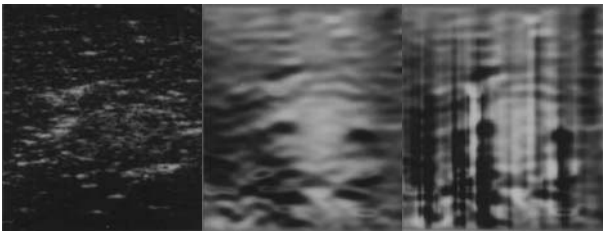

(b)

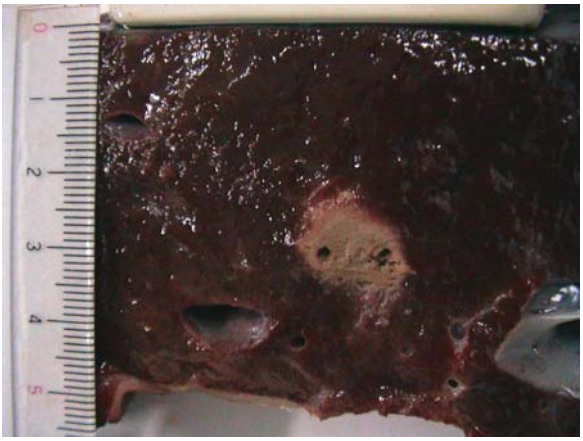

(c)

FIG. 6. In vitro calf liver (ROI size of 23.3 mm × 19.6 mm, depth from 2.3 mm). B-mode image (*left*, precompression), and reconstructed relative shear modulus images (*right*, two respectively obtained with 2-D- and 1-D-regularization, image DR, 62.8 dB). **a** With the inserted two paired needle electrodes before applying current (2-D DR, 64.8 dB; 1-D DR, 1.24e2 dB). **b** With no electrodes after applying current (2-D, 30.5 dB; 1D, 55.1 dB). **c** Photograph of cutting surface including the ROI

(a)–1

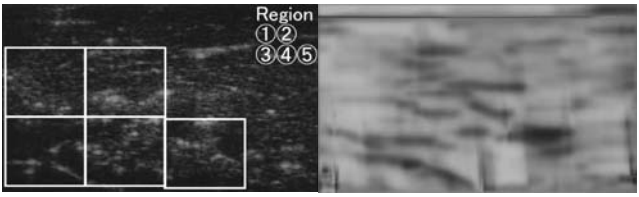

(a)–2

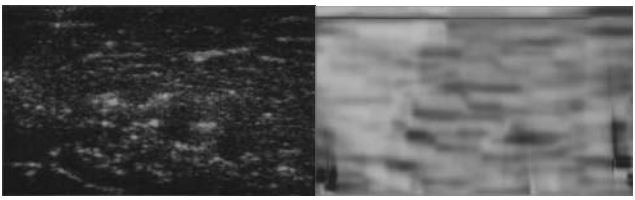

(a)–3

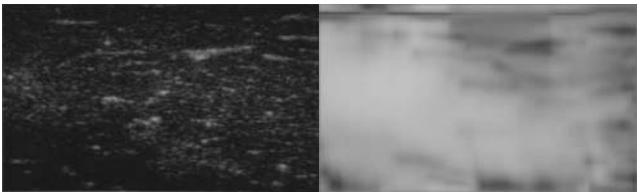

(a)–4

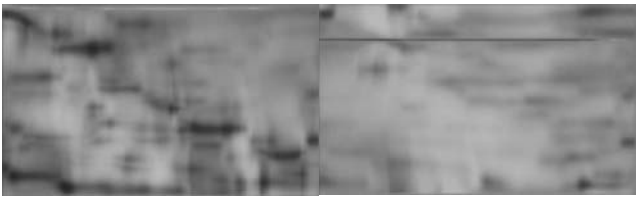

(a)–5 (a)–6

FIG. 7. Spatiotemporal change of shear modulus on in vitro calf liver. ROI (size of 25.1 mm × 39.4 mm, depth from 3.9 mm) was set in the central plane between the paired electrodes. The current was applied twice for 5 min followed by a 10-min interval. Six points are observed: (1) before heating, (2) after 5 min of heating, (3) 1 min after heating stopped, (4) 10 min after heating stopped, (5) after 5 min of heating, and (6) 10 min after heating stopped. **a** B-mode images and reconstructed relative shear modulus images (image DR, 79.8 dB) at the points

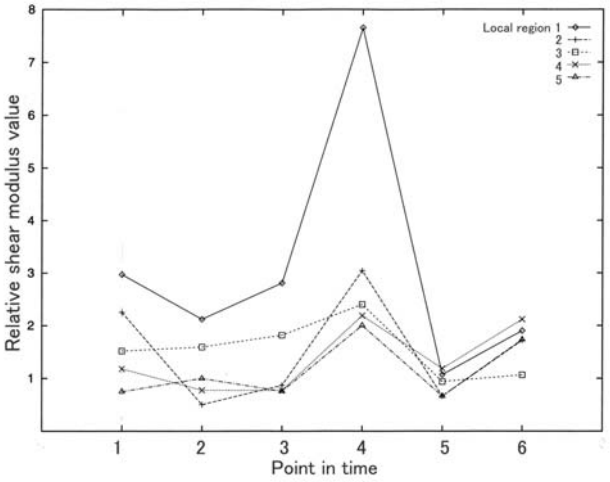

(b)

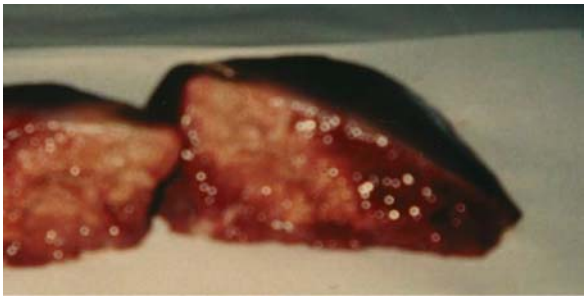

(c)

FIG. 7. *Continued*. **b** Measured points (1)–(6) versus the mean shear modulus values calculated from five local regions (8.3 mm × 10.0 mm). **c** Cutting surface. The heated region cannot be discerned in the B-mode images [points (1)–(6)], although one can observe the generation of bubbles due to tissue boiling and the fading of the bubbles during cooling down. In any case, however, the spatiotemporal change of tissue elasticity is noticeable in the shear modulus images. Note that the tissue is softened by heating [points (2) and (5)] and stiffened from outside to inside by cooling down [points (3), (4), and (6)]. After the second heating period [point (6)], the mean values in local regions 1 and 3 did not reach the mean values after the first heating [point (4)], being frangible. The coagulated region detected in the shear modulus image of point (4) coincides well with that of the white region detected along the cutting surface, although it is difficult to see in the shear modulus image of the final point (6). These results confirm that such monitoring can provide distinct merits during thermal therapy

heating, (3) 1 min after heating stopped, (4) 10 min after heating stopped, (5) after 5 min of heating, and (6) 10 min after heating stopped. At each point the specimen was mechanically compressed such that echo data frames could be collected in the central plane between the paired electrodes (US frequency, 8.0 MHz). Figure 7a (left) shows sequential B-mode images of the ROI (25.1 mm × 39.4 mm, at a depth of 3.9 mm) obtained under precompression at points (1) to (6). The reference line was set at a depth of 5.8 mm, and the reference values were determined by calculating the ratios of the measured strains.

Specimen 3 (Fig. 8)

The spatiotemporal change of the shear modulus was monitored for blood vessels with diameters of about 0.1 mm (Fig. 8e: photograph of the cutting surface.). The distance was 20 mm between the needle electrodes. One of the inserted two paired needle electrodes is visualized in Fig. 8d (the last B-mode image). The currents were applied twice for 5 min followed by a 10-min interval. From the B-mode image after heating shown in Fig. 8b (12 min after the first heating), a branched blood vessel was visualized although it is difficult to see from the B-mode image before heating (Fig. 8a). With about a 1-min interval, the specimen was mechanically compressed such that the echo data frames could be acquired (US frequency of 7.5 MHz) in the central plane between the paired electrodes. The ROI was set in the plane (23.0 mm × 14.0 mm, depth from 5.0 mm), and the reference line was set at a depth of 5.5 mm.

Specimen 4 (Fig. 9)

The superficial end of the liver had many blood vessels with diameters of about 1 mm (Fig. 9c), and the region of the ultrasonically detected changes was larger compared with that in the cutting surface of the visibly detected coagulation. The distance between the electrodes was 10 mm. This specimen was compressed such that acquisition could be performed of the echo data frames crossed with the paired electrodes (US frequency of 7.5 MHz). In Fig. 9a,b, B-mode images are shown of the ROI (18.6 mm × 17.8 mm, depth from 4.7 mm) before and after heating under precompression, respectively. The reference line was set at a depth of 6.3 mm.

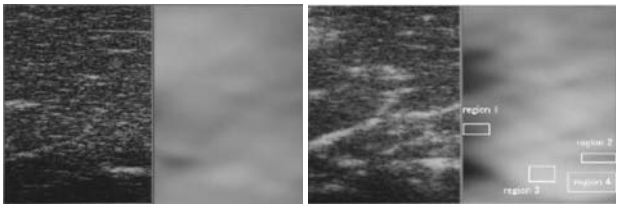

(a) (b)

FIG. 8. In vitro calf liver (ROI size of 23.0 mm × 16.4 mm, depth from 5.0 mm). B-mode (*left*) and shear modulus images (*right*, image DR, 29.2 dB). **a** Before the first heating (data no. 0, DR, 8.25 dB). **b** After the first heating (data no. 13, 24.2 dB). Blood vessel regions 1 and 2, respectively, with the 0.1-mm-diameter vessel and the slightly larger diameter vessel, and parenchyma regions 3 and 4

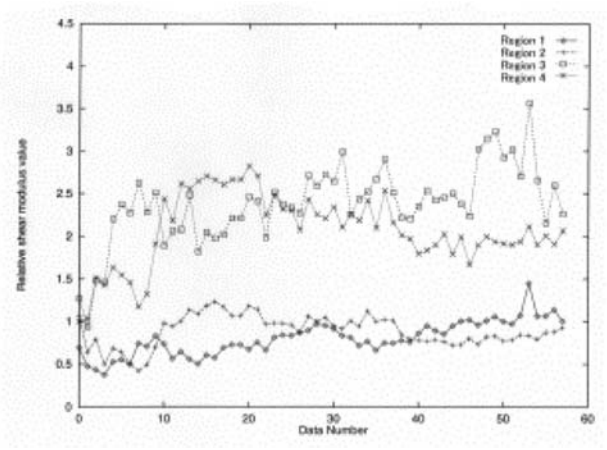

(c-1)

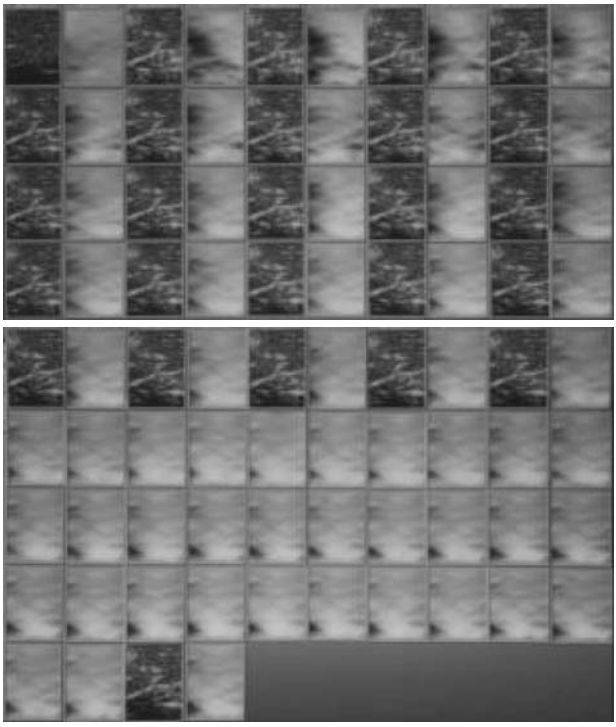

(c-2)

FIG. 8. *Continued*. **c** First heating [data no. 0 (nonheated) to no. 57 with interval of about 1 min] vs. relative shear modulus values of regions 1–4 depicted in **b**. (c-2) From first heating, data no. 0 (nonheated) to 57 (from *left* to *right*, *upper* to *lower*)

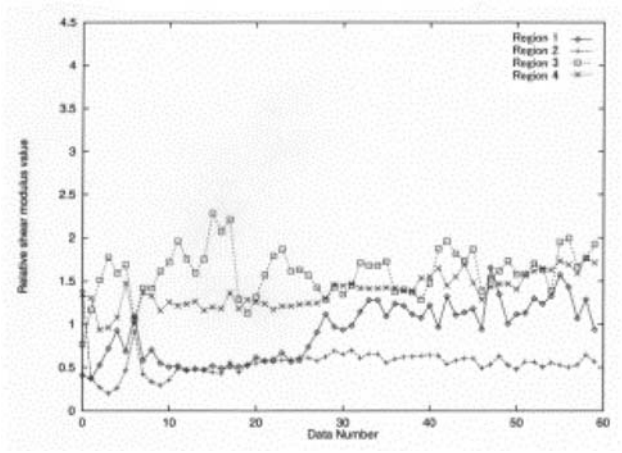

(d-1)

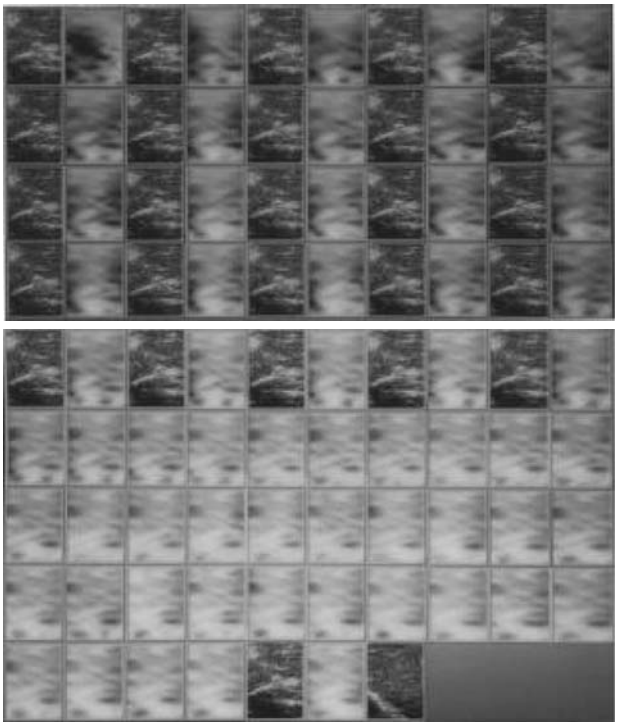

(d-2)

FIG. 8. *Continued*. **d** Second heating (data no. 0 to no. 59 with interval of about 1 min) vs. relative shear modulus values of regions 1–4. (d-2) From second heating, data no. 0 to no. 59 (From *left* to *right*, from *upper* to *lower*), and B-mode image with one of paired needle electrodes before heating

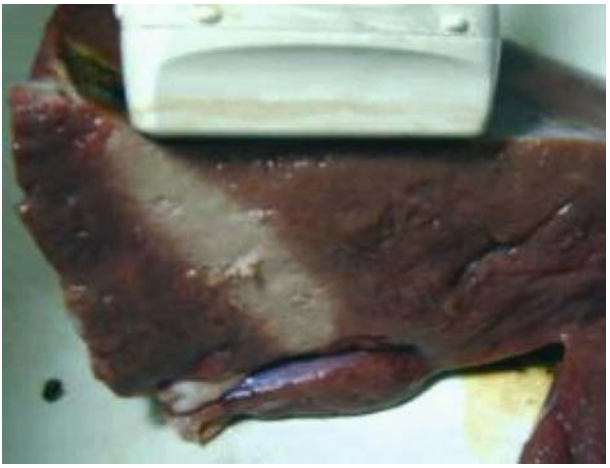

(e)

FIG. 8. *Continued.* **e** Cutting surface

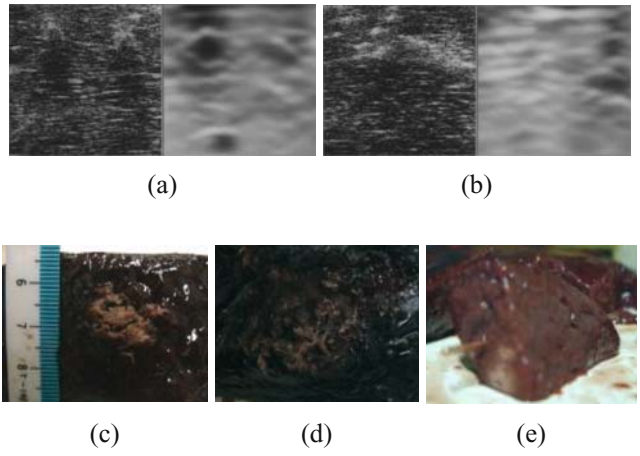

FIG. 9. In vitro calf liver (superficial end; ROI size of 18.6 mm × 17.8 mm, depth from 4.7 mm). B-mode (*left*) and reconstructed relative shear modulus images in a log gray scale (*right*), in which the bright region indicates that the region is relatively soft and vice versa (image DR, 36.3 dB). **a** With the inserted two paired electrodes before applying currents (DR, 29.9 dB). **b** With no electrodes after applying current (27.6 dB ranging). Photographs of (**c**) cutting surface including the ROI, (**d**) coagulated blood vessels, and (**e**) other specimen

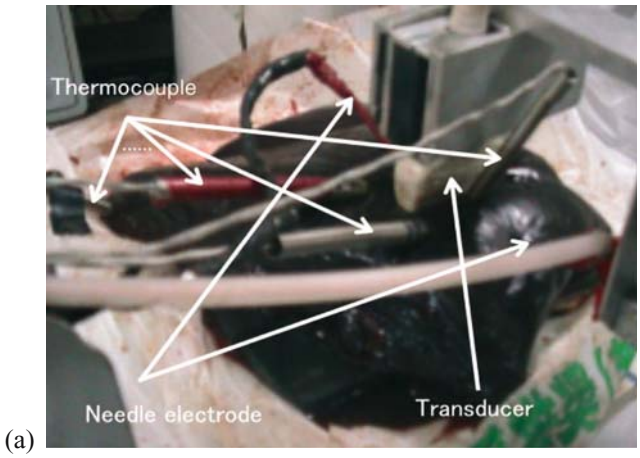

(a)

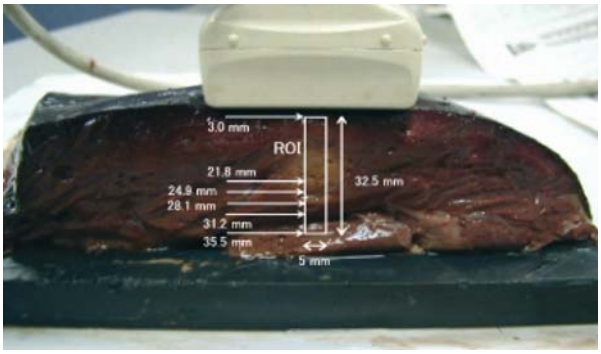

(b)

Fig. 10. **a** Experimental setup. **b** Cutting surface and three local regions, respectively, set in the coagulated region with lateral length of 5 mm, and with depths 21.8–24.9 mm, 24.9–28.1 mm, and 28.1–31.2 mm

Specimen 5 (Figs. 10, 11)

As shown in the photograph (Fig. 10a), currents with the low power of 60 W were injected into the calf liver specimen through the paired needle electrodes inserted from opposite directions. The distance between the points of the needles was 20 mm, and their depth was 25 mm. The currents were applied five times with 60-min intervals, respectively, for 1, 2, 3, 4, and 5 min such that the temperature at depth of 25 mm reached room temperature, 20.3°C. The echo data frames were collected (US frequency of 7.5 MHz) in the central plane between the points of the needle electrodes. The spatiotemporal changes were monitored of shear modulus versus the effective electric energy and the temperature (depth of 25 mm, thermocouple utilized). Specifically, three local regions were set in the detected coagulated region (Fig. 10b, with the

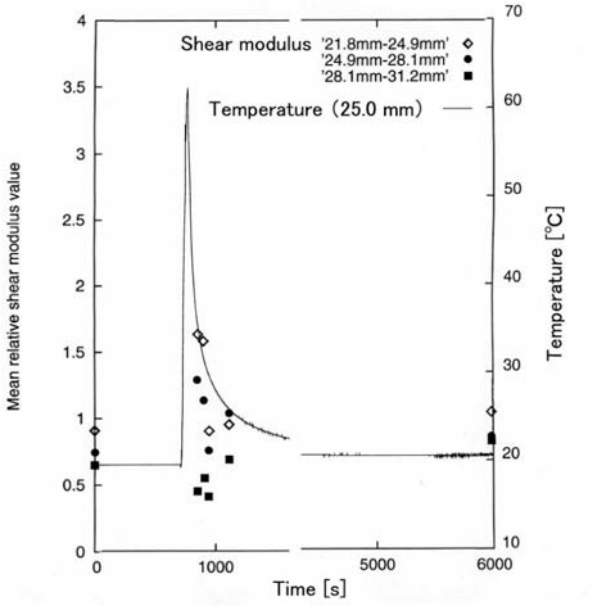

(a)

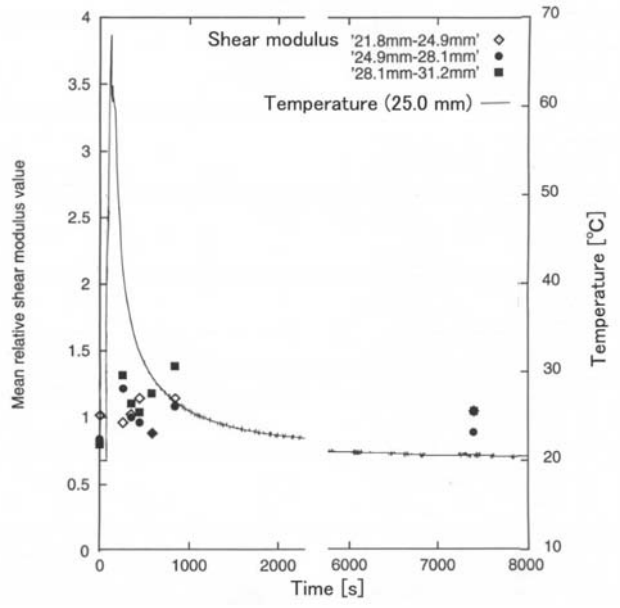

(b)

FIG. 11. Time vs. temperature (depth, 25.0 mm), and mean relative shear modulus values (depths 21.8–24.9 mm, 24.9–28.1 mm, 28.1–31.2 mm; lateral length, 5.0 mm). Total effective electric energies of (**a**) 3305 J (total 1-min heating), (**b**) 9635 J (total 3-min heating)

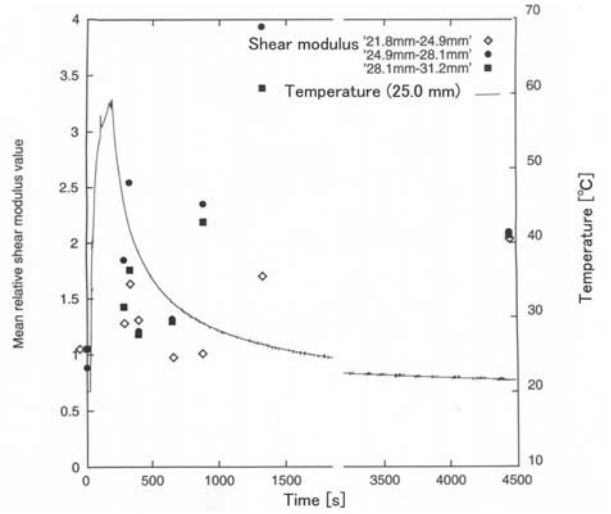

(c)

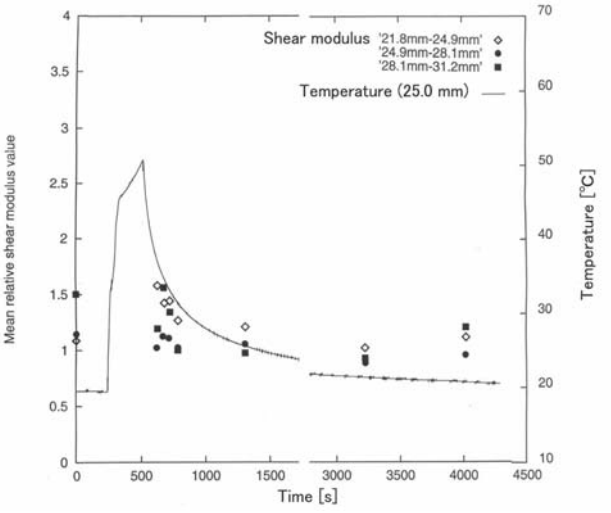

(d)

FIG. 11. *Continued.* (**c**) 19 545 J (6-min heating), and (**d**) 50 706 J (15-min heating)

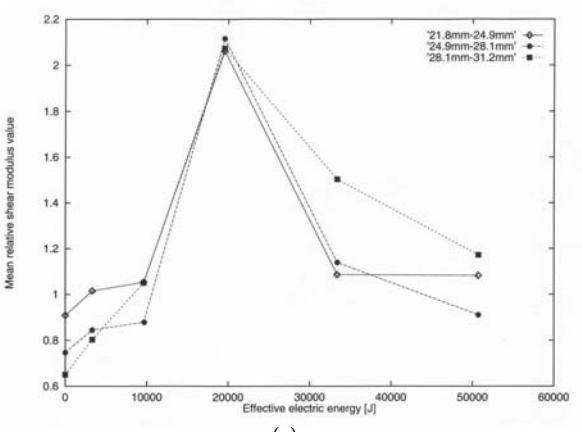

(e)

FIG. 11. *Continued*. **e** The effective electric energies of **a–d** and 33 375 J (10-min heating) vs. the final mean relative shear modulus values

lateral length of 5.0 mm, and respective depths 21.8–24.9, 24.9–28.1, and 28.1–31.2 mm), and the mean relative shear modulus value was monitored with respect to the mean shear modulus value evaluated in the depth from 3.1 to 6.2 mm.

Specimen 6 (Fig. 12)

The viscoshear modulus was imaged. The distance was 10 mm between the electrodes. The specimen was compressed by the ultrasound transducer (US frequency of 7.5 MHz) such that acquisition was successively obtained of the echo data frames crossed with the paired electrodes during compression. In Fig. 12a,b, B-mode images are shown of the ROI (16.2 mm × 16.4 mm, depth from 4.8 mm) before and after heating under precompression, respectively. The reference line was set at the upper borderline of the ROI.

Results

Artifacts of Low Dimensional Reconstruction

Figure 1a,b, respectively, shows the axial x-profiles and lateral y-profiles passing through the center of the spherical inhomogeneous region, and Fig. 1c shows maximum and minimum values obtained at each x–y plane with elevational position z = 10.0 to 40.0 mm. Figure 1d–g, respectively, shows the 3-D reconstruction, 2-D reconstructions (2-D stress and 2-D strain assumptions), and 1-D reconstruction with elevational position z = 25.0 mm.

For the 3-D reconstruction and 2-D reconstruction, which assumes a 2-D stress distribution, the shear modulus of the stiff region is quantitatively estimated. The quantitativeness is successively degraded based on the assumption of 2-D strain and 1-D

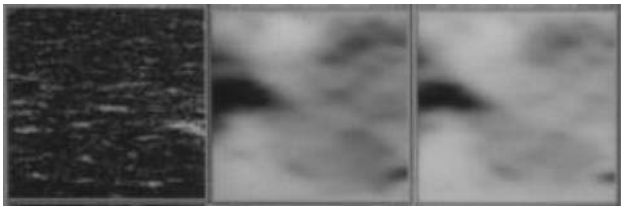

(a)

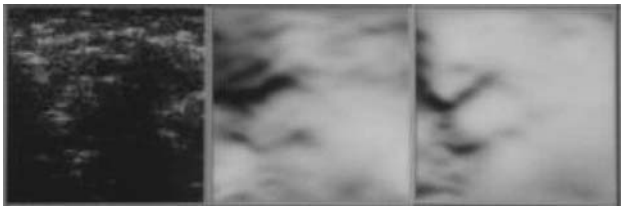

(b)

(c)

FIG. 12. In vitro calf liver (ROI size of 16.2 mm × 16.4 mm, depth from 4.8 mm). B-mode images (*left*), shear modulus images (*center*), and viscoshear modulus images (*right*). **a** Before heating; **b** after heating; **c** cutting surface. The mean values of strain velocities were, respectively, -1.60×10^{-2}/s and -3.35×10^{-2}/s

stress. That is, the inhomogeneity is estimated to be successively smaller. It should be realized that for the 2-D reconstruction (2-D stress assumption) the shear moduli of both lateral sides of the stiff region are estimated to be lower than the original value (Fig. 1b). Moreover, on the low dimensional reconstructions, an artifact formed by stress concentration is present in front of and behind the stiff region. This artifact successively appears due to the assumption of 1-D stress, 2-D strain, and 2-D stress

(Figs. 1a, 2e–g); that is, the shear modulus there is estimated to be lower compared to the original value. As previously stated, this artifact can be reduced by setting the reference region to pass through the stress concentration region (results omitted). Furthermore, Fig. 1b,c shows that a low dimensional reconstruction results in a misleading diagnosis in that the size of the stiff lesion is larger than that of the original. Specifically, in the lateral direction the artifact is apparent on the 1-D reconstruction, while in elevational direction the artifact is apparent on the 1-D reconstruction and both 2-D reconstructions.

When the inhomogeneous region is small, similar to that of the employed phantoms, the shear moduli values are small compared to the surrounding medium such that artifacts are similarly found in low dimensional reconstructions (results omitted). That is, (1) the quantitativeness is successively degraded based on the assumption of 2-D strain and 1-D stress, (2) for the 2-D reconstruction (2-D stress assumption) the shear moduli of both lateral sides of the soft region are estimated to be higher than the original value, (3) the small stress regions in front of and behind the soft region are estimated to be stiffer, and (4) in the lateral direction of the 1-D reconstruction, the size of the soft lesion is estimated to be larger, whereas in the elevation direction of the 1-D reconstruction and in both 2-D reconstructions, the artifact is apparent.

Taken together, these results indicate that low dimensional reconstructions are affected by 3-D inhomogeneity-dependent artifacts, which in turn decreases spatial resolution.

Experiments on Human Breast and Liver In Vivo

Breast Scirrhous Carcinoma Case

Figure 2 shows the spatially anisotropic 2-D-regularized stable shear modulus reconstruction images having a high spatial resolution of $0.8\,\text{mm} \times 3.2\,\text{mm}$. The reconstruction image on the upper right was obtained with the very large dynamic range (DR) of 65.4 dB by solving PDE having the inverse of shear modulus as unknown with the lower bound provided by the shear modulus value. This image is in a log gray scale, in which the bright region indicates that the region is relatively soft and vice versa. The images on the middle left and middle right were obtained by solving PDE having shear modulus as unknown with the upper bounds, respectively, provided by strain value and shear modulus value. The image of lower is inversion of that of upper right. These images are also in a log gray scale, in which the bright region indicates that the region is relatively stiff and vice versa. The initial estimates were obtained by calculating the ratio of measured strain. The lesion was estimated to have considerably high shear modulus value, and the estimated highest value was $2.35 \times 10^7\,\text{N/m}^2$.

Normal Liver Case

Figure 3b shows the stable shear modulus reconstruction image with a very large dynamic range of 70.2 dB (spatial resolution of $4.8\,\text{mm} \times 5.8\,\text{mm}$). As shown, several blood vessels with diameters of the order of millimeters were estimated to be considerably soft compared with the surrounding tissues.

Liver Carcinoma Case

Figure 4a shows the stable shear modulus reconstruction image with the spatial resolution of 1.7 mm × 1.9 mm (DR of 18.7 dB). This image is in a log gray scale, in which the bright region indicates that the region is relatively soft and vice versa. As shown, this tumor was estimated to be considerably stiff compared with the surrounding tissue, particularly the upper tissue.

Experiments on Calf Liver In Vitro

The reconstructed shear modulus images are in a log gray scale, in which the bright region indicates that the region is relatively stiff and vice versa.

Specimen 1

In respective Fig. 6a,b, respectively, the shear modulus images are shown with the inserted two paired needle electrodes before heating and with no electrodes after heating following a 15-min wait (left: 2-D regularization with lateral smoothing as well; right: 1-D regularization). The image DR is 62.8 dB, and the spatial resolution is 1.6 mm × 1.6 mm. The photograph (Fig. 6c) shows the cutting surface including the ROI that the visibly detected coagulated elliptical region coincided with that of the quantitatively detected coagulation region. We should note that although the 1-D-regularized reconstruction shows instability laterally, we can read in the coagulated region the specific variations of the shear modulus value. The instability of 1-D regularization can be handled with the multidimensional process.

Specimen 2

Figure 7a (right) shows shear modulus images reconstructed at points (1)–(6), where the image DR is 79.8 dB at a spatial resolution of 2.4 mm × 7.2 mm. The heated region cannot be discerned in the B-mode images [points (1) to (6)], although one can observe the generation of bubbles due to tissue boiling and the fading of the bubbles during cooling down [24, 25]. In any case, however, the spatiotemporal change of tissue elasticity is noticeable in the shear modulus images. To quantitatively evaluate the change, Fig. 7b shows the measured points versus the mean shear modulus values calculated from five local regions (8.3 mm × 10.0 mm) indicated in the B-mode image of point (2). Note that the tissue is softened by heating [points (2) and (5)] and stiffened from outside to inside by cooling down [points (3), (4), and (6)]. After the first heating period, the mean shear modulus value of local region 1 [point (4)] increased by about five times compared to that of point (1). Also of interest, after the second heating period [point (6)], the mean values in local regions 1 and 3 did not reach the mean values after the first heating [point (4)], being frangible. Figure 7c shows the cutting surface including the ROI. The coagulated region detected in the shear modulus image of point (4) coincides well with that of the white region detected along the cutting surface, although it is difficult to see in the shear modulus image of the final point (6). These results confirm that such monitoring can provide distinct merits during thermal therapy.

Specimen 3

Figure 8a, 8b, respectively, shows the shear modulus images obtained before heating (first heating data no. 0; DR, 8.25 dB) and after first heating followed by a 12-min wait (no. 13; 24.2 dB). The image DR is 29.2 dB, and the spatial resolution is 1.6 mm × 1.6 mm. Figure 8c,d, respectively, shows the first heating data (no. 0–no. 57 with interval of about 1 min) versus the relative shear modulus values of the local regions 1–4 depicted in Fig. 8b, and the second heating data (no. 0–no. 59 with interval about 1 min) versus the local relative shear modulus values. The photograph (Fig. 8e) of the cutting surface including the ROI shows that the region had acquired a high shear modulus value that almost coincided with that of the visibly detected coagulation. Shear modulus value of parenchyma (e.g., regions 3 and 4) similarly changed as that of parenchyma as reported previously [16–23], namely, softened, stiffened, and became frangible (extraheated). Visibly detected blood vessels and their neighborhoods (e.g., region 1 with the 0.1-mm-diameter vessel, and region 2 with the slightly larger diameter vessel) had originally low shear modulus values (Fig. 8a,c), and by heating (Fig. 8c,d) they softened and stiffened with cooling down. Shear modulus values of regions 1 and 2 of blood vessels retained lower values compared with those of parenchyma. Particularly, region 2 remained soft compared with the parenchyma before heating. As the shear modulus image also exhibits variations in the elevational direction (artifact), more quantitative data will be obtained by 3-D reconstruction with high spatial resolution [8, 9] (also see earlier).

Specimen 4

Figure 9a,b, respectively, shows the shear modulus reconstructions obtained before and after heating followed by a 15-min wait (DRs of 34.0 dB versus 24.7 dB). The reconstruction images are in a log gray scale, in which the bright region indicates that the region is relatively soft and vice versa. The image DR is 36.3 dB, and the spatial resolution is 1.6 mm × 1.6 mm. The photograph (Fig. 9c) of the cutting surface including the ROI shows that unexpectedly the lower elliptical tissues and both side blood vessels of the inserted needles were coagulated. By digging among the coagulated tissues, many blood vessels could be found with diameters of less than 1 mm (Fig. 9d). During cooling down, at the early stage the shear modulus value of the side blood vessels became higher. However, the shear modulus of the lower elliptical region became not so high compared with the side blood vessels. These coagulations are explicitly dependent on the running paths of blood vessels and remaining blood, specifically, the electrical resistances and thermal conductivities. As also confirmed on other specimens (e.g., Fig. 9e), blood vessels and their neighborhoods become coagulated in an early stage compared with parenchyma. The large region of sonic changes also seems dependent on the running blood vessels. Blood vessels with a diameter larger than several millimeters were significantly robust with respect to exposed thermal energy (data omitted).

Specimen 5

The total effective electric energies were 3305 J (1-min heating), 9635 J (2-min heating more), 19 545 J (3-min heating more), and 33 375 J (4-min heating more), and 50 706 J

(5-min heating more). Figure 11a–d shows the time courses after the respective heating of the measured temperature (depth, 25.0 mm), and the mean relative shear modulus values (Fig. 10b; depths from 21.8 to 24.9 mm, from 24.9 to 28.1 mm, and from 28.1 to 31.2 mm). Figure 11e shows the total effective electric energy versus the measured final mean relative shear modulus values.

The measured highest temperature values lowered with the total effective electric energy value increase. Particularly, before tissues became extraheated (Fig. 11e), that is, when the total effective energies were 3305, 9635, and 19 545 J, the shear modulus had high values immediately after stopping heating, after which shear modulus became lower as the temperature lowered (Fig. 11a–c). These phenomena for 3 or 4 min (during temperature higher than 30°C) were not confirmed on specimens 1, 2, and 3 where high-power currents of 100 W were applied. When the total energies were 3305 J and 9635 J, and subsequently the temperature became lower, the shear modulus drastically heightened to slightly higher values (i.e., almost reversibly changed), whereas when the energy was 19 545 J, the shear modulus heightened to about a four-fold higher value (i.e., obviously coagulated). However, due to tissues being extra-heated (Fig. 11e), that is, when the energy was 50 706 J (Fig. 11d), the shear modulus of the coagulated central local region consistently reached lower values after heating, although at the upper and lower regions, the interesting changes were still observed.

Specimen 6

Figure 12a,b, respectively, shows shear modulus image (center) and viscoshear modulus image (right) before and after heating, from which the viscoshear modulus image would provide us distinct mechanical properties from shear modulus image. The mean values of strain velocities were, respectively, -1.60×10^{-2}/s and -3.35×10^{-2}/s.

Monitoring of Effectiveness of Microwave Thermal Treatment on Human Liver Carcinoma In Vivo

Figure 4b,d, respectively, shows the stable shear modulus reconstruction images, during the treatment (for 4 min) under ventrotomy (two images) and after the treatment (closed up). These images are in a log gray scale, in which the bright region indicates that the region is relatively soft and vice versa. The spatial resolutions of these images are, respectively, 0.8 mm × 1.4 mm and 1.7 mm × 1.9 mm. As shown, during the treatment this tumor and the margin of several millimeters, respectively, became considerably soft and considerably stiff, although before the treatment the tumor was estimated to be considerably stiff compared with the surrounding tissue. We should note that in the tumor there exist estimated many considerably soft regions. These cannot be detected from the B-mode image. Furthermore, it is difficult to detect the elasticity of the tumor and the surrounding from strain images (Fig. 4c). The dynamic ranges of the reconstructions became very large compared with that before the treatment, that is, the dynamic range of 38.7 dB (left) and 34.7 dB (right) versus 18.7 dB. Furthermore, we could confirm that after the treatment the tumor and the margin of several millimeters, respectively, was rather soft and considerably stiff compared with

those before the treatment, that is, the dynamic range of 27.8 dB versus 18.7 dB. Thus, our reconstruction/imaging technique was useful to differentiate the malignancy and monitor the effectiveness of the thermal treatment.

Discussions and Conclusions

Time for our shear modulus and viscoshear modulus reconstruction/imaging being dependent on the ROI size, utilization of our technique and the conventional work station (Compaq XP1000, Alpha 500 MHz) could visualize in quasi-real time the tissue low frequency mechanical property distributions (in fact, less than 1 s from measured strain data). On the calf in vitro liver, viscoshear modulus reconstruction/image exhibited distinct mechanical properties from shear modulus reconstruction/image. Moreover, on the human in vivo liver and breast malignancies, the absolute shear modulus distributions could be stably reconstructed/imaged. In the near future, the limitations for differentiating malignancies of our technique will be reported.

Furthermore, on the calf livers in vitro, the spatiotemporal change of shear modulus was monitored due to the rf electromagnetic wave heating (high spatial resolutions), cooling down, and the extraheating, particularly, including blood vessels with diameters of approximately 0.1 and 1 mm. On human liver carcinoma in vivo, microwave treatment was also monitored. Although our relative reconstruction/imaging was also useful to monitor the effectiveness of thermal treatment, we could confirm that our absolute reconstruction/imaging utilizing reference material must be performed to enhance the efficiency, safety, and reliability of thermal treatments. Low-invasively obtained various insights about tissue thermal and elastic properties will significantly contribute to heightening the effectiveness of various thermal therapies such as HIFU [24, 25] and laser as well. When performing this kind of thermal therapy, the energy exposure time should be shortened as much as possible by increasing the exposure power. Some cooling device should also be utilized to confirm the treatment effectiveness in a short time. Moreover, the tissue inhomogeneity of electric, thermal, and elastic properties was also confirmed. Thus, together with such a high spatial resolution thermal treatment technique, the temperature monitoring technique [26], and total effective energy monitoring technique, utilization of our reconstruction/imaging technique will allow thermal therapy to be widely used by enhancing the efficiency, safety, and reliability of the thermal treatment. That is, monitored temperature, effective energy, and reconstructed shear modulus data will be efficiently utilized as the measure for controlling the intention, the foci, the exposure interval, etc. Our monitoring technique can also be applied to various treatments including cryotherapy and chemical therapy (e.g., anticancer drug, ethanol). The limitations for monitoring and differentiation of posttreatment lesions of our technique will be reported.

Our absolute reconstruction/imaging technique is available although our 3-D reconstruction will be more useful. In the near future, suitable combination of simple and low-invasive therapy techniques with our imaging technique will open up a new clinical style allowing diagnosis and the subsequently immediate treatment. This approach should substantially reduce total medical expenses. Our combination will also be utilized for screenings.

Acknowledgments. This research was in part supported by the JSPS and NEDO.

References

1. Sumi C, Suzuki A, Nakayama K (1993) Estimation of shear modulus distribution in soft tissue from strain measurement. Jpn J ME BE 31(suppl):390 (in Japanese)
2. Sumi C, et al. USA Patent 5495771. Elasticity measuring method and elasticity measuring apparatus, August 12, 1993
3. Sumi C, Suzuki A, Nakayama K (1995) Estimation of shear modulus distribution in soft tissue from strain distribution. IEEE Trans Biomed Eng 42:193–202
4. Sumi C, Nakayama K (1997) A robust numerical solution to reconstruct a globally relative shear modulus distribution from strain measurements. IEEE Trans Med Imag 17:419–428
5. Sumi C, Suzuki A, Nakayama K (1995) Phantom experiment on estimation of shear modulus distribution in soft tissue from ultrasonic measurement of displacement vector field. IEICE Trans Fund E78-A:1655–1664
6. Sumi C (1999) Fine elasticity imaging utilizing the iterative rf-echo phase matching method. IEEE Trans Ultrason Ferroelectr Freq Control 46:158–166
7. Sumi C, Nakayama K, Kubota M (2000) An effective ultrasonic strain measurement-based shear modulus reconstruction technique for superficial tissues—demonstration on in vitro pork ribs and in vivo human breast tissues. Phys Med Biol 45:1511–1520
8. Sumi C (1999) Toward 3D reconstruction/imaging shear modulus distribution in living soft tissues. Proc ASJ March:1201–1202
9. Sumi C, Ahiko K (2002) Tissue shear modulus reconstruction—affection of 3D inhomogeneity on 2D and 1D reconstruction. Proc ASJ March:1159–1160
10. Wright NT, Chen SS, Humphrey JD (1998) Time-temperature equivalence of heat-induced changes in cells and proteins. Trans ASME 20:20–26
11. Stafford RJ, Kallel F, Price RE, et al (1998) Elastographic imaging of thermal lesions in soft tissue: a preliminary study in vitro. Ultrasound Med Biol 24(9):1449–1458
12. Kallel F, Stafford RJ, Price RE, et al (1999) The feasibility of elastographic visualization of HIFU-induced thermal lesions in soft tissues. Ultrasound Med Biol 25(4):641–647
13. Righetti R, Kallel F, Stafford RJ (1999) Elastographic characterization of HIFU-induced lesions in canine livers. Ultrasound Med Biol 25:1099–1113
14. Kallel F, Hirasaki K, Alaniz A, et al (1999) Monitoring low-power heat deposition with elastography. Proc IEEE Ultrasonics Symp 1999:1409–1412
15. Doley MM, Bamber JC, Rivens I, et al (1999) Elastographic Imaging of thermally ablated tissue in vivo. Proc 1999 IEEE Ultrasonics Symp 1999:1631–1634
16. Sumi C, Kanai H (2000) Feasibility of monitoring the thermal therapy by elasticity imaging. Abstracts, 8th Int Cong Hyperthermic Oncol April:191
17. Sumi C, Ichiki Y, Kanai H (2000) Feasibility of monitoring thermal therapy by ultrasonic strain measurement-based shear modulus reconstruction. Jpn J Med Electronics Biol Eng 38(suppl I):284 (in Japanese)
18. Sumi C, Takegahara S, Kanai H (2000) Feasibility of shear modulus imaging for monitoring the effectiveness of the interstitial RF electromagnetc wave therapy. Jpn J Hyperthermic Oncol 16(suppl):118 (in Japanese)
19. Sumi C, Takegahara S, Kanai H (2001) Feasibility of shear modulus imaging technique for monitoring the effectiveness of the interstitial RF electromagnetic wave thermal therapy. Proc SPIE—Thermal Treatment of Tissue: Energy Delivery and Assessment 4247:151–157
20. Sumi C, Kojima R (2001) Realization of combined diagnosis/treatment system by ultrasound strain measurement-based shear modulus reconstruction/imaging technique—

examples with application on the new type interstitial RF electromagnetic wave thermal therapy. Proc 23rd Annu Int Conf IEEE Eng Med Biol Soc (CD-ROM), 6 p, Istanbul, October 2001
21. Sumi C (2002) Realization of combined diagnosis/treatment style by ultrasonic strain measurement-based mechanical properties imaging technique—examples with applications on the interstitial rf-electromagnetic wave thermal therapy. Abstr First Int Conf Ultrasonic Measurement Imaging Tissue Elasticity, 23, Niagara Falls, October 2002
22. Sumi C (2002) Realization of combined diagnosis/treatment system by utilizing ultrasonic strain measurement-based shear modulus and viscoshear modulus imaging technique. Proc 2nd Eur Med Biol Eng Conf EMBEC '02, 880–889, Vienna, December 2002
23. Sumi C, Kubota M, Wakabayashi G, et al (2003) Usefulness of ultrasonic strain measurement-based mechanical properties imaging technique—toward realization of short time diagnosis/treatment. Proc SPIE—Thermal Treatment of Tissue: Energy Delivery and Assessment, vol 4954 (CD-ROM), San Jose, January 2003
24. Hill CR, Ter Haar GR (1995) Review article: high intensity focused ultrasound-potential for cancer treatment. Br J Radiol 68:1296–1303
25. Watkin NA, Ter Haar GR, Morris SB, et al (1995) The urological applications of focused ultrasound surgery. Br J Urol 75 (suppl 1):1–8
26. Seip R, Ebbini (1995) Non-invasive estimation of tissue/temperature response to heating fields using diagnostic ultrasound. IEEE Trans Biomed Eng 42:829–839

Mass Detection Using a Texture Feature Coding Method

Ping-Sung Liao[1], Shu-Mei Guo[2], Yu-China Liao[2], Sheng-Chih Yang[3], Ching-Wen Yang[4], Hsiang-Ming Chen[5], Pau-Choo Chung[3], San Kan Lee[5,6], and Chein-I Chang[7]

Summary. Detection of masses is much more difficult than that of microcalcifications (MCCs) because breast masses are part of tissues that may not be detected effectively by the techniques developed for detection of MCCs. In this chapter, we present a texture feature coding method (TFCM) to extract features that could characterize special properties of masses. It extracts gradient variations of gray level co-occurrence matrix as texture features. As a result, the TFCM is more sensitive to changes in texture. Three neural network architectures, backpropagation neural network, probabilistic neural network, and radial basis function neural network are used for mass detection with inputs provided by TFCM-extracted features. The experimental results show that our TFCM-based neural network approaches can achieve a detection rate of approximately 87% with a 10% false alarm rate.

Key words. Gray level co-occurrence matrix, Mass detection, Texture feature coding method (TFCM), Texture spectrum (TS)

Introduction

The mortality and incidence of breast cancer for women in Taiwan is currently increasing. Hence, to prevent the worst cases of breast cancer happening in women is an important discipline for the Ministry of health and hospitals. Mammography is a

[1] Department of Electrical Engineering, Cheng Shiu Institute of Technology, 840 Chengching Road, (A33) Niaosung, Kaohshung, Taiwan, Republic of China
[2] Department of Information Engineering, National Cheng Kung University, Tainan 70101, Taiwan, Republic of China
[3] Department of Electrical Engineering, National Cheng Kung University, Tainan 70101, Taiwan, Republic of China
[4] Computer Center, Taichung Veterans General Hospital, Taichung, Taiwan, Republic of China
[5] Department of Radiology, Taichung Veterans General Hospital, Taichung 40705, Taiwan, Republic of China
[6] Department of Diagnostic Radiology, National Defense Medical Center, Taipei 100, Taiwan, Republic of China
[7] Remote Sensing Signal and Image Processing Laboratory, Department of Computer Science and Electrical Engineering, University of Maryland, Baltimore County, Baltimore, MD 21250, USA

useful screening tool recommended for early detection of suspicious regions of breast cancer by the American Cancer Society. The major symptom of breast cancer is either microcalcifications or masses as shown on mammograms. However, mass detection is much more difficult than that of microcalcifications because masses are part of breast tissues and the appearance of breast parenchyma is more complicated than that of MCCs. In particular, the intensity and contrast of masses are not easily characterized by a robust model. Because the spatial gray level dependence method (SGLDM) has been widely used in mass detection and classification [1–3], in this chapter, we propose a new SGLDM-based approach, referred to as the texture feature coding method (TFCM) [4, 5], to detect the existence of masses. TFCM extracts derivative features, referred to texture feature numbers (TFNs) from a spatial gray level co-occurrence matrix, and these TFNs could describe successive gradient changes in gray level among three consecutive pixels using the concepts of 4-neighbor connectivity and 8-neighbor connectivity. Therefore, the TFCM could be considered as a second-order SGLDM, and its feature vector associated to a suspicious region in a mammogram is chosen as the input in three neural network architectures for mass detection.

Texture Feature Coding Method

Let an image be of size $M \times N$ with $I(l, k)$ being the gray level of the pixel at the spatial location (l, k). The gray level co-occurrence matrix $N_{d,\theta}(i, j)$ denotes the number of transitions between two pixels whose gray levels are i and j with d-pixel apart and angular rotation θ. Normalizing $N_{d,\theta}(i, j)$ yields the probability of gray level transitions between i and j:

$$p(i, j \mid d, \theta) = \frac{N_{d,\theta}(i, j)}{\sum_{i,j} N_{d,\theta}(i, j)} \tag{1}$$

Using Eq. 1, the co-occurrence matrix specified by displacement d and angular orientation θ is defined by $\mathbf{W}_{d,\theta} = [p(i, j \mid d, \theta)]$.

For a 3×3 window mask over a pixel, there are eight orientations, 0°, 45°, 90°, 135°, 180°, 225°, 270°, and 315° as shown in Fig. 1a. According to the definition given in earlier reports [4, 5], the 4-neighbor connectivity of the pixel is described in Fig. 1b by four pixels labeled by 1, 3, 5, 7, and the other four pixels in the 8-neighbor connectivity labeled by 2, 4, 6, 8, as shown in Fig. 1c.

The idea of the TFCM is to consider three consecutive pixels along with certain specific directions and calculate gradient changes in gray levels of two successive adjacent pixels among these three pixels. Two directions are of interest, three pixels aligned in a perpendicular or diagonal direction. In the former case, the three pixels are first-order neighboring pixels connected by two perpendicular lines specified by 0°–180° and 90°–270° as shown in Fig. 1b, whereas in the latter case, the three pixels are second-order neighboring pixels connected by two diagonal lines specified by 45°–225° and 135°–315° in Fig. 1c. If we denote three consecutive pixels by their spatial coordinates at a, b, c and associated gray levels by $I(a)$, $I(b)$, and $I(c)$ respectively, the difference between the gray intensity in the center $I(b)$ and that of its neighborhood $I(b)$ and $I(c)$ may indicate the degree of roughness along a specified line. Let Δ be a desired

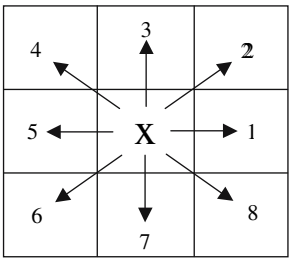

(a) 8 orientations

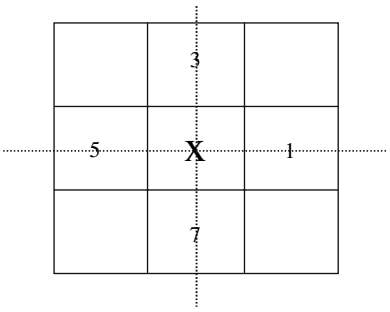

(b) first-order 4-neighbor connectivity

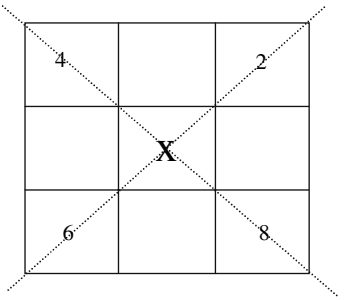

(c) second-order 4-neighbor connectivity

FIG. 1. 8-neighbor connectivity

gray level tolerance. Thus four types of successive gradient changes in gray level along the corresponding direction are defined below:

$$\text{(Type 1)} \left| I(a) - I(b) \right| \le \Delta, \left| I(b) - I(c) \right| \le \Delta$$

$$\text{(Type 2)} \left| I(a) - I(b) \right| \le \Delta, \left| I(b) - I(c) \right| > \Delta \text{ or } \left| I(a) - I(b) \right| > \Delta, \left| I(b) - I(c) \right| \le \Delta$$

$$\text{(Type 3)} I(a) - I(b) > \Delta, I(b) - I(c) > \Delta \text{ or } I(b) - I(a) > \Delta, I(c) - I(b) > \Delta$$

$$\text{(Type 4)} I(a) - I(b) > \Delta, I(c) - I(b) > \Delta \text{ or } I(b) - I(a) > \Delta, I(b) - I(c) > \Delta$$

According to degrees of successive gradient changes in gray level among three consecutive pixels, type 1 corresponds to zero-order variation because there are no gradient changes in gray level of two successive adjacent pixels, type 2 represents first-order variation because there is one gradient change in gray level that occurs in only one pair of two adjacent pixels, and type 3 and type 4 describe second-order variation because there are drastic gradient changes in gray level among three pixels.

Let $\alpha 1$ (0°–180° line), $\beta 1$ (90°–270° line), $\alpha 2$ (45°–225° line), and $\beta 2$ (135°–315° line) denote line types on which the three consecutive pixels are aligned respectively. As a result, each parameter of $\alpha 1$, $\alpha 2$, $\beta 1$, and $\beta 2$ takes values from {1, 2, 3, 4} where a number i represents type (i) of successive gradient variation. For each pixel of an image, its TFN is derived by Eq. 2 as below:

$$TFN(x, y) = \alpha(x, y) \times \beta(x, y) \tag{2}$$

where $\alpha(x, y)$ equals to $\alpha 1(x, y)$ times $\alpha 2(x, y)$, and $\beta(x, y)$ equals to $\beta 1(x, y)$ times $\beta 2(x, y)$. Obviously, there are 256 possible combined types of successive gradient variations. However, by reindexing after removing the illegal cases, the number of all reasonable cases is 41 [4, 5]. Furthermore, based on the histogram of texture feature number, we define several one-dimensional (1D) TFN descriptors such as coarseness, homogeneity, mean convergence, and variance as 1D features for mass detection [6].

Similar to the co-occurrence matrix in SGLDM, the TFN co-occurrence matrix is defined in Eq. 3:

$$W_{TFN_{\Delta^*,d,\theta}}(i,j) = \sum_{l=1}^{M}\sum_{k=1}^{N} \delta_{TFN_{\Delta^*,d,\theta}}(l,k) \tag{3}$$

where $0 \le i \le 40$, $0 \le j \le 40$, and optimal tolerance Δ^* is set to 3 in our experiment.

$$\delta_{TFN_{\Delta^*,d,\theta}}(l,k) = \begin{cases} 1 & \text{if } TFN_{\Delta^*}(l,k) = i, TFN_{\Delta^*}(l + d\cos\theta, k + d\sin\theta) = j \\ 0 & \text{otherwise} \end{cases} \tag{4}$$

Normalizing the Eq. 3 of the TFN co-occurrence matrix yields the probability function of TFN co-occurrence matrix:

$$P_{TFN_{\Delta^*,d,\theta}}(i,j) = \frac{W_{TFN_{\Delta^*,d,\theta}}(i,j)}{\sum_{i=0}^{41}\sum_{j=0}^{41} W_{TFN_{\Delta^*,d,\theta}}(i,j)} \tag{5}$$

Next, like 1D TFN descriptors, we also define three two-dimensional (2D) TFN descriptors such as entropy, similarity, and regularity as 2D features for mass detection [6]. As a result, these 1D texture descriptors and 2D texture descriptors are packed together as a feature vector that could describe the gray variations in a suspicious region in a mammogram. Certainly, this feature vector will be fed into the input nodes of neural networks being briefly introduced in the next section.

Three neural network architectures, probabilistic neural network (PNN), radial basis function neural network (RBFNN), and backpropagation neural network (BPNN) are proposed in this section for mass detection. The basic concept of PNN roots in statistical Bayesian classifier using Gaussian distributions. It is a network with no need of training [7]. The BPNN is a three-layer neural network with its performance completely determined by training samples with backpropagation as the training algorithm [8]. The RBFNN is also a three-layer neural network and implements a hidden layer with the hidden nodes being the training samples using Gaussian kernels as activation functions [8].

Experiments and Discussion

In our experiments, the MIAS MiniMammographic Database [9] provided by the Mammographic Image Analysis Society (MIAS) is used. There are 207 normal mammograms compared to 115 mammograms that contain abnormal tissues. Three classes are considered in accordance with breast parenchyma—dense-glandular, fatty, and fatty-glandular. Among 207 normal mammograms there are 76 dense-glandular, 66 fatty, and 65 fatty-glandular. For each mammogram of dense-glandular, fatty, and

fatty-glandular, we randomly pick up three regions with size 65×65 pixels as the normal tissues for training and classification. As to 115 abnormal mammograms, there are 23 dense-glandular, 35 fatty, and 29 fatty-glandular.

To evaluate the effectiveness of mass detection, we consider the following three parameters as performance measures:

1. Detection rate: $DR = TPN/N_p$
2. False alarm rate: $FAR = FPN/N_n$
3. Correct classification rate: $CR = (TPN + TNN)/(N_p + N_n)$

where TPN is the number of masses detected among total tumor tissues, FNN is the number of failures to detect mass among total tumor tissues, TNN is the number of normal cases detected as normal tissues, FTN is the number of failures to detect masses among total normal tissue, N_p is the number of abnormal cases with masses, and N_n is the number of normal tissue cases.

When all 1D texture descriptors and 2D texture descriptors are computed, they are first normalized into [0–1] to prevent from overflow during computation in classification. As for abnormal breast tissues, we randomly chose 12 dense-glandular, 18 fatty, and 15 fatty-glandular as the training samples with the rest used as text images. Similarly, to the normal tissues were randomly and evenly divided into two groups, one for training samples and another for test samples.

Because there are too few real cases to validate our proposed texture feature coding method in conjunction with three neural network platforms, our experiments were conducted as 100 iterations by randomly selecting the training samples and testing samples. The results are finally given by the means under 100 experiments. Table 1 tabulates the experimental results of detecting masses by using three different neural networks where TPN is true positive number, FNN is false negative number, TNN is true negative number, FPN is false positive number, DR is detection rate, FAR is false alarm rate, and CR is correct classification rate.

Table 1. Performance comparison under different neural networks

Backpropagation neural network (BPNN):							
Breast tissue	TPN	FNN	TNN	FPN	DR%	FAR%	CR%
Dense-glandular	9.17	1.83	187.68	28.32	83.36	13.11	86.72
Fatty	15.52	1.48	168.83	11.17	91.29	6.21	93.58
Fatty-glandular	11.88	2.12	161.31	18.69	84.86	10.38	89.27
Radial basis function neural network (RBFNN):							
Breast tissue	TPN	FNN	TNN	FPN	DR%	FAR%	CR%
Dense-glandular	6.97	4.03	153.44	62.56	63.36	28.96	70.67
Fatty	11.78	5.22	142.32	37.68	69.29	20.93	78.22
Fatty-glandular	8.6	5.4	128.74	51.26	61.43	28.48	70.79
Probabilistic neural network (PNN):							
Breast tissue	TPN	FNN	TNN	FPN	DR%	FAR%	CR%
Dense-glandular	9.31	1.69	189.71	26.29	84.64	12.17	87.67
Fatty	15.51	1.49	170.92	9.08	91.24	5.04	94.63
Fatty-glandular	12.18	1.82	159.3	20.7	87	11.5	88.39

From Table 1, the detection abilities of BPNN and PNN outperformed the RBFNN. Based on the obtained statistical means, BPNN could an achieve an approximate 86% detection rate with a false alarm rate 10% whereas the PNN could reach an approximate 87% detection rate with 10% false alarm rate.

Conclusion

In this chapter, TFCM is proposed to extract the gradient variations along two specific directions. The experimental results show that our TFCM-based neural network approaches can achieve an approximate 87% detection rate with a 10% false alarm rate. It implies that the texture feature from TFCM could effectively discriminate between abnormal and normal tissues in a mammogram.

Acknowledgments. This work is supported by a grant received from the Taichung Veterans General Hospital number TCVGH-915509C. The authors are grateful for the database provided by Mammographic Image Analysis Society (MIAS).

References

1. Chan HP, Wei D, Helvie MA, et al (1995) Computer-aided classification of mammographic masses and normal tissue: linear discriminant analysis in texture feature space. Phys Med Biol 40:857–876
2. Christoyianni I, Dermatas E, Kokkinakis G (1999) Neural classification of abnormal tissue in digital mammography using statistical features of the texture. ICECS99 1:117–120
3. Hadjiiski L, Sahiner B, Chan HP, et al (1999) Classification of malignant and benign masses based on hybrid ART2LDA approach. IEEE Trans Med Imaging 18:1178–1187
4. Chang CI (1995) Final report NSC-84-2213-E-006-086. National Science Council in Taiwan
5. Hong MH, Sung YN, Lin XZ (2002) Texture feature coding method for classification of liver sonography. Comput Med Imaging Graphics 26:33–42
6. Liao YC (2002) Mass detection using texture analysis. Master thesis, Department of Computer Science and Information Engineering, Chen Kung University, Taiwan
7. Specht DF (1990) Probabilistic neural networks and the polynomial adaline as complementary techniques for classification. IEEE Trans Neural Networks 1:111–121
8. Bishop CM (1995) Neural networks for pattern recognition. Oxford University Press, New York
9. The Mammographic Image Analysis Society, Digital Mammography Database. www.wiau.man.ac.uk/services/MIAS/MIASweb.html

Breast Tissue Assessments Based on High Order Mechanical Properties

Naotaka Nitta[1] and Tsuyoshi Shiina[2]

Summary. Ultrasonic tissue elasticity imaging, which can visualize diseased tissues based on their stiffness, is a useful technique for breast cancer detection. In general, soft tissues including the breast have nonlinear elasticity and viscoelasticity referred to as high order mechanical properties. These properties make the conventional elasticity evaluations based on strain and Young's modulus images difficult because these images vary depending on various conditions, in which high order mechanical properties cannot be neglected. For mechanical assessment independent of such conditions, high order mechanical properties must be assessed. Moreover, these properties also change in diseased tissues. Therefore, in this chapter, a method to assess high order mechanical properties is proposed with the aim of improvement of diagnostic ability. In actual breast assessment, cyclic loading and unloading were applied to the body surface by freehand manipulation of an ultrasonic probe; then, the nonlinear elasticity and viscoelastic hysteresis parameters were estimated and visualized based on the surface pressure measured with the pressure sensor, and the local strain distribution was estimated by the combined autocorrelation method. Nonlinear elasticity and hysteresis parameters, which can be estimated by the proposed method, clearly discriminated the breast tumor from the surrounding normal tissue.

Key words. Strain, Nonlinear elasticity, Hysteresis, High order, Breast tissue assessment

Introduction

Ultrasonic tissue elasticity imaging, which can visualize the diseased tissues based on their stiffness, is a useful technique for breast cancer detection because the cancer is generally harder than normal tissue. Conventional elasticity imaging is mainly based on the primary elastic properties such as strain and Young's modulus under small

[1] Institute for Human Science and Biomedical Engineering, National Institute of Advanced Industrial Science and Technology (AIST), 1-2-1 Namiki, Tsukuba, Ibaraki 305-8564, Japan
[2] Institute of Information Sciences and Electronics, University of Tsukuba, 1-1-1 Tennodai, Tsukuba, Ibaraki 305-8573, Japan

deformation, in which linear elasticity assumption is valid. In general, soft tissues including the breast have nonlinear elasticity and viscoelasticity [1], which are referred to as high order mechanical properties in this chapter. High order mechanical properties make the conventional elasticity evaluations difficult because these image patterns vary depending on the magnitude and speed of compression, in which high order mechanical properties cannot be neglected. For mechanical assessment independently of these conditions, high order mechanical properties must be assessed. Moreover, these properties also change in diseased tissues. Therefore, the assessments of high order mechanical properties are prospective for improvement of diagnostic ability.

In this chapter, high order mechanical parameters to characterize the nonlinear elasticity and the hysteresis in viscoelastic property are introduced, and a method to estimate these parameters is proposed. The potential of this method was investigated through in vivo measurement of breast tissue.

A Method to Estimate High Order Mechanical Prameters

Figure 1 shows a typical uniaxial stress–strain relationship of soft tissue in the loading and unloading processes within a certain time period. Each curve is nonlinear, and both processes produce a hysteresis loop due to viscoelasticity. In the biomechanics field, it is well known that the stress–strain relationship of soft tissue exhibits an exponential character. From this empirical information, the stress–strain curve in the loading process is approximated by including an exponential function as follows [2]:

$$\sigma = (A/B)\{\exp(B \cdot \varepsilon) - 1\} \tag{1}$$

where σ and ε are the axial stress and strain, and A is the Young's modulus when the small deformation is applied; B is the nonlinear elasticity parameter defined in this chapter and can express the intensity of nonlinearity. By fitting the measured values of stress and strain to Eq. 1, B can be extracted.

On the other hand, the hysteresis parameter to characterize the hysteresis property in viscoelasticity can be defined based on the area of hysteresis loop H as shown in Fig. 1. Because the area of hysteresis loop depends on the turning strain ε_0 between the loading and unloading, this index should be normalized by the strain energy function S_l in the loading process as follows [3]:

$$R = H/S_l \tag{2}$$

where R is the hysteresis parameter defined here and takes values from zero to 100%. Therefore, R can evaluate the hysteretic property quantitatively.

Not only Young's modulus, but also high order mechanical parameters B and R vary depending on tissue component and degeneration. Moreover, B is constant independently of the compression magnitude if the exponential formulation is valid, and R is also close to constant independently of the compression speed because the hysteretic property is almost constant to the varying deformation rate [1]. Therefore, high order mechanical parameters have potential to provide useful diagnostic information

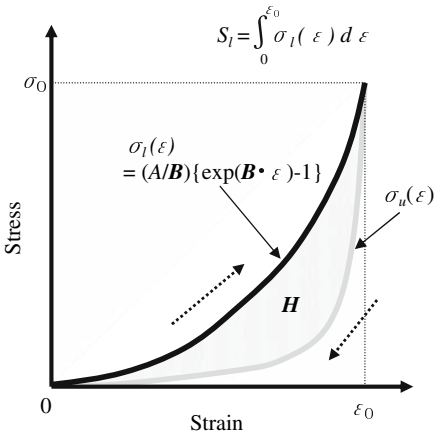

FIG. 1. Typical uniaxial stress–strain relationship of soft tissue in the loading and unloading processes during a certain time period

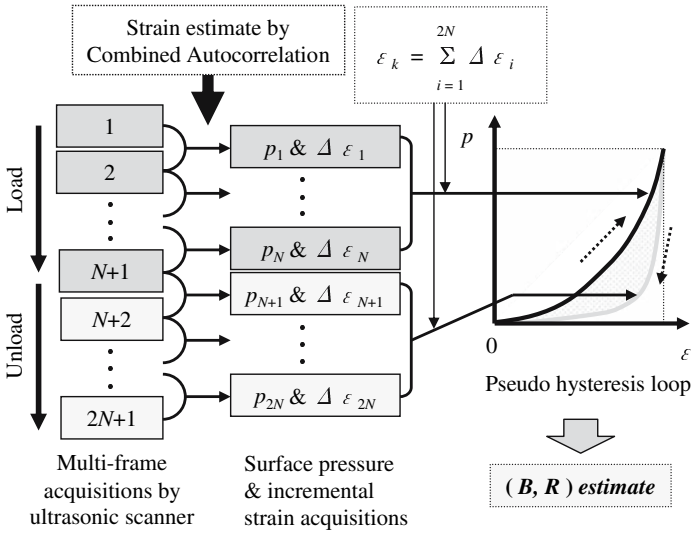

FIG. 2. A method to estimate the distribution of high order mechanical parameters

for improvement of diagnostic ability independently of the magnitude and speed of compression.

Figure 2 shows a method to estimate the distributions of high order mechanical parameters. To achieve this, local stress–strain curves are required. First, in parallel with cyclic loading and unloading applied to the body surface at constant speed, multiple rf frames are acquired with the ultrasonic scanner. Between the adjacent frames, incremental strain $\Delta\varepsilon_k$ ($k = 1, 2, \ldots, N, N+1, \ldots, 2N$) distributions are estimated by differentiating the axial component of a two-dimensional displacement vector obtained based on the combined autocorrelation method [4]. Strains ε_k, which corre-

spond to the horizontal axis in the local stress–strain curves, are calculated by accumulating the traced incremental strain based on the two-dimensional displacement vector. At the same time as multiple rf frame acquisitions, time-series surface pressures p_k are acquired with the pressure sensor for obtaining the stresses, which correspond to the vertical axis in the local stress–strain curves. However, stress estimation is one of the most difficult problems in the elasticity imaging. In this chapter, instead of the internal stress estimation, the measured value of surface pressure is used for obtaining the pseudo stress–strain curves as a trial. Once the pseudo stress–strain curves are obtained, the nonlinear elasticity and the hysteresis parameters can be locally estimated by the aforementioned procedures. The usefulness of this method has been investigated by preliminary experiments for the porcine femur and kidney [2, 3].

In Vivo Experiment of Breast Tissue

An in vivo experiment of breast tissue that had suffered from fibroadenoma was performed. Cyclic loading and unloading forces to the body surface were applied by free-hand manipulation of an ultrasonic linear array probe (Hitachi; 7.5 MHz) for about 2 s. A small acrylic compressor was fixed to the probe, and a pressure sensor was embedded in the compressor near the probe for surface pressure measurement.

Figure 3a,b shows the B-mode and the conventional strain images of the fibroadenoma obtained at the initial stage in the loading process. Although the fibroadenoma is unclear in the B-mode image, the strain image displays the fibroadenoma as a low strain area. On the other hand, Fig. 3c,d shows the nonlinear elasticity and the hysteresis parameter images. The nonlinear elasticity parameter image provides a high-contrast image and clearly displays the fibroadenoma as a high nonlinearity area. The hysteresis parameter image can also visualize the fibroadenoma as a low hysteresis area. Although the high order mechanical parameter images substantially seem to reflect the morphological structure of the breast as shown in the B-mode image, they depict different patterns from the conventional B-mode and strain images. Therefore, high order mechanical parameters might also provide useful information for breast tissue diagnosis independently of the conventional images such as B-mode and strain.

Conclusions

With the aim of improvement of diagnostic ability and mechanical assessment independently of the magnitude and speed of compression, a method to estimate the high order mechanical parameters was proposed in this chapter. As understood in the experimental results, high order mechanical parameters might provide useful information that differs from the conventional images such as B-mode and strain. These parameters can be chosen according to any case in the clinical diagnosis. To clarify the meaning of high order mechanical parameters, the relationship between these parameters and the pathology should be investigated in the future.

Moreover, in this work, because the internal stress distribution is not obtained, the estimated high order mechanical parameters are not quantitative. For quantitative

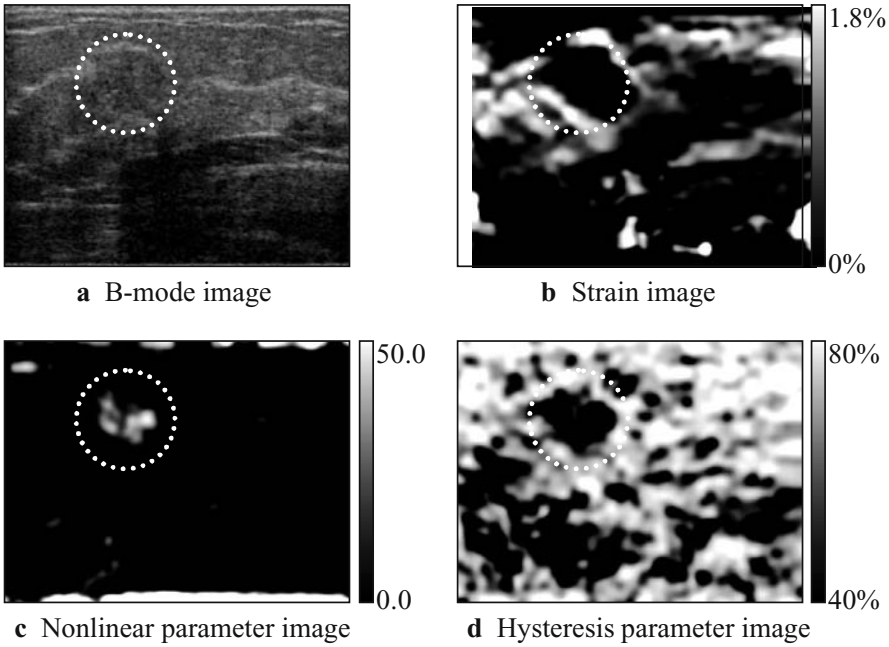

FIG. 3. In vivo experimental results with breast tissue that suffered a fibroadenoma. **a** B-mode image at initial stage in the loading process. **b** Strain image at initial stage in the loading process. **c** Nonlinear elasticity parameter image. **d** Hysteresis parameter image. *Open circle with dotted line* on each image indicates the region of fibroadenoma

estimations, the internal stress distributions should be estimated, or the influence of them should be eliminated. In future research, we intend to resolve these problems.

References

1. Fung YC (1993) Biomechanics: mechanical properties of living tissues, 2nd edn. Springer, New York, pp 242–320
2. Nitta N, Shiina T (2002) Estimation of nonlinear elasticity parameter of tissues by ultrasound. Jpn J Appl Phys 41:3572–3578
3. Nitta N, Shiina T, Ueno E (2002) Quantitative assessment and imaging of viscoelastic properties of soft tissue. Proc IEEE Ultrasonics Symp 2:1839–1843
4. Shiina T, Doyley MM, Bamber JC (1996) Strain imaging using combined RF and envelope autocorrelation processing. Proc IEEE Ultrasonics Symp 2:1331–1336

Forms of Tumors

Takanori Watanabe, Ei Ueno, Tokiko Endo, Mitsuhiro Kubota, Yutaka Konishi, Hiroshi Sakuma, Kazuhiro Shimamoto, Hiroko Tsunoda-Shimizu, Hideyuki Hashimoto, Norikazu Masuda, Mitsuhiro Mizutani, Isamu Morishima, and Hidemitsu Yasuda

Definition

The classifications refer to the impression of shape given from the whole image of a tumor. Tumors are assessed for classification by their cross sections.

Fig. 1. Classification

Explanation

Tumor forms are used to describe tumor shapes casually. When doing so, tumor marginal properties may be ignored. When it comes to each type of item, they can be defined by presence of "constriction" and "angularity." Let the terms constriction and

The Japan Association of Breast and Thyroid Sonology, Japan

Table 1. Definitions of shape

Shape	Constriction	Angularity
Round / oval	–	–
Polygonal	–	+
Lobulated	+	–
Irregular	+	+

angularity (Table 1) be used when a tumor has remarkable discontinuous changes in its shape: the former means convex or indented characteristics, the latter indicates concave or projecting characteristics. Even if the impression of shape given from the whole tumor only depends on the observer's subjectivity, judging must be more objective referring to a criterion. Even malignancy can sometimes show a round or oval shape while benignity can sometimes appear irregular.

Criteria by Ultrasonography

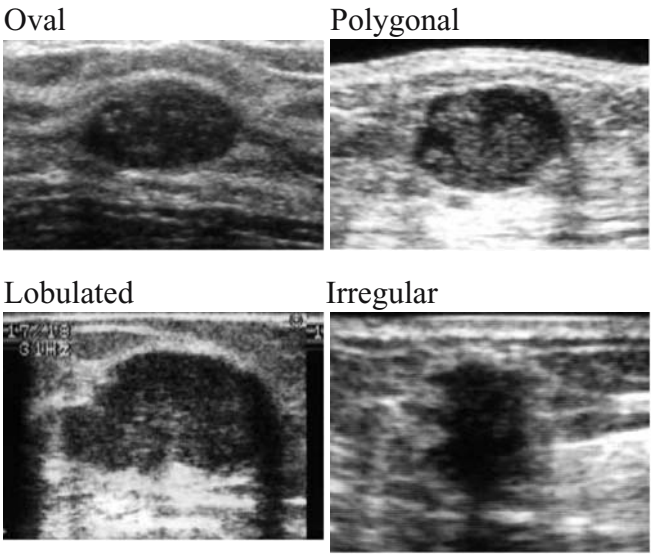

Notes:

1. With intracystic lesions, the forms of intracystic lesion are mentioned as well as cyst.
2. Judgment should include no forms of intramammary-ductal lesion extending outside the tumor.

Usefulness of Depth to Width Ratio in Differentiation of Regular Invasive Ductal Carcinoma from Fibroadenoma

Hiroko Tsunoda-Shimizu, Yasuyuki Kato, Ei Ueno, Tokiko Endo, Mitsunori Shirouzu, Ryouji Watanabe, Hideyuki Hashimoto, Yoshinari Ogawa, Tsutomu Takashima, Yasuhisa Fujimoto, Hideaki Shirai, Manabu Nagae, Noriko Unuma, Norikazu Masuda, Norikazu Obane, Isamu Morishima, Yuka Kujiraoka, Kiyoka Omoto, and Nobuyuki Taniguchi

Summary. Depth to width ratio (D/W) is the only quantitive item in seven criteria used to evaluate breast masses by the Japanese Ultrasound Society. Recent technical improvement of ultrasound is remarkable, but the usefulness of the D/W has not fully been evaluated. We reviewed prospectively the D/W estimation of breast masses by using dedicated ultrasound units in ten hospitals that belong to the Japanese Breast and Thyroid Sonology and the Japanese Ultrasound Society. The materials included 163 regular invasive ductal carcinomas (CA) and 219 fibroadenomas (FA) that were selected from consecutive cases and which were smaller than 30 mm in diameter. The mean size of CA was 17 mm and that of FA was 14.5 mm. The D/W of CA was 0.76, significantly larger than that of FA, 0.57. The larger the size of the tumor, the smaller became the D/W in both CA and FA. The D/W of these two kinds of tumors was significantly different in cases with tumors larger than 5 mm in diameter. We also reviewed the D/W of three groups divided by the posterior echoes; that is, attenuating masses, no change, and accentuating. The D/W of the attenuating mass was larger than that of the other two groups. We reconfirmed that the D/W was useful in differentiating CA from FA.

Key words. Breast ultrasound, Breast cancer, Fibroadenoma, Depth to width ratio

Introduction

Our title is usefulness of depth to width ratio in the differentiation of regular invasive ductal carcinoma (CA) from fibroadenoma (FA). The depth to width ratio (D/W) was first established by the Japanese Ultrasound Society in 1989 as a useful diagnostic tool in differentiating malignant from benign tumors [1, 2]. Technical improvement of ultrasound during the post decade is remarkable, but the usefulness of the D/W has not been fully evaluated.

The Committee of the Breast Ultrasound Criteria, Japanese Association of Breast and Thyroid Ultrasound Sonology, Department of Radiology, St. Luke's Hospital, 9-1 Akashi-cho, Chuo-ku, Tokyo 104-8560, Japan

The definition of the D/W is a division of depth by transverse diameter of the mass. The transverse diameter is the maximum diameter of the mass on ultrasound and is measured in the direction running parallel to the skin. The depth diameter is the vertical length of the mass perpendicular to the transverse diameter. The measurement is performed using only the low-echoic area without the echogenic boundary echoes or halo. The purpose of this study is to evaluate the usefulness of the D/W in differentiation of regular invasive ductal carcinomas from fibroadenomas using dedicated units. This investigation was performed with the collaboration of ten institutes that belong to the Japanese Breast and Thyroid Sonology and Japanese Ultrasound Society.

Methods and Materials

A questionnaire was sent by e-mail to these 10 institutes. The questionnaire included patient's age, depth and transverse diameter of the mass, final diagnosis, ultrasound units, and so on. The physicians and sonographers filled in the items of this questionnaire from their results of the ultrasound examinations. The participating institutes for this study are shown in Table 1.

The materials included breast masses examined during the period between January 1998 and June 1998. Masses of a size equal to or smaller than 30 mm in maximum diameter were selected. Twenty consecutive malignant lesions were selected per each institution. All benign lesions were selected during the period when these 20 malignant lesions were collected. The tumors that did not change in size and nature for 3 years were included as benign lesions without histological confirmation. Total number of the materials was 223 malignant cases, including 163 regular ductal carcinomas, and 313 benign cases including 219 fibroadenomas.

The ultrasound equipment used is listed in Table 2. The frequency of the transducers was from 6 to 13 MHz. Multifrequency transducers were used in some institutes. The scan methods were mechanical sector, electric linear, and annular array scan.

Table 1. Participating institutes

Institution	Investigator
Breastopia Namba Hospital	K. Shirouzu, R. Watanabe
Chiba University	H. Hashimoto
Osaka City Hospital	Y. Katoh, Y. Ogawa, T. Takashima
Osaka City Medical Center	Y. Fujimoto
Sapporo Kotoni Breast Clinic	H. Shirai
St. Marianna Medical School	M. Nagae, N. Unuma
Sakai City Hospital	N. Masuda
Sumitomo Hospital	N. Obane
Tsukuba University	H. Tsunoda-Shimizu, I. Morishima Y. Kujiraoka, E. Ueno
Jichi Medical School	K. Omoto, N. Taniguchi

Table 2. Ultrasound equipment

Manufacturer	Model	Frequency	Scan type
Aloka	SSD 650 CL	10 MHz	Electric linear
	1700	7.5 MHz	Mechanical sector
	2000	10 MHz	Electric linear
GE	Logiqe 500	6–13 MHz	Electric linear
		8.3–13 MHz	Electric linear
	700 MR	7.5 MHz	Electric linear
Toshiba	SSA 250 A	7.5 MHz	Anular array
	340 A	6, 8 MHz	Anular array
Siemens		7.5 MHz	Electric linear

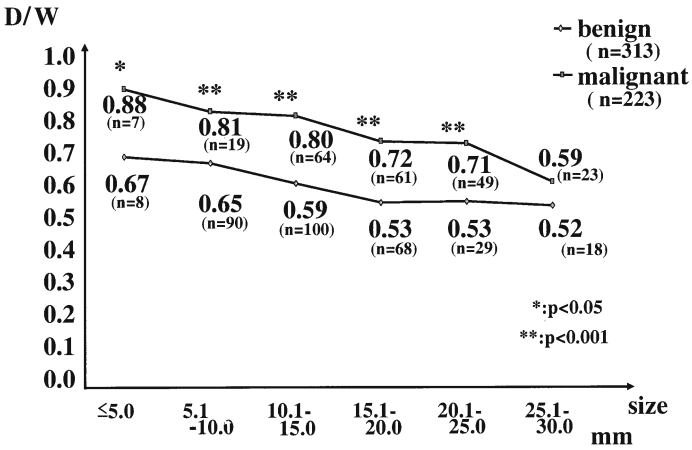

Fig. 1. Depth to width ratio (*D*/*W*) ratio by tumor size

Results

The D/W by tumor size is shown in Fig. 1. The transverse axis is tumor size divided by 5 mm and the vertical axis is the D/W. As shown here, the smaller the tumor size, the larger the D/W in both malignant and benign cases. In any tumor size, D/W of the malignant tumors was larger than that of benign tumors. This difference was statistically significant in cases with tumor size smaller than 25 mm but not for cases with tumors larger than 25 mm.

The D/W of fibroadenomas and regular type of invasive ductal carcinomas is shown in Fig. 2. The D/W of FA was 0.57, and the D/W of CA was larger than 0.7 in the any type of regular invasive ductal carcinomas. Scirrhous carcinoma showed the largest D/W, 0.79; in solid-tubular carcinoma, the D/W was 0.75; and in papillotubular carcinoma, it was 0.71. The D/W of FA and invasive ductal carcinoma that were evaluated by tumor size are shown in Fig. 3. The D/W of fibroadenoma was smaller than that

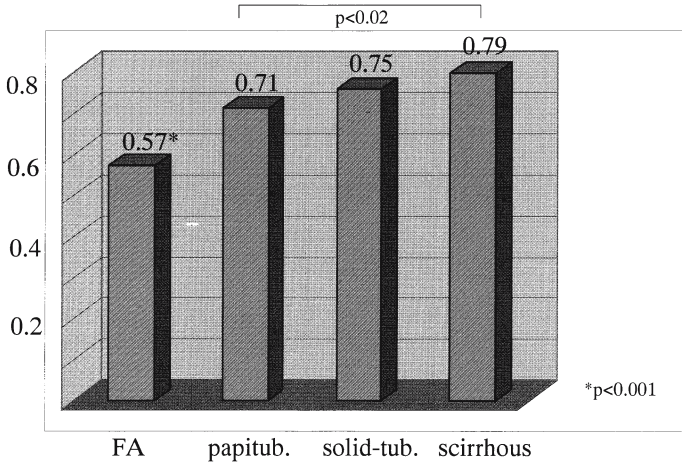

Fig. 2. D/W of fibroadenomas and invasive ductal carcinomas. *FA*, fibroadenoma; *papitub.*, papillotubular; *solid-tub.*, solid-tubular

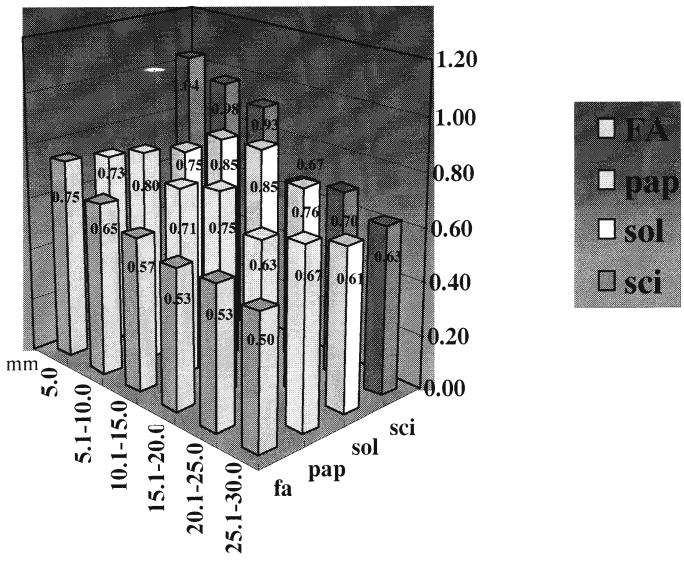

Fig. 3. D/W of fibroadenomas (FA) and invasive ductal carcinomas. *fa*, fibroadenoma; *pap*, papillotubular; *sol*, solid-tubular; *sci*, scirrhous

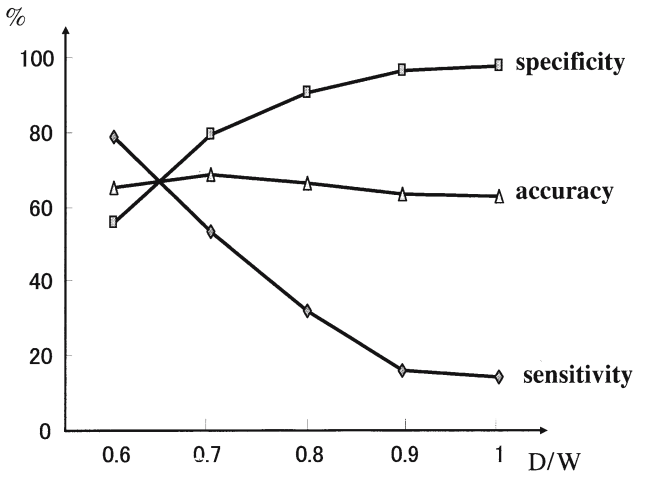

Fig. 4. Threshold of D/W

of any type of carcinomas except for those smaller than 5 mm in size in papillotubular carcinomas. The D/W of scirrhous carcinoma was significantly larger in tumors larger than 15 mm.

Discussion

We studied the most useful threshold in D/W to differentiate malignancy from benign lesions. The sensitivity, specificity, and accuracy in each value of the D/W are shown in Fig. 4. The larger the D/W is, the higher is the specificity but the lower is the sensitivity. Sensitivity and specificity cross between 0.6 and 0.7 in the D/W. The highest accuracy, 68.5%, was noted when the D/W was 0.7.

In conclusion, the D/W of malignant tumors was larger than that of benign tumors. This difference was statistically significant in cases with tumors smaller than 25 mm. The D/W of fibroadenoma was smaller than that of any type of invasive ductal carcinomas of any size, except for papillotubular carcinomas smaller than 5 mm. The threshold of the D/W in malignant and benign tumors was approximately 0.7.

References

1. Tajima T, et al (1983) Longitudinal/transverse ratio of tumor echogram as a diagnostic criterion of breast carcinoma. In: Jellins J, Kobayashi, T (eds) Ultrasonic examination of the breast. John Wiley, pp 69–70
2. Tohno E, et al (1994) Diagnostic features on ultrasound. In: Ultrasound diagnosis of breast disease. Churchill Livingstone, pp 50–53

Margin, Border, and Boundary Zone of Breast Tumor Ultrasonography

Hidemitsu Yasuda, Ei Ueno, Tokiko Endo, Mitsuhiro Kubota, Yutaka Konishi, Hiroshi Sakuma, Kazuhiro Shimamoto, Hiroko Tsunoda-Shimizu, Isamu Morishima, and Takanori Watanabe

Key words. Margin, Border, Boundary zone, Periphery, Halo

Introduction

In November 1999, the first meeting of the Subcommittee of Diagnostic Criteria for Breast Diseases under the Japan Association of Breast and Thyroid Sonology was held. The diagnostic criteria and the lexicon used for breast diseases were discussed. About 40 conferences were held over 5 years. More than 200 cases of breast disease were discussed, and experiments were done to define the consistency of diagnostic criteria.

Methods

Two hundred photographs of breast diseases were gathered from ten institutions, and 20 standard cases were selected. The precise features of the breast lesion were recorded on a diagnosis sheet. The items for diagnostic criteria were the shape and boundary, the existence of boundary high echo, and the intensity and homogeneity of the internal echo. The results were estimated, and appropriate technical terms were chosen.

Results

In the subcommittee of the Japan Association of Breast and Thyroid Sonology, margin is defined as the peripheral part of the tumor adjacent to the border (Fig. 1).

The border is a plane located between the tumor and the tissue around the tumor. Many other expressions are possible, such as boundary, borderline, margin, and limit line [1–3]. The periphery is the area surrounding the tumor.

The boundary zone means the area including margin, border, and periphery [4]. The border may not always be able to be defined clearly. Sometimes it may be diffi-

Subcommittee of Diagnostic Criteria for Breast Diseases under the Japan Association of Breast and Thyroid Sonology, International Medical Center of Japan, 1-21-1 Toyama, Shinjuku-ku, Tokyo 162-8655, Japan

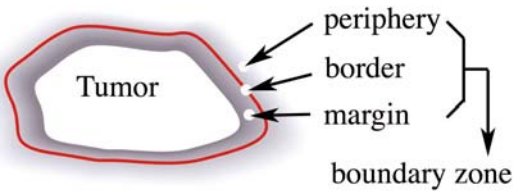

Fig. 1. The border (*solid line*) is a plane located between the tumor and the tissue around the tumor, the periphery is the area surrounding the tumor, and the boundary zone means the area including margin, border, and periphery

cult to define margin or periphery clearly; therefore, we propose to use "boundary zone" to include margin, border, and adjacent zone.

The properties of the border are classified into four categories:

1. Well defined and smooth.
2. Well defined and rough.
3. Not clear, ill-defined, unclear. In this category, we classify two subgroups according to whether a halo (boundary high echo) appears at the boundary zone or not:
   a. Appears at the boundary zone
   b. Does not appear at the boundary zone
4. Difficult to evaluate.

"Difficult to evaluate" means a condition where is difficult to evaluate the posterior or lateral boundary of a tumor due to attenuation or deficiency of ultrasound.

Diagnosis must be made at the most suitable plane that represents the property of the lesion. The properties of one lesion may have plural findings. If the border is well defined, it means that the margin and periphery can be divided by a single line. "Boundary high echo," "marginal hyperechoic zone," echogenic halo "or" halo, "hyperechoic boundary echo," "echogenic rim"—all these phrases could mean the hyperechoic area appearing at the boundary zone (Fig. 2). Although we have not reached a conclusion, "halo" may be the most simple and plain word as well as that most commonly used in Japan.

At the hyperechoic boundary zone, it is difficult to define the precise point of the boundary (Fig. 3); therefore, it is better to define the property of the boundary as not clear.

Conclusions

To make a standard diagnosis, it is important to have a standard lexicon. Although many kinds of expression are possible for the same feature of a breast tumor, a technical term must be a word that is seldom confused with another different concept. Especially, a halo or boundary high echo must be a word that is used to express a malignant sign.

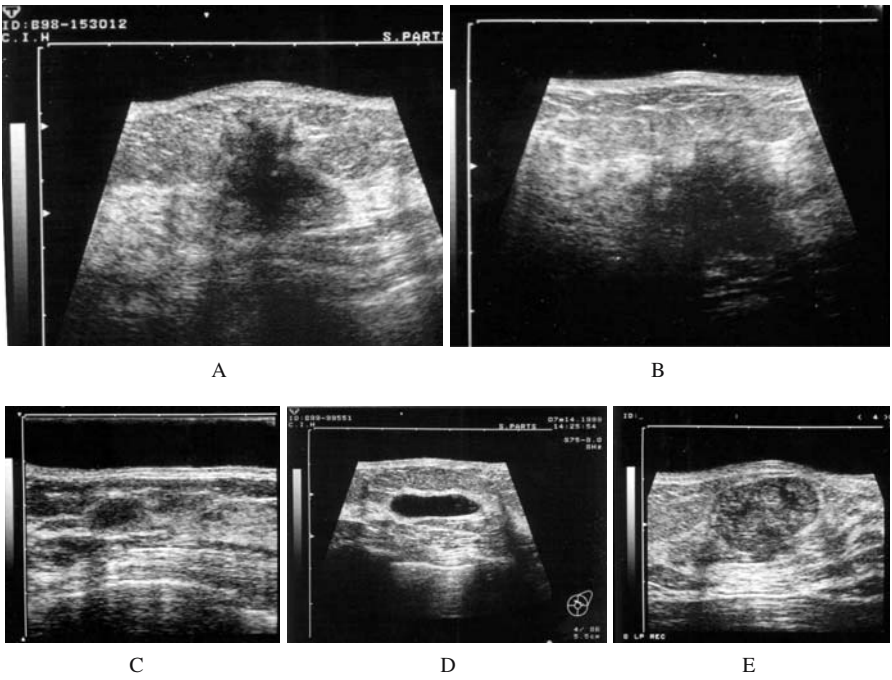

Fig. 2. Two cases (**A**, **B**) show halos on both sides, the typical boundary high echo observed in malignant tumors. Images **C**–**E** present findings that look similar to halos at a glance, but these are not true halos. The case in **C** is a tumor associated with mastopathy. The beltlike zone seen around the hypoechoic area corresponds to the site where a group of gland cavities are located. This echo level of the beltlike lesion is intermediate between the adjacent mammary gland and the hypoechoic area. True malignant halos are higher than the adjacent tissue. The case in **D** is a cyst and the case in **E** is a fibroadenoma. Both cases are surrounded by a thin rim of normal mammary gland; these also are not true halos

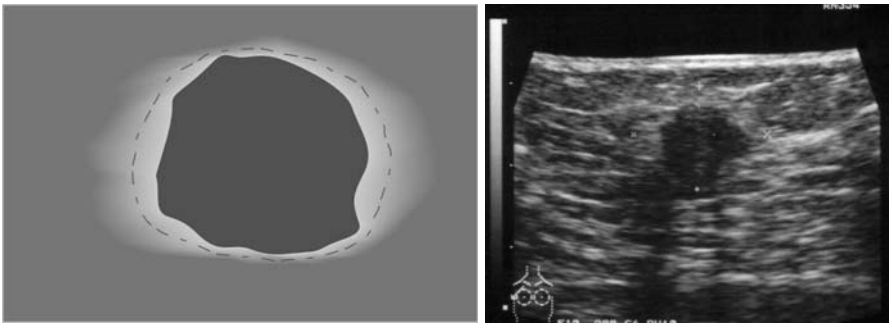

Fig. 3. At a hyperechoic boundary zone, it is difficult to define the precise point of the boundary; therefore, it is better to define the property of the boundary as not clear

References

1. Sawaki A, Shimamoto K, Satake H, et al (1999) Breast ultrasonography: diagnostic efficacy of a computer-aided diagnostic system using fuzzy inference. Radiat Med 17(1):41–45
2. Jackson VP, Rothschild PA, Kreipke DL, et al (1986) The spectrum of sonographic findings of fibroadenoma of the breast. Invest Radiol 21(1):34–40
3. Chen CM, Chou YH, Han KC, et al (2003) Breast lesions on sonograms: computer-aided diagnosis with nearly setting-independent features and artificial neural networks. Radiology 226(2):504–514
4. Kim KG, Kim JH, Min BG (2002) Classification of malignant and benign tumors using boundary characteristics in breast ultrasonograms. J Digit Imaging 15(suppl 1):224–227

Revised Diagnostic Criteria for the Breast (Draft): Internal Echoes

Mitsuhiro Kubota[1,2], Yutaka Konishi[2], Kazuhiro Shimamoto[2], Kumiko Tanaka[2], Hiroko Tsunoda-Shimizu[2], Hideyuki Hashimoto[2], Norikazu Masuda[2], Mitsuhiro Mizutani[2], Isamu Morishima[2], Hidemitsu Yasuda[2], Takanori Watanabe[2], Ei Ueno[2], and Tokiko Endo[2]

Introduction

In discussion, the committee has consumed more than 4 years for revision of the lexicon and diagnostic criteria of breast lesions. Internal echoes of mass image-forming lesions were also one of the themes. These have been summarized as follows. The criteria are not yet final and are presented with discussion.

Definition and Lexicon of Internal Echoes

Internal echoes means echoes from the inside of the mass. They do not concern echoes from a marginal area. Homogeneity and echo level of internal echoes from some area are assessed. If there are two or more regions with a different nature of internal echoes, they should be recorded together. If it is a mass with mixed pattern, that is, having both cystic and solid parts, only internal echoes of solid parts are assessed.

1. Homogeneity

Regularity of internal echoes (texture) is assessed.

   a. Homogeneous
   b. Heterogeneous

2. Echo level

Echo level means intensity of internal echoes. It is classified into five levels, as follows, comparing with the subcutaneous fatty layer, not with mammary tissue.

   a. Free
   b. Very low
   c. Low
   d. Equal
   e. High

3. Additional findings

Findings as follows are recorded if present:

[1] Yamachika Memorial Hospital, 3-19-14 Koyawata, Odawara, Kanagawa 256-0815, Japan
[2] JABTS Committee of Lexicon and Diagnostic Criteria, Japan

a. High echo spots
b. Cyst
c. Fluid–fluid level (FFL)

High echo spots are classified into three types as follows:

Fine
Small
Coarse

Examples

Several ultrasound (US) images of breast tumors are shown, particularly concerning internal echoes. These images are part of samples delivered from institutes or hospitals of members of the committee (Figs. 1–8).

Discussion

Internal echoes have been one of the important items in diagnostic criteria of breast tumors since the beginning of modern breast ultrasonography. In the diagnostic criteria of breast tumor proposed by the Japan Society of Ultrasonics in Medicine (JSUM) in 1987, internal echoes were one of the seven items. There were three categories, that is, echo-free, fine homogeneous, and coarse heterogeneous, combined with the likeliness of benignancy to malignancy.

The most conspicuous difference between the previous diagnostic criteria of JSUM and the revised criteria of the Japan Association of Breast and Thyroid Sonology (JABTS) is that the echo level of internal echoes has been discussed in the latter. Echoes from the inside of a tumor present its tissue characteristics. In ultrasonography, the tissue characteristics of a tumor are defined through the nature of both its internal and posterior echoes. Internal echoes mean the summation of intratumoral attenuation and reflections and backscattering.

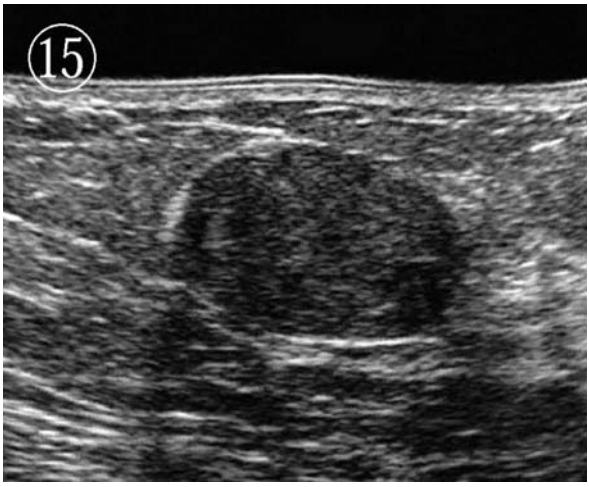

Fig. 1. Papillotubular carcinoma. Internal echoes are low and homogeneous

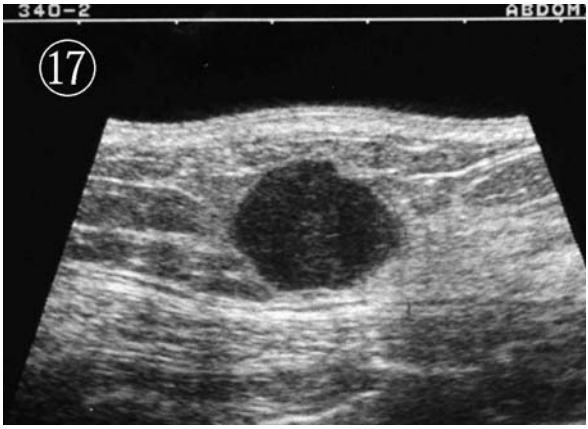

Fig. 2. Solid tubular carcinoma. Internal echoes are low rather than very low and homogeneous rather than heterogeneous

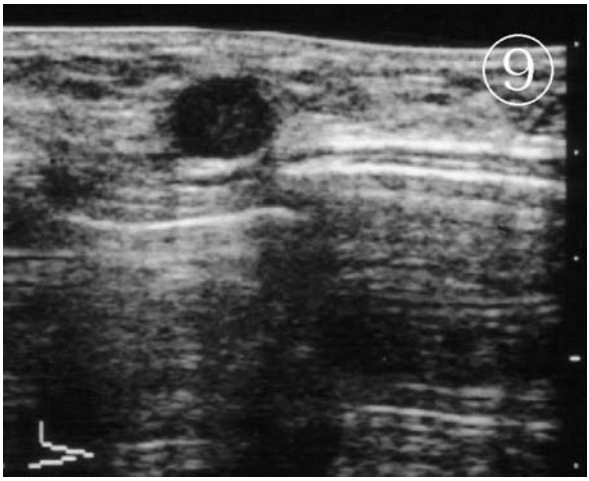

Fig. 3. Solid tubular carcinoma. Internal echoes are low or very low, and heterogeneous rather than homogeneous. Fine high echo spots are present

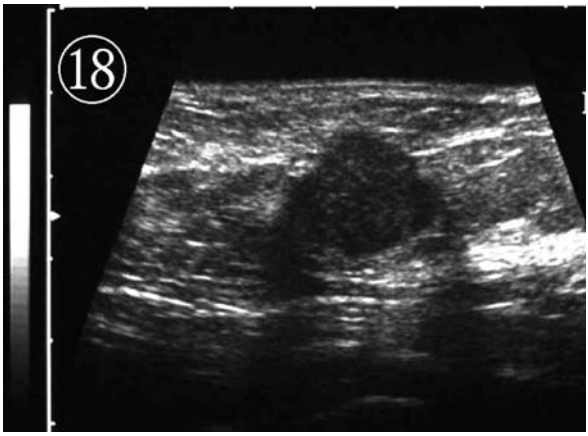

Fig. 4. Scirrhous carcinoma. Internal echoes are low rather than very low. They are heterogeneous rather than homogeneous. High echo spots are fine

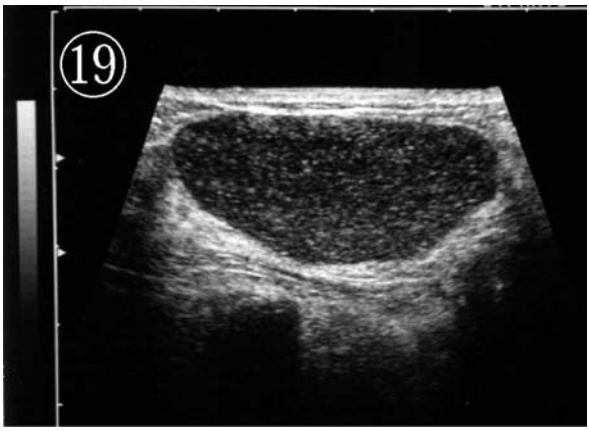

Fig. 5. Internal echoes are low rather than very low. They are homogeneous rather than heterogeneous. High echo spots are fine.This tumor was revealed to be a cyst

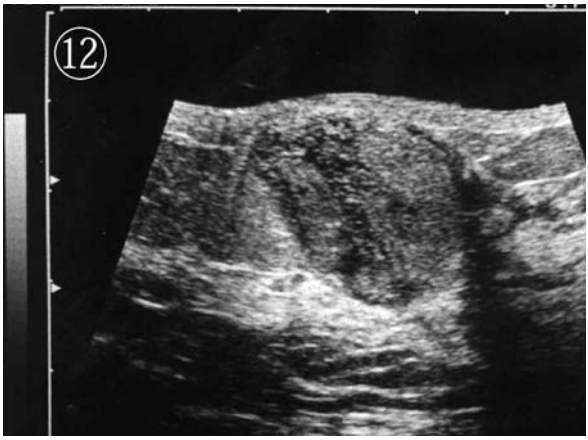

Fig. 6. Internal echoes are equal or hyperechoic, and heterogeneous. Fine high echo spots are present

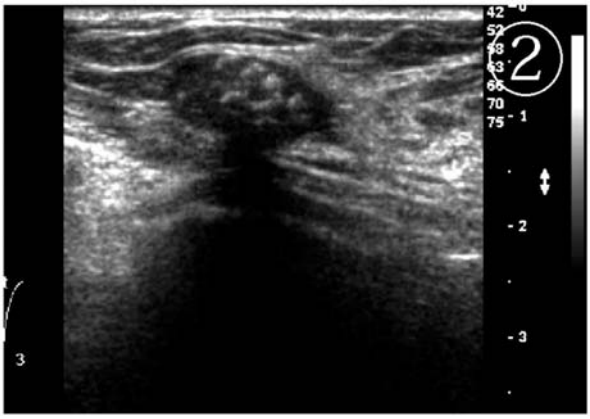

Fig. 7. Fibroadenoma. Internal echoes are low, and heterogeneous. High echo spots are coarse

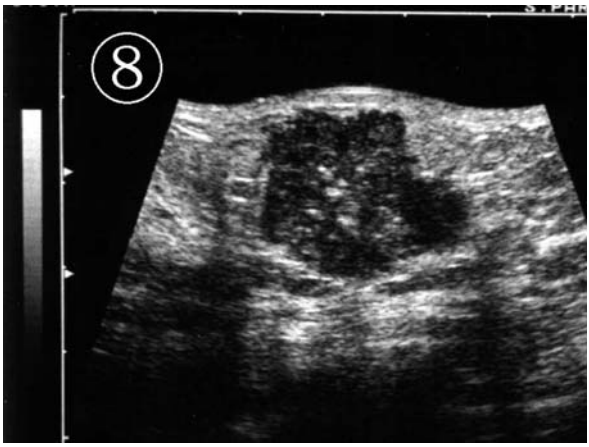

FIG. 8. Cancer. Internal echoes are low or very low. High echo spots are fine rather than coarse

As to internal echo level, it was discussed why the subcutaneous fatty layer, not the surrounding mammary gland, should be referred to as the standard. The most important point is that the echo level of the mammary gland is too variable, according to many factors including age, reproductive stage, and obesity, to be a stable standard of echo level. Furthermore, if ordinarily a hyperechoic mammary gland is referred to as the standard, a mass in the gland is always assessed to be hypoechoic. The subcutaneous fatty layer is relatively invariable and is better as the standard of echo level than the mammary gland, although it is not always directly beside the tumor and, rarely, is almost absent, particularly when the patient is young and very thin.

In general, benign tumors such as fibroadenoma have a tendency to be high and malignant tumors low in internal echo level. In other words, this may mean that tumors with various tissue components have a tendency to be high and tumors histologically more monotonous low in internal echo level, according to their level of reflection and backscattering. Tumors with a high internal echo level include fat-containing benign tumors such as lipoma and hamartoma. They also include malignant tumors such as mucinous carcinoma in which multilayered many fine mucinous lakes cause high reflection or backscattering, thus a high echo level. It is also insisted that ductal or lobular carcinoma with extremely high invasiveness occasionally presents as a mass with a high internal echo level. An isoechoic mass with echo level equal to subcutaneous fatty tissue is recognized with some difficulty if it is located superficially; this happens occasionally in fibroadenoma and rarely in carcinoma.

Another discussion as to echo level is whether it is necessary to divide low from very low. It may be important if this division contributes to a suggestion of two different natures of the tumor. In highly cellular tumors such as malignant lymphoma or medullary carcinoma, the internal echo level is very low because of high penetration of ultrasound without much reflection or backscattering associated with posterior echo accentuation. In contrast, in highly fibrous tumors such as scirrhous carcinoma, the internal echo level is also very low because of high attenuation of ultrasound in the tumor associated with a posterior echo attenuation or defect. Other types

of carcinoma or benign tumors usually show their echo level to be simply low, but this is not yet conclusive. Further study is needed.

Assessment of homogeneity of internal echoes is frequently complicated. Should high echo spots be included? This is also still in debate. Homogeneity can be said of different categories, such as distribution of echoes, size, or brightness of each echoes and so on. These are not a concern at this time. Instead, here regularity of internal texture was considered important.

As to high echo spots, one of the discussions was their classification by size. The tentative proposition is that fine high echo spots are less than 1 mm, small are 1 mm or more, and coarse high echo spots correspond with spots of 3 mm or more in size. These should be documented further through studies in many institutes.

Fluid–fluid level (FFL) usually means hemorrhage in the cystic lesion. With this phenomenon, the possibility of malignancy of the lesion is increased. Other causes of FFL are oil cyst and the concentrated type of cyst (complicated cyst). In a cystic lesion with internal hemorrhage, the lower part below the FFL is more hyperechoic. In an oil cyst, the oily component is lighter than the watery one and is located above the FFL. In concentrated cysts, a thick concentrated fluid component occasionally gathers in the upper part, forming FFL, and is hyperechoic.

Conclusions

Many aspects of internal echoes of mass image-forming breast lesions have been discussed. These points, as well as other themes, should be documented or corrected through further investigation in wide clinical practice.

Incident Angle of the Plunging Artery of Breast Tumors

Yuka Kujiraoka[1], Ei Ueno[2], Eriko Tohno[2], Isamu Morishima[3], and Hiroko Tsunoda-Shimizu[4]

Summary. We measured the incident angle of the feeding artery of breast tumors on color Doppler ultrasonography. Ninety-two tumors that had plunging arteries (21 fibroadenomas and 71 breast cancers) were retrospectively evaluated. Breast cancers were divided into three types [accentuating type (ACC), 25; intermediate type (INT), 35; and attenuating type (ATT), 11] by posterior echo. Color Doppler ultrasonography was performed using an HDI 5000 (ATL Ultrasound, USA) with a 7- to 10-MHz linear probe. We measured the incident angle of the feeding artery on color Doppler imaging. If the tumor had many plunging vessels, we measured all of them. The average incident angle of the artery of fibroadenoma was 47.5° and that of breast cancer was 17.6°. Fibroadenoma ranged from 15° to 70° and breast cancer from 0° to 70°. In breast cancer, there were no significant differences among the three types (ACC, INT, and ATT). We concluded that the incident angle of the feeding artery adds valuable information to the color Doppler ultrasonographic diagnosis for breast tumors.

Key words. Incident angle, Breast tumor, Fibroadenoma, Breast cancer, Color Doppler ultrasonography

Introduction

Recently, morphological characteristics of tumor vessels have been evaluated by color Doppler and power Doppler imaging [1]. Experimental evidence indicates that proliferation and distribution of tumor vessels are linked to tumor growth pattern [2]. Malignant tumors grow rapidly and involve surrounding tissue, so the arteries plunge and penetrate into tumors. Benign tumors grow slowly and press surrounding tissue, so the arteries go around the margin of tumors [3–5]. However, sometimes we find

[1] Department of Radiology, Tsukuba Memorial Hospital, 1187-299 Kaname, Tsukuba, Ibaraki 300-2622, Japan
[2] Institute of Clinical Medicine, Tsukuba University, 2-1-1 Amakubo, Tsukuba, Ibaraki 305-8576, Japan
[3] Department of Surgery, Tsukuba Medical Center, 1-3-1 Amakubo, Tsukuba, Ibaraki 305-8558, Japan
[4] Department of Radiology, St. Luke's Hospital, 9-1 Akashi, Chuo-ku, Tokyo 104-8560, Japan

cases of fibroadenoma that have plunging arteries. Are there any differences about the plunging pattern between breast cancer and fibroadenoma? We measured incident angle of plunging arteries of breast tumors on color and power Doppler imaging. We compared the incident angle of breast cancer with that of fibroadenoma to know the potential of incident angle to differentiate benign from malignant solid breast tumors.

Materials and Methods

Ninety-two breast tumors that had plunging arteries were evaluated; 21 were fibroadenoma and 71 were breast cancer. If the tumor had many plunging arteries we measured all of them, so in total 131 plunging arteries were evaluated. Color and power Doppler ultrasonography was performed using an HDI 5000 (ATL Ultrasound, USA) with a 7- to 10-MHz linear probe. One representative color or power Doppler echogram was chosen for each tumor, and the incident angle was measured on it. We drew two lines on the point of plunging arteries. One was drawn tangential to the tumor, and the other was drawn vertical to this tangential line. The angle between this vertical line and the plunging artery ranged from 0° to 90° (Fig. 1).

The average of incident angle in breast cancer was compared with that of fibroadenoma by means of the two-tailed Student's *t* test for unpaired data. With the *F* test, the mean of incident angle in the attenuating type (ATT) group was compared with the intermediate type (INT) group and the accentuating type (ACC) group. A *P* value of less than 0.05 was considered to indicate a statistically significant difference. The receiver operating characteristic (ROC) curve was constructed and the cutoff point determined.

Results

The average incident angle of fibroadenoma was 47.5° and that of breast cancer was 17.6° (Table 1). The incident angle of fibroadenoma ranged from 15° to 70° while that of breast cancer ranged from 0° to 70° (Fig. 2). The average incident angle of breast cancer is significantly lower than that of fibroadenoma. There are no significant dif-

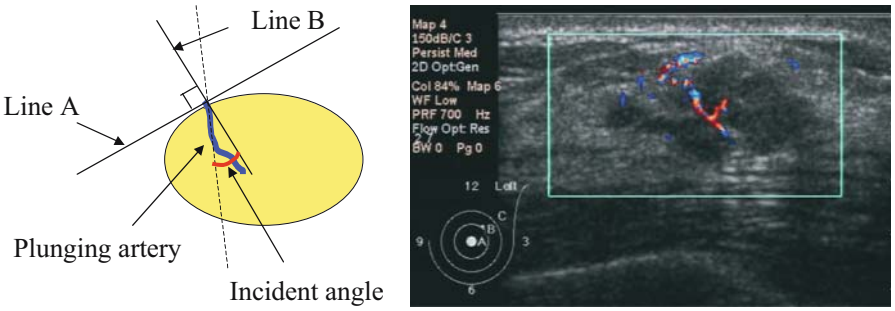

Fig. 1. Schematic drawing of measurement of incident angle. We drew two lines on the point of plunging arteries, one tangential to the tumor (*line A*) and the other vertical to this tangential line (*line B*). The angle between this vertical line and the plunging artery was measured

Table 1. Statistical analysis: fibroadenoma (Fa) versus breast cancer (Ca)

	Number	Average	Range	Distribution	SD
Fa	31	47.5	20–70	209.7	14.4
Ca	100	17.6*	0–70	262.3	16.1
ATT	17	16.4	0–45	180.5	13.4
INT	49	17.5	0–70	299.0	17.2
ACC	34	18.2	0–50	263.4	16.2

SD, standard deviation; ATT, attenuating type; INT, intermediate type; ACC, accentuating type
*Average of incident angle of the breast cancers is lower than that of fibroadenomas ($P < 0.05$)

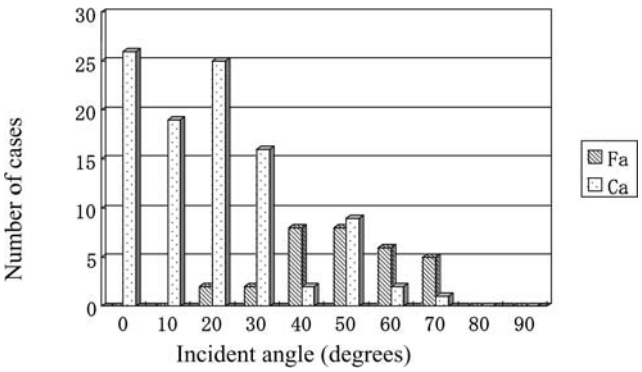

Fig. 2. Distribution of incident angle in fibroadenoma and breast cancer. *Fa*, fibroadenoma; *Ca*, breast cancer

ferences among the three groups (ATT, INT, and ACC) of breast cancer (Fig. 3). From the ROC curve, 30° was adopted for the cutoff point. At this point, sensitivity of malignancy is 86% and specificity is 88%.

Discussion

Previous study of the morphological features of tumor vessels has indicated that penetrating arteries are highly suggestive of malignancy and surrounding marginal arteries are suggestive of benignity [1]. Plunging arteries are frequently seen in breast cancer, but are also seen in fibroadenoma in some cases. We investigated the incident angle of plunging arteries of breast tumors on color and power Doppler imaging. We found that the incident angle of breast cancer was lower than that of fibroadenoma. Although their range overlaps, if the cutoff point is set at 30°, the sensitivity of malignancy is 86% and the specificity is 88%. Incident angle seems to be useful to differentiate a benign tumor from malignancy. On the other hand, 4 of 31 (12%) cases were false positive at this cutoff point. In these fibroadenomas, the shape of tumors tends to be lobulated and their plunging arteries lie among the lobes; this might be the reason why the tumors have a low incident angle. Establishment of the combination of incident angle and other features increases the accuracy.

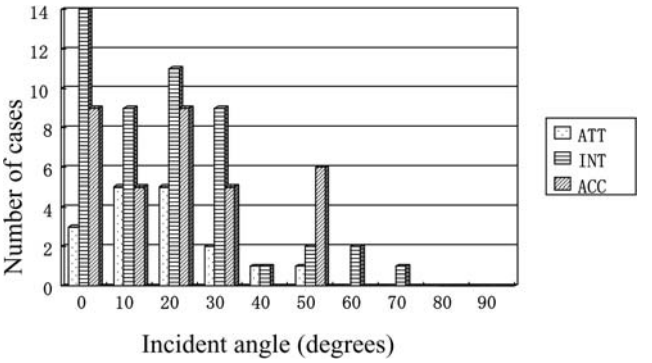

Fig. 3. Distribution of incident angle of breast cancer. *ATT*, attenuating type; *INT*, intermediate type; *ACC*, accentuating type

Conclusion

Incident angle is one of the important values in the differentiation of breast tumors on color and power Doppler imaging. Establishment of the combination of incident angle and other features would be useful in daily practice.

References

1. Raza S, Baum JK (1997) Solid breast lesions: evaluation with power Doppler US. Radiology 203:164–168
2. Lee WJ, Chu JS, Houng SJ, et al. (1995) Breast cancer angiogenesis: a quantitative morphologic and Doppler imaging study. Ann Surg Oncol 2(3):246–251
3. Weind KL, Maier BCF, Rutt BK, et al. (1998) Invasive carcinomas and fibroadenomas of the breast: comparison of microvessel distributions—implications for imaging modalities. Radiology 208:477–483
4. Skaane P, Engedal K (1998) Analysis of sonographic features in the differentiation of fibroadenoma and invasive ductal carcinoma. AJR (Am J Roentgenol) 170:109–114
5. Morishima I (1993) Color Doppler imaging of fibroadenoma; 8th ICUBE. Bildgebung Imaging (suppl 2 zu Band) 60:45

Draft JSUM Diagnostic Guidelines for Mass Image-Forming Lesions

Ei Ueno[1,2], Tokiko Endo[1,2], Mitsuhiro Kubota[1,2], Akihiro Kawauchi[1], Yasuyuki Kato[1], Yutaka Konishi[1,2], Mitsuhiro Mizutani[1,2], Eriko Tohno[1], Hiroko Tsunoda-Shimizu[1,2], Nobuyuki Taniguchi[1], Hidemitsu Yasuda[1,2], Takanori Watanabe[2], Kazuhiro Shimamoto[2], Hideyuki Hashimoto[1,2], Norikazu Masuda[2], and Isamu Morishima[2]

Diagnostic Criteria for Breast Lesions has been widely used since its release in 1988 by the Japan Society of Ultrasonics in Medicine (JSUM). However, improved diagnostic procedures and new data led to a growing desire for revisions to this publication. Prompted by that growing demand, in 2000 the JSUM set up a Subcommittee on Diagnostic Criteria for Breast Diseases (SCDCBD-JSUM; chairman, Ei Ueno), thus launching a study of new diagnostic guidelines for these diseases.

The subcommittee classified breast diseases into two categories, mass image-forming and non-mass image-forming lesions as shown on ultrasonograms, and won approval of its classification for mass image-forming lesions as part of the revision process. These revisions were published in the *Journal of Medical Ultrasonics* and JSUM members have been invited to comment. The Japan Association of Breast and Thyroid Sonology's Committee on Diagnostic Criteria for Breast Diseases (CDCBD-JABTS; chairman, Tokiko Endo) also engaged in a study of the terminology that provides the basis for these classifications. Details of these studies are elaborated here.

Key Revisions by the JSUM Subcommittee

The three main revisions are as follows.

1. "Diagnostic Criteria" has been deleted from the title and replaced with "Diagnostic Guidelines for Ultrasonic Diagnosis."

A definite diagnosis of breast cancer cannot be made solely on the basis of an imaging procedure. Ultimately, a histological evaluation will be required. For this reason, it was concluded that a title with the expression "diagnostic criteria" is not suited to a document on diagnostic imaging. In addition, on the understanding that

[1] Subcommittee on Diagnostic Criteria for Breast Diseases, Japan Society of Ultrasonics in Medicine, Department of Breast-Thyroid-Endocrine Surgery, Institute of Clinical Medicine, University of Tsukuba, 1-1-1 Tennodai, Tsukuba, Ibaraki 305-8577, Japan
[2] Committee on Diagnostic Criteria for Breast Diseases, Japan Association of Breast and Thyroid Sonology, University of Tsukuba, 1-1-1 Tennodai, Tsukuba, Ibaraki 305-8577, Japan

insufficient criteria could be detrimental to the advancement of ultrasonic medicine in the years ahead, the document was reframed as "guidelines" based on a minimum level of agreement and a new title containing the term "Guidelines" was formulated.

2. Breast lesions are categorized into mass image-forming lesions and non-mass image-forming lesions, and in the new guidelines, the definition of a mass image-forming lesion has been revised.

In the past, ultrasonic diagnostic procedures were aimed at diagnosing palpable tumors. However, advances in the field have expanded the scope of application to non-palpable lesions and asymptomatic breast lesions. This has facilitated the detection of many breast carcinomas that do not form a mass image and, conversely, the occasional detection of palpable breast carcinomas that do not form a well-defined mass image. Drawing from these findings, Ueno and Tohno [1] proposed that lesions be classified into two types: mass image forming and non-mass image forming. The latest revisions adopt this proposal, first by introducing the classifications for mass image-forming and non-mass image-forming lesions. Because the classifications are based not on whether a lesion is palpable, but whether or not it forms a mass image on ultrasonograms, the terms "image" and "mass image-forming lesion" have been used instead of "mass-forming lesion." Furthermore, the previously used term "type" has been replaced by "lesion" in the revised edition.

The CDCBD-JABTS debated the definition of a lesion, and defined a mass as follows: A mass image-forming lesion (tumor mass) is a space-occupying lesion that is thought to be a lump of material that differs from the surrounding tissue [2]. Hence, a non-mass image-forming lesion is not identical to a diffuse lesion, and a mass image-forming lesion is not identical to a circumscribed lesion.

3. An explanation of tissue characterization has been added.

Histological and ultrasound findings are often consistent with one another. It is possible to make assumptions about histological typing on the basis of ultrasound findings. Furthermore, more precise diagnoses are possible with diagnostic procedures that make assumptions about the histological findings. Accordingly, the guidelines incorporate a new comparison with histological data.

Ultrasound Findings and the Differential Diagnosis of Malignancy

SCDCBD-JSUM cited six criteria of value to the differential diagnosis of malignancy—shape, border, internal echoes, compressibility, depth/width, and vascularity—and demonstrated patterns of malignancy based on these criteria (Table 1). A posterior echo is of no direct aid in determining whether a lesion is malignant, but is an important factor for consideration when speculating about the features of lesion tissue. As such, it was treated in a section on tissue characterization, not the differential diagnosis of malignancy.

Table 1. Ultrasonic findings and benign/malignant findings

	Benign ◄——————————►		Malignant
Findings			
Shape	Round or oval/lobulated		
		Polygonal	
			Irregular
Border			
Definition	Well defined		Not clear
Irregularity	Smooth		Rough
Halo	Absent		Present
Gland surface	Continuous		Interrupted
Internal echoes			
Homogeneity	Homogeneous		Heterogeneous
High echo spot	Coarse		Micro/small
Compressibility	Easily deformed		Nondeformable
Depth/width	Small		Large
Vascularity	Avascular or hypovascular		Hypervascular

Shape (1)

Shape refers to the morphological impression of a lesion image in its entirety. As a system of terminology for the expression of shape, JABTS adopted the following: round/oval, polygonal, lobulated, and irregular (Fig. 1). Watanabe proposed that the definitions of shape could be expressed through the presence or absence of constriction or angularity [3], and JSUM and JABTS decided to adopt this proposal. The probability of malignancy was considered to increase with certain shapes in the following order: round/oval, lobulated, polygonal, and irregular (Table 2).

Border (2)

For border-related data, attention was focused on four criteria: definition, irregularity, halo (hyperechoic marginal zone), and gland surface. Border definition and irregularity were selected as diagnostic criteria. Lesion borders contrast with surrounding tissue. Border definition is a function of variations in echo level and lesion structure and the presence or absence of a capsule. Irregularity reflects the condition of a border. JABTS has recommended a compound expression, with the term "boundary zone" consolidating the definitions of periphery, border, and margin [4].

Halo (Hyperechoic Marginal Zone)

When a breast carcinoma invades and spreads into surrounding tissue, the affected locus is characterized by tangles of fatty and fibrous tissue, which results in backscattering. Accordingly, a hyperechoic marginal zone will be expressed by scirrhous carcinomas that are strongly likely to invade surrounding tissues (Fig. 2). This diagnostic sign was proposed by Takehara in 1976 [5]. As to its etymological origin, the term "halo" refers to the strong aura of light often shown in depictions of Buddha, Christ, Allah, and other religious deities. It was thus concluded that "halo" is a

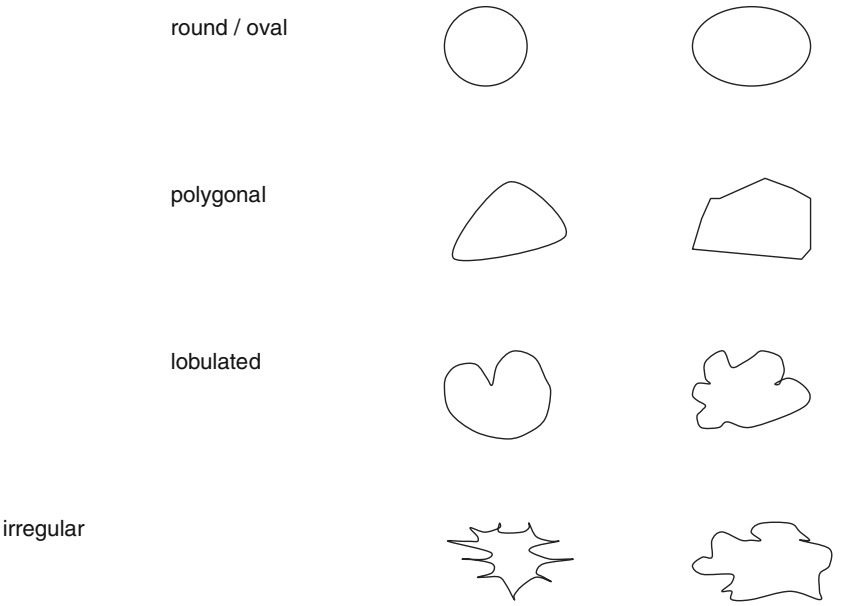

Fig. 1. Various shapes of lesions

Table 2. Shape is defined by the combination of constriction and angularity

	Constriction	Angularity	Figure no.
Round/oval	–	–	Fig. 2
Lobulated	+	–	Fig. 3
Polygonal	–	+	Fig. 4
Irregular	+	+	Fig. 5

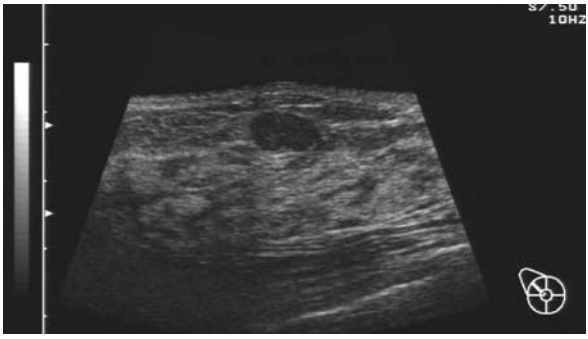

Fig. 2. Oval-shaped fibroadenoma

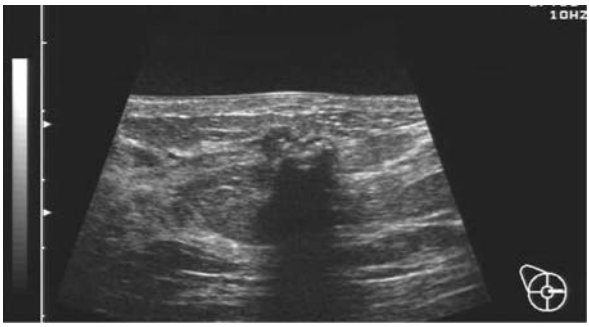

Fig. 3. Lobulated fibroadenoma. The inside of the fibroadenoma has calcified and has become heterogeneous

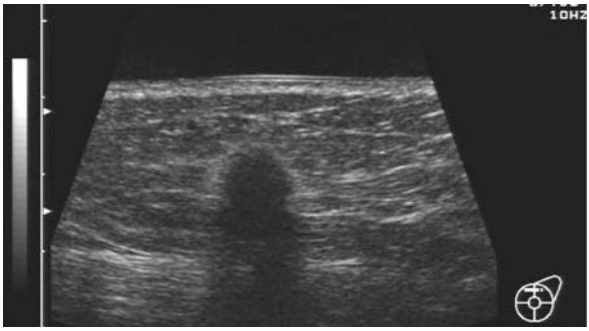

Fig. 4. Scirrhous carcinoma in a 59-year-old female patient. Halo and posterior echo attenuation can be observed

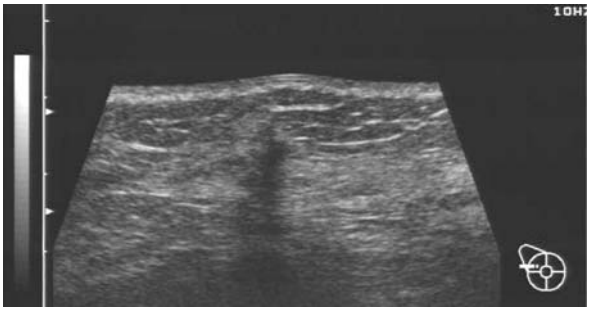

Fig. 5. Invasive ductal carcinoma. Interruption of the anterior border of the mammary gland is visible

misnomer when applied in reference to a weak-signaled hypoechoic marginal zone. Conversely, the halo on a mammogram is a negative film finding, and considered appropriate terminology in view of the strong signal for the echo data.

Interruption of Mammary Gland Surface

Breast carcinomas destroy the capsule of the mammary gland surface when they invade fatty tissue; this is recognized to be a finding of gland surface interruption (Figs. 3, 4, 5). As a diagnostic sign, it has been proposed by Konishi et al. and is indicative of a high probability of malignancy when it is present [6].

Internal Echoes (3)

Methods of observing internal echoes and the histological relationships are elaborated in a separate section below.

Compressibility (4)

Compressibility is visually assessed by noting the degree of deformation caused by applying external pressure to the lesion. Tumor cell proliferation or fibrosis increases the elasticity of a breast carcinoma. Benign tumors readily deform under external pressure, but cancer tumors do not change their shape when external pressure is applied. Ueno et al. have devised dynamic tests to observe this compressibility [7].

Depth/Width (5)

Definition of the depth/width ratio (DW ratio): the depth of the mass divided by the width of the mass. The largest part of the mass is used in measuring the DW ratio. In the image, the width is shown parallel to the skin and the depth crosses the width vertically. The DW ratio does not include the echogenic halo and is measured only in the hypoechoic part of the mass. This diagnostic sign was proposed by Kato [8]. Working with various other facilities, the Subcommittee sought to identify a suitable cutoff value for this sign, and determined that a value of 0.7 is appropriate [9]. When values larger than 0.7 are considered to indicate malignancy and those of 0.7 or less benignity, the rates of sensitivity, specificity, and accuracy are 70.5%, 64.7%, and 68.5%, respectively.

Vascularity (6)

As vascularity is currently difficult to quantify, we decided to semiquantify it in terms of four levels of intensity: hypervascular, vascular, hypovascular, and avascular. Assessments of vascularity are subjective. Figure 6 is a sample illustrating three levels of vascularity, excluding the avascular level. It is assumed that avascular and hypovascular tumors are more likely to be benign and that vascular and hypervascular tumors are more likely to be malignant. However, vascularity is lower in carcinomas characterized by increased fibrous tissue, such as scirrhous carcinoma, whereas in proliferative fibroadenoma and papilloma, the tumors are typically hypervascular. At present, no consensus has been formed on diagnostic approaches that utilize morphological findings in tandem with the vascularity index.

Tissue Characterization and Ultrasonic Diagnosis

Performing a systematic ultrasonic diagnosis demands that one have an advanced understanding of the relationships between histology and ultrasound. Ultrasonic tissue characterization is explained in the guidelines. Although ultrasonic tissue characterization was formerly expressed in terms of sound speed, attenuation coefficients, and certain other parameters, in recent years the correlations with histology have taken on more importance.

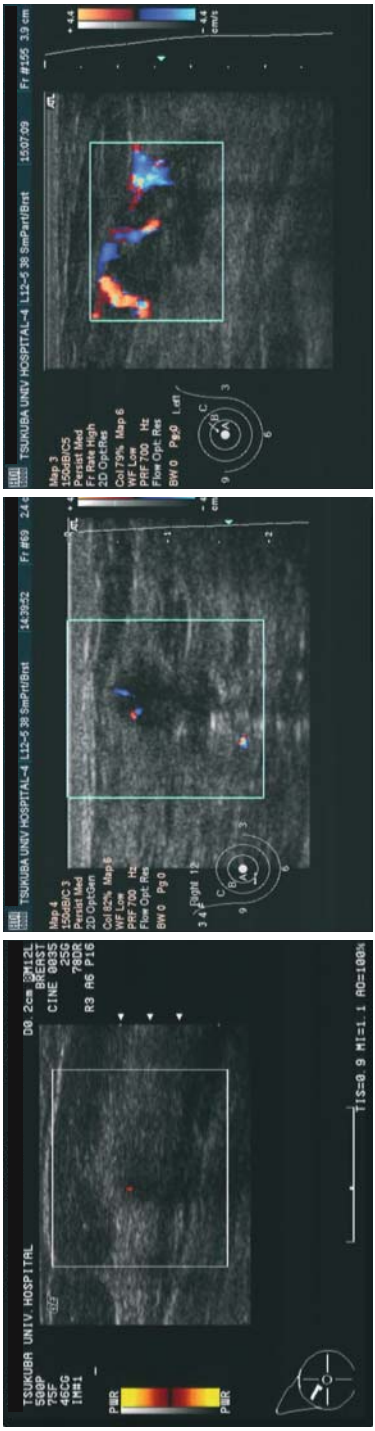

FIG. 6. Vascularity is classified into four levels: avascular, hypovascular, vascular, and hypervascular, the latter three shown in this figure

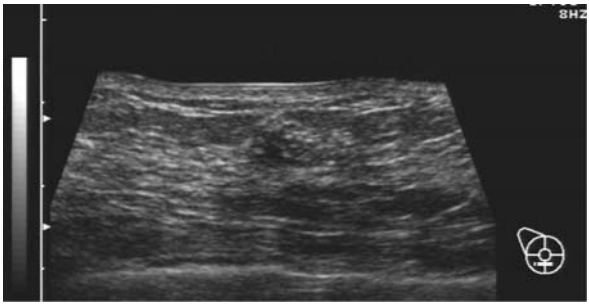

Fig. 7. Invasive ductal carcinoma with a dominant intraductal component. No change can be observed in the posterior echo

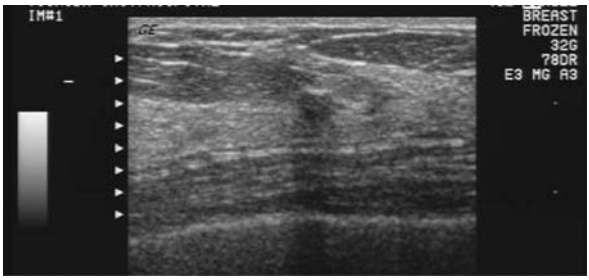

Fig. 8. Condensed milk cyst. Even though it is a cyst, the posterior echo has not enhanced it

Intensity of Posterior Echoes

Posterior echoes reflect the attenuation of an ultrasonic wave within a tumor mass. Posterior echoes are described in terms of four levels of intensity:

1. Accentuating (Fig. 2)
2. No change (Fig. 7)
3. Attenuating (Figs. 4, 5)
4. Deficient (Fig. 3)

Low-intensity posterior echoes are indicative of heightened attenuation within a tumor mass, whereas high-intensity posterior echoes indicate that the attenuation of the ultrasonic wave is lower within the mass than it is in surrounding breast or fatty tissues.

Within living tissue, the fibrous component is the feature that correlates most closely with the level of attenuation. In a tumor such as scirrhous carcinoma that is marked by proliferative fibrosis, the posterior echo is weak. This pattern is also observed in infiltrating lobular carcinoma. Ultrasonic waves are unable to penetrate a calcified mass or a cyst with a hardened capsule and, as a consequence, the posterior echo is attenuated or absent (Fig. 8).

By contrast, tissue with high water content rarely attenuates ultrasonic waves. For example, the posterior echo is more intense for a cyst. Given that cancer cells have high water content and little fibrous material, posterior echoes are more intense for solid-tubular carcinomas (see Note 1, following) or medullary carcinomas (Fig. 9) that consist of tightly packed cells. The posterior echo is also intense for a mucinous carcinoma because it contains profuse amounts of water-soluble mucin (Fig. 10).

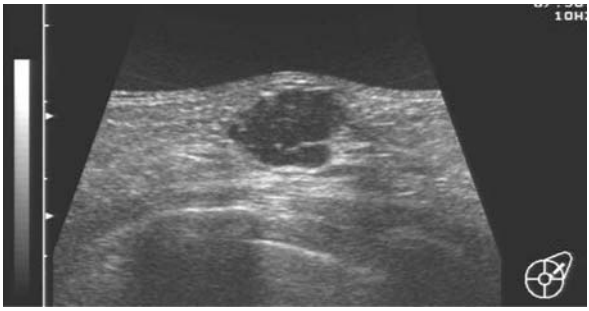

Fig. 9. Medullary carcinoma spreads rapidly and is characterized by posterior echo accentuation and low internal echo levels

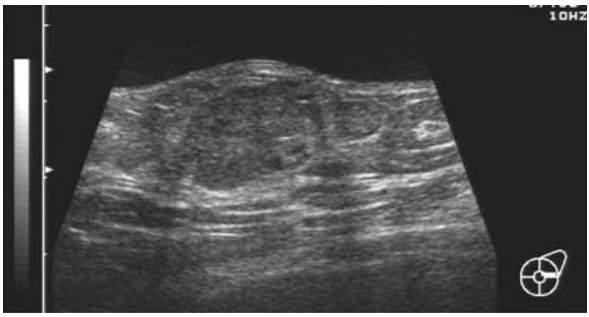

Fig. 10. Mucinous carcinoma is characterized by posterior echo accentuation and high internal echo levels

In papillotubular carcinoma (see Note 2, following), the ratio of fibrous tissue to cancer cells resembles that of normal mammary gland tissue, resulting in a median level of attenuation and, hence, a posterior echo that is unchanged.

In juvenile cystadenofibroma, there is little fibrous tissue, but fibrosis becomes elevated with advancing age. Hence, in the early stages, the posterior echo is more intense (see Fig. 2), but in elderly patients it is attenuated. With calcification, the ultrasonic wave is unable to penetrate and the posterior echo thus is absent (see Fig. 3).

A differential diagnosis of malignancy cannot be made directly on the basis of posterior echo data alone. However, in view of the fact that the posterior echo correlates most closely with tissue characteristics, as described above, correlations between posterior echo intensity and tissue type have been presented in Table 3. The breast cancer tissue types shown in this table are based on general rules issued by the Japanese Breast Cancer Society for the clinical and pathological recording of breast cancer [10].

Notes

1. Solid-tubular carcinoma: This is an invasive ductal carcinoma in which solid nests demonstrate expansive development. The cancer nests are marked by medullary or microtubular proliferation. This presentation is consistent with a circumscribed carcinoma and is differentiated cytomorphologically from medullary carcinoma.
2. Papillotubular carcinoma: This is an invasive ductal carcinoma characterized by papillary proliferation and tubular formation. Comedo carcinoma is also in this category.

Table 3. Tissue characterization and ultrasonic diagnosis

Posterior echoes	Benign	Malignant
Accentuating	Cyst, fibroadenoma Papilloma Phyllodes tumor	Solid-tubular carcinoma, mucinous carcinoma Intracystic papillary carcinoma Medullary carcinoma Malignant lymphoma
No change	Fibroadenoma, lipoma Sclerosing adenosis	Papillotubular carcinoma
Attenuating or deficient	Scar, old fibroadenoma Sclerosing adenosis Silicone granuloma	Scirrhous carcinoma Invasive lobular carcinoma

Table 4. Intensity of internal echoes

Internal echoes	Benign	Malignant
Anechoic	Cyst	Medullary carcinoma Malignant lymphoma
Extremely low	Sclerosing adenosis	Medullary carcinoma Malignant lymphoma Scirrhous carcinoma Solid-tubular carcinoma
Low	Fibroadenoma Papilloma	Papillotubular carcinoma
Equal	Fibroadenoma Papilloma	Mucinous carcinoma Papillotubular carcinoma
High	Lipoma, panniculitis	Mucinous carcinoma

Intensity of Internal Echoes (Echo Level)

The intensity of an internal echo is determined by the amount of backscattering within the lesion. Usually, the echo level is expressed in comparison with the tissue surrounding the lesion. Given that the breast contains mammary glands as well as fatty tissue, discussion focused on the question of which of these to treat as the baseline standard for comparison. Mammary gland tissue was considered unsuited as a standard because it changes with age and is also the tissue in the breast with the most intense echo level. On that basis, subcutaneous fatty tissue was chosen as a standard for comparison because it is more stable.

Echo levels were divided into five stages: echo-free, extremely low, low, equal, and high. Although it was not possible to establish a borderline value to differentiate between the extremely low and low levels, it was decided that the extremely low level would be assigned to solid masses that are virtually echo-free and that the low level would be assigned to masses that are virtually isoechoic with surrounding tissue. The correlations between internal echo intensity and tissue type are illustrated in the guidelines (Table 4).

Disorders That Are Free of Internal Echoes

Because water content tends to be acoustically uniform, internal echoes are not observed in most cysts. Similarly, they are also not observed in some lymphomas, medullary carcinomas, and other solid, proliferative tumors.

Disorders Characterized by Internal Echoes of Extremely Low Intensity

In general, the internal echo level is low for malignant tumors, particularly for medullary carcinoma (see Fig. 9) and malignant lymphoma. The internal echo for scirrhous carcinoma is extremely low because of strong attenuation (see Fig. 4).

Disorders Characterized by Internal Echoes of Low Intensity

Although slight, backscattering does occur within lesions that are histomorphologically well differentiated, and the internal echo level increases. In fibroadenoma, backscattering is observed in glandular tissue and fibrous stroma (see Fig. 2). The echo level decreases in atrophied epithelium and hyalinized stroma. In papilloma, the branching core of vascular fibrous tissue also causes backscattering (Fig. 11).

Papillotubular carcinomas are a relatively well differentiated form of invasive ductal carcinoma with a high echo level.

Disorders Characterized by Internal Echoes of Equal Intensity

Fibroadenoma, papilloma, mucinous carcinoma (see Fig. 10), and papillotubular carcinoma are among the disorders that have internal echo levels equal in intensity to those of fatty tissue. In mucinous carcinoma, the proliferation of honeycomb fibrous tissue causes backscattering.

Disorders Characterized by Internal Echoes of High Intensity

The lesions of lipoma, panniculitis, and mucinous carcinoma typically exhibit higher echo levels than fatty tissues. The echo levels from most lipomas are higher than those for fatty tissues. In early-stage scirrhous carcinoma, almost all lesions exhibit a halo image because they lack a core and are characterized by a high echo level (Fig. 12).

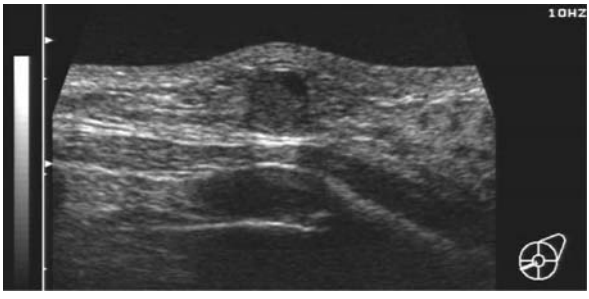

Fig. 11. Internal echo levels for papilloma are either low or isoechoic

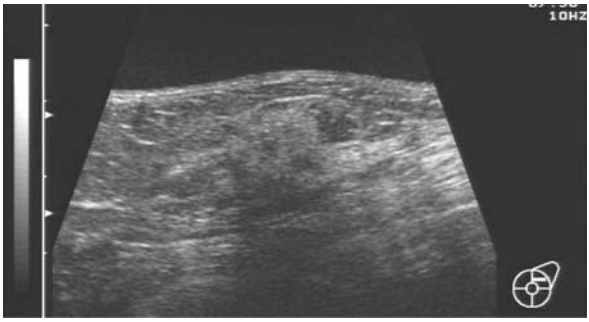

Fig. 12. Coreless scirrhous carcinoma

Table 5. Correlations between histology and various combinations of posterior and internal echoes

	Deficient or Attenuating	No Change	Accentuating
Free	Scirrhous carcinoma		Cyst, lymphoma
Extremely low	Scirrhous carcinoma Concentrated milk cyst Sclerosing adenosis Lobular carcinoma	Papillotubular carcinoma Sclerosing adenosis	Medullary carcinoma Solid-tubular carcinoma
Low	Fibroadenoma	Papillotubular carcinoma Fibroadenoma Ductal hyperplasia Adenosis Lobular carcinoma Tubular carcinoma	Fibroadenoma Papilloma Papillary carcinoma
Equal			Papilloma Fibroadenoma Mucinous carcinoma Papillary carcinoma
High	Silicone granuloma Panniculitis Scirrhous carcinoma No core	Lipoma Panniculitis	Mucinous carcinoma

Table 5 shows the correlations between histology and various combinations of posterior and internal echoes.

Determining Degrees of Certainty for a Diagnosis of Malignancy

Various attempts have been made to express degrees of certainty when evaluating a lesion for malignancy. In Japan, a system derived from the Papanicolaou classification, as used in cytology, was in use for about two decades. As a result of the influence from the American College of Radiology's breast imaging and reporting system [11], in recent years a category classification system (Table 6) has been used for mam-

Table 6. BIRADS category classifications (second edition, 1995)

Category 1. Negative
Category 2. Benign
Category 3. Benign, but malignancy cannot be ruled out
Category 4. Suspicious abnormality
Category 5. Highly suggestive of malignancy

mography evaluations. Because there are essentially no differences with grading based on the Papanicolaou classification, JABTS decided to adopt the category classification for use in ultrasound examinations in the interest of facilitating comparisons both on an international level and with the results of mammography tests. This subcommittee has urged that JSUM also approve the category classification system in the near future.

Draft Diagnostic Guidelines for Non-Mass Image-Forming Lesions by the Japan Association of Breast and Thyroid Sonology (JABTS) and the Japan Society of Ultrasonics in Medicine

Tokiko Endo[1,2], Mitsuhiro Kubota[1], Yutaka Konishi[1], Kazuhiro Shimamoto[1], Kumiko Tanaka[1], Hiroko Tsunoda-Shimizu[1], Hideyuki Hashimoto[1], Norikazu Masuda[1], Mitsuhiro Mizutani[1], Isamu Morishima[1], Hidemitsu Yasuda[1], Takanori Watanabe[1], and Ei Ueno[1]

Background

Recently, ultrasonic instruments have remarkably improved, and smaller or earlier breast cancers have been found. Also, mammographic screening for breast cancer for women of 50 years and older has heightened people's desire to find and diagnose smaller or earlier lesions. The lesions that do not form mass images have been recognized, and a lexicon for reporting these is desired.

We have been discussing the diagnostic guidelines for breast cancer for the past 3 years. Non-mass image-forming lesions are contained as the objects of diagnosis. We present the tentative plan of the guidelines for non-mass image-forming lesions here.

Definition of the Non-Mass Image-Forming Lesions

Non-mass image-forming lesions are those lesions that are difficult to recognize as a "mass image." They may associate with "mass image-forming lesions." The ultrasonic images of breast disease consist of mass image-forming lesions and non-mass image-forming lesions.

Normal Breast Sonograms and Variants

Normal breast sonograms and their variants are the essential knowledge for understanding non-mass image-forming lesions. These factors may have an effect on ultrasonic breast images:

[1] Japan Association of Breast and Thyroid Sonology, Japan
[2] Department of Radiology, National Nagoya Hospital, 4-1-1 Sannomaru, Naka-ku, Nagoya 460-0001, Japan

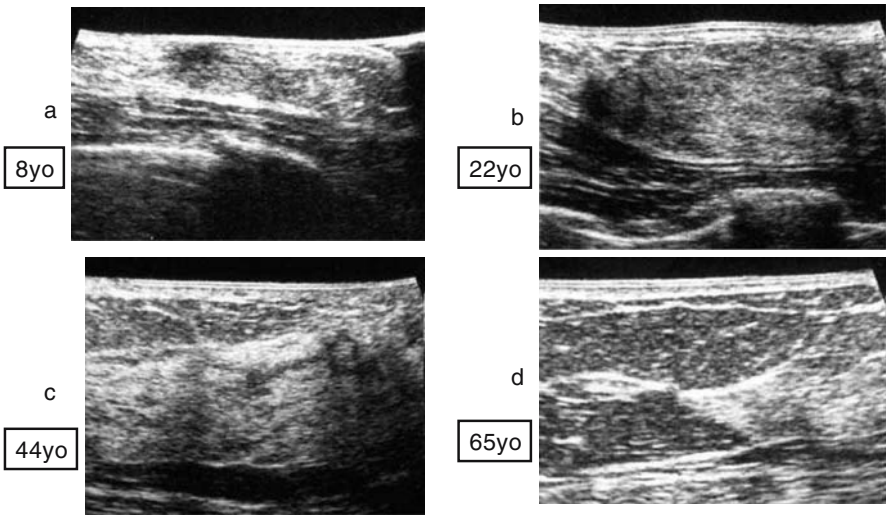

Fig. 1. Ultrasonic breast images and patient age

Age (Fig. 1)
Pregnancy
Breast-feeding
Hormone replacement therapy

Lesions That May Be Observed by Ultrasonic Examination as Non-Mass Image-Forming Lesions

- Duct dilatation
- Duct ectasia (contains plasma cell mastitis)
- Intraductal papilloma, multiple intraductal papilloma
- Mastopathy
- Epithelial hyperplasia
  - Adenosis
  - Multiple cyst
  - Fibroadenomatoid hyperplasia
  - Fibrosis
- Mastitis
  - Lymphocytic mastitis
  - Acute mastitis.
- Radial scar, complex sclerosing lesion
- Noninvasive ductal carcinoma
- Invasive ductal carcinoma with a predominant intraductal component
- Invasive carcinoma

Lexicon for Non-Mass Image-Forming Lesions

- Dilation of the duct
  Dilated ducts with or without internal echoes that may be in any area
- Wall thickening of the duct
  The wall of the duct is increased in thickness more than usual
- Irregularity of the caliber of the duct
  Irregularity of the anechoic area in the duct
- Internal echoes in the duct or tiny cysts
  Echoes in the duct or tiny cysts as follows:
    Solid echoes
    Floating echoes
    Linear high echoes
    High echo spots
    Fine high echo spots (smaller than 1 mm in diameter)
- Multi-vesicular pattern
  Multiple tiny or small cysts in the breast tissue
- Low echo area in the breast tissue
  Low echo area whose character is different from surrounding gland or same area in the ipsilateral breast (Fig. 2)
  Spotted or mottled low echo area
    Relatively small low echo areas form the spotted (or mottled) pattern
- Geographical low echo area
  Low echo area looks like geography as if spotted low echo areas fused into one
- Low echo area with indistinct margin
  Low echo area whose margins are not clearly defined
- Architectural distortion
  Distorted structure without mass image

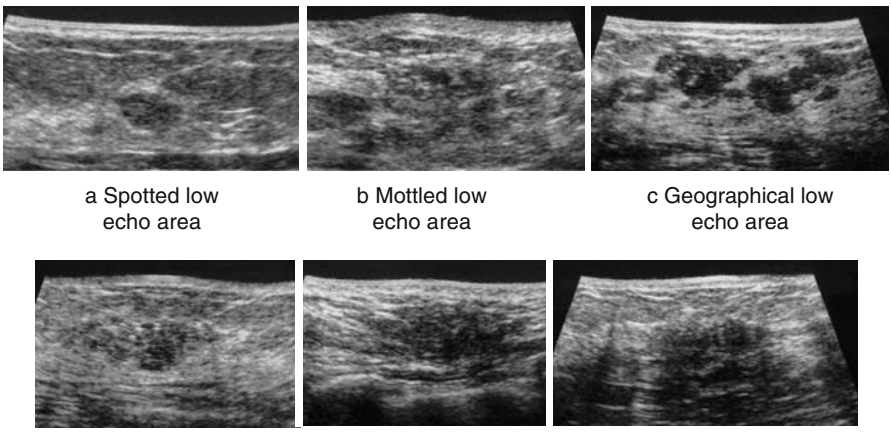

Fig. 2. Low echo area in the breast tissue

Assessment and Categories

Assessment categories are decided as follows:

Category 0: Assessment is incomplete
Category 1: Negative
Category 2: Benign
Category 3: Benign, but malignancy cannot be ruled out
Category 4: Suspicious abnormality
Category 5: Highly suggestive of malignancy

Duct Dilatation (a): Duct Dilatation Without Internal Echoes (Fig. 3)

Dilated ducts with no internal echoes can be seen in the peripheral area outside the areola. They may be complicated with wall thickening by inflammation.

Bilaterally and multiple: category 2
  Dilated ducts
Solitary: category 3
  Dilated duct
  Duct ectasia

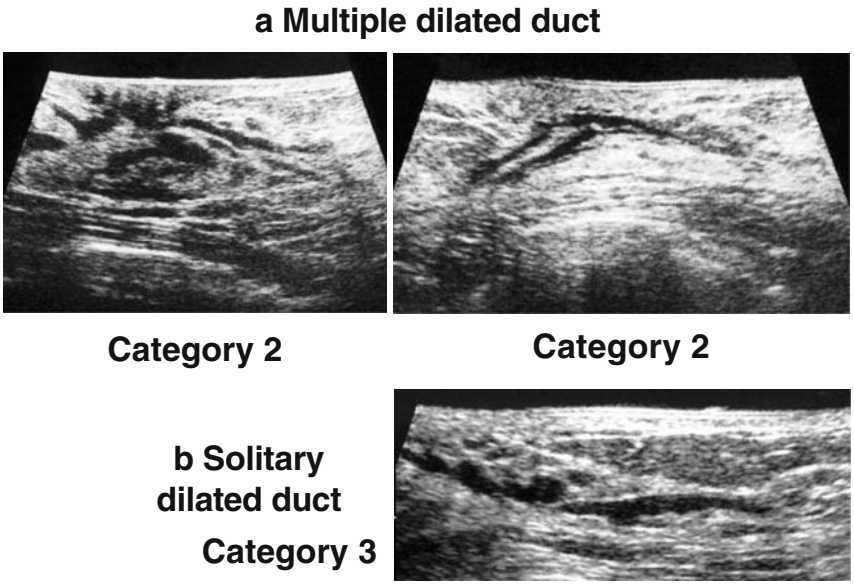

Fig. 3. Duct dilatation without internal echoes

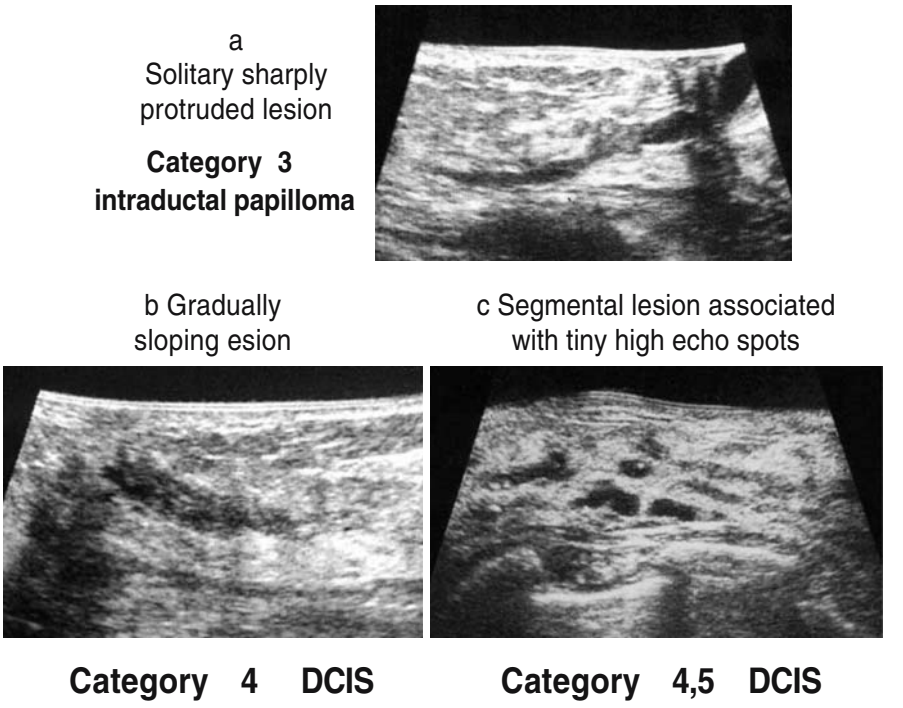

Fig. 4. Dilated ducts with internal solid echoes. *DCIS*, ductal careinoma in situ

Epithelial hyperplasia
Intraductal papillomas, noninvasive ductal carcinoma

*Secondary duct dilatation may be developed from intraductal proliferative lesions.
*When it is difficult to judge whether the internal echoes are there or not, it should be regarded as (b) (below).

Duct Dilation (b): Duct Dilatation with Internal Echoes (Fig. 4)

Intraductal echoes consist of solid echoes, floating echoes, linear high echoes, high echo spots, and fine high echo spots. Solid echoes often result from proliferative lesions; careful observation of the wall is needed. Internal echoes are produced by the floating components in the fluid. Condensed milk or blood is common.

Assessment of Duct Dilatation with Internal Echoes

Shape of the solid echoes

- Sharply protruded: Category 3
  Intraductal papilloma

- Gradually sloping (broad base lesion): Category 3,4,5 (irregularities of the ductal caliber are not rare)
  Intraductal papilloma
  Epithelial hyperplasia
  Noninvasive ductal carcinoma

Distribution of the solid echoes

- Bilaterally and multiple: Category 2
  Condensed milk
- Solitary lesion near the nipple: Category 3
  Intraductal papilloma
- Segmental or chainlike lesions: Category 3,4
  Epithelial hyperplasia,
  Intraductal papilloma
  Noninvasive ductal carcinoma

*Associated with tiny high echo spots suggesting malignant calcifications:
Category 4,5
Noninvasive ductal carcinoma
Invasive ductal carcinoma with a predominant intraductal component
Epithelial hyperplasia
Intraductal papilloma

Multi-Vesicular Pattern (Fig. 5)

Multiple tiny or small cysts in the mammary gland
*Include the lesions whose internal echoes are free or not is difficult to judge.

- Diffuse distribution: Category 2
  Mastopathy
- Regional or segmental distribution: Category 3
  Mastopathy
  Noninvasive ductal carcinoma

*When high echo spots suspected the calcifications are associated: mastopathy, probably

Low Echo Area in the Mammary Gland (Figs. 6, 7, 8, 9)

Low echo area whose character is different from surrounding breast tissue or the same area in the ipsilateral breast

Distribution
The distribution is very important to assess.

- Diffusely or scattered
- Focal
- Segmental
- Unilateral whole breast

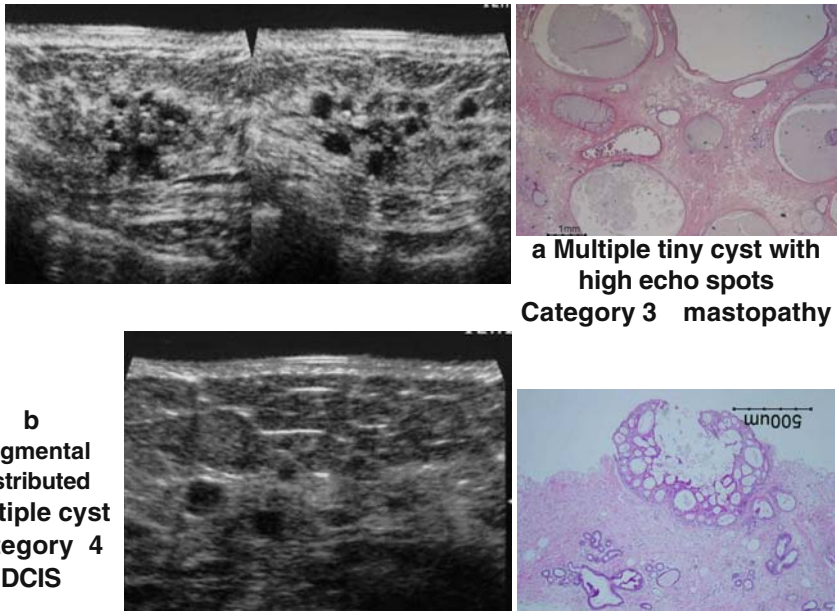

Fig. 5. Multiple tiny or small cysts

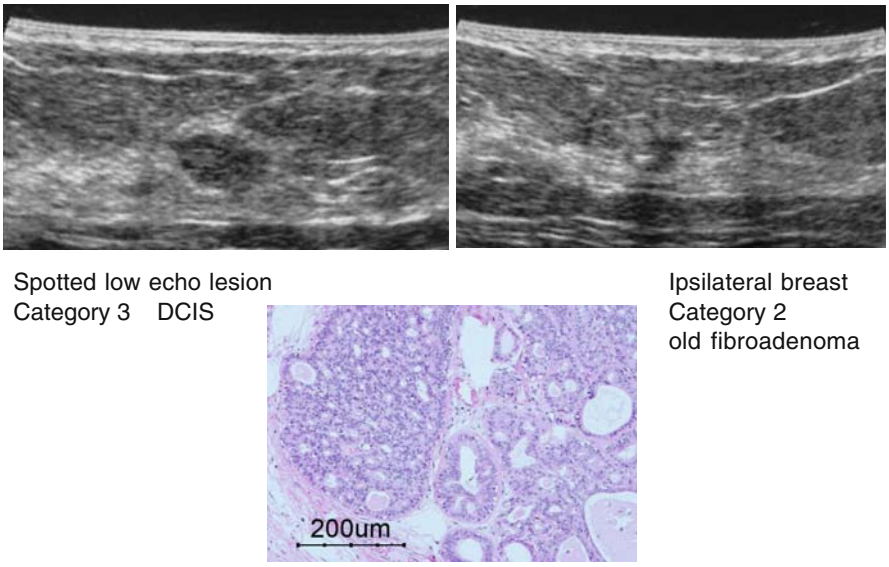

Fig. 6. Spotted low echo area

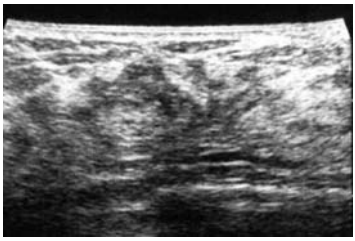

a Diffusely distributed
Category 2 mastopathy

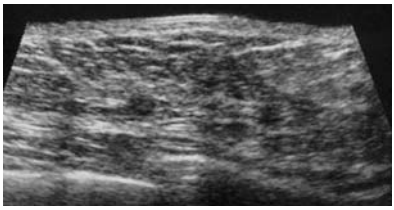

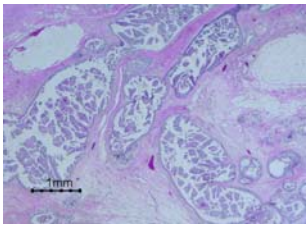

b
Segmental
distribution
Category 4
DCIS

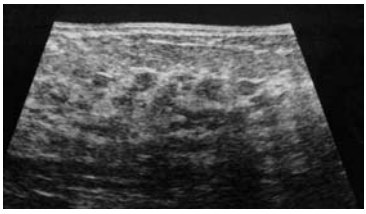

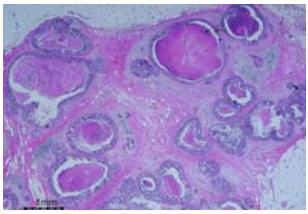

c
Segmental lesion
associated with
high echo spots
Category 5
DCIS

d Segmental Mottled low echo lesion
associated with faint high echo spots
Category 4 DCIS

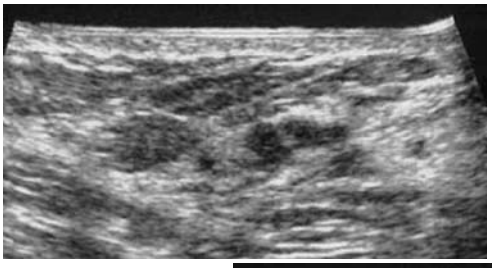

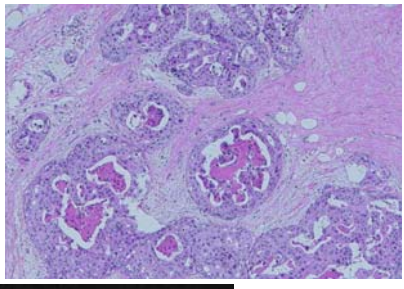

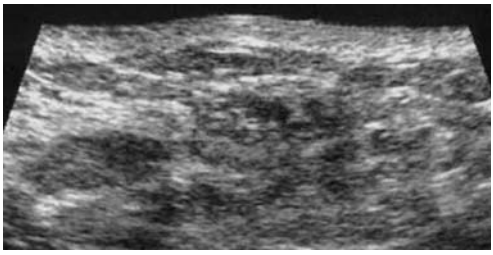

Fig. 7. Mottled low echo area

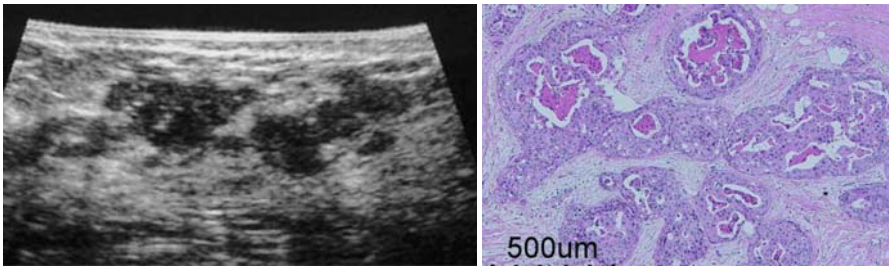

Fig. 8. Geographical low echo area

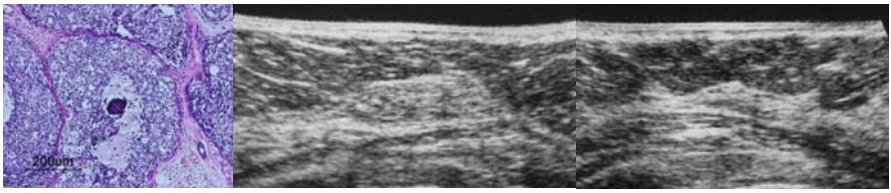

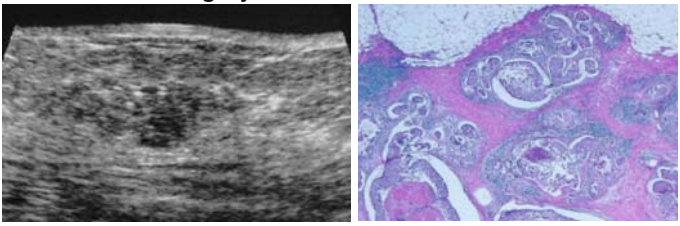

Fig. 9. Low echo area with indistinct margin

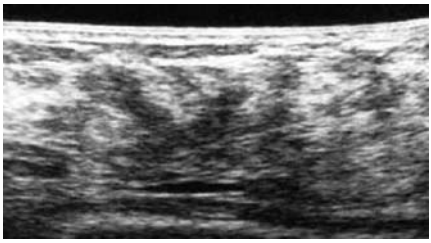

c Diffuse distribution
Category 2 mastopathy

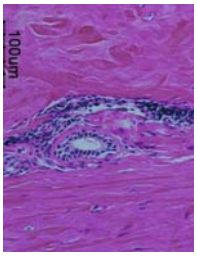

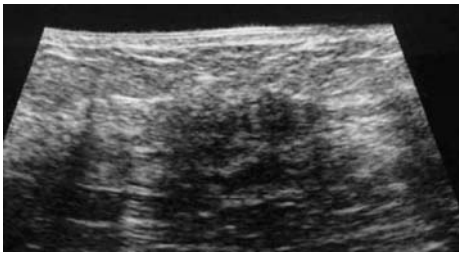

d Focal distribution
Category 4
lymphocytic mastitis

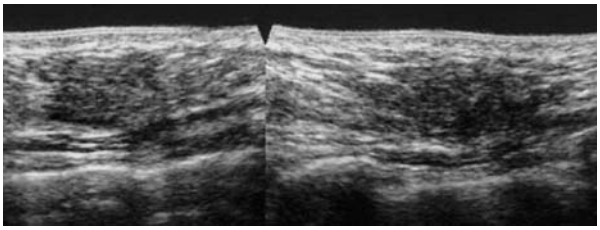

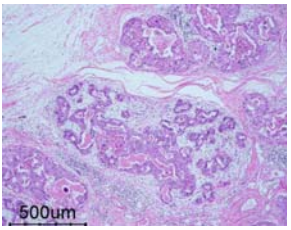

e Focal distribution
Category 4 DCIS

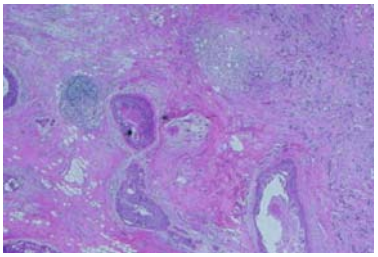

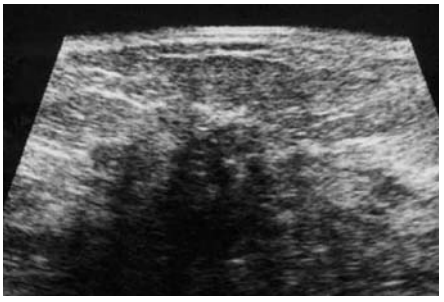

f Focal lesion
Category 5
invasive ductal carcinoma

Fig. 9. *Continued*

Types
(a) Spotted or mottled low echo area, geographical low echo area (Fig. 6, spotted low echo area; Fig. 7, mottled low echo area; Fig. 8, geographic low echo area)
(b) Low echo area with indistinct margin (Fig. 9)
Assessment of the low echo area in the mammary gland
- Diffusely or scattered: Category 2
  Mastopathy (inflammation)
- Focal: Category 3
  Mastopathy (inflammation)
  Noninvasive ductal carcinoma

*When the lesion is associated with the high echo spots, suspected intraductal calcifications: Category 4, 5
  Noninvasive ductal carcinoma
  Invasive ductal carcinoma with a predominant intraductal component
  Invasive carcinoma
- Segmental: Category 4
  Noninvasive ductal carcinoma
  Mastopathy
  Invasive lobular carcinoma

*When the lesion is associated with the high echo spots, suspected intraductal calcifications: Category 5
  Noninvasive ductal carcinoma
  Invasive ductal carcinoma with a predominant intraductal component
  Invasive carcinoma
- Unilateral whole breast: Category 2–5
  Normal variation
  Mastopathy
  Locally advanced breast cancer

Architectural Distortion (Fig. 10)

Distorted breast tissue without mass image formation
  *Architectural distortion associated with mass image forming lesion is the secondary one.

It is the distortion and/or retraction of the normal tissue inside and/or outside of the breast tissue:

- Associated with scar: Category 2
  Surgical scar
- Without scar: Category 4
  Invasive carcinoma (scirrhous carcinoma, invasive lobular carcinoma)
  Noninvasive ductal carcinoma
  Radial scar/complex sclerosing lesion
  Surgical scar

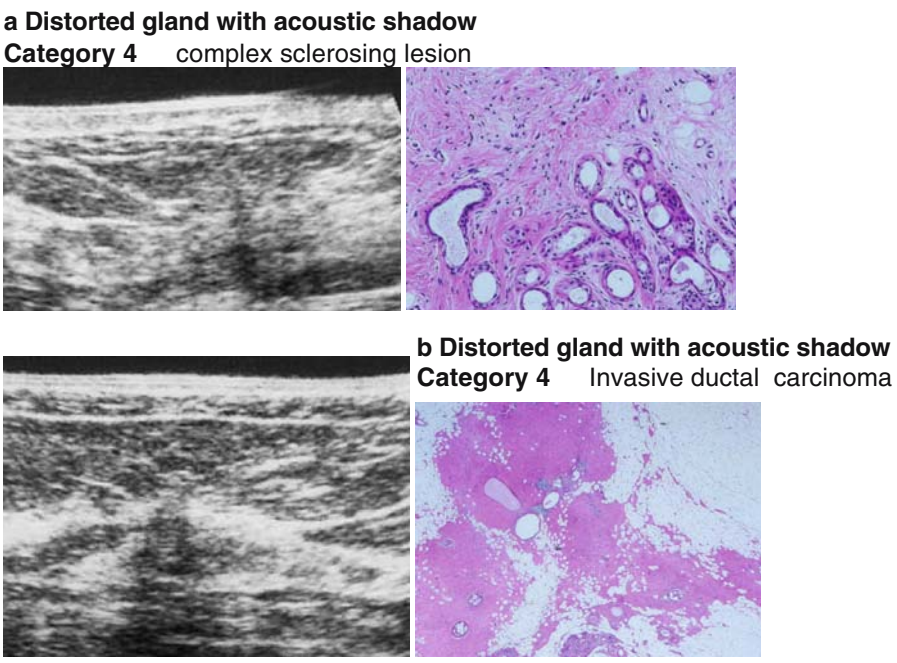

Fig. 10. Architectural distortion

Conclusions

We have reported the Diagnostic Guidelines for Non-Mass Image-Forming Lesions. These have been discussed in the subcommittee of the Japan Association of Breast and Thyroid Sonology (JABTS) and the Japan Society of Ultrasonics in Medicine.

This report is now the draft. We will discuss it further, and it will become a useful guideline for the ultrasonic diagnosis of breast cancers.

Bibliography

1. Endo T, Ueno E, Kubota M, et al. (2002) Report of the committee on Breast Ultrasonic Imaging Lexicon and Diagnostic Criteria: "Non-Mass Image-Forming Lesion." New Wave of Breast and Thyroid Sonology 5(2): 41–44
2. Tsunoda H, Ueno E, Tohno E, et al. (1990) Echogram of ductal spreading of breast carcinoma. Jpn J Med Ultrasonics 17:44–49
3. The Japan Society of Ultrasonics in Medicine (2000) Current textbook of ultrasonics in medicine, vol. 4. Igakushoin, Tokyo, pp 332–345
4. Stavros AT (2002) Ultrasound of ductal carcinoma in situ. Ductal carcinoma in situ of the breast, 2nd edn. Lippincott Williams & Lagios, Philadelphia, pp 128–169
5. Tohno E, Cosgrove DO, Sloane JP, et al. (1994) Malignant disease: primary carcinoma-ductal carcinoma in situ. In: Ultrasound diagnosis of breast disease. Churchill Livingstone, New York, pp 178–179
6. Tochio H, Konishi Y, Hashimoto T, et al. (1989) Ultrasonographic features of noninvasive breast cancer. Jpn J Medi Ultrasonics 16(suppl 2):543–544

JABTS Breast Ultrasound Training Course: Program and Results

Eriko Tohno[1], Kiyoshi Sawai[2], and the Members of the Education Committee of JABTS

Summary. The educational committee of the JABTS (Japanese Association of Breast and Thyroid Sonology) organized a breast ultrasound training course as a method for quality control. The course consisted of pre- and posttests, lectures, and small group learning. To simulate an actual examination, moving images of clinical cases were used in some of the small learning groups and the tests. After the course, although the specificity deteriorated from 75.4% to 68.0%, the sensitivity rose from 62.5% to 75.4%. The training course was considered to be effective in improving the ability to find lesions.

Key words. Breast, Ultrasound, Screening, Training, Efficacy

Introduction

We are now trying to introduce ultrasound as a modality of breast screening in Japan, but there are problems. If the examination is done using ordinary ultrasound equipment, that is, with handheld real-time scanners, cancers might be missed by technical failure, or due to lack of skill of the operators. If we were to recall women in whom any lesion was found, the recall rate would be extremely high, perhaps up to 15%. So, quality control is necessary in scanning technique, evaluation of lesions, standards for recall, and so on. There are also problems in ordinary training courses. For example, lectures are usually done in large classrooms and ultrasound is taught through still images, whereas actual ultrasound examinations are done in real time. It is difficult to train personnel in ways to find lesions. Also, there is no method to evaluate the effectiveness of the course. Thus, we set up training courses to achieve these requirements and analyzed the results.

[1] Institute of Clinical Medicine, University of Tsukuba, 1-1-1 Tennodai, Tsukuba, Ibaraki 305-8577, Japan
[2] Department of Endocrine Surgery & Breast Surgery, Kyoto Prefectural University of Medicine, Kyoto, Japan

Materials and Methods

The educational committee was organized within JABTS, the Japanese Association of Breast and Thyroid Sonology. We, the members of the committee, planned the breast ultrasound training course. The course was held for the first time in Tsukuba from January 11 to 13, and the second one was held from April 4 to 6 in Kyoto. To provide intensive teaching, the maximum number of attendees in each course was limited to 36.

The courses consisted of pretest, lectures, small group learning, and posttest. Table 1 shows the titles of the lectures, and Table 2 shows the titles of the small group learning. Following short lectures, using PC projection, attendants were asked how to analyze and categorize the ultrasound images of the cases that were distributed individually. As educational material, we provided ultrasoncgraphy (US) images of important diseases to train the ability to find lesions. Clinical cases were edited and saved on CD. Using laptop computers, the attendees observed the cases, and made the most likely diagnoses.

Before and after the course, attendees had tests to evaluate the effectiveness of the training course. Again, the attendees diagnosed moving ultrasound images of 80 cases. The average length of each case was 30 s, and the time limit for this test was 100 min.

Results

The results of the course in Tsukuba show that the sensitivity (finding lesions above category 3) rose from 62.5% to 78.1%, while the specificity dropped from 75.4% to 68.0%.

Table 1. Titles and lengths of the lectures

1. General aspects of breast diseases (30 min)
2. Scanning technique (30 min)
3. Breast ultrasound lexicon (120 min)
4. Basic aspects of ultrasound; pitfalls and artifacts (30 min)
5. US tissue characterization (30 min)
6. Standards for recall (30 min)

Table 2. Titles of the small group learning

1. Accentuating type of breast disease
2. Intermediate type and attenuating type of breast diseases
3. Nonmass-forming diseases, intraductal diseases
4. Hands-on
5. US images of important diseases
6. Practice for finding lesions

Conclusions

1. We are trying to establish an effective teaching course for quality control of breast ultrasound screening.
2. To train with real-time breast ultrasound, we made training materials consisting of moving pictures from clinical cases.
3. Pre- and posttests were done to evaluate the effectiveness of the course.
4. Although the specificity dropped, improvement of sensitivity is important to avoid missing cancers during screening.

Ductal Carcinoma In Situ of the Breast: The Pathological Reason for the Diversity of Its Clinical Imaging

Shu Ichihara[1], Suzuko Moritani[1], Tohru Ohtake[2], and Noriaki Ohuchi[3]

Summary. The hormone-sensitive epithelial cells within the lobules are the major source of ductal carcinoma in situ (DCIS) of the breast. The neoplastic cells grow, and fill and increase the volume of the spaces bound by the basement membrane until they disrupt them. Even extensive cases of DCIS are unifocal in three dimensions and are usually confined to a single segment of the mammary duct system. The neoplastic cells can proliferate within the spaces that have been altered by benign proliferative diseases such as adenosis and multiple papilloma. The concept of unfolding is the key to understanding the morphology of DCIS as well as benign breast cysts, both of which have larger and fewer structures although they originated in the small blind-ending structures within the lobules. Atypical ductal hyperplasia (ADH) can be understood as minimal low-grade DCIS that incompletely fills the spaces bound by the basement membrane. Although ADH, atypical lobular hyperplasia, and lobular carcinoma in situ (LCIS) carry a general risk for later development of invasive mammary carcinoma, DCIS carries a localized risk. The management of the DCIS should be determined based on pathological evidence including grade, size, and surgical margin status.

Introduction

A clear understanding of the normal and pathological anatomy is essential for a correct interpretation of the clinical imaging of the ductal carcinoma in situ (DCIS). For example, the fact that most DCIS originate in the epithelial cells of the ductules rather than the ducts explains why the spaces filled with noninvasive carcinoma cells always have rounded contours and are clustered close together although they measure several millimeters in size. Anatomy also indicates that the ductules have only one exit. If it is blocked, the elevated pressure in the closed spaces caused by cancerous

[1] Department of Pathology, Nagoya Medical Center, 4-1-1 Naka-ku, Nagoya 460-0001, Japan
[2] The Second Department of Surgery, Fukushima Medical University School of Medicine, 1 Hikarigaoka, Fukushima 960-1295, Japan
[3] Division of Surgical Oncology, Tohoku University Graduate School of Medicine, Aoba-ku, Sendai 980-8574, Japan

growth and accumulation of necrotic material results in fewer and larger spaces containing cancer cells and central necrosis, a so-called comedo pattern characteristic to DCIS. This report focuses on the anatomical aspects of DCIS and benign breast lesions that are relevant to understanding the diversity of their clinical imaging.

Anatomy of the Breast

The breast consists of 15 to 25 segments, or lobes. Each lobe is based on a branching duct system leading from the collecting ducts via segmental and subsegmental ducts to the lobules.

The intraductal spread of breast carcinoma occur along the duct lobular system of one lobe, with no invasion beyond the basement membrane. According to a three-dimensional reconstruction study using computer technology performed by Ohtake et al. [1], the individual duct system is arranged radially, with the nipple at the center, and shows an irregular branching pattern and a sector-shaped overall distribution.

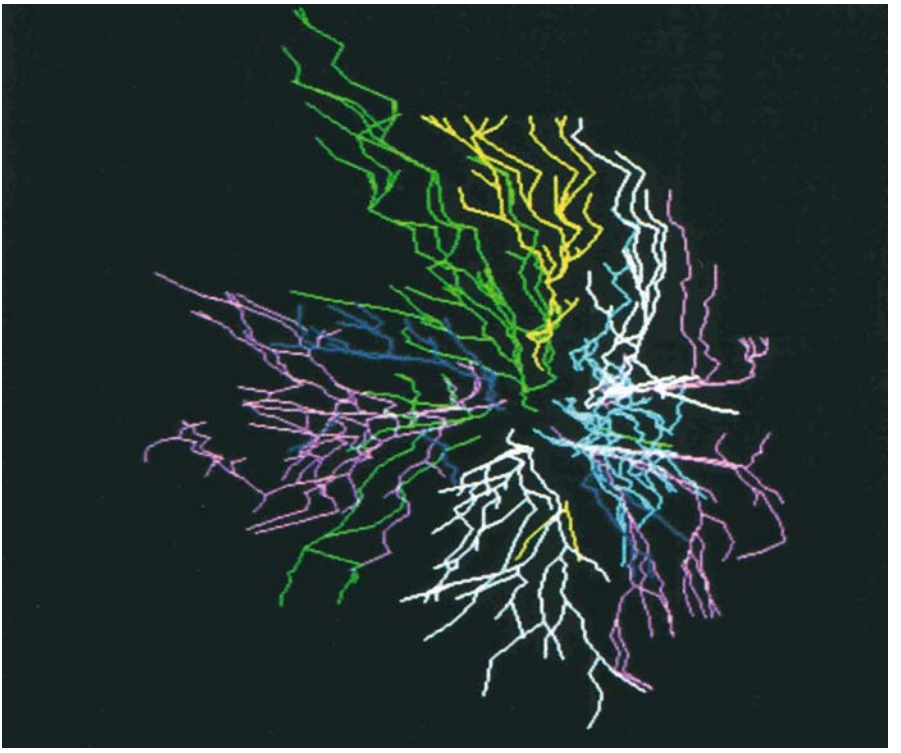

Fig. 1. Complete three-dimensional network model showing all mammary ductal/lobular system (MDLS) individually identified by different colors. This breast specimen included 16 sector-shaped MDLS exhibiting repeated and irregular branching of ducts, here shown skeletally or schematically. (From [1] with permission)

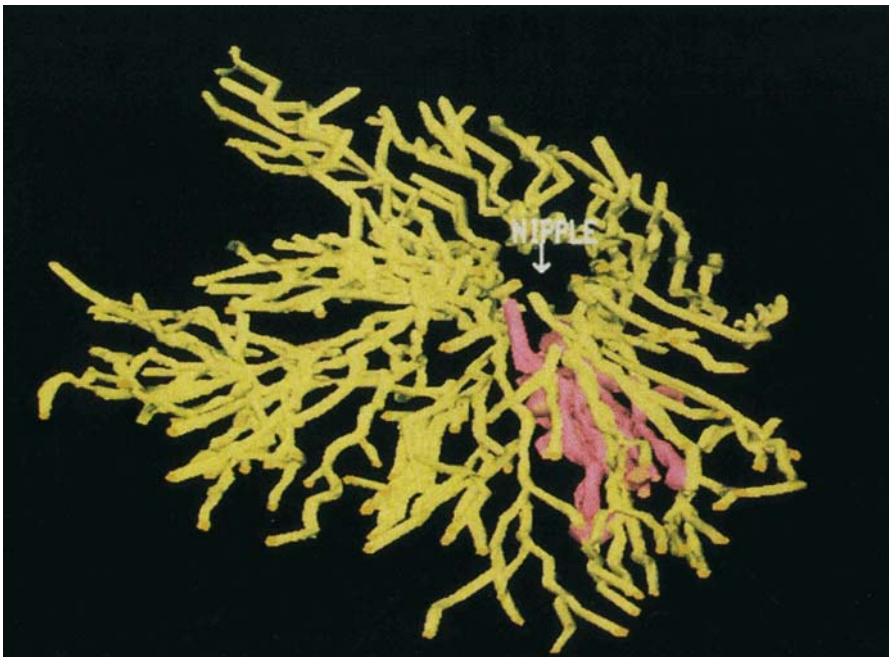

Fig. 2. Complete three-dimensional solid model of the full extent of all mammary ductal/lobular systems (MDLS) in the entire breast. All MDLS are oriented radially, with the nipple at the center (*arrow*). Not a single MDLS is involved by ductal carcinoma (DCIS) (DCIS is shown in *red* and the normal ducts are shown in *yellow*). (From [1], with permission)

Several duct systems overlap one another in the same region of the breast (Figs. 1, 2). Ohtake et al. also noted the presence of intersegmental anastomosing ducts in some of the cases they examined. However, the frequency and the clinical significance of such anastomoses are not known and will need further investigation.

The lobules are functional units for milk production. The terminal ducts give rise to multiple blind-ending branches called ductules or acini. A small portion of the terminal duct together with the ductule (acini) constitutes the lobule. The three-dimensional structure of the lobule is best understood using three-dimensional reconstruction studies, although it is also perceived on aspiration cytology specimens (Fig. 3). A normal lobule measures 0.5 to 8 mm (the average being 1–2 mm).

The breast lobules are the major sources of both benign and malignant breast diseases. Common benign lesions of the breast such as fibroadenoma, cysts, adenosis, epithelial hyperplasia, and multiple papillomas are disorders of the lobules. Furthermore, most breast malignancies also originate in the lobules.

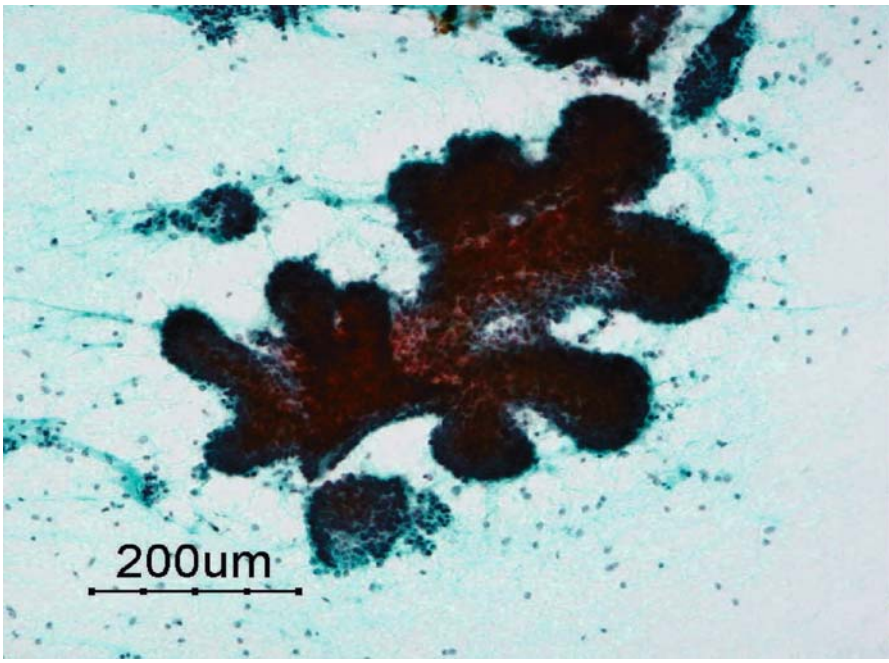

Fig. 3. A breast lobule in aspiration cytology. The three-dimensional structure of the lobule is best understood using three-dimensional reconstruction studies, although it is also perceived on an aspiration cytology specimen

Breast Cysts

The ductule has only one exit. If it is blocked, the increased hydrostatic pressure in the ductules results in a tension cyst. A few larger cysts develop by a "running together" of ductules with concomitant disappearance of the specialized lobular stroma [2]. It is important to note that the cysts can be larger than the dilated ducts in size, although they are derived from the smallest unit of the duct-lobular system. At low magnification, cysts are grouped together and always have rounded contours, demonstrating their lobular origin (Fig. 4).

Fibroadenomas

Polyclonal proliferation of both intralobular epithelial and stromal cells results in fibroadenoma. Therefore, fibroadenoma is also a disorder of the lobule. The relationship between terminal ducts and multiple blind-ending branches (ductules) is well maintained in earlier stages of fibroadenomas, which are refered to as fibroadenomatous nodules or fibroadenomatous hyperplasia. A well-developed fibroadenoma is formed by coalescence of the separate and smaller fibroadenomatous nodules; this means that a fibroadenoma enlarges by central expansion as well as accretion.

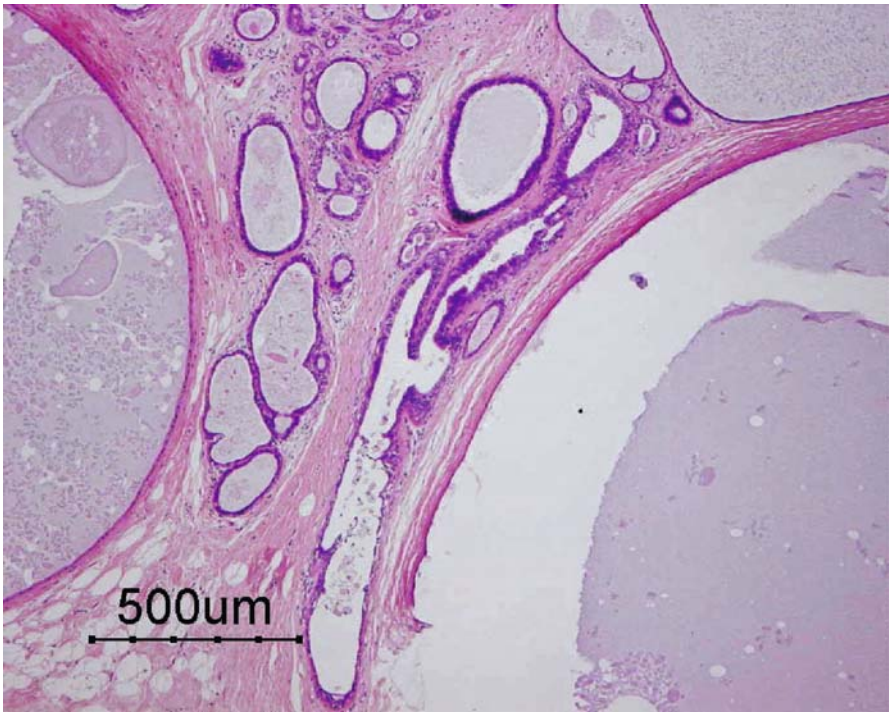

Fig. 4. Breast cysts. At low magnification, cysts are grouped together and always have rounded contours, demonstrating their lobular origin. (Hematoxylin eosin stain)

The process occurs either spontaneously or under hyperestrogenic status; it is arrested at any stage and undergoes hyalinization. Mammographic screening will detect such old fibroadenomas with characteristic coarse calcifications with a popcorn-like appearance.

Adenosis

Adenosis is a proliferation of ductules, resulting in an enlargement of the lobules. Therefore, there is an increase in the number of spaces bound by the basement membrane in adenosis. In sclerosing adenosis, the lesion acquire infiltrative margins. At low-power examination, however, an organoid pattern is recognized. A DCIS may occasionally occur in lobules exhibiting sclerosing adenosis. Such lesions may give a spurious impression of invasion. Recognizing that the space can be altered is the key to understanding the histopathological appearance and the clinical imaging of the DCIS arising in adenosis. In addition to uncomplicated sclerosing adenosis around the lesion, the clue to the correct diagnosis is the retention of lobular architecture. Demonstration of the basement membrane and myoepithelium around the ductules using the imunohistochemical technique is also helpful.

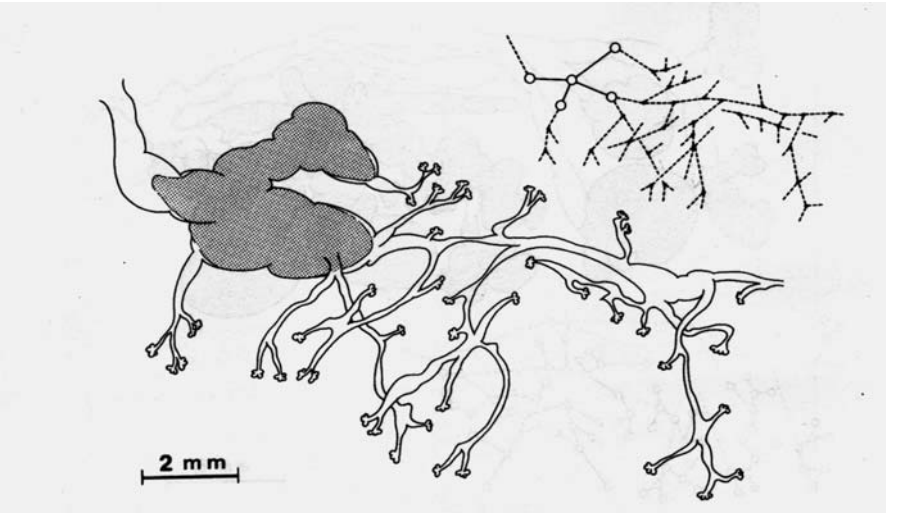

Fig. 5. A solitary papilloma involving only the large ducts. (From [3], with permission)

Papilloma

The term papilloma should be used for villous or arborescent lesions that have a fibrovascular core in the interior of their branches and which are covered by an epithelial layer [2]. In papilloma, the epithelial layer is composed of two cell types, namely, epithelial and myoepithelial cells. The basement membrane exists between the fibrovascular cores and the epithelial and myopithelial cells. Papilloma is occasionally involved by DCIS as well as epithelilal hyperplasia. When the proportion of DCIS relative to the papilloma is small in extent, the diagnosis of atypical papilloma is recommended by some authors.

Sclerosed papilloma is a variant of papilloma complicated by marked sclerosis. Such papilloma often presents a palpable lump, occasionally fixed to the overlying skin. On microscopic examination, the sclerotic areas shows distorted and entrapped epithelial elements, mimicking an invasive carcinoma. For a correct diagnosis, core-needle biopsy and even excisional biopsy may be needed. Some sclerosed papillomas are characterized by an occlusive, adenosis growth pattern surrounded by a fibrotic duct wall. A diagnosis of ductal adenoma is suitable for this variant of sclerosed papilloma.

Conventionally, papillomas are divided into solitary and multiple types. According to a three-dimensional study by Ohuchi et al. [3], solitary papilloma involved only the large ducts (Fig. 5). In contrast, multiple papillomas have their root in the lobule and may spread to the large ducts, suggesting their lobular origin (Fig. 6).

Encysted papillary carcinoma is a special type of DCIS that originates in large ducts. In contrast to the benign papilloma, the epithelial layer of the papillary carcinoma is composed only of neoplastic epithelial cells.

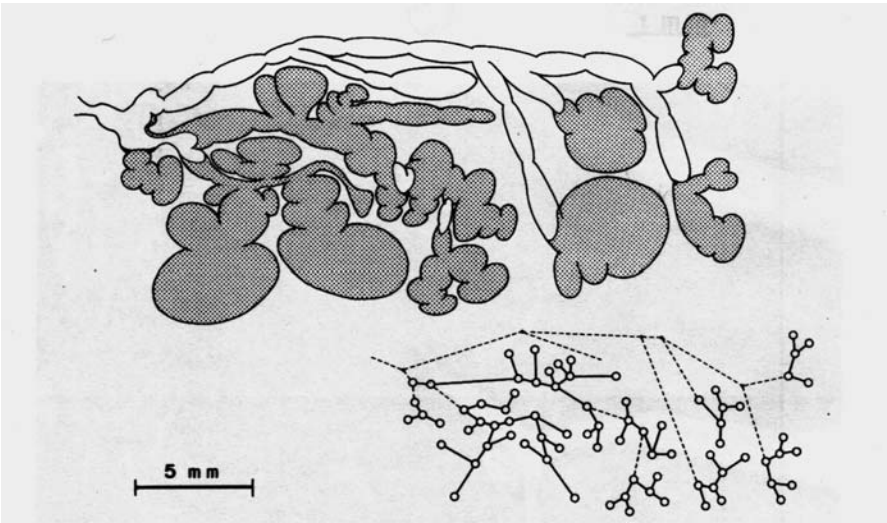

Fig. 6. Multiple papillomas with the roots in the lobule. (From [3], with permission)

Radial Scar

Radial scar consists of ducts and lobules with various amounts of epithelial hyperplasia, adenosis, or ectasia, arranged in a stellate configuration, sometimes indistinguishable from invasive carcinoma on clinical imaging. However, the epithelial elements lack cytological features of malignancy and are surrounded by basement membrane and myoepithelium. DCIS does arise in the spaces bound by the basement membrane in a radial scar. It is difficult to determine whether DCIS arise in the radial scar or preexisting adenosis involved by DCIS takes on a radial scarlike configuration. Demonstration of the basement membrane and myoepithelium around the ductules by imunohistological technique is also helpful.

Epithelial Hyperplasia

Epithelial hyperplasia is an increase in the number of benign cells in the basement membrane-bound spaces. It occurs not only in the spaces bound by the basement membrane in normal breast lobules but also those in benign conditions such as adenosis and papilloma. In mild epithelial hyperplasia, there are three or four cells above the basement membrane. Mild hyperplasia indicates no increased risk for later breast carcinoma. In moderate to severe hyperplasia, the number of cells above the basement membrane is more than four, and this constitutes a mild risk for later breast carcinoma.

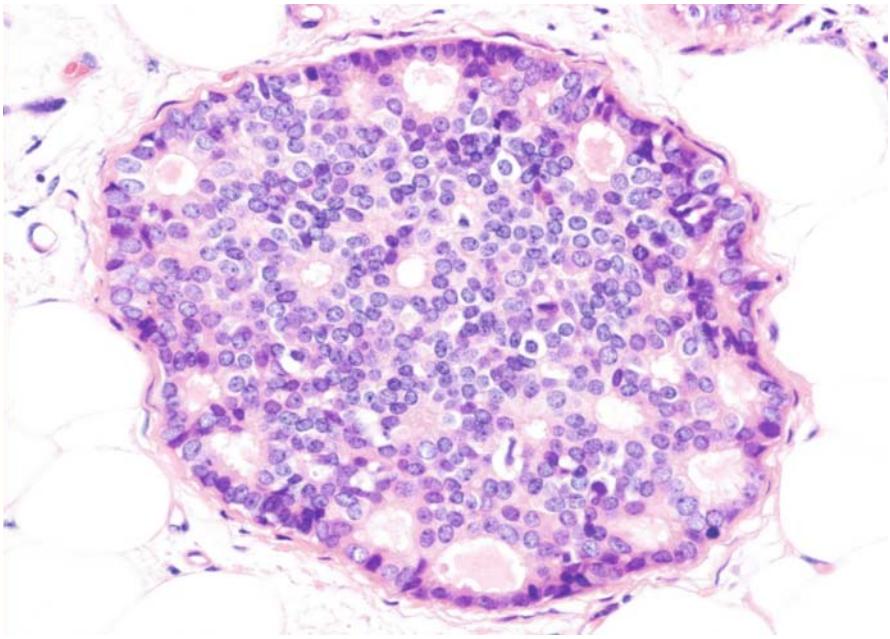

Fig. 7. Atypical ductal hyperplasia (ADH). There is a monotonous cell population resembling low-grade DCIS in the spaces bound by the basement membrane

Atypical Ductal Hyperplasia

The diagnosis of atypical ductal hyperplasia (ADH) requires the presence of a monotonous cell population resembling low-grade DCIS anywhere in the spaces bound by the basement membrane (Fig. 7). However, a major point that distinguishes ADH from low-grade DCIS is that the number of the proliferating cells is limited and the architecture is not fully developed. Lesions of ADH are usually less than 3 mm in size and confined to a lobule. Atypical ductal hyperplasia can be understood as minimal low-grade DCIS that incompletely fills the spaces bound by the basement membrane. Although atypical hyperplasia of ducal and lobular type and lobular carcinoma in situ are believed to carry a general risk for later development of invasive mammary carcinoma, ductal carcinoma in situ is considered to carry a localized risk.

DCIS

The majority of DCIS arise in the hormone-sensitive epithelial cells of the lobule of the mammary duct system. The neoplastic cells grow, then fill and increase the volume of the spaces bound by the basement membrane until they disrupt them. In a case submitted for the three-dimensional reconstruction study by Ohuchi et al. [4], two microscopic foci of DCIS were found, both of them located at the periphery (Fig. 8).

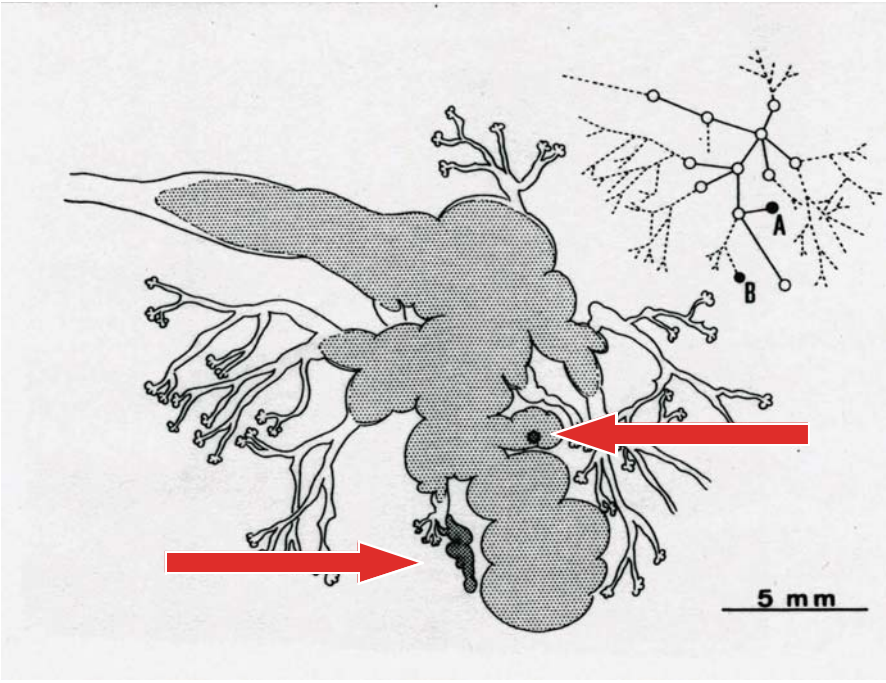

Fig. 8. Two microscopic foci of DCIS are located at the periphery of the mammary duct system. (From [4], with permission)

In another case studied by the same authors, the DCIS is located at the periphery and the papilloma is located in the large duct (Fig. 9). The lobular units distended by cancer cells are often mistaken for cancer of large ducts because of their comparatively large size. The concept of unfolding is essential for understanding the macroscopical appearances of DCIS. With unfolding, a number of small epithelial units merge to give rise to fewer but larger structures.

The origin of most breast carcinomas in the lobule is best appreciated by the study of early cancers at a very low scanning magnification. The spaces bound by the basement membrane are easily distended by increased pressure because they are mostly ductules or terminal ducts that have only one exit. Progressive distension is usually accompanied by unfolding, so that there are only a few, much larger spaces in a diseased lobule. The difference in size between normal and cancerous lobules is striking. The ductule distended and filled by DCIS gives us a false impression of ducts.

Microcalcification is an important diagnostic clue to the presence of DCIS. Microcalcifications characteristic of high-grade DCIS are summarized as follows: these are numerous, have segmental distribution, and exhibit irregularity in density, size, and shape (may be linear or branching). These points are easily understood if one considers that the calcification occurs in the necrotic material in the ductules, terminal ducts, and occasionally large ducts. Although the ductules have rounded contours, the

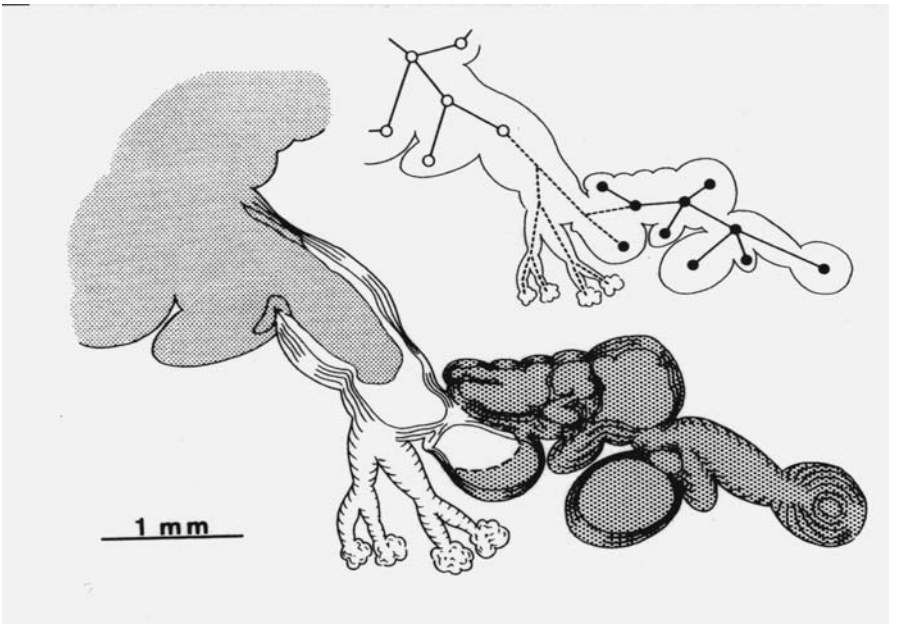

Fig. 9. The DCIS is located at the periphery and the papilloma is located in the large duct. (From [4], with permission)

terminal ducts and large ducts have treelike structures. Therefore, linear or branching calcifications suggest ductal spreading of the carcinoma cells.

Acknowledgments. We thank Prof. Ei Ueno, Dr. Tokiko Endo, Dr. Tae Niwa, and Dr. Takako Morita for encouraging us in performing this review.

References

1. Ohtake T, Kimijima I, Fukushima T, et al (2001) Computer-assisted complete three-dimensional reconstruction of the mammary ductal/lobular systems. Cancer (Phila) 91:2263–2272
2. Azzopardi JG (1979) Problems in breast pathology. W. B. Saunders, London
3. Ohuchi N, Abe R, Takahashi T, et al (1984) Origin and extension of intraductal papillomas of the breast. A 3-D reconstruction study. Breast Cancer Res Treatment 4:117–128
4. Ohuchi N, Abe R, Kasai M (1984) Possible cancerous change of intraductal papillomas of the breast. A 3-D reconstruction study of 25 cases. Cancer (Phila) 54:605–611

Ductal Carcinoma In Situ (DCIS): Incidence, Prognosis, and Diagnostic Aspects of Mammography, Galactography, and Needle Biopsies

Gunilla Svane

Summary. Ductal carcinoma in situ (DCIS) is mostly diagnosed by mammography. The incidence is between 1% and 5% in countries without widespread use of mammography, but the incidence in mammography screening programs is between 8% and 25%. However, DCIS can also be diagnosed by galactography in patients with nipple discharge, by ultrasound, and sometimes also by MRI. These methods can tell precisely how big the cancer is and exactly where in the breast. However, to morphologically verify a suspicion of malignancy from any of these imaging methods, needle biopsy can be performed. By using needle biopsy, surgery can be planned more accurately as a curative measure instead of as a diagnostic biopsy. Fine-needle biopsy with thin needles for cytological diagnosis can be used successfully, especially in DCIS of the comedo type, but this technique is more operator dependent than core-needle biopsy and vacuum-assisted biopsy techniques where small pieces of tissue are sampled for histopathological analyses and diagnosis. There are no real complications for all these techniques. Patients diagnosed with DCIS have an excellent prognosis to survive without any local recurrences and general metastases.

Key words. Breast cancer, Ductal carcinoma in situ, Mammography, Galactography, Needle biopsy

Breast cancer is the most common malignancy in women in many countries. In Europe alone, more than 300 000 cases were estimated in 1995 and approximately 124 000 women died of breast cancer [1]. However, there are geographical differences in the risk of developing breast cancer. High rates of incidence are observed, especially in Western Europe and the United States, while the incidence is low in, for example, Japan. Family history of breast cancer might be important also for the development of cancer in situ. Claus and coworkers found that patients with ductal carcinoma in situ (DCIS) were 2.4 times more likely than controls to have both mother and sister previously diagnosed with breast cancer. Their risk of developing DCIS before the age of 50 was 2.1 fold the risk of controls [2]. However, the prognosis of breast cancer is improving in some countries, most probably as a consequence of earlier

Department of Diagnostic Radiology, Karolinska Hospital, S-171 76 Stockholm, Sweden

detection by mammography and thereby earlier surgical treatment, but also because of improvement of endocrine therapy and chemotherapy of advanced tumors. Mortality in breast cancer has been reduced, especially where mammography screening programs are ongoing. In these programs, most of the tumors are stage I, without lymph node metastases and about 50% have a diameter of less than 1 cm. The prognosis for noninvasive breast cancers and of invasive cancers with a diameter of only 1 cm or less is excellent [3, 4]. Mokbel found the specific breast cancer mortality to be 0.59% for patients diagnosed with DCIS only. He found that local recurrences of DCIS are rare, only 1.4%, which can be reduced even further by radiotherapy [4].

Cancer in situ was first described 70 years ago as a tumor where the cells show marked atypia like malignant cells but the cells are not infiltrating into surrounding tissue. There are two different types of in situ cancer, the ductal type and the lobular type. The lobular type (LCIS) is usually not detected preoperatively by clinical examination or by any of our breast imaging methods. It is usually detected under the microscope when a surgical specimen of another tumor is examined.

The incidence of DCIS without any invasive tumor is very low in clinical practice, usually 1% to 3%. Rarely, DCIS presents as a palpable lump found by the patient herself or by a physician. However, in mammography screening programs DCIS is more common, usually between 8% and 25%. DCIS are mainly detected by mammography, where the tumor usually presents as calcifications but sometimes also as parenchymal distortion. Only rarely does DCIS show an increased density. Due to technical improvement of ultrasound equipment and more trained physicians performing ultrasound examinations, DCIS can nowadays be diagnosed by ultrasound as well. Also, magnetic resonance imaging (MRI) can show DCIS.

Since three to four decades ago, patients presenting with discharge from the nipple can be examined by galactography where contrast is injected into the duct from which the discharge is coming. The common finding is a lobulated filling defect corresponding to a papilloma, but irregular contrast filling defects along the ductal walls can represent epithelial proliferations that sometimes correspond to DCIS. The sensitivity of galactography for any neoplasm, according to Dinkel and coworkers, is 94% and the specificity is 55% [5]. They found sensitivity and specificity for malignancy to be slightly lower, 83% and 41%, respectively. The color of the discharge is an important factor. Hou et al. reported that cancer was found in 26.8% of patients with bloody discharge and in 13% of patients with serous discharge. No patients with discharge of other types had a malignant tumor [6]. They also found that cancer in 75.7% presented as irregular contrast filling defects whereas benign lesions showed dilatation of the ducts in 71.7% and lobular smooth contrast filling defects in 79.6%. DCIS can also be detected by fiber ductoscopy (FDS), which is used in clinical practice, especially in Japan [7]. FDS is a very sophisticated and impressive method by which the intraductal changes can be visually observed [8]. However, the most common way to detect DCIS is still by mammography, where the tumor mostly presents as clustered or scattered microcalcifications only. A meticulous evaluation of the calcifications from magnification views is necessary to correctly handle the patient and to decide if further investigations are necessary.

A morphological evaluation of the lesions to confirm the mammographic evaluation can be done by needle biopsy [8]. A benign morphological report can confirm the mammographic evaluation of a benign lesion and surgery can be avoided. When

morphology shows malignancy, surgery can be performed as a curative measure at once instead of as a surgical diagnostic biopsy. Because DCIS rarely presents as a palpable lump or a retraction of the skin, needle biopsy can rarely be performed by free-hand. Two-dimensional localization methods that can be used to sample cells or tissue from invasive cancers are usually not precise enough to sample cells or tissue from noninvasive tumors, especially because an increase in density is almost never found; this means that very little or no difference in resistance of the tumor compared to surrounding tissue can be felt through the needle. A three-dimensional localization method is necessary, especially as many of the DCIS are only a couple of millimeters in diameter and sometimes several foci of only 1 to 2 mm are separated by normal ducts. The three-dimensional stereotaxic technique has been used since 1976 in clinical practice for needle biopsies of both invasive and in situ tumors; the precision has been ±1 mm from the very beginning [9, 10].

Ultrasound guidance can be used in all tumors detected by ultrasound. The next step is to choose a needle. Both fine needles for cytological diagnosis and bigger needles for histopathology can be used. Fine-needle cytology is more demanding and very much dependent on the skill of the operators. Both the doctor performing the sampling of the cells and the cytologist reading the smears have to be well trained and experienced. An abundant amount of cells is necessary for a correct evaluation. Some DCIS show only little cell atypia and can be difficult to diagnose, whereas DCIS of the comedo type usually are easy to sample cells from and also to analyze correctly because the cells show pronounced atypia. Core-needle biopsy and vacuum-assisted biopsy are less operator dependent [11]. A fragment of tissue might be easier for the pathologist to analyze than cells only. However, it might sometimes be easier to sample representative material from the exact area by a thin needle than by a big needle, especially if the diameter of the tumor is only, 2 to 3 mm. Shortage of experienced cytologists is a problem in many places, and this is one important reason not to use fine-needle biopsy.

In general, fine-needle biopsy of DCIS is reported to result in a higher percentage of false-negative reports than core biopsy or vacuum-assisted biopsy [12, 13]. However, there are false-negative reports also when these needles are used [14]. Especially, a preoperative morphological diagnosis of atypical ductal hyperplasia (ADH) might turn out to be a false-negative report [15–17]. A postoperative diagnosis of DCIS or invasive ductal cancer can be found in some of the lesions diagnosed preoperatively as ADH. The false-negative reports for fine-needle biopsy in DCIS is generally 15% to 30%, but there are reports of 60% false-negative reports. The false-negative figures for core-needle biopsy vary from 10% to 40% depending upon the size of the needle and the number of passes. Vacuum-assisted biopsy is more precise according to some authors, but false-negative reports in 5% to 25% have been reported. A cytologist rarely can tell if the tumor is invasive. Also, tissue from core-needle biopsy and vacuum-assisted biopsy showing DCIS might turn out to correspond to an invasive cancer when the surgical specimen is examined [18–20]. However, mammography and/or ultrasound can be used to determine if the tumor is invasive. The tumor is most probably invasive when the mammograms show an increased density and/or spiculae and not only calcifications.

A preoperative evaluation of the mammograms, the galactograms, and/or the ultrasound examination performed by physicians experienced in reading the images is

essential for a correct handling of the patient even if a needle biopsy is performed. The report from the cytologist/pathologist should always be evaluated together with our breast imaging methods in order not to miss a cancer and thereby delay diagnosis of a DCIS, which then might grow to become an invasive tumor. There are almost no real complications after needle biopsy. However, there are some reports of seeding of tumor cells in the needle track after large-needle biopsy [21–23].

Local recurrences of DCIS are rare when mastectomy has been performed. Spiegel and co-workers reported no local recurrence after a mean follow-up period of 9.8 years in 44 patients with DCIS alone who were operated upon with skin-sparing mastectomy and immediate breast reconstruction [24]. Also, breast conservative surgery with postoperative radiation therapy seems to be sufficient in most of the cases. However, a radical excision is important. Aref et al. showed residual microcalcifications in 16 postlumpectomy mammograms in 90 patients with DCIS [25]. Despite peroperative radiography of the excised specimen, a postoperative mammography examination might be necessary to verify that all calcifications have been excised, especially if the calcifications are scattered and not in a small cluster.

References

1. Bray F, Sankila R, Ferlay J, et al (2002) Estimates of cancer incidence and mortality in Europe in 1995. Eur J Cancer 39:99
2. Claus EB, Stowe M, Carter D (2003) Family history of breast and ovarian cancer and the risk of breast cancer in situ. Cancer Res Treat 78(1):7–15
3. Tabár L, Dean P, Kaufman CS, et al (2000) A new era in the diagnosis of breast cancer. Surg Oncol Clin N Am 9(2):233
4. Mokbel K (2003) Towards optimal management of DCIS of the breast. Eur J Surg Oncol 29(2):191–197
5. Dinkel HP, Gassel AM, Muller T, et al (2001) Galactography and exfoliative cytology in women with abnormal nipple discharge. Obstct Gynecol 784:625–629
6. Hou MF, Huang TJ, Liu GC (2001) The diagnostic value of galactography in patients with nipple discharge. Clin Imaging 25(2):75–81
7. Okazaki A, Hirata K, Okazaki M, et al (1999) Nipple discharge disorders: current management and the role of fiber-ductoscopy. Eur Radiol 9:583–590
8. Martin HE, Ellis EB (1930) Biopsy by needle puncture and aspiration. Ann Surg 92: 169–181
9. Nordenström B, Rydén H, Svane G (1981) Breast. In: Zornoza J (ed) Percutaneous needle biopsy. Williams & Wilkins, Baltimore, p 43
10. Svane G, Silfverswärd C (1983) Stereotaxic needle biopsy of non-palpable breast lesions. Cytologic and histopathologic findings. Acta Radiol Diagn 24 (4):283
11. Elvin A, Andersson T, Jaremko G, et al (1994) Significance of operator experience in diagnostic accuracy of biopsy gun biopsies. Eur Radiol 4:430
12. Lifrange E, Kridelka F, Colin C (1997) Stereotaxic needle core biopsy and fine needle aspiration biopsy in the diagnosis of non-palpable breast lesions: controversies and future prospects. Eur J Radiol 24:39
13. Leifland K, Lundquist H, Lagerstedt U, et al (2003) Comparison of preoperative simultaneous fine needle aspiration biopsy and core needle biopsy in ductal carcinoma in situ of the breast. Acta Radiol Diagn 44:213–217
14. Liberman L, la Trenta LR, Van Zee KJ, et al (1997) Stereotaxic core biopsy of calcifications highly suggestive of malignancy. Radiology 203:673

15. Cangiarella J, Waisman J, Symmers WF, et al (2001) Mammotome core biopsy for mammary microcalcification: analysis of 160 biopsies from 142 women with surgical and radiological follow up. Cancer (Phila) 119(1):173
16. Adrales G, Turk P, Wallace T, et al (2000) Is surgical excision necessary for atypical ductal hyperplasia of the breast diagnosed by Mammotome? Am J Surg 180(4):313
17. Joshi M, Duva-Frissora A, Padmanabhan R, et al (2001) Atypical ductal hyperplasia in stereotactic breast biopsies: enhanced accuracy of diagnosis with the mammotome. Breast J 7(4):207
18. Renshaw AA (2002) Predicting invasion in the excision specimen from breast core needle biopsy specimens with only ductal carcinoma in situ. Arch Pathol Lab Med 126(1):39–41
19. King TA, Farr GH Jr, Cederbom GJ, et al (2001) A mass on breast imaging predicts coexisting invasive carcinoma in patients with a core biopsy diagnosis of ductal carcinoma in situ. Am Surg 67(9):907–912
20. Wahedna Y (2001) Mammographic size of ductal carcinoma in situ does not predict the presence of an invasive focus. Eur J Cancer 37(4):459–462
21. Diaz LK, Wiley EL, Venta LA (1989) Are malignant cells displaced by large-gauge needle core biopsy of the breast? AJR (Am J Roentgenol) 173(5):1303–1313
22. Stolier A, Skinner J, Levine EA (2000) A prospective study of seeding of the skin after core biopsy of the breast. Am J Surg 180(2):104–107
23. Davies JD, Nonni A, D'Costa HF (1997) Mammary epidermoid inclusion cysts after wide-core needle biopsies. Histopathology (Oxf) 31(6):549–551
24. Speigel AJ, Butler CE (2003) Recurrence following treatment of DCIS with skin-sparing mastectomy and immediate breast reconstruction. Plast Reconstr Surg 111(2):706–711
25. Aref A, Youssef E, Washington T, et al (2000) The value of postlumpectomy mammogram in the management of breast cancer patients presenting with suspicious microcalcifications. Cancer J Sci Am 6(1):11–12

The Ultrasonic Diagnosis of Nonpalpable DCIS Without Calcification on MMG and Nipple Discharge: Advocacy of a New Term, 3 Non-DCIS

Koji Takebe and Ayumi Izumori

Summary. Ductal carcinoma in situ (DCIS) has been detected primarily by palpation, calcification on mammogram (MMG), and nipple discharge. Ultrasonographic investigation of DCIS has been performed, but has not up to now revealed any form of DCIS that could not be discovered by the above three methods. In the present report, we describe a form of DCIS that has not been detected by earlier methods, and propose to refer to this new DCIS as 3 non-DCIS to distinguish it from conventional DCIS: 3 non-DCIS represents nonpalpable DCIS without calcification on MMG and without nipple discharge. Only the method of ultrasound screening described in this chapter can detect 3 non-DCIS. We diagnosed 23 patients as 3 non-DCIS at this institution between May 1997 and March 2003. There was neither calcification, mass, nor distortion on MMG in these patients. On ultrasonography, a small mass measuring 10 mm or less was revealed. Thorough examination by fine-needle aspiration cytology showed 90% of the patients were positive. On analysis of subtype of DCIS, 22 of the 23 cases of DCIS were classified into pure noncomedo type and 1 was mixed type. Lesions in 3 non-DCIS were frequently less extensive than those in conventional DCIS.

Key words. Ductal carcinoma in situ, Ultrasonography, Nonpalpable breast cancer, Breast conservation therapy

Introduction

Ductal carcinoma in situ (DCIS) has been detected primarily by palpation, calcification on mammogram (MMG), and nipple discharge. Ultrasonographic investigation of DCIS has been performed but has not up to now revealed any form of DCIS that could not be discovered by these three methods [1, 2]. In the present report, we describe a form of DCIS that has not been detected by earlier methods, and propose to refer to this new DCIS as 3 non-DCIS to distinguish it from the conventional DCIS. Thus, 3 non-DCIS represents nonpalpable DCIS without calcification on MMG and without nipple discharge. Only the method of ultrasound screening described in this report can detect 3 non-DCIS.

Takebe Breast Care Clinic, Tahishimomachi 365-9, Takamatsu 761-8075, Japan

We diagnosed 23 patients as 3 non-DCIS at this institution between May 1997 and March 2003. There was neither calcification, mass, nor distortion on MMG in these patients. On the ultrasonograph, a small mass measuring 10 mm or less was revealed. Thorough examination by fine-needle aspiration cytology showed 90% of the patients were positive. On analysis of subtype of DCIS, 22 of the 23 cases of DCIS were classified into pure noncomedo type and 1 was mixed type. Lesions in 3 non-DCIS were frequently less extensive than those in old DCIS.

The Crux of Detecting 3 Non-DCIS

We performed ultrasonography with a unit of SSD-1000 (Aloka) of annular alley type. To detect 3 non-DCIS, we need to discover a very slight change in the breast on ultrasound whole-breast scanning. It is hard to detect 3 non-DCIS by just looking for a mass. It is important for ultrasonographers to have their attention concentrated on the continuity of internal patterns of the breast structure on the border between the mammary region and adipose tissue, and the duct, mottle, and adipose tissues, to instantly catch any fine break in the continuity of the monitoring images [3].

Findings on Ultrasonography

The ultrasound findings in the 23 cases (Fig. 1) were classified into five groups. (1) Relatively well-defined small masses were detected in 18 cases. The major diameter of the masses was 3–10 mm on ultrasonograph. The lesions were too small to

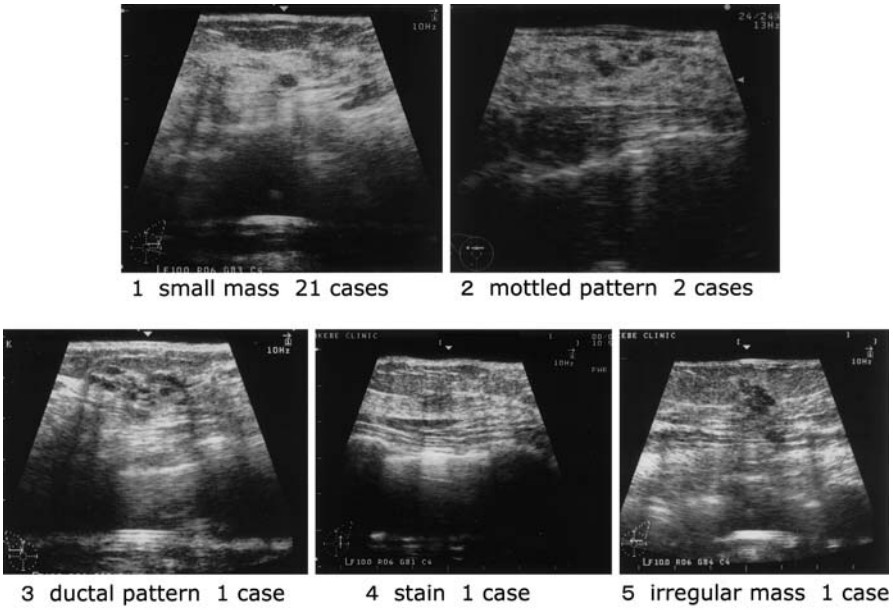

Fig. 1. Ultrasonography (US) findings of 3 non-DCIS

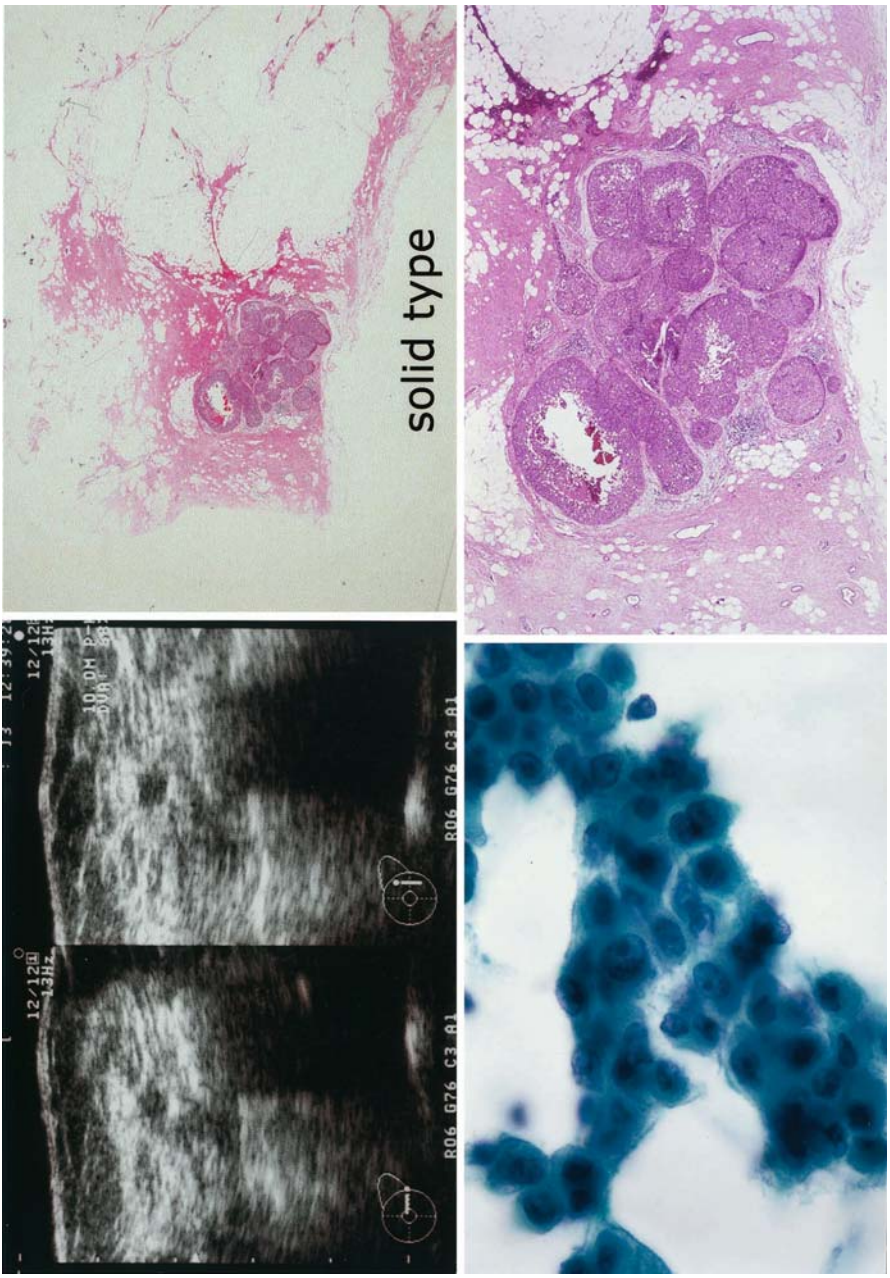

FIG. 2. Case 1. A 68-year-old woman was found to have a low-echo area measuring 5 mm in the left breast on mass screening. The area was well defined, with a small DW ratio, and the findings appeared to be suggestive of a benign cyst or adenoma. A large amount of slightly atypical cells were obtained by fine-needle aspiration cytology, and class 5 (suspected papillotubular cancer) was diagnosed. Pathologically, the lesion was a localized solid-type ductal carcinoma in situ (DCIS)

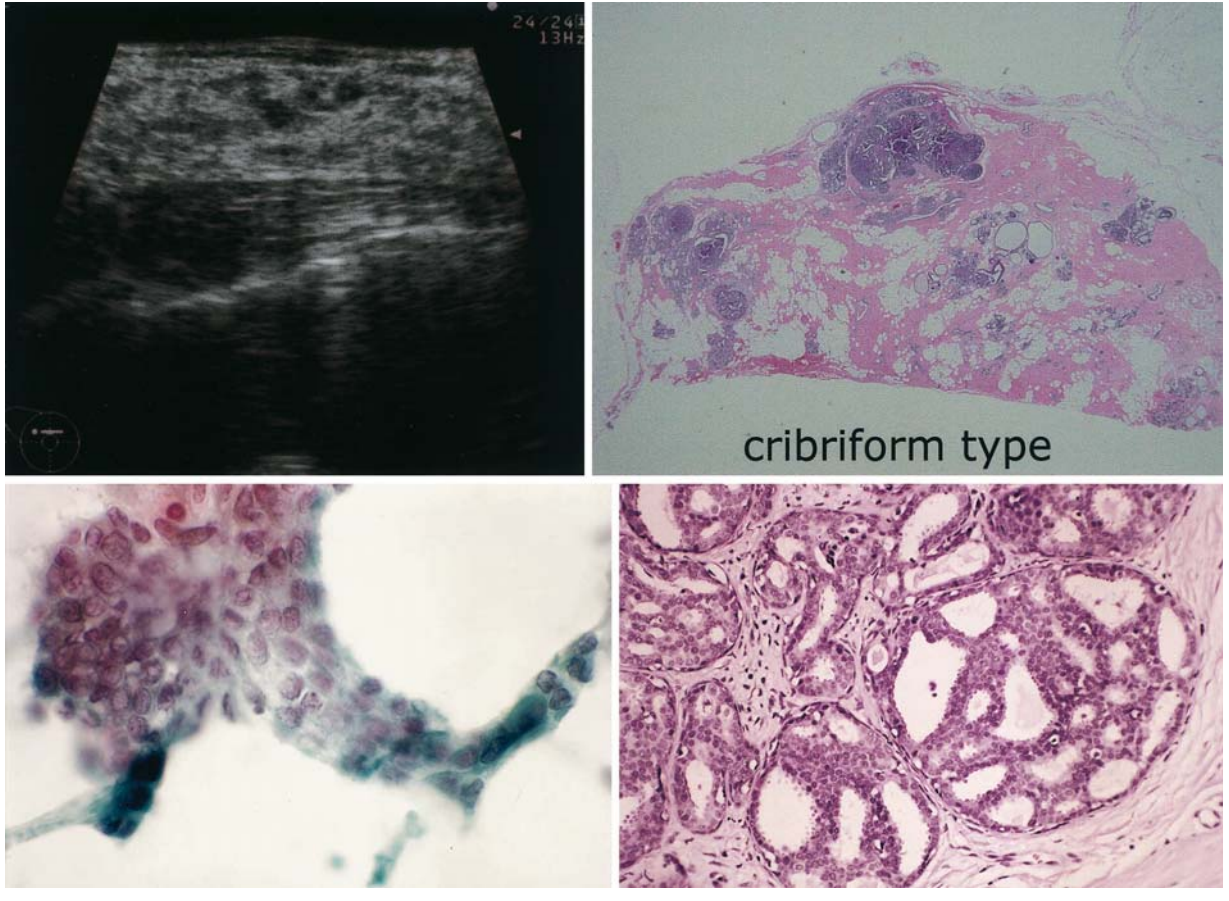

FIG. 3. Case 2. A 46-year-old woman came to the hospital because of premenstrual pain in the breasts. There was an area measuring 10 mm in diameter with slight irregularity in the mottled pattern at the upper region of the right breast. Because fine-needle aspiration cytology yielded a large amount of strongly atypical cells, class 5 (suspected invasive cancer) was diagnosed. Histopathological examination showed a cribriform-type DCIS spread over an area measuring 30 mm

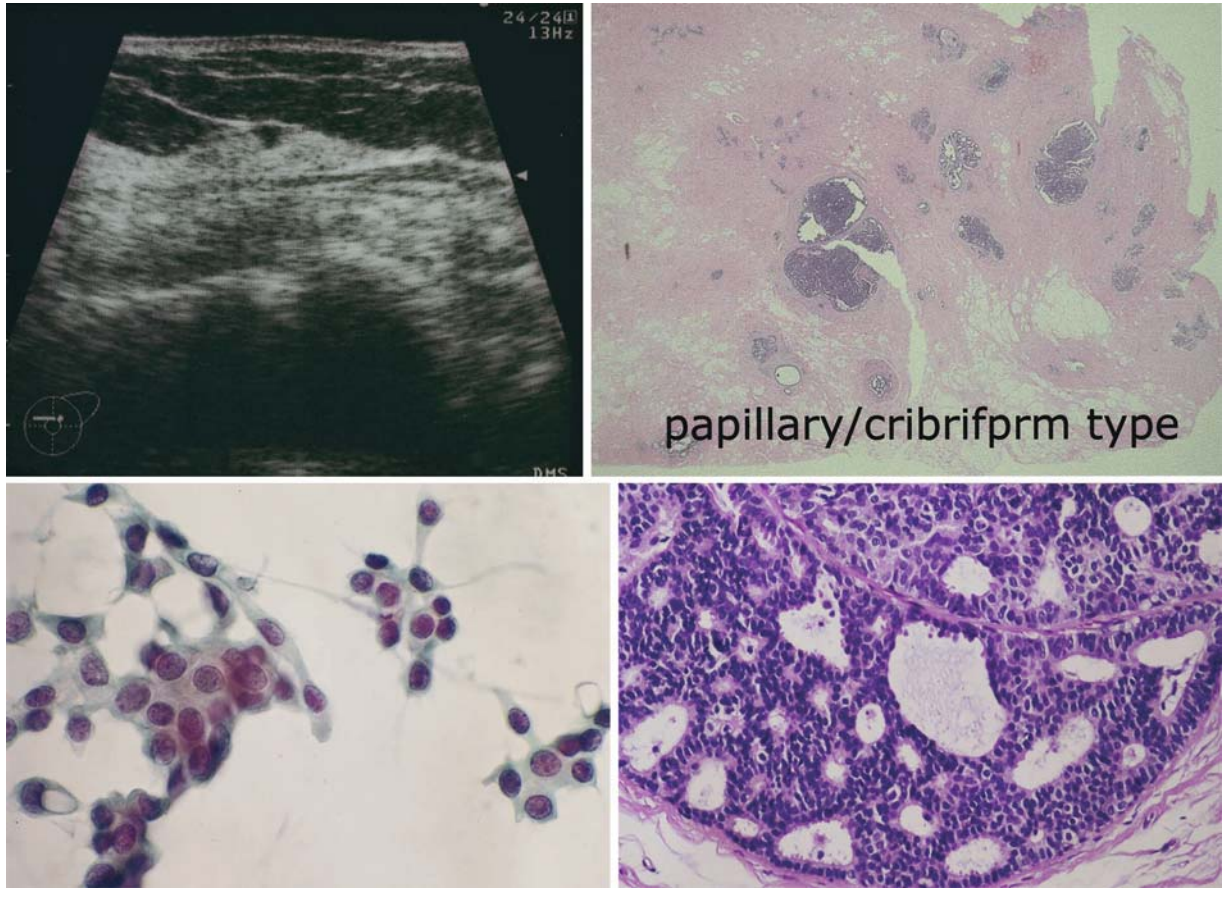

FIG. 4. Case 3. A 67-year-old woman was diagnosed as having a cystic lesion measuring 3 mm at the upper region of the right breast on mass screening. Surrounding it were several smaller low-echo areas in a segment. The diagnosis by cytology was class 4 (suspected DCIS). Histopathological examination revealed a papillary-type DCIS spread over a 50-mm area. In such older patients, especially those who had menopause 10 years or more before, small cystic lesions in the breast frequently seem to be DCIS, and therefore, fine-needle aspiration cytology should be actively performed

evaluate the shape, internal echo, and DW ratio, etc. There was no attenuation in posterior echoes. (2) An irregular mottled pattern within a 10-mm area was detected in 2 cases. (3) A cluster of ducts with a dilated ductal pattern was seen in 1 case. (4) There was a stain, a poorly defined area with lower echoes than those in the surrounding mammary gland tissue; it was termed a "stain" because it seemed like a stain on a shirt that cannot be cleaned by washing. (5) Typical ultrasonographic findings for breast cancer, that is, an irregular mass invading adipose tissue, appeared in 1 case.

Close Examination

Fine-needle aspiration cytology alone was performed, and core-needle biopsy was not used. Core-needle biopsy is too expensive to use in evaluating 3 non-DCIS because needle biopsy at many sites is needed. In addition, we consider that cytology with a fine needle is more convenient in accurately inserting a needle to reach a small lesion measuring only approximately 5 mm. Fine-needle aspiration is performed manually without using an adapter. A 7-cm, 23-gauge needle is inserted at a site on the right side of a scanner under the guidance of ultrasound. Caution should be taken in handling the needle so it does not stick out of the lesion. Considerable amounts of cell specimens were collected by aspiration in all of the 23 cases with 3 non-DCIS. The results of cytology were evaluated as class 5 (suspected invasive cancer) in 3 cases, class 4 (suspected DCIS) in 15 cases, class 3b (suspected DCIS, but papilloma cannot be ruled out) in 2 cases, and class 3a (suspected papilloma) in 2 cases. The sensitivity of cytology was considered 90% if class 3b or more severe classes are considered positive. This finding shows that fine-needle aspiration cytology allows diagnosis without using core-needle biopsy.

Histological Findings

Almost all the histopathological findings in cases of 3 non-DCIS (Table 1) indicated the features of noncomedo type of DCIS. Only 1 case was evaluated as a significant mixed type. Thin slices with the thickness of 5 mm of tissue specimens were examined. Localized lesions were found in 13 cases, lesions measuring 4 cm or less in 9 cases, and extended lesions measuring more than 4 cm in 4 cases. DCIS lesions were smaller in cases of 3 non-DCIS than DCIS with calcification diagnosed in our facility.

Table 1. Pathological features of 3 non-DCIS

FNAC	Class IIIa	Class IIIb	Class IV	Class V
	2	2	14	8
Subtype	Pure noncomedo	Comedo mixed	Pure comedo	
	25	1	0	
Spread	No spread	Spread ≦4 cm	Spread >4 cm	
	13	9	4	

DCIS, ductal carcinoma in situ; FNAC, fine-needle aspiration cytology

Table 2. Differential diagnosis of small cystic lesion

	Concentrated cyst?	DCIS?
Age (years)	Less than 40	More than 60
Size	Less than 3 mm, more than 10 mm	3–10 mm
Shape	Regular	Irregular
Spread	Scattered	Solitary or clustered
Internal echo	Homogeneous	Irregular
Posterior echo	Attenuated	Unchanged

Differential Diagnosis

On ultrasonography, a cyst, especially one containing condensed material, is hard to differentiate from 3 non-DCIS. Even a skilled investigator with long experience finds it hard to differentiate the two only by findings on ultrasonography. Differentiation of the two needs the investigation of the following factors. DCIS was frequently detected in older patients (Table 2). The area of concern is likely to be a cyst if posterior echoes attenuate and to be DCIS if posterior echoes do not change. The posterior echo attenuation is the point of differentiation between a cyst and palpable carcinomas. It is impossible to differentiate 3 non-DCIS from papilloma on an ultrasonograph. Screening skill and high diagnostic ability are required for differential diagnosis.

Results of Screening

The results of a mass screening by whole-breast scanning using ultrasonography follow. The greatest proportion of the participants were enrolled in this hospital. The number of participants includes that of repeat participants. Over 6 years, 12 404 persons were examined and 60 were diagnosed as having breast cancer; 29 had nonpalpable breast cancer and 14 had 3 non-DCIS. The detection rate of breast cancer by the above method was 0.48%, which is more than four times the detection rate by macroscopic observation combined with palpation in Japan, and higher than that by mammography. This high detection rate is due to the detection of nonpalpable breast cancers, especially 3 non-DCIS. With skills to diagnose 3 non-DCIS, ultrasonography will be more useful than mammography.

Concept of 3 Non-DCIS

There is a question about DCIS that has remained unresolved for us. Invasive carcinoma is not confined to those cases of carcinoma that show calcification on MMG or which are accompanied by discharge from the nipple. Of all cases of invasive carcinoma, calcification is positive on MMG in about half of all cases, and the percentage of invasive carcinoma accompanied by nipple discharge is lower and estimated to be about 10%. Most invasive carcinoma should first assume the form of DCIS within the breast. Then, why do most of the nonpalpable small DCIS undergo calcification? Why

is their detection precipitated only by discharge from the nipple? There should be many cases of DCIS not accompanied by calcification or nipple discharge. We think 3 non-DCIS represents such cases of DCIS.

In Western countries, the outcome of breast conservative therapy for DCIS shows that lumpectomy alone resulted in recurrence of 15% or more, and lumpectomy combined with radiotherapy resulted in recurrence of 10% or more [4, 5] . Most DCIS is detected on the basis of calcification on MMG in Western countries. Of 15 patients with 3 non-DCIS in whom we performed breast conservative therapy in the previous and present hospitals, all have survived for 5 years, and no recurrence has been noted in these patients. Although no inference can be made from the results of such a small number of cases, localized lesions and noncomedo type of DCIS, as evaluated on histopathological examination, are likely to have contributed to such a low recurrence rate. We consider that breast conservative therapy should be indicated for 3 non-DCIS separately from regular DCIS in each treatment plan.

Conclusion

1. The category 3 non-DCIS is nonpalpable DCIS without calcification on MMG and without nipple discharge.
2. Diagnosing 3 non-DCIS requires excellent ability on the part of the investigator in detecting small lesions on the ultrasonograph, the accurate application of fine-needle aspiration, and experience in diagnosing by cytology.
3. Frequently, 3 non-DCIS is revealed as a well-defined mass on the ultrasonograph. Small cystic lesions (approximately 5 mm) in elderly patients who had menopause 10 years or more before were frequently diagnosed as 3 non-DCIS.
4. In the present cases of 3 non-DCIS, the histopathological type was diagnosed as noncomedo type, which was more localized than DCIS with calcification.

References

1. Ueno E (1996) Recent progress of imaging diagnosis for breast cancer: breast ultrasound and color Doppler. Jpn J Breast Cancer 11(2):216–231
2. Kamio T, Kameoka S, Muraki H, et al. (1991) Significance of ductal findings in ultrasonic examination of the breast. Diagnosis of intraductal tumor and intraductal spreading of braeast cancer. In: Topics in breast ultrasound. Shinohara, Tokyo, pp 200–205
3. Takebe K, Nakamura K, Yamamoto Y (1999) The contribution of ultrasound examination to the diagnosis of nonpalpable breast cancer. Jpn J Breast Cancer 14(4):444–450
4. Fisher B, Dignam J, Walmark N, et al. (1998) Lumpectomy and radiation therapy for the treatment of intraductal breast cancer: findings from National Ajduvant Breast and Bowel Project B17. J Clin Oncol 16:441–452
5. Julien JP, Bijker N, Fentiman IS (2000) Radiotherapy in breast-conserving treatment for ductal carcinoma in situ: first results of the EORTC randomaised phase III trial 10853. Lancet 355:528–533

Ultrasonic Diagnosis of Non-Mass Image-Forming Breast Cancer

Isamu Morishima[1], Ei Ueno[2], Eriko Tohno[2], Hiroko Tsunoda-Shimizu[3], Yuka Kujiraoka[4], and Masako Takasaki[2]

Summary. We investigated the characteristics of non-mass image-forming breast cancer and the relationship between non-mass image-forming breast cancer and ductal carcinoma in situ (DCIS). We reviewed 47 non-mass image-forming breast cancers and 75 ultrasonic images of DCIS. We classified non-mass image-forming breast cancers into four subtypes: a homogeneous pattern, a ductal pattern, a mottled pattern, and a geographic pattern. The 47 cases were classified into 2, 6, 12, and 27 cases, respectively. Histological findings were 24 DCIS, 19 invasive ductal carcinomas with predominant intraductal components, and 4 invasive carcinomas. The 16 of 27 cases with a geographic pattern included invasive components. The 15 of 24 geographic cases had a comedo type of intraductal component. Of the 75 cases of DCIS, 51 cases were a mass image-forming type and 24 cases were a non-mass image-forming type. The histological findings for non-mass image-forming breast cancer tend to be DCIS and/or invasive ductal carcinoma with a predominant intraductal component. The geographic pattern often contained invasive components. The geographic pattern and/or the lesion with echogenic spots often had a comedo type. These results revealed the close relationship between the progress of breast cancer and ultrasonic imaging.

Key words. Ultrasonic diagnosis, Non-mass image-forming breast cancer, DCIS

Introduction

The diagnosis of non-mass image-forming lesions is still controversial, but it is important because some cases of breast cancer present such images. The purpose of this study is to investigate the characteristics of non-mass image-forming breast cancer and particularly the relationship between non-mass image-forming breast cancer and ductal carcinoma in situ (DCIS).

[1] Tsukuba Medical Center Hospital, 1-3-1 Amakubo, Tsukuba, Ibaraki 305-0005, Japan
[2] University of Tsukuba, Tsukuba, Ibaraki, Japan
[3] St. Lukes International Hospital, Tokyo, Japan
[4] Tsukuba Memorial Hospital, Ibaraki, Japan

Materials and Methods

We reviewed 47 non-mass image-forming breast cancers to compare ultrasonic images and histological findings. The lesions were nonpalpable in 24 cases and palpable in 23 cases. In addition, 9 of the 24 nonpalpable cases had abnormal nipple discharge and 2 of the 23 palpable cases had abnormal nipple discharge. These cases were encountered at Tsukuba University Hospital between January 1995 and December 2002 and at Tsukuba Medical Center Hospital between May 1999 and December 2002. Ultrasonic equipment used was a Toshiba SSA-250A, a LOGOQ 700MR, an ATL HDI 5000, and an Aloka SSD 5500. In the next step, we examined 75 ultrasonic images of DCIS during the same period.

According to the echoic patterns of the mammary gland with the lesions, we classified non-mass image-forming breast cancers into four subtypes: a homogeneous pattern, a ductal pattern, a mottled pattern, and a geographic pattern. The homogeneous pattern is defined as displaying a uniform echoic pattern. The echo level varies from high to low. The ductal pattern is defined as displaying a dilated duct extending to the periphery beyond the subareolar area without extraductal mass. The mottled pattern is defined as displaying a number of small, island-like low echoic areas in the mammary parenchyma. The geographic pattern is defined as displaying an irregular low echoic area, including an aggregation of small, island-like low echoic areas (Figs. 1–5).

Results

The 47 cases were classified into 2 cases with a homogeneous pattern, 6 with a ductal pattern, 12 with a mottled pattern, and 27 with a geographic pattern. Histological findings of 47 cases were 24 DCIS, 19 invasive ductal carcinomas with predominant intraductal components (including 9 cases with microinvasive carcinoma), 3 invasive ductal carcinomas, and 1 invasive lobular carcinoma [1–3]. Twenty-four of 47 cases, 51.1%, were DCIS; 33 of 47 cases, 70.2%, were DCIS and microinvasive ductal carcinoma; 43 of 47 cases, 91.5%, were DCIS and invasive ductal carcinoma with a predominant intraductal component. These results indicate that the histological findings for non-mass image-forming breast cancer tend to be DCIS and/or invasive

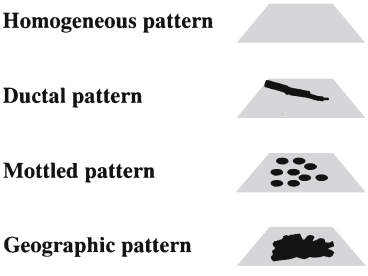

Fig. 1. Subtypes of ultrasonic images

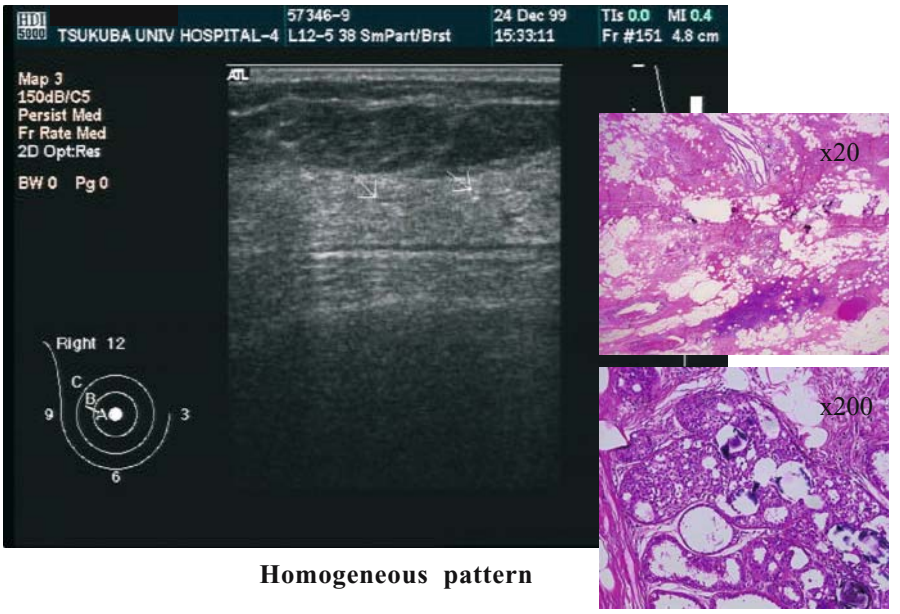

FIG. 2. A case with a homogeneous pattern. The patient is 56 years old. Echogenic spots are seen in the uniform mammary parenchyma. The histological diagnosis was a non-comedo type of ductal carcinoma in situ (DCIS)

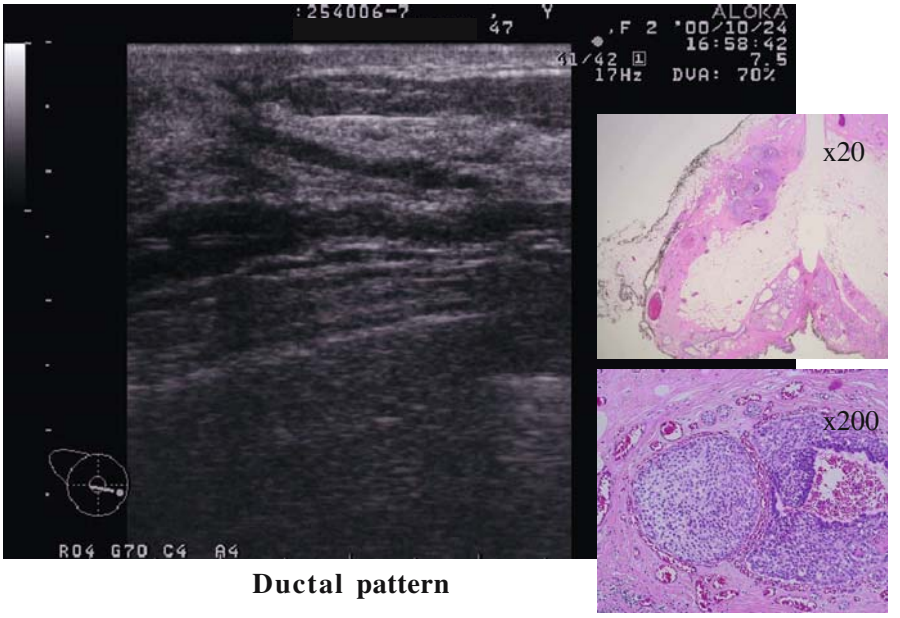

FIG. 3. A case with a ductal pattern. The patient is 47 years old, with bloody nipple discharge. A single dilated duct with internal echoes is seen. The histological diagnosis was a solid type of DCIS

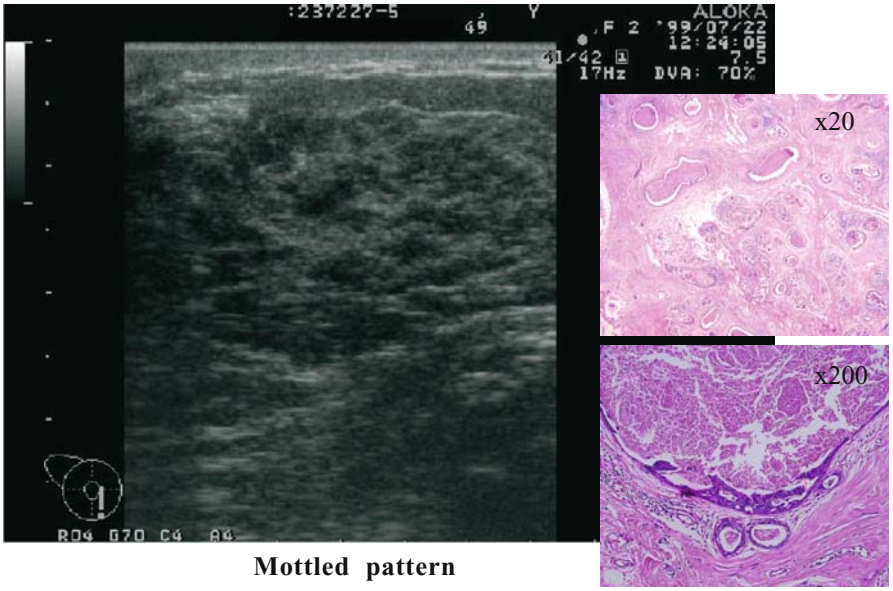

FIG. 4. A case with a mottled pattern. The patient is 49 years old. Some small island-like low echoic areas are seen in the mammary parenchyma. The polarity of the low echoic area is disturbed. The histological diagnosis was microinvasive ductal carcinoma, and intraductal components were a comedo type

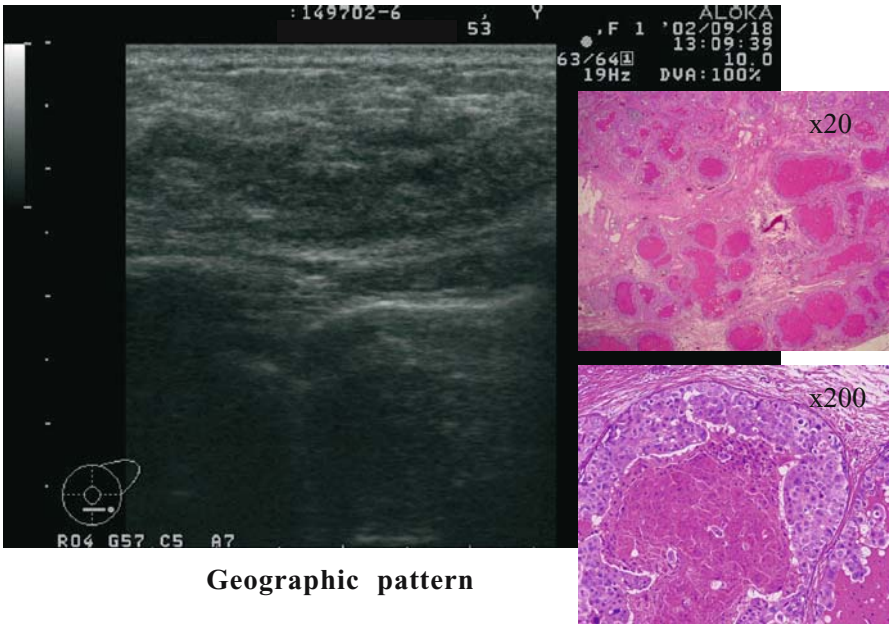

FIG. 5. A case with a geographic pattern. The patient is 53 years old. An irregular low echoic area is seen. The histological diagnosis was microinvasive ductal carcinoma, and intraductal components were a comedo type

Table 1. Relationship between ultrasonic images and histological findings

Pattern	DCIS	IDC with a predominant intraductal component		IDC	ILC	Total
		Microinvasive	Others			
Homogeneous	2	0	0	0	0	2
Ductal	5	1	0	0	0	6
Mottled	6	4	1	0	1	12
Geographic	11	4	9	3	0	27
Total	24	9	10	3	1	47

DCIS, ductal carcinoma in situ; IDC, invasive ductal carcinoma; ILC, invasive lobular carcinoma

ductal carcinoma with a predominant intraductal component. Another important point is that, with attention to the subtypes of the ultrasonic images, 16 of 27 cases with a geographic pattern, 59.3%, included invasive components. Cases with a geographic pattern had a high rate of having invasive components (Table 1).

We divided intraductal components into either a non-comedo type or a comedo type. With attention to the subtypes of the ultrasonic images, 15 of 24 geographic cases, 62.5%, had a comedo type of intraductal component. There was a high rate of the comedo type in cases with a geographic pattern. Twenty-four cases had echogenic spots. Fifteen of 24 cases, 62.5%, had a comedo type of intraductal component (Fig. 6). In conclusion, the geographic pattern and/or the lesion with echogenic spots tends to have a comedo type of intraductal component (Table 2).

Of the 75 cases of DCIS, 51 cases, 68%, were a mass image-forming type and 24 cases, 32%, were a non-mass image-forming type. Of the 51 cases that were a mass image-forming type, 39 cases formed an image of a mass, 7 cases formed an image of duct dilatation and a mass, and 5 cases formed an image of an intracystic mass. Previously we have explained that 51.1% of the non-mass image-forming breast cancer was DCIS. On the other hand, nearly 70% of DCIS presented with the mass image-forming type, with features that were mainly small and/or multiple masses (Table 3).

Discussion

From these results, we considered the relationship between the progress of breast cancer and ultrasonic imaging.

First, breast cancer occurs at the terminal duct lobular units (TDLU) of a single segment of the mammary gland and proliferating cells fill the ducts [4, 5]. When cancer cells proliferate intraductally in a relatively localized area, the image displays a small mass. When the cancer cells spread predominantly to the central side with the accumulation of secretion, the image displays a ductal pattern. In DCIS, the cancer cells proliferate within the ducts without acquiring infiltrating ability [6]. According to the grade of proliferation of cancer and interaction between the intraductal component and the stroma, they present a homogeneous pattern, a mottled pattern, or a

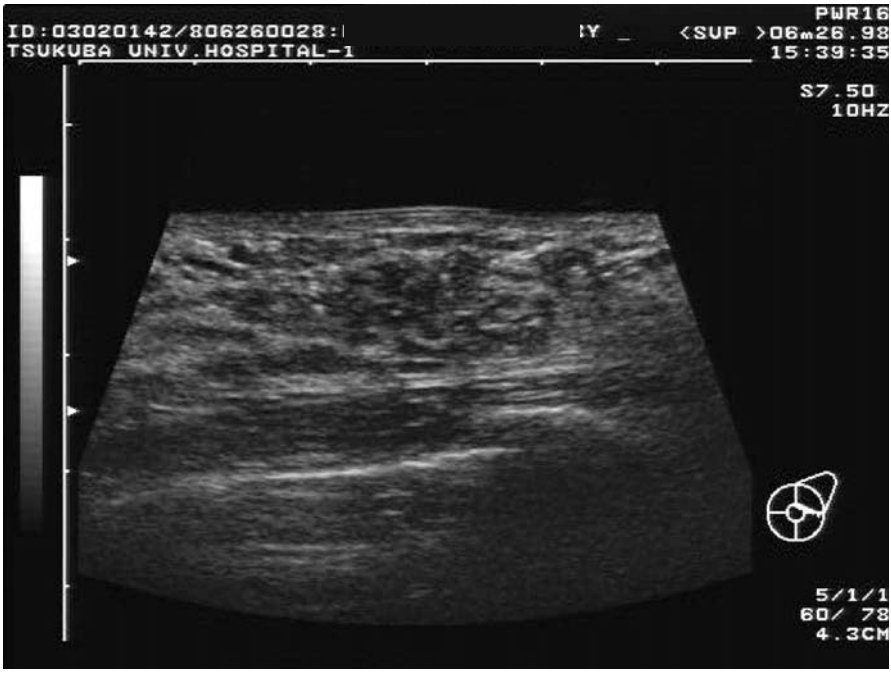

Echogenic spots +

Fig. 6. This case has echogenic spots. This is a geographic pattern. The patient is 42 years old. The histological diagnosis was invasive ductal carcinoma with a predominant intraductal component, and the intraductal component was comedo type

Table 2. Relationship between intraductal component and ultrasonic images

Pattern	Non-comedo type	Comedo type
Homogeneous	2 (2)	0 (0)
Ductal	2 (0)	4 (1)
Mottled	8 (2)	3 (2)
Geographic	9 (5)	15 (12)
Total	21 (9)	22 (15)

Number of cases with echogenic spots is indicated in parentheses

geographic pattern. In many cases with a mottled pattern or a geographic pattern, the cancer cells spread widely. If calcification exists, echogenic spots are visible regardless of the pattern. If infiltrating ability is acquired after spreading, the image displays a mass plus dilated duct, a mottled pattern, or a geographic pattern [7]. If infiltrating ability is immediately acquired after the development of cancer, it displays a mass image, which is the most common type of breast cancer (Fig. 7).

Table 3. Ultrasonic images of ductal carcinoma in situ (DCIS)

Mass image-forming type	51 (68.0%)
Mass (small, multiple etc)	39
Duct dilatation + mass	7
Intracystic mass	5
Non-mass image-forming type	24 (32.0%)
Total	75 (100%)

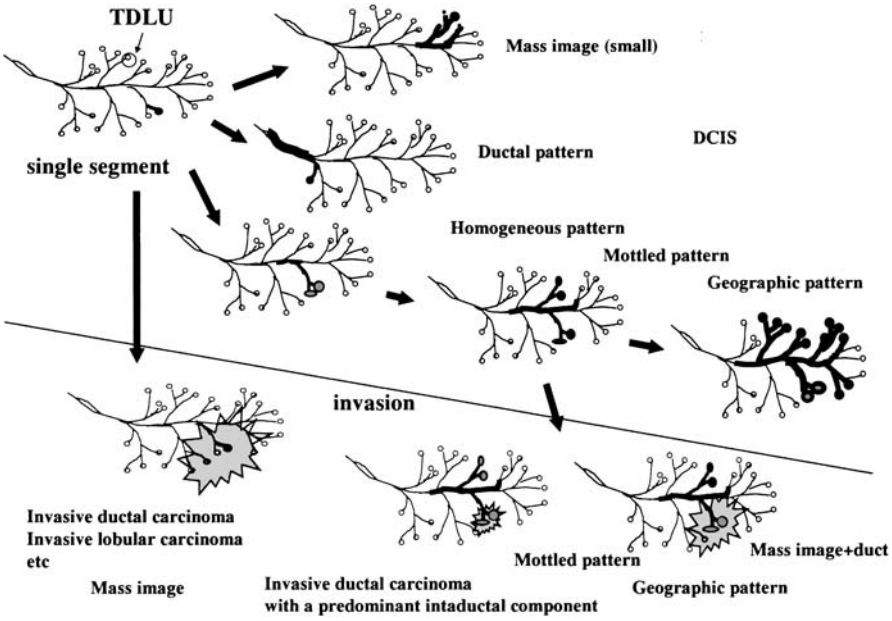

Fig. 7. Schema of the relationship between the progress of breast cancer and ultrasonic imaging

Conclusions

1. Although mass image-forming lesions are commonly seen in breast cancer, there are some cases with a non-mass image-forming type. In this study, we investigated the characteristics of non-mass image-forming breast cancer. With non-mass image-forming breast cancer, more than 50% was DCIS, about 70% was DCIS and micro-invasive carcinoma, and about 90% was DCIS and invasive ductal carcinoma with a predominant intraductal component. In contrast, about 30% of DCIS was non-mass image-forming breast cancer.

2. According to the echoic pattern of the mammary gland with the lesion, we classified non-mass image-forming breast cancers into four subtypes: a homogeneous

pattern, a ductal pattern, a mottled pattern, and a geographic pattern. Forty-seven cases were classified into 2 with a homogeneous pattern, 6 with a ductal pattern, 12 with a mottled pattern, and 27 with a geographic pattern.

3. The geographic pattern often contains invasive components.

4. The geographic pattern and/or the lesion with echogenic spots often has a comedo type of intraductal component.

5. These results revealed the close relationship between the progress of breast cancer and ultrasonic imaging.

References

1. World Health Organization (1981) Histological typing of breast tumours, 2nd edn. WHO, Geneva
2. Singletary SE, Allred C, Ashley P, et al (2002) Revision of the American Joint Committee on Cancer Staging for Breast Cancer. J Clin Oncol 20:3628–3636
3. Rosen PP (1999) Breast pathology. Diagnosis by core needle biopsy. Lippincott Williams & Wilkins, Baltimore
4. Silverstein MJ (ed) (1997) Ductal carcinoma in situ of the breast. William & Wilkins, Baltimore
5. Wellings SR, Jensen MH, Marcum RG (1975) An atlas of subgross pathology of the human breast with special reference to possible precancerous lesions. J Natl Cancer Inst 55:231–273
6. Ohuchi N, Furuta A, Mori S (1994) Management of ductal carcinoma in situ with nipple discharge. Intraductal spreading of carcinoma is an unfavorable pathologic factor for breast-conserving surgery. Cancer 74(4):1294–1302
7. Ichihara S, Aoyama H, Matsuyama T, et al (1989) Relationship between the extent of intraductal component and that of invasive component of ductal carcinoma of the breast. Acta Pathol Jpn 39(12):786–794

Characteristic Mammography and Ultrasonography Findings of Ductal Carcinoma In Situ of the Breast Arising in Sclerosing Adenosis

Kumiko Tanaka[1], Hiroshi Sakuma[2], Goi Sakamoto[1], Futoshi Akiyama[1], and Fujio Kasumi[3]

Summary. Some cases of ductal carcinoma in situ (DCIS) of the breast are arising in sclerosing adenosis. Sclerosing adenosis can sometimes resemble invasive carcinoma, especially in mammography (MMG). We attemped to reevaluate images from DCIS arising in sclerosing adenosis in MMG and ultrasonography (US) by comparing pathological reports. Four of the 90 (4.4%) cases of DCIS operated on at the Cancer Institute Hospital in 2001 arose from sclerosing adenosis. Three of the 4 cases showed characteristic images, focal distortion without mass lesion in MMG and indistinct and irregularly shaped hypoechoic area in US. It is usually easy to conclude the presence of malignancies from MMG findings. However, using US findings, it can difficult not only to detect abnormalities but also to determine the presence of malignancy. It is important to be able to detect this type of DCIS to make the correct diagnosis and to select suitable treatment.

Key words. DCIS, Sclerosing adenosis, Distortion, Irregularly shaped hypoechoic lesion

Introduction

Some cases of ductal carcinoma in situ (DCIS) of the breast are arising in sclerosing adenosis. However, sclerosing adenosis can sometimes resemble invasive carcinoma. Thus, DCIS arising in ducts affected by sclerosing adenosis can be misinterpreted as invasive carcinoma. In this study we attempted to reevaluate images from DCIS cases with sclerosing adenosis.

Patients and Methods

Ninety cases of DCIS were operated on at the Cancer Institute Hospital in 2001. Cases of DCIS arising in sclerosing adenosis were identified from pathological reports, and mammography (MMG) and ultrasonography (US) images were compared.

[1] Department of Breast Pathology, Cancer Institute Hospital, 1-37-1 Kamiikebukuro, Toshima-ku, Tokyo 170-8455, Japan
[2] Department of Ultrasonology, Cancer Institute Hospital, Tokyo, Japan
[3] Department of Breast Surgery, Cancer Institute Hospital, Tokyo, Japan

Results

Four of the 90 (4.4%) patients showed DCIS arising from sclerosing adenosis. We examined the MMG and US images from the patients and found that 3 of the 4 cases showed similar characteristics.

Case 1

A 56-year-old woman. The tumor was not palpable. Distortion in the MMG was prominent, and an irregularly shaped hypoechoic lesion was seen by US (Fig. 1). Microscopic appearance showed carcinoma spreading into the sclerosing adenosis and distorted parenchyma, which reflected the distortion in the MMG (Fig. 2).

Case 2

A 59-year-old woman. Physical findings were a 40 × 20 mm induration. Distortion in the MMG was associated with coarse calcification caused by an old fibroadenoma and was not related to the tumor. An irregularly shaped hypoechoic lesion was seen by US (Fig. 3). The microscopic appearance was similar to case 1 (Fig. 4).

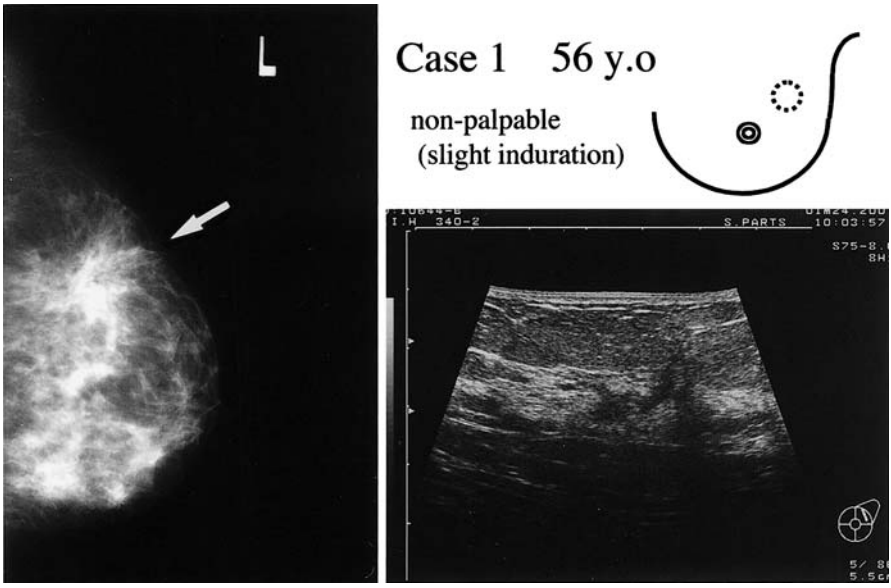

Fig. 1. Focal distortion in mammography (MMG) (*arrow*); irregularly shaped hypoechoic area seen by ultrasonography

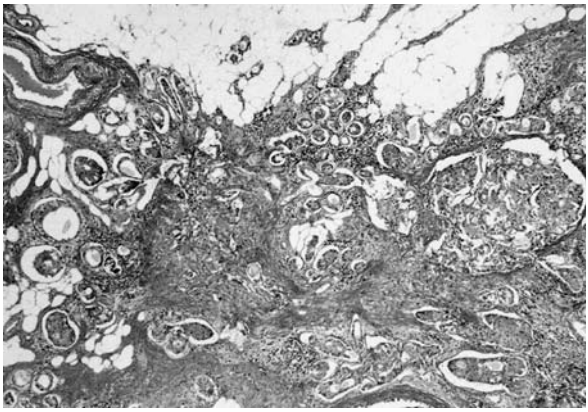

FIG. 2. Microscopic appearance of case 1. Ductal carcinoma in situ (DCIS) is spreading into sclerosing adenosis

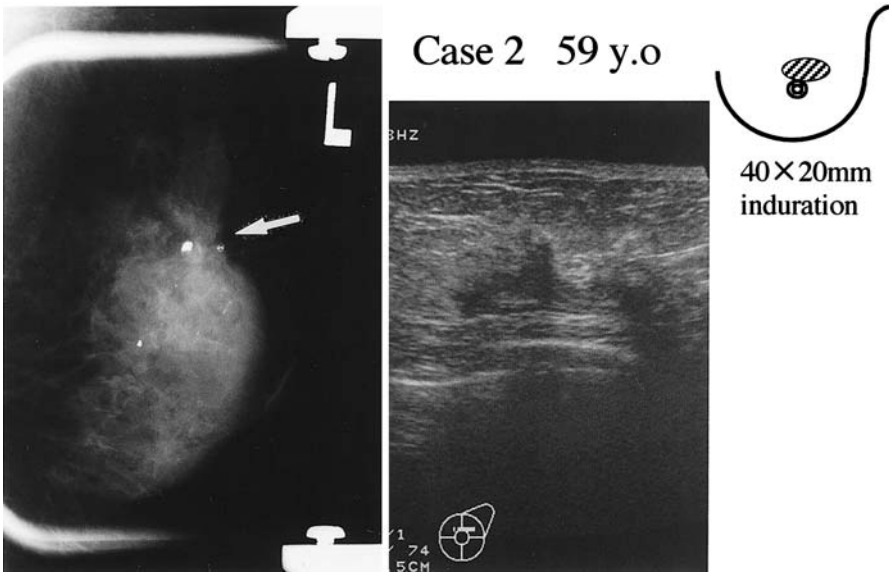

FIG. 3. Focal distortion in MMG (*arrow*); irregularly shaped hypoechoic area by ultrasonography

Case 3

A 60-year-old woman. A small round tumor (14 × 14 mm) was palpable. A slight distortion was observed by MMG and an irregular hypoechoic tumor was seen by US (Fig. 5). Microscopically, carcinoma was observed in the ducts of the sclerosing adenosis, but had spread to a relatively small area.

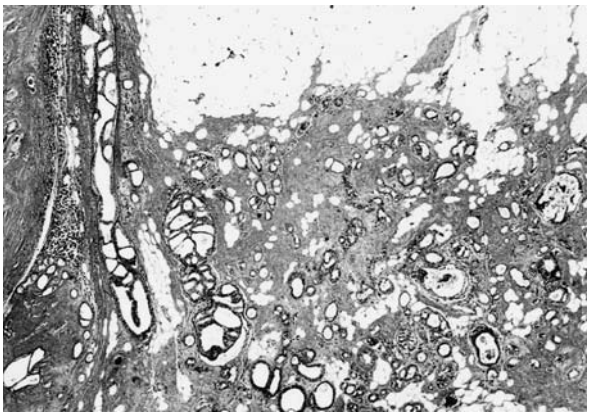

FIG. 4. Microscopic appearance of case 2 was similar to that of case 1, i.e., DCIS spreading into sclerosing adenosis

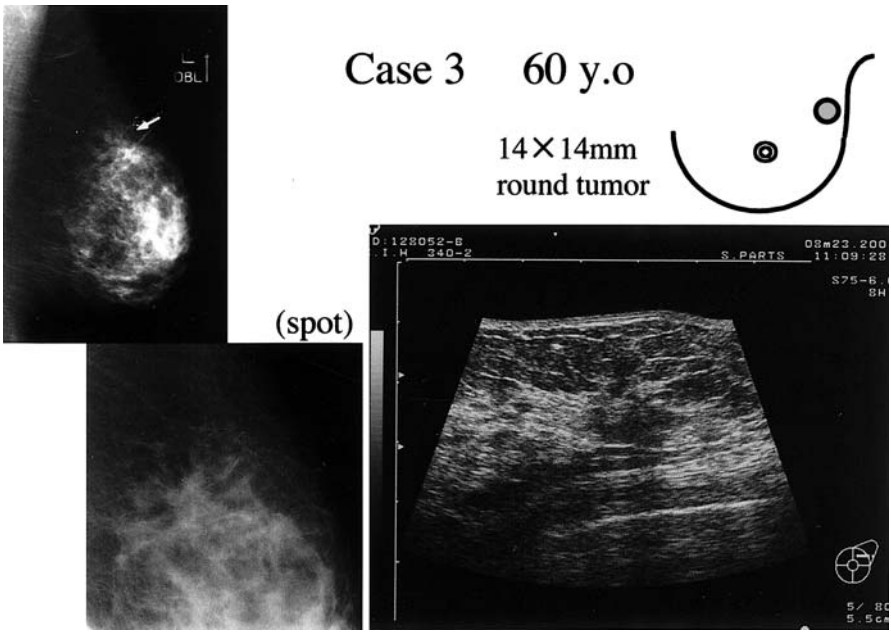

FIG. 5. There was slight distortion in MMG (*arrow*) and an irregularly shaped, hypoechoic small tumor by ultrasonography

Case 4

A 69-year-old woman. An oval, hard, 30 × 23 mm tumor was palpable. This case is different from the others, with a high-density mass detectable by MMG and an irregular hypoechoic tumor by US (Fig. 6). Microscopically, intraductal carcinoma foci were gathering and in the process of forming a tumor.

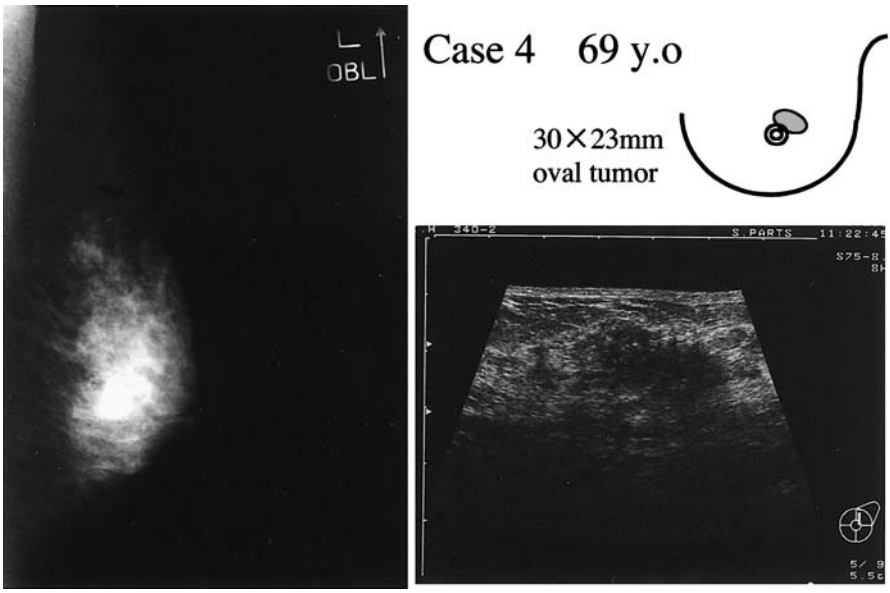

Fig. 6. High-density mass in MMG; oval tumor by ultrasonography. This case was different from the others

Discussion

1. Sclerosing adenosis causes architectural distortion by MMG, such that if DCIS arises in sclerosing adenosis, the MMG distortion is emphasized by the carcinoma foci. This kind of distortion observed by MMG can often be misinterpreted as invasive carcinoma.
2. Although sclerosing adenosis is difficult to detect by US, if DCIS does arise in sclerosing adenosis, an indistinct and irregularly shaped hypoechoic lesion can often be observed. However, this kind of nonmass-forming image can be missed or overlooked.

Conclusion

It is important to be able to detect DCIS arising in sclerosing adenosis. However, this type of carcinoma tends not to show typical malignant features, especially by ultrasound examination. Our findings showed that a characteristic distortion was observed by MMG, and an indistinct and an irregularly shaped hypoechoic lesion was observed by US in three of four cases of DCIS arising in sclerosing adenosis.

References

1. Rosen PP (2001) Rosen's breast pathology. Lippincott/Williams & Wilkins, Philadelphia, pp 282–285
2. Page DL, Anderson TJ (1987) Diagnostic histopathology of the breast. Churchill Livingstone, Edinburgh, pp 89–103
3. Muto N, Akiyama F, Sakamoto G, et al (2000) Breast cancer arising in the duct of sclerosing adenosis. Jpn J Breast Cancer 15(2):239–241

Preoperative Ultrasonic Assessment for Breast-Conserving Treatment

Tamotsu Kudo[1], Yoshino Kiyosawa[1], Iwao Ono[2], and Masaaki Kubota[3]

Summary. Our aim was to appreciate the value of our newly equipped ultrasonic device in assessing margin status and to evaluate the policy of oncoplastic surgery in breast-conserving treatment (BCT). Of 783 cases of primary breast cancer treated between January 1991 and December 2001, 407 cases undergoing BCT were studied. A GE-YMS Logiq 700 MR was introduced as the new device in January 2000 and its outcome was calculated. In BCT, we intended to take the policy of oncoplastic surgery with the goal of ultimately obtaining a negative margin using both image-guided biopsy and frozen section analysis. Ninety percent (366/407) of patients received radiation therapy. Outcome was calculated using crude rates of first site of failure. After introducing the new device, the rate of BCT increased to 80% (86/108) from 69% and the rate of pathologically negative margins (>5 mm; PNM) also increased to 91% (78/86) from 82%. At a mean follow-up time of 49 months, the overall local recurrence rate was 0.5% (2/407). Comparatively high percentages of BCT and PNM were obtained mainly by introducing the Logiq 700 MR. A small local recurrence rate (0.5%) was derived from taking the policy of oncoplastic surgery.

Key words. Breast neoplasms, Breast conservation therapy, Surgical margin, Local recurrence, Breast ultrasound

Introduction

From the standpoint of breast-conserving treatment (BCT) and quality of life, increase in the rate of BCT and in the rate of pathologically negative margins (PNM), and, ultimately, reduction of the risk of local recurrence rate (LRR), are the most important points and a paramount goal. The purposes of this study were to evaluate the newly equipped ultrasonic device for its contribution to the increase in rate of BCT and PNM, and to evaluate the policy of oncoplastic surgery [1] in BCT with respect to a reduction of LRR.

Departments of [1]Breast-Endocrine Surgery, [2]Pathology, and [3]Unit of Clinical Physiology, Nakadoori General Hospital, 3-15 Minamidoori Misono-cho, Akita 010-0012, Japan

Table 1. Characteristics of the 407 treated cases

Factor	
Age (years)	
<36	15
36–45	93
45–55	147
>55	152
T factor	
≦3.0 cm	334
>3.0 cm	73
Histology	
Ductal	387
Lobular	7
Other	13
n factor[a]	
Negative	260
Positive	98
Unknown	49
Chemotherapy	
Yes	150
No	257
Tamoxifen and/or goserelin	
Yes	243
No	164

[a] Pathologic factor

Materials and Methods

We studied 407 consecutive patients undergoing BCT from 783 cases of primary breast cancer between January 1991 and December 2001 in our hospital. The average age of the population was 51 years, with a range of 21 to 90 years. Eighteen percent (73/407) had a tumor size of more than 3 cm. The characteristics of the patient population are given in Table 1.

The conservative surgical technique generally employed was wide excision with axillary dissection. In terms of indications for BCT, patients with a diffuse malignant lesion or collagen vascular disease were not candidates for BCT. We intended to take the policy of oncoplastic surgery with the goal of ultimately obtaining a negative margin using preoperative breast imaging and intraoperative frozen section analysis (FSA). If the margin was identified as positive, additional tissue was taken from the exact site during the same surgery. Sometimes, we performed multiple reexcision for positive margins.

In terms of equipment, the GE-YMS Logiq 700MR Expert was introduced as a new ultrasonographic (US) device in January 2000. Previous US equipment was the Aloka SSD-650CL and GE-YMS Logiq 500 MR. The Gyroscan NT 1.5T. (magnetic resonance imaging, MRI) was introduced in 1997. The GE-YMS Senograph 600 and Lorad M-IV with Stereo Guide were used as mammography equipment.

In January 2000, we started to use the Logiq 700 combined with MRI for preoperative marginal diagnosis on a full scale. Preoperative fine-needle aspiration biopsy cytology, core biopsy under US guidance, and/or intraoperative FSA under marking by US with using a "line of sight" technique were performed to better define the boundaries.

Ninety percent (366/407) of the patients received postoperative radiation therapy (50.4–60.4 Gy). Follow-up including annual mammography was obtained as of March 2003, which resulted in average and median follow-up of 49 and 45 months, respectively.

Results

After introducing the Logiq 700MR, the rate of BCT increased to 80% (86/108) from 69% (1998) and 67% (1999). The rate of PNM (>5 mm) also increased to 91% (78/86) from 85% and 82% (Fig. 1). With respect to the prognosis, LRR (LR only or LR before distant metastasis) was 0.5% (2/407), and mortality was 4.4% (18/407), at an average follow-up time of 49 months (Fig. 2).

One LR case underwent BCT at 26 years of age with axillary lymph node metastases and positive margins were found (LR) at 28 years of age by clinical examination. Seven months after salvage mastectomy, liver metastasis was apparent, and the patient died at 30 years of age. In another LR case, mammography was indispensable in leading to the diagnosis. The LR was found at 58 years of age, 2 years after first treatment (BCT), and the patient underwent salvage mastectomy. She is now well without recurrence. We experienced salvage mastectomy in these 2 patients only (2/407).

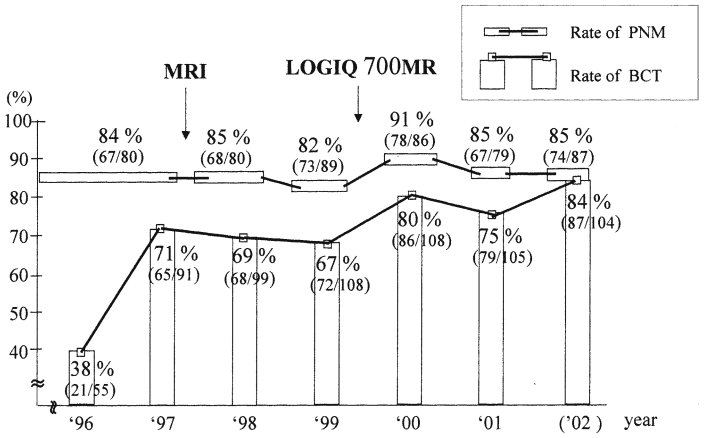

FIG. 1. Changes in the rate of pathologically negative margins (*PNM*) and breast-conserving treatment (*BCT*)

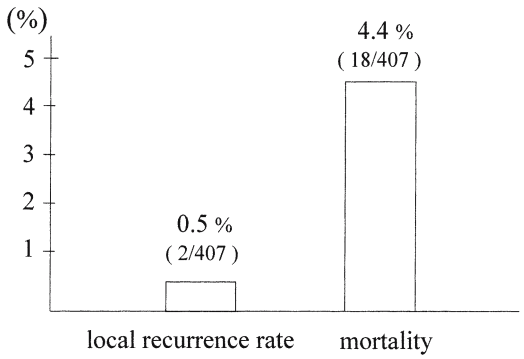

FIG. 2. Prognosis. Average follow-up time was 49 months; *local recurrence rate* only or LR before distant metastasis

Discussion

The development of equipment and technological support has provided physicians with the tools to perform accurate biopsy and diagnosis. An approach that has been explored for its utility in yielding negative margins uses intraoperative US to guide the initial surgery [2]. Breast MRI is helpful in preoperative evaluation of local tumor extent, however, with false-positive and false-negative diagnoses. Therefore, we started to use the Logiq 700 MR combined with MRI for marginal diagnosis. In addition to preoperative US-guided cytology or histology, we used FSA under US marking in various situation. As a result, the rate of BCT and PNM increased about 10% more than in previous years, and a high percentage of BCT was also maintained in the next year (75%, 2001) and the past year (84%, 2002). These high rates of BCT are thought to have been supported mainly by the Logiq 700 MR.

In respect of breast-conserving surgery, the battle is between margins and cosmesis. Our practice, in patients who wish and are candidates for breast preservation, was to attempt to widely excise the entire cancer lesion, invasive or noninvasive, achieving 5 mm or more margin in every direction, beginning in 1991. As a result, the LRR (at average follow-up time of 49 months) is extremely low (0.5%) in comparison with other reports [2–5]. This fact strongly suggests that the policy of oncoplastic surgery should be advocated.

Conclusions

1. A comparatively high percentage (75%–84%) of BCT, while maintaining a moderately high rate of PNM, was obtained by introducing the Logiq 700 MR.
2. A small number of local recurrences (0.5%; average follow-up time of 49 months) were derived from taking the policy of oncoplastic surgery, using FSA as well as preoperative image-guided biopsy.

References

1. Image-Detected Breast Cancer (IDBC) Consensus Conference. Palm Beach, FL, March 22–24, 2001

2. Singletary SE (2002) Surgical margins in patients with early-stage breast cancer treated with breast conservation therapy. Am J Surg 184:383–393
3. Kurtz JM, Amalric R, Brandone H, et al (1989) Local recurrence after breast-conserving surgery and radiotherapy. Cancer (Phila) 63:1912–1917
4. Haffty BG, Goldberg NB, Rose M, et al (1989) Conservative surgery with radiation therapy in clinical stage I and II breast cancer. Arch Surg 124:1266–1270
5. Smitt MC, Nowels KW, Zdeblick MJ, et al (1995) The importance of the lumpectomy surgical margin status in long-term results of breast conservation. Cancer (Phila) 76:259–267

Recent Advances in Multidimensional 3D/4D Breast Imaging

Christian Weismann

Introduction

Three-dimensional (3D) mammasonography is the most recent development in breast ultrasound imaging and intervention, providing additional aspects to conventional two-dimensional (2D) sonography: completely new superior diagnostic information to study a breast mass and the surrounding tissue in three orthogonal planes. Four-dimensional (4D) ultrasound offers real-time 3D rendered image information and is taken as a basis of multidimensional imaging of the breast. In the following section about 3D and 4D breast ultrasound (US), after a short introduction to technical considerations, multidimensional imaging of solid benign and malignant breast lesions, 3D targeting, and real-time 4D breast biopsy technique are discussed.

3D Ultrasound Technique and Display

Two principal techniques and the combination of both exist to obtain three-dimensional (3D) ultrasound (US) information: manual or automatic scanner movement with echo data processing along the US beam. All demonstrated cases were investigated with a linear array 2D and 3D US volume transducer, 5–13 MHz, with a 29° volume sector angle, combined with the Voluson 530D and 730 (GE Medical Systems Kretz Ultrasound, Zipf, Austria). The Voluson technique offers the option to acquire a 3D US volume data set automatically with one and the same transducer without freehand movement of the probe. In about 3 s the system obtains the entire 3D data volume set (about 10 MB) and displays the information in a multiplanar image display mode.

Multiplanar Display Mode

The multiplanar representation uses the 3D US information from three planes (A, B, and C plane) that cut the voxel and are orthogonal to each other. The A plane shows

Department of Diagnostic Radiology, St. Johanns Hospital, Landeskliniken Salzburg, Muellner Hauptstrasse 48, 5020 Salzburg, Austria

the original scan plane during typical 2D US investigation and volume acquisition. The B plane is orthogonal to A and C and offers the typical rectangular US information of 2D scanning, for example, the sagittal or transversal plane. Completely new diagnostic information is obtained by the coronal plane (C plane), which is orthogonal to A and B. Furthermore, the system allows navigation through the entire acquired volume conducting parallel interactive movement through the image slices. In all three planes, a colored dot (A, yellow; B, orange; C, blue) indicating an identical voxel can be identified in every activated plane in the volume of interest (VOI). Synchronous parallel image movement in all the corresponding orthogonal planes can be observed as the information in the VOI rectangle is updated. A dynamic analysis of the 3D-acquired US information of an anatomical detail is available and is easier to understand; for example, complex collecting duct branching.

Rendering Modes

The acquired US volume data allow a variety of 3D rendering modes, and the most effective for visibility of the biopsy needle inside the 3D data set are transparency modes. Fading, for example, between maximum or minimum modes, gives reliable information of ductal anatomy and pathology such as intraductal papilloma. Combined with an animated rotation of the transparent rendered tissue block, the position of the needle in relation to the lesion can also be better evaluated.

2D and 3D US Characterization of Solid Breast Lesions

All 2D and 3D US investigations were performed with the patients in supine position with elevated arms. The typical 2D US analysis of breast lesion shape, width-to-depth ratio, margin characterization, lesion compressibility, lesion echogenicity, and echo texture, followed. The additional 3D US information first displayed in the multiplanar mode offers the new coronal plane lesion aspect ancd allows marking of the different breast masses by retracting and compressing lesion patterns as described by Rotten and colleagues [1, 2].

Fibroadenoma

3D US gives reliable information about the lesion shape. Fibroadenomas often show a round base, like a coin positioned parallel to the skin, embedded by breast tissue. Due to their transversal width-to-sagittal depth ratio of more than 1 on 2D cross-sectional images, they have a more cylindrical morphology than assumed by 2D US. Also, real-time 2D US usually is not sufficient to give a clear understanding of the 3D lesion aspect in cases of the more complex bases of fibroadenomas with lobulation of their surfaces and dumbbell-like or irregular aspects. In about 3–4 s, the Voluson technique offers a 3D multiplanar image of the fibroadenoma without any dependence on long or short axis lesion diameter or angulation. Different measurements of width and depth distances can be accurately obtained, guided by all three planes.

3D US volume datasets show more objective fibroadenoma compressibility than 2D US, because during echo palpation a well-defined embedded lesion is movable and the probability increases that 2D US causes depth–axis diameter measurement in dif-

ferent positions, with the consequence of measuring incorrect distances. Comparing the 3D morphology of the lesion before and after compression with 3D US datasets provide correct measurements of comparable slices.

Invasive Breast Carcinoma

According to the study of Rahbar et al. [3], 2D US features that characterize lesions as malignant are irregular shape (61% malignant), microlobulated (67% malignant), spiculated (67% malignant), and a width-to-depth (anteroposterior dimension) ratio of 1.4 or less (40% malignant). Most of the time the tumor center is characterized by a homogeneous echo-poor fibrohyalinosis followed by a dorsal shadowing due to ultrasound energy absorption. The echo-rich margins are the expression of many different tissue components of tumor cells, fibrous strands, fatty tissue, and surrounding glandular parenchyma indicating the tumorous growth and infiltration zone. Mammography clearly shows this stellate infiltration pattern with the architectural distortion of the neighboring structures.

3D US is the first ultrasound imaging modality that offers simultaneously the coronal, transversal, and sagittal plane for eliminating the architectural distortion as in mammography. Although 2D US shows signs of disrupted connective tissue layers and changes of the shape and disruption of the superficial fascia in the transversal and sagittal planes, these signs are less impressive compared with the tissue distortion and retraction presented in the 3D coronal plane. Even in stellate carcinomas smaller than 1 cm in diameter, the retraction pattern is visible in the coronal plane.

In particular, invasive lobular carcinomas sometimes develop without a mammographically and sonographically visible dominating mass. In such a situation the coronal plane helps to visualize the architectural distortion and enables understanding of the underlying pathology. Therefore, dense, palpable, especially asymmetrical breast tissue should be investigated by 3D US to detect architectural distortion. When invasive lobular carcinoma forms a more circumscribed mass or tends to produce multifocal lesions, these tumorous lesions have a similar ultrasound aspect such as an invasive ductal carcinoma. Although Rotten described the retraction pattern highly characteristic for malignant masses, we have to consider benign differential diagnoses such as the radial scar, sclerosing adenosis, or postoperative scarring.

3D Targeting Technique

The sonographic visibility of a suspicious lesion is the basis for an ultrasound-guided biopsy. 3D breast US offers a correlation of typical “freehand” 2D US guided core or fine-needle biopsy and hookwire localization of palpable and nonpalpable lesions to optimize tissue sampling and to reduce the miss rate [4, 5]. The consequence of 3D targeting should be a reduction of needle passes without an increase of miss rate due to objective 3D demonstration of correct or incorrect core or fine-needle position [6]. First, a 3D US volume dataset is acquired to study the morphology of the lesion. The multiplanar scan plane analysis offers comprehensive information of the lesion and the surrounding structures. For large-core needle biopsy (14 gauge) with local anesthesia, a 3-mm skin incision is performed. In typical freehand 2D US guidance [7], the needle path should be as horizontal as possible to optimize visualization of the

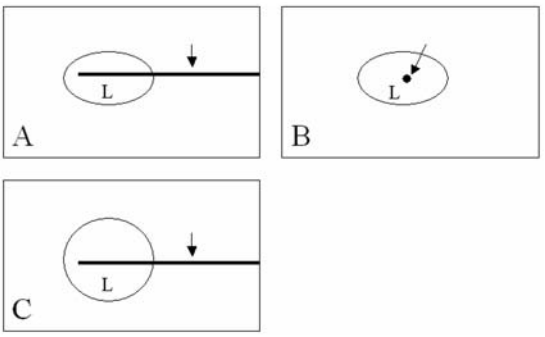

Fig. 1. Multiplanar display and 3D-targeting: needle (*arrows*) in all three planes (*A*, sagittal; *B*, transversal; *C*, coronal plane) inside the lesion (*L*)

needle length and needle tip. Via the 13-gauge coaxial cannula, a 14-gauge core needle is positioned in front of the lesion. After a 22-mm core needle stroke using a BIP (High Speed-Multi) biopsy gun (Biomed Instrumente und Produkte, Türkenfeld, Germany), the Voluson technique offers the option to acquire a 3D US volume data set with one and the same transducer without freehand movement of the probe. In about 3 s, the system acquires the entire 3D data volume and displays information about the needle position in relation to the lesion accurately in a multiplanar imaging mode. This needle position check in all three planes is called 3D targeting [8].

Real-Time 4D US Breast Biopsy

A newly developed software allows real-time 4D US needle guidance during breast biopsy. The permanently acquired real-time 4D US volume data are displayed in a multiplanar scan plane analysis mode. Compared to conventional freehand 2D, US needle guidance real-time 4D offers additional permanent information of all three planes in the multiplanar display mode, a rendered image of the breast lesion, and the needle position. The three-dimensional permanent analysis of lesion position as well as needle position in all three planes allows one to navigate the core needle in an optimal prefire position. After the core needle stroke, 3D targeting follows, showing the correct or incorrect needle position.

References

1. Rotten D, Levaillant J-M, Zerat L (1998) Use of three-dimensional ultrasound mammography to analyze normal breast tissue and solid breast masses. In: Merz E (ed) 3-D ultrasonography in obstetrics and gynecology. Lippincott Willams & Wilkins, Philadelphia, pp 73–78
2. Rotten D, Levaillant J-M, Zerat L (1999) Analysis of normal breast tissue and of solid breast masses using three-dimensional ultrasound mammography. Ultrasound Obstet Gynecol 14:114–124
3. Rahbar G, Sie AC, Hansen GC, et al (1999) Benign versus malignant solid breast masses: US differentiation. Radiology 213:889–894
4. Jackman RJ, Nowels KW, Rodriguez-Soto J, et al (1999) Stereotactic, automated, large core needle biopsy of nonpalpable breast lesions: false-negative and histologic underestimation rates after long-term follow-up. Radiology 210:799–805

5. Libermann L, Dershaw DD, Glassman JR, et al (1997) Analysis of cancers not diagnosed at stereotactic core breast biopsy. Radiology 203:151–157
6. Weismann CF (2001) Ultra-som tridimensional da mama. In: Montenegro CAB, Rezende Filho J, Almeida Lima ML (eds) Ultra-som tridimensional atlas comentado, vol 6. Guanabara Koogan S.A., Rio de Janeiro, pp 151–172
7. Parker SH, Jobe WE, Dennis MA, et al (1993) US-guided automated large-core biopsy. Radiology 187:507–511
8. Weismann CF, Forstner R, Prokop E, et al (2000) Three-dimensional targeting: a new three-dimensional ultrasound technique to evaluate needle position during breast biopsy. Ultrasound Obstet Gynecol 16:359–364

3D Ultrasound-Based Evaluation of Lesions in the Uncompressed Breast

Carsten Riis[1], Anders Lernevall[2], Flemming B. Sorensen[2], and Hans Nygaard[1,3]

Summary. Ultrasound-based evaluation of breast lesions is most often performed by recognizing characteristic ultrasonic properties of the findings, such as shape, orientation, border characteristics, and echogenicity. During traditional ultrasound examination of the breast, the patient lies supine, and the ultrasound probe is moved manually over the breast. Probe pressure must be applied to ensure good acoustic contact to the tissue. By applying pressure, however, the true shape characteristics of the suspected lesions are distorted and tissues or lesions may be displaced. Further, the examination technique is not systematic and the result is user dependent. Systematic 3D breast scanning minimizes the user dependency of the examination and makes the reporting of findings easier. One advantage of 3D ultrasound is the ability to view arbitrary 2D scan planes, to evaluate size and shape of findings. True evaluation of these parameters, however, requires a scanning performed on the uncompressed breast. A system for systematic 3D scanning of the uncompressed breast has been developed. During examination, the patient lies prone on an examination bed, with the breast immersed in a water-filled cup. A transducer is moved in a systematic rotational pattern, covering the full breast. Compound imaging techniques minimize shadow and enhancement artifacts before 3D reconstruction.

Key words. Breast cancer, Ultrasound, Compound ultrasound imaging, 3D breast ultrasound

Introduction

An important diagnostic feature in breast ultrasound mammography is the possibility of evaluating the shape and orientation of breast lesions. In traditional two-dimensional (2D) ultrasound mammography, manipulating and rotating the transducer selectively over suspect lesions achieves this information. This technique

[1] Engineering College of Aarhus, Dalgas Avenue 2, DK-8000 Aarhus C, Denmark
[2] Aarhus University Hospital, Aarhus Amtssygehus, Tage Hansens Gade 2, DK-8000 Aarhus C, Denmark
[3] Aarhus University Hospital, Skejby Sygehus, Brendstrupgaardsvej, DK-8200 Aarhus N, Denmark

is, of course, operator dependent, and requires the presence of the patient during diagnosis. Further, the breast is compressed during scanning, which disturbs the true shape and characteristics of the evaluated lesions. If systematic three-dimensional (3D) ultrasound of the breast is utilized, shape, orientation, borders, and other clinically discriminating signs of malignancy can be evaluated offline without the patient being present. Further, arbitrary slicing allows reconstruction of scan planes in any orientation of the acquired volume. Useful original 3D information should help in assessing the duct network and the relationship of a mass or lesion to the ducts, and should better demonstrate the vascularity associated with neoplasms [1].

One approach to 3D ultrasound is to acquire a series of 2D ultrasound images covering the volume of interest, and build a 3D voxel-based Cartesian volume (or 3D grid) by placing each of these images in its correct location in the volume. A system for breast ultrasound scanning has been implemented and evaluated, using linear translation of an ultrasound transducer in small incremental steps covering the breast immersed in water. This method has been widely used and described for 3D ultrasound scanning. However, in breast ultrasound scanning, the method suffers from some limitations; a majority of breast cancers are located in the upper quadrant of the breast, adjacent to the lymphatic complex in the axilla area. This area is poorly covered with the present scan method, as it is situated in the far field of the ultrasound transducer. As the incidence angle to the tissue is skewed, refraction artifacts occur in the periphery of the breast, and further, in water immersion scanning the strong reflection from the papilla shadows anatomically important structures such as the papillary ducts. These limitations make linear transversal scanning less suitable for evaluation of lesions in the uncompressed breast. The aim of the present study is to implement and evaluate a new method for systematic 3D ultrasound scanning of the uncompressed breast. The system should use high-quality ultrasound equipment of choice for the diagnostician, combined with dedicated hardware for systematic 3D ultrasound data acquisition, and software for 3D reconstruction and analysis.

Materials and Methods

A prototype system for systematic water immersion breast scanning has been developed. During scanning the patient lies prone on an examination bed, with the breast immersed in a water-filled cup, through a circular aperture in the examination bed (Fig. 1). The water is close to body temperature to ensure good acoustical coupling to the breast [2,3] and make the scanning more comfortable for the patient.

Scanning of a full breast is achieved by performing a 360° rotation of the cup in rapid and accurate angular steps, while acquiring image data from the ultrasound scanner. Images are recorded along with information about angular orientation to a fixed reference point. As the system is made of rigid mechanical components and a high-precision stepper motor, no positioning sensors need to be attached to the probe. Depending on the required precision of the scanning, and the nature of the breast, between 400 and 1200 images are acquired for each rotation. A series of 800 ultrasound images can be acquired in about 1 min, enabling the patient to lie still during scanning to minimize movement artifacts.

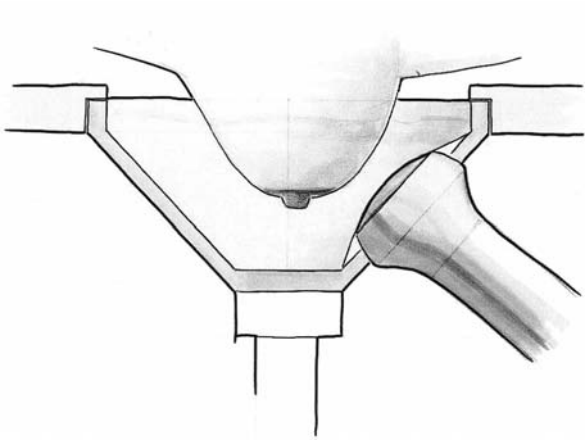

Fig. 1. Rotation device. The breast is immersed in a water-filled rotating cup, controlled by a computer. An ultrasound transducer is fixed to the side of the rotating cup, scanning the tissue through a membrane

Minimizing Propagation Artifacts

In 3D ultrasound applications, sound propagation artifacts, such as shadow and enhancement phenomena, can cause errors and misinterpretation. One example of such an error is the shadowed region behind the papilla, caused by the interface between water and tissue. In multiplanar reslicing, this shadow is projected onto the coronal plane, normal to the incidence, giving an impression of a hypoechoic mass. In the same fashion, ultrasound enhancement behind simple cysts gives the impression of hyperechoic masses in the coronal plane. One way to minimize these errors is to insonate the breast tissue from different angles [4]. Spatial compound ultrasound imaging can then be achieved by combining two or more images in the same 2D scan plane, minimizing the effect of propagation artifacts (Fig. 2a–c).

Compound ultrasound techniques further have the potential to reduce speckle noise and enhance edges in ultrasound images. As the intersecting scan lines of the images have different angles of incidence to the reflecting tissue boundaries, combination of these images will enhance the definition of the boundaries. The images must be very accurately registered and corrected for motion artifacts to avoid loss of spatial resolution [5–8]. The characteristics of the resulting image can be changed according to the algorithm chosen for the combination of overlapping image data.

3D Reconstruction and Analysis

Before reconstruction in 3D, the images representing the same 2D plane, that is, acquired 180° apart in the rotational pattern, are subjected to spatial compounding. 3D reconstruction, segmentation, and analysis can be performed by placing these compound images in a voxel coordinate system. Several commercial applications can be used to view and manipulate 3D voxel data. The organization of the spatial compound images resembles a cone-shaped image acquisition pattern.

Calibration

Before scanning, the system is calibrated using a dedicated phantom, consisting of an accurate grid of nylon strings. The phantom is fixed at the top of the water-filled cup,

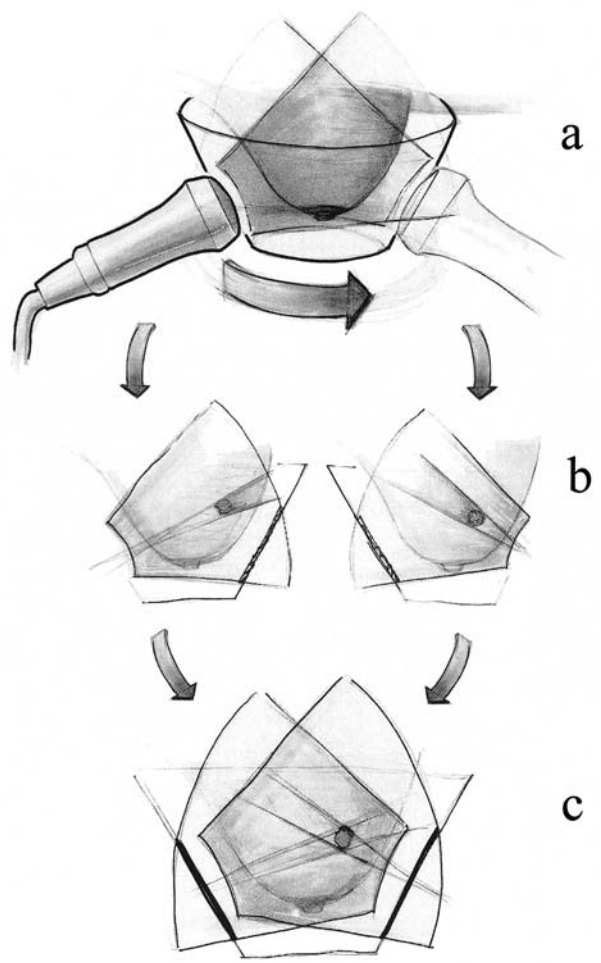

Fig. 2. **a** Image acquisition. By rotating the transducer 360° during acquisition, the full volume of the breast is covered, utilizing 3D imaging. **b** Registration. Two images acquired 180° apart will represent the same 2D image plane in the acquired volume. **c** Compound imaging. Combination of two images representing the same 2D plane will minimize propagation artifacts

and by identifying the grid points in the ultrasound image, the exact position and angular orientation of the transducer with respect to the center axis of the rotation cup is verified. With the breast immersed in the water cup, the average ultrasound propagation velocity for the breast tissue can be estimated by measuring the distance from the transducer to the reflecting wall of the cup through the tissue and comparing this with the same distance through water. This parameter can be used to compensate for geometric distortion due to refraction.

Discussion

Presently, the developed system is evaluated on normal healthy volunteers aged 18 to 25 years. The purpose of this study is to optimize the method, adjust system parameters, and acquire knowledge of the appearance and properties of normal and dense

breast tissue. Several practical problems in the system design and scanning method need yet to be solved before high-quality compound scanning and 3D reconstruction can be achieved with the existing system. When the system is optimized, the method will be evaluated in a study including symptomatic women undergoing breast cancer investigation and mammography. Further, a comparative study of recessed pathological breast tissue is planned. For this purpose a dedicated in vitro model, implementing the rotational compound scanning method, has been developed.

The compressibility and stiffness of a breast lesion is a vital diagnostic parameter for differentiating benign breast lesions from solid tumors. When performing automated immersion scanning of the uncompressed breast, however, this parameter is not evaluated. The central shadowing from the papilla, and other refraction- and propagation-based artifacts, is very common in water-coupled ultrasound imaging of the uncompressed breast. Adding a slight compression to the breast will minimize these artifacts [9]. However, this step will introduce a new source of user dependency, and the compression will distort the natural shape and characteristics of the lesions.

Conclusions

A technique for systematic 3D scanning of the uncompressed breast has been developed, and is presently being subjected to evaluation and optimization. Examination is performed with the patient lying prone on an examination bed, with the uncompressed breast immersed in a water-filled cup. A transducer is moved in a systematic rotational pattern enabling compound scanning of the full breast in a radial pattern. High-quality 3D reconstruction can be achieved, because compound scanning is used for minimizing shadow and enhancement artifacts before 3D reconstruction.

References

1. Fornage BD (2000) Recent advances in breast sonography. JBR–BTR 83(2):75–80
2. Einighammer HJ (1985) Ultrasonic rotational compound scans of the breast. Diagn Imaging Clin Med 54(3–4):223–228
3. Jellins J, Kossoff G (1973) Velocity compensation in water-coupled breast echography. Ultrasonics 11:223–226
4. Hernandez A, Basset O, Chirossel P, et al (1996) Spatial compounding in ultrasonic imaging using an articulated scan arm. Ultrasound Med Biol 22(2):229–238
5. Jespersen SK, Wilhjelm JE, Sillesen H (1998) Multi-angle compound imaging. Ultrasonic Imaging 20(2):81–102
6. Leotta DF, Martin RW (2000) Three-dimensional spatial compounding of ultrasound scans with weighting by incidence angle. Ultrasonic Imaging 22(1):1–19
7. Moskalik A, Carson PL, Meyer CR, et al (1985) Registration of three-dimensional compound ultrasound scans of the breast for refraction and motion correction. Ultrasound Med Biol 21(6):769–778
8. Rohling R, Gee A, Berman L (1997) Three-dimensional spatial compounding of ultrasound images. Med Image Anal 1(3):177–193
9. Madjar H (2000) The practice of breast ultrasound. Thieme, Stuttgart, pp 27–47

The Role of Ultrasound in Population-Based Breast Cancer Screening Programs

Edward Azavedo

Breast cancer is the most common malignancy that can affect a woman during her lifetime. In Sweden, breast cancer accounts for 26% of all the malignancies that affect women in our country. Even though we have made tremendous progress with both surgical and nonsurgical therapies, it is well documented that early detection is the best way to handle this disease. It is only through early detection that we can change the natural course of this disease with benefits both to individuals and to the entire society.

The first report regarding the beneficial use of early detection to fight this disease came from the HIP study in New York, wherein women who were offered mammography had a statistically significant lower mortality in breast cancer as compared to women who were not offered mammography. The other major report that revolutionized early detection was from the two-county study from Sweden published by Tabar et al. [1]. After that report many countries implemented nationwide screening programs to detect breast cancers at an early stage. The age groups that are screened vary within and among countries and are in a wide range, between 40 years at the lower level and 74 years at the upper level. Even the interval for screening varies a bit, but around 2 years is the generally accepted time interval for a screening program. The main tool for early mass detection of breast cancers is mammography. When something abnormal or questionable is seen on a mammogram or when a woman reports breast symptoms, these women are recalled for further analysis.

The population-based breast cancer screening program in Sweden invites every single woman within the ages of 40 to 74 years, in certain cases 50 to 69 years, to have a mammogram every 2 years. In Stockholm we offer mammography screening for women aged between 50 and 69 years of age every 2 years. The first time a woman attends a screening examination, she always gets a two-view mammogram, that is, a MLO (mediolateral-oblique) and a CC (craniocaudal) view. If and when we see something abnormal or questionable or if a woman reports actionable symptoms, then these women are recalled for further workups. At this stage, these women undergo a physical examination and get all the necessary extra views that include spot compressions, magnifications, and rolled views. During the past two decades, ultrasound

Faculty of Medicine, Karolinska Institute, Solna, 17176 Stockholm, Sweden

(US) examinations have been on the increase all over the world. Although US has been performed on breasts for a long time, its general use has increased exponentially with screening programs.

It is a well-known fact that the sensitivity of US to detect malignancies in dense breasts is higher as compared to mammography. This is one of the main reasons, in addition to the technological possibilities to study tumor details and multifocality, etc., that has made US so popular. Once the technology was mainly used to differentiate a solid from a cystic lesion, but that was long ago. The technological advancement in US is amazing, and we have today the possibility of seeing calcifications that are detected on mammograms and also the possibility of studying intraductal areas. When we started our screening program, it was believed through the reported literature that postmenopausal women have radiolucent breasts that are easy to analyze on mammograms. Our experience today reveals that the breasts, at least in Stockholm, do not show such a big difference between pre- and postmenopausal women. To add to that, we have today increasing use of hormone replacement therapy (HRT), which in many cases leads to increase in breast density. US helps us to rule out abnormalities in dense breasts with a higher degree of confidence.

Once a tumor is detected on a mammogram, it can be biopsied with either fine-needle aspiration (FNA) and/or a core biopsy to get a morphological preoperative diagnosis. These procedures can in many cases be done more easily and in a shorter time if the lesions detected on mammograms are visible on US, which they often are. US can also help us to see the extent of the disease and study the margins toward the surrounding tissue. An US examination is often followed by the patient on our monitors, and when we see no abnormality or when we empty a cyst, the patients feel more relaxed than if they only had heard the result without visualizing such an event.

During the past few years, the use of HRT is on the increase, not only because of climacteric subjective reasons but also because of reports of the beneficial effects of HRT on osteoporosis, cardiovascular diseases, etc. As the age groups that attend a breast cancer screening program are usually around the peri- and postmenopausal ages, we have in many a case seen adverse effects of HRT on breast density. A mammogram may change from N1 (Wolfe's classification of breast densities) to P2 and Dy patterns, making it a challenge to read these mammograms. In these situations the additional use of US increases our confidence to give the concerned women a trustworthy report.

Another development on the therapeutic side is preoperative chemotherapy in advanced disease. In this cases an US examination can be of help in two different ways: one is to monitor the effect of therapy and the other is to localize the tumor precisely with either a metal clip or charcoal. This will help the pathologists to identify the area to be examined microscopically in case the preoperative therapy shows a good response.

Today we have US as an integrated part of a breast cancer screening program starting from the recalled women. The first screening examination in population-based screening programs where the turnover is very high is mammography. A normal screening unit in countries that perform mammography screening for the whole population can have up to 180 women per day, a number too high for performing US exams. Neither personnel nor time resources allow the use of US as the primary tool, but US has its given place in case of any doubt, may it be significant or not.

To conclude, I can state that we have gradually increased the number of US exams and US-guided interventions in our screening programs.

Bibliography

Azavedo E, Svane G (1992) Radial scars detected mammographically in a breast cancer screening programme. Eur J Radiol 15(1):18–21

Dennis MA, Parker SH, Klaus AJ, et al (2001) Breast biopsy avoidance: the value of normal mammograms and normal sonograms in the setting of a palpable lump. Radiology 219(1):186–191

Jellins J (1998) Combining imaging and vascularity assessment of breast lesions. Ultrasound Med Biol 14 (suppl 1):121–130

Kauenen-Boumeester V, Menke-Pluymers M, de Kanter AY, et al (2003) Ultrasound-guided fine needle aspiration cytology of axillary lymph nodes in breast cancer patients. A preoperative staging procedure. Eur J Cancer 39(2):170–174

Kossoff G, Garrett WJ, Carpenter DA, et al (1976) Principles and classification of soft tissues by grey scale echography. Ultrasound Med Biol 2(2):89–111

Kuenen-Boumeester V, Menke-Pluymers M, de Kanter AY, et al (1991) The role of the radiologist in screening for nonpalpable breast tumors in Sweden. Invest Radiol 26(2):174–178

Madjar H, Rickard M, Jellins J, Otto R (1999) IBUS guidelines for the ultrasonic examination of the breast. IBUS International Faculty. International Breast Ultrasound School. Eur J Ultrasound 9(1):99–102

Rahusen FD, Bremers AJ, Fabry HF, et al (2002) Ultrasound-guided lumpectomy of nonpalpable breast cancer versus wire-guided resection: a randomised clinical trial. Ann Surg Oncol 9(10):994–998

Rizzatto G, Chersevani R, Abbona M, et al (1997) High-resolution sonography of breast carcinoma. Eur J Radiol 24(1):11–19

Rizzatto G, Martegani A, Chersevani R, et al (2001) Importance of staging of breast cancer and role of contrast ultrasound. Eur Radiol 11 (suppl 3):E47–E51

Rizzatto GJ (2001) Towards a more sophisticated use of breast ultrasound. Eur Radiol 11(12):2425–2435

Shapiro S, Strax P, Venet L (1971) Periodic breast cancer screening in reducing mortality from breast cancer. JAMA 15;215(11):1777–1785

Tabar L, Fagerberg CJ, Gad A, et al (1885) Reduction in mortality from breast cancer after mass screening with mammography. Randomised trial from the Breast Cancer Screening Working Group of the Swedish National Board of Health and Welfare. Lancet 13;1(8433):829–832

Breast Cancer Screening by Palpation, Ultrasound, and Mammography

Hiroshi Morikubo

Summary. Breast cancer screening was carried out in 3455 subjects living in Tochigi Prefecture during 1999. All subjects underwent palpation, ultrasonic examination and mammography. The detection rate of each method was examined and compared. Breast cancer was discovered in 11 (0.32%) cases, of which 72.7% was early cancer. Three cases were discovered by ultrasonic examination alone, while 4 cases were discovered by mammography alone. No case was discovered by palpation only. Those that were discovered by ultrasonic examination were detected as a mass (two schirrhous carcinoma, one papillotubular carcinoma). Three cases that were discovered by mammography showed microcalcification without forming a mass and all were noninvasive carcinoma. In conclusion, mammography and ultrasonic examination were considered complementary to each other for the detection of breast cancer in mass screenings.

Key words. Breast cancer screening, Ultrasound, Mammography

Introduction

The Tochigi Public Health Service Association has conducted breast cancer screening on citizens, partly using ultrasound in combination with palpation, since 1988. Since 1997, ultrasound examination has been performed on all examinees, a total of about 20 000 persons a year, which has improved the detection and early detection rates of breast cancer (Table 1). In 1999, as part of a research project conducted in Tochigi Prefecture, the Association performed breast cancer screening using three independent modalities concomitantly, including mammography, ultrasound, and palpation. Furthermore, we conducted a follow-up study on examinees who joined the research project in 2000 to evaluate the sensitivity and specificity of each modality. Currently, the Tochigi Public Health Service Association is performing breast cancer screening by combining ultrasound and palpation or ultrasound and mammography, depending on the selection of local authorities.

Department of Radiology, Rosai Hospital for Silicosis, 632 Takatoku, Fujihara-machi, Shioya-gun, Tochigi 321-2523, Japan

Table 1. Implementation overview of breast cancer screening by Tochigi Public Health Service Association

	1988–1996: some cases were examined using ultrasound in combination with palpation	1997: all cases were examined by palpation and ultrasound	1999: all cases were examined by palpation and ultrasound; some cases were examined in combination with mammography	1999: research project on combined use of palpation, ultrasound, and mammography
Total number of examinees	174 521	17 958	27 206	3455
Rate of cases requiring detailed examinations	1.8%	4.0%	5.7%	15.3%
Detection rate of breast cancer	0.06%	0.13%	0.12%	0.32%
Early detection rate of breast cancer	47.7%	69.6%	69.7%	72.7%

Table 2. Examination methods of ultrasound and mammography

	Ultrasound	Mammography
Devices	7.5 MHz mechanical scanner or electronic linear scanner (Aloka SSD-900)	Toshiba MGU-200B
Scanning and imaging direction	Bilateral whole-breast ultrasound using freehand technique by a technician	Mediolateral oblique (MLO) view Unilateral
Image recording media	MO disk for digital still image	Screen-film system (Kodak Min-R2000/Min-R200)
Time required for examination	4 min	3 min
Interpretation and diagnostic method	Interpretation of still images by ultrasound specialists, 200 cases/h	Independent evaluation by two doctors

Methods

In the research project conducted in 1999, the number of examinees who had received breast cancer screening by the combined use of three modalities was 3455 (mean age, 52 years), the rate of cases requiring detailed examinations was 15.3%, the detection rate of breast cancer was 0.32%, and the early detection rate of breast cancer was 72.7%. This high rate of cases requiring detailed examinations was the result of differences in the independent evaluation of two doctors on the mammography results and between modalities. Table 2 shows the ultrasound and mammography examination methods.

Results

Among 11 breast cancer cases detected by screening, no case was detected by palpation alone, 3 cases were detected by ultrasound alone, and 4 cases by mammography alone. These results are shown in Tables 3 and 4.

As shown in Table 3, all the breast cancers detected by ultrasound alone were invasive ductal carcinoma, and a tumor image was demonstrated by ultrasound in these cases. The age of all three examinees was 50 years or older. Also, as shown in Table 4, three of four cases of breast cancer found by mammography alone were noninvasive ductal carcinoma, and microcalcification was detected by mammography in these cases. Three of four examinees were under 50 years old. Table 5 shows the detection rates of breast cancer by modality.

According to the results of the follow-up study on 3455 examinees who joined the research project in 1999, 1842 examinees received mass breast cancer screening or

Table 3. Results in cases detected by ultrasound alone

Case no (age, years)	Ultrasound findings	Mammography findings	TNM stage classification	Pathological diagnosis
Case 1 (50)	Tumor: detailed examination required	Benign calcification	Stage I	Scirrhous carcinoma
Case 2 (55)	Tumor: detailed examination required	Normal lymph nodes	Stage I	Scirrhous carcinoma
Case 3 (68)	Tumor: detailed examination required	Normal	Stage I	Solid tubular carcinoma

Table 4. Results in cases detected by mammography alone

Case no (age, years)	Ultrasound findings	Mammography findings	TNM stage classification	Pathological diagnosis
Case 1 (36)	Cyst	Calcification: detailed examination required	Stage 0	Noninvasive ductal carcinoma
Case 2 (54)	Normal	Calcification: detailed examination required	Stage 0	Noninvasive ductal carcinoma
Case 3 (47)	Normal	Calcification, tumor	Stage II	Papillotubular carcinoma
Case 4 (40)	Normal	Calcification: detailed examination required	Stage 0	Noninvasive ductal carcinoma

Table 5. Detection rate of breast cancer by modality

	Palpation	Ultrasound	Mammography	Concomitant use of the three modalities
Detection rate of breast cancer	0.09%	0.20%	0.20%	0.32%

Table 6. Sensitivity and specificity of each modality and combined methods

	Palpation	Ultrasound	Mammography	Palpation + ultrasound + mammography	Ultrasound + Mammography
Sensitivity	27.3%	63.6%	63.6%	100%	100%
Specificity	95.4%	95.5%	91.1%	84.2%	88.1%

examinations at medical institutions in 2000. We confirmed that none of them was newly diagnosed as having breast cancer. From the results of the research project in 1999, the sensitivity of ultrasound, mammography, and palpation alone was 63.6%, 63.6%, and 27.3%, respectively. The sensitivity of the concomitant use of three modalities and that of two modalities, ultrasound and mammography, were 100% (Table 6).

Discussion

In terms of the ages of examinees in whom breast cancer was detected and the examination modality, contrary to our expectations, mammography was effective for those under 50 years because many cases of microcalcification were found in relatively younger examinees.

As already mentioned, the types of breast cancer detected by ultrasound and mammography are clearly different. The characteristics of each modality affect the types of cancer detected. Ultrasound examination reveals more invasive ductal carcinoma associated with relatively small tumors. On the other hand, mammography tends to detect more noninvasive ductal carcinoma associated with microcalcification. Although it is difficult to accurately determine the actual ratio of these types of cancer, this research project showed the ratio of these types of cancer to be almost equal.

In conclusion, mass screening for breast cancer becomes effective when ultrasound and mammography are concomitantly used. With this method, each modality functions at almost the same level in a complementary way to achieve adequate detection and early detection rates of breast cancer.

A Review of Breast Cancer Undetectable by Ultrasonography in a Screening Setting

Miki Yamasaki[1], Shigeru Nasu[2], Hisaharu Mori[2], Sunao Koga[2], and Shunichi Koga[1]

Summary. In 89 breast cancer lesions found during clinical breast cancer screening with combined usage of mammography (MMG) and ultrasonography (US) between February 1995 and August 2002, we found 13 cases were negative for US detection. In this study, we reexamined those cases of breast cancer undetectable by breast US. In the 12 US-negative lesions, a secondary extended examination performed using US showed 7 lesions were positive for detection; the remaining 5 lesions were still negative for US examination. In summary, of the 89 breast cancer lesions, US failed to detect 10 (11.2%) during clinical breast cancer screening.

Key words. Breast cancer screening, Breast ultrasonography

Introduction

We have previously reported the effectiveness of breast cancer screening by the combined usage of ultrasonography (US) and mammography (MMG) [1]. In this Chapter, to improve our screening technique of breast cancer we reviewed the cases of breast cancer with negative findings on ultrasonographic study.

Materials and Methods

In the period from February 1995 to August 2002, we detected 89 cases of breast cancer by a combination of US and MMG at our institute of health examination service. In those cases, 13 were undetectable by US screening. We tried further US detection by the full view of US with reference to the MMG findings. US examination was performed either by SSD-650CL or SSD-2000 with a 10-MHz mechanical sector probe (Aloka) or SSA-250A with an annular array probe (Toshiba). MMG were carried out with a mediolateral oblique view (MLO) by either Senograph 500T or 500TS (GE-CGR).

[1] Hakuaikai Medical Association Group, Human Dry Dock Center Wellness, [2] Hakuaikai Hospital, 1-17-29 Sasaoka, Chuo-ku, Fukuoka 810-0034, Japan

Table 1. Result of reexamination by ultrasonography (US) for the 12 undetectable cases in the first US screening examination

Case	Age (years)	Stage	MMG	Histology	US (closer examination)
1	47	0	C	DCIS	Negative
2	48	0	C	DCIS	Negative
3	54	0	C	DCIS	Negative
4	67	I	C	IDC, papillotubular carcinoma	Negative
5	42	I	C	IDC, papillotubular carcinoma	Negative
6	50	0	C	DCIS	SE spots
7	54	0	C	DCIS	Hypoechoic area
8	58	0	C	DCIS	SE spots
9	66	I	C	Unknown	SE spots
10	35	I	C	IDC, papillotubular carcinoma	Hypoechoic area, SE spots
11	44	I	C	IDC, papillotubular carcinoma	Mass, SE spots
12	54	IIA	M	IDC, papillotubular carcinoma	Mass
13	45	IIIA	D	IDC, papillotubular carcinoma	No examination

C, microcalcification; M, mass; D, architectural distortion; DCIS, ductal carcinoma in situ; IDC, invasive ductal carcinoma; SE, strong echo

Results

Results of reexamination by US on the 13 US-undetectable lesions that had been shown positive by MMG are summarized in Table 1. Case 13 was not available for US reexamination. Further investigation by US was carried out in 12 of US-undetectable cases by a detailed closer method of examination. Five cases (cases 1–5) were still undetectable by the repeated US trial, but another 7 cases (cases 6–12) showed some evidences of abnormality. In cases 1 to 5, histology showed noninvasive ductal carcinoma or partially invasive ductal carcinoma papillotubular carcinoma. In 5 of those 7 cases (cases 6–10), we observed some strong echo spots in the area of the MMG-detected lesion. The 5 lesions showed similar histological findings: they could be delineated with US but required an extended examination after imaging microcalcifications using MMG. Case 11 and 12 were invasive ductal carcinomas, which could be detected as mass lesions by closer US reexamination (Figs. 1, 2).

Discussion

We have been using a combination of MMG and US in breast cancer screening since 1995. We have reported that in human dry dock examination, where high levels of accuracy are sought, a combined usage of MMG and US is advantageous [1]. In this study, we analyzed undetectable cancer cases using US and investigated the limits of cancer detection ability at the time of screening examination using the US examination method.

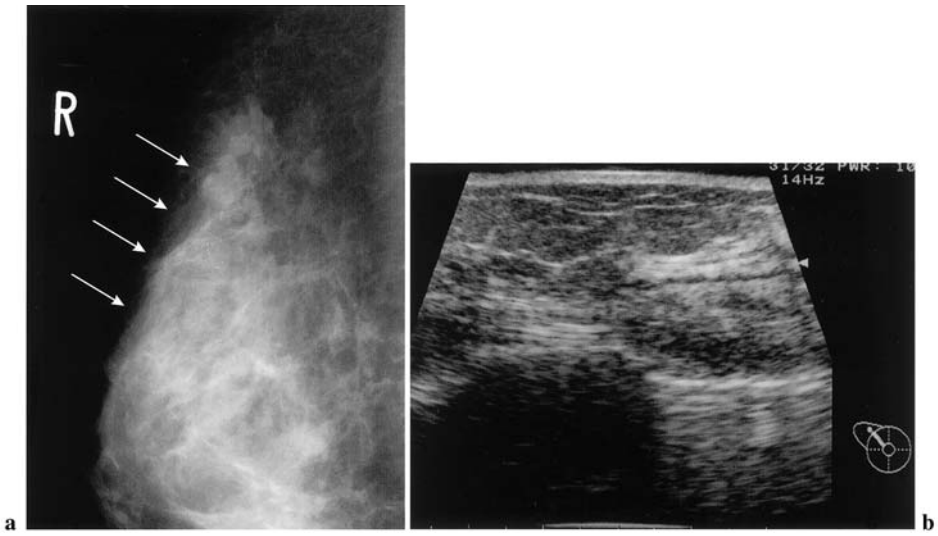

FIG. 1. Case 11. As we had detected microcalcification (*arrows* in **a**) by screening mammography (MMG), the case was recalled for closer examination. Multiple cysts in both mammary glands had been shown by screening US. On closer US examination, we were able to detect strong echo spots in dilated ducts and a mass lesion. We should be more careful in scanning around the nipple because the duct ectasia was overlooked in the multiple cysts, which suggesed the diagnosis of mastopathy. **a** Screening MMG. **b** Closer US examination

We investigated 12 lesions undetectable by US, with the exception of 1 case, which was unavailable for US reexamination. The 5 lesions were still undetectable during the secondary examination, and the remaining 5 lesions were, through diligent scanning with a probe, finally detected by high-frequency wave echoes of calcified lesions. These 10 lesions, which were detected as a microcalcification image by MMG, were cases of noninvasive ductal carcinoma or partially invasive ductal carcinama papillotublar carcinoma. It is thought that detection was difficult at the time of the first examination by US. Consequently, 10 lesions (11.2%) of the 89 cancer lesions discovered were difficult to detect using US. The limit of detection ability by US was about 90%. In the remaining 2 cases, however, some mass lesions were detectable by closer US examination. We looked for the reasons of this oversight. In 1 case, the mass was isoechoic to the fat tissue and located on the edge of the mammary ground, which made it difficult to detect. Metastatic axillary gland swelling also existed, however, suggesting we had a chance to detect it in the screening setting. Another case showed mastopathy with multiple cysts but also showed the duct ectasia, suggesting a chance to detect the mass with careful scanning around the nipple.

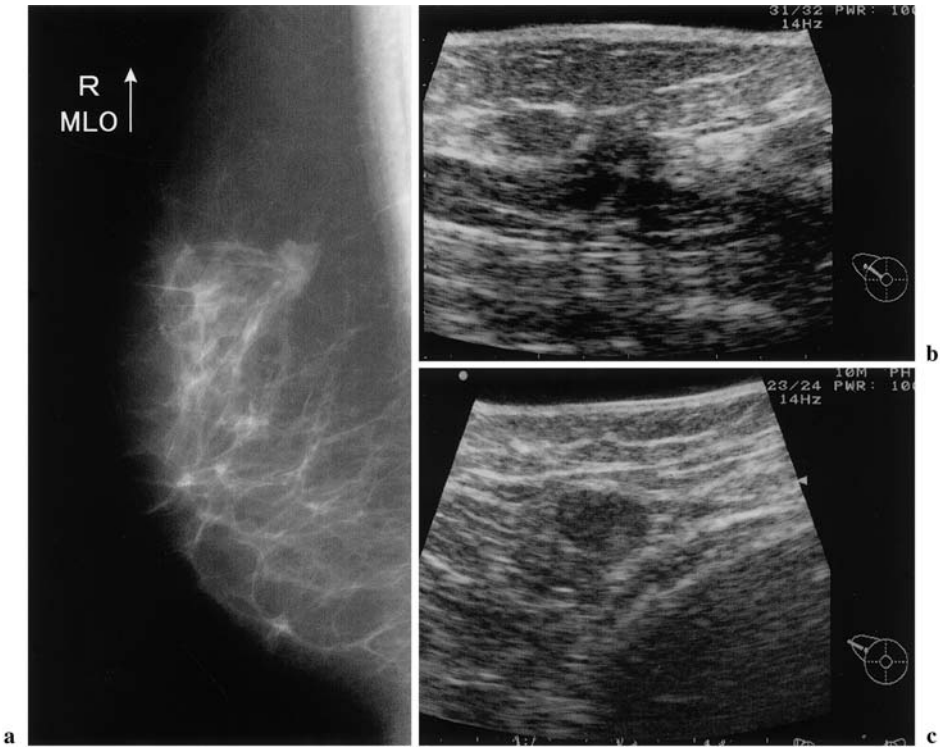

Fig. 2. Case 12. As we had detected a mass lesion by screening MMG, the case was recalled for closer examination. Reexamination revealed a mass in addition to a suggestive axillary gland swelling. The oversight might have occurred because the mass was isoechoic to the fat tissue and located on the edge of the mammary gland. However, we missed the chance to detect it because there was an axillary gland swelling. **a** Expansion photography in closer examination MMG. **b** Closer US examination (mass lesion). **c** Closer US examination (axillary gland swelling). *MLO*, mediolateral oblique view

Conclusions

With US, about 10% of breast cancer cases could not be detected. We should keep in mind the limitations of using only US in the screening of breast cancer. A continued effort is being made to improve our techniques of early diagnosis of breast cancer.

Reference

1. Nasu S, Yamasaki M, Tojo M, et al (2002) Efficacy of ultrasonography for breast cancer screening. Health Eval Promotion 29:804–805

Ultrasonic Screening of the Thyroid in Patients with Breast Complaints

Yasuhisa Fujimoto[1], Masahiro Hatama[1], Kenji Tezuka[1], Hiroshi Otani[1], Yuuichi Arimoto[1], Katsumi Ikeda[2], Sadatoshi Shimizu[2], Yoshinari Ogawa[2], and Yukio Nishiguchi[2]

Summary. From 1994 until 2002, we performed 6956 ultrasonic screenings of the thyroid for all patients who received breast examination by ultrasonography. We discovered 14 thyroid cancers (0.32%) from 4327 cases with breast complaints. The incidence of thyroid cancer with breast cancer (0.25%) was three times higher than that of thyroid cancer without breast cancer (0.73%). It was concluded that ultrasonic screening of the thyroid was useful in patients with breast complaints.

Key words. Ultrasonic screening of thyroid, Thyroid cancer, Thyroid cancer with breast cancer

Purpose

A possible association between breast disease and thyroid disease has been discussed in many reports. In 1988, we reported the usefulness of the ultrasonic screening of thyroid in patients with breast complaints at the 5th World Federation for Ultrasound in Medicine and Biology in Washington D.C. [1]. In 1994, we started a new series of ultrasonic screening of the thyroid for all patients who received breast examination by ultrasonography at the newly opened Osaka City General Hospital. The purpose of the present study is to reevaluate its usefulness.

Materials and Methods

From 1994 until 2002, we performed 6956 ultrasonic examinations of the thyroid and breast concurrently on 4327 patients who came to Osaka City General Hospital with breast complaints. The number of the patients with breast cancer was 682. We used Aloka SSD 650CL, GE Logiq 500, GE Logiq 700, and ATL HDI 5000. In most cases, at the time of examination, we placed a pillow under the left shoulder and examined the left breast first. We then moved the pillow under the neck, and examined the thyroid.

[1] Osaka City Sumiyoshi Hospital, 1-2-16 Higashikagaya, Suminoe-ku, Osaka 559-0012, Japan
[2] Osaka City General Hospital, 2-3-22 Miyakojimahondori, Miyakojima-ku, Osaka 534-0021, Japan

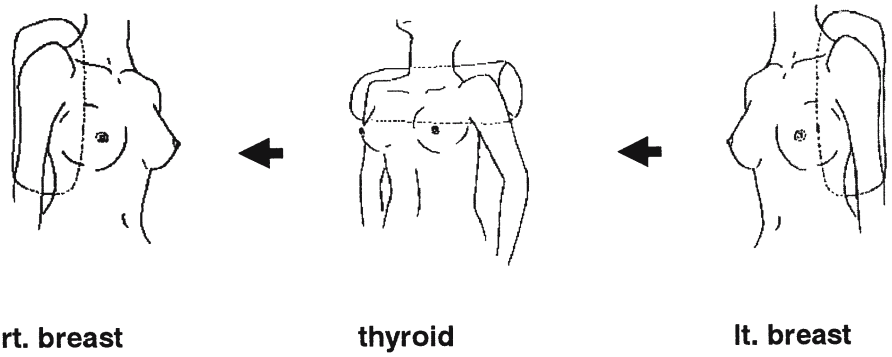

Fig. 1. Position for the examination

Finally, we examined the right breast with the pillow under the right shoulder (Fig. 1).

Results

In 4327 examinations, 35 cases (0.81%) had malignant findings in the thyroid by ultrasonography. The maximum size of these 35 nodules was 1.11 ± 0.41 cm. Of the 682 cases with breast cancer, 9 cases (1.32%) had malignant findings in the thyroid by ultrasonography. Of the 3645 cases without breast cancer, 26 cases (0.71%) had malignant findings in thyroid by ultrasonography.

Fourteen cases were operated and diagnosed histologically. In the 14 cases, we found 13 thyroid cancers, which included 12 papillary carcinomas and 1 medullary carcinoma, with 6 negative, 6 positive, and 1 unknown for lymph node metastasis. One nonoperative case was diagnosed cytologically as thyroid cancer and 14 cases (0.32%) were thyroid cancers diagnosed pathologically. Maximum size of these 14 cancer nodules was 1.14 ± 0.23 cm.

Of the 682 cases with breast cancer, 5 cases (0.73%) were thyroid cancer. Of the 3645 cases without breast cancer, 9 cases (0.25%) were thyroid cancer. The incidence of thyroid cancer with breast cancer was three times higher than that of thyroid cancer without breast cancer.

Of the 35 cases with malignant findings, 21 cases were tracked. There were 8 cases that were tracked over 2 years by ultrasonography. Of the 8 cases, 3 cases had an increase in tumor size and 5 cases had no change in size. The increase was 1.3 to 1.6 cm in diameter over 4 years, 1.7 to 2.1 cm in diameter over 3 years, and 0.9 to 1.0 cm in diameter over 2 years.

Discussion

In this study, the discovery rate of thyroid cancer was 0.25% in the cases without breast cancer. This incidence of thyroid cancer may show in general in people who come to common mass screening. It was concluded that the ultrasonic screening of thyroid

was useful in the patients with breast complaints. The incidence rate, which was three times higher with breast cancer, was noteworthy. This result showed that a relationship between thyroid cancer and breast cancer might be present.

There is no evidence for this explanation. However, there is the Cowden syndrome, which is characterized by a high risk of breast and thyroid cancers. Perren et al. [2] reported that this syndrome causes genetic disorders. With the exception of genetic factors, environmental factors, such as exposure to X-rays of the thyroid and the breast, may be a candidate for this explanation.

References

1. Fujimoto Y, Kato Y, Maekawa H, et al (1988) Ultrasonic screening of thyroid in the patients with breast complaints. J Ultrasound Med 7:39–S283
2. Perren A, Weng L, Boag AH, et al (1999) Immunohistochemical evidence of loss of PTEN expression in primary ductal adeocarcinomas of the breast. Am J Pathology 155: 1253–1260

Phantom and Human Experiments for Breast Cancer Detection by Ultrasound Transmission Technique

Yoshinori Hayakawa, Aya Sakasegawa, and Kiichi Tsuji

Summary. A new technique named the ultrasound transmission technique has been proposed by the authors. The idea was developed from the clinical findings that sound velocity in breast cancer is higher than in normal tissue by 49–90 m/s. Phantom experiments were conducted. Plexiglas (PMMA) plates 3 mm, 2 mm, or 1 mm thick were put into a cubic container (86 × 86 × 86 mm) filled with degassed water. In the echogram, the apparent distance between the back wall of the container and transducer was shortened because of the higher velocity of sound waves in plexiglas (2700 m/s) than degassed water (1500 m/s). This result showed the validity of the method. A breast to be examined can be sandwiched between a planar ultrasound transducer and reflector plate. Similar experiments were performed using a slice of pork (42 mm thick) instead of degassed water. The shortening of the reflector was apparent. The forearm of a human volunteer was also examined with plexiglas 2 mm or 1 mm thick with similar results, suggesting the validity of the method.

Key words. Breast cancer, Early detection, Ultrasound, Transmission period, Sound velocity

Introduction

Breast cancer is the leading cause of death among American women and the second most common cause among Japanese women. The disease is related to the Western-style diet and is increasing in incidence.

In every cancer, early detection and early treatment are the best ways to decrease mortality of patients. Moreover, early detection of breast cancer increases the possibility of breast conservation treatment. Although mammography is the most powerful modality for early detection, it is hazardous for use in young women due to X-ray exposure. Another modality of image diagnosis is ultrasound echo technique, but it is not as powerful in detecting breast cancer as mammography. Palpation, another modality, is largely dependent on the skill and experience of medical doctors. A new

Department of Biomedical Engineering, Toin University of Yokohama, 1614 Kuragane-cho, Aoba-ku, Yokohama 225-8502, Japan

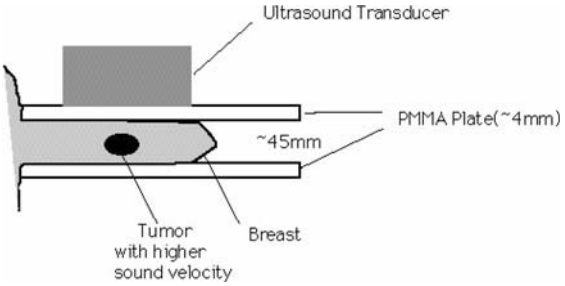

Fig. 1. Schematic view of proposed breast examination apparatus. A breast will be sandwiched between an ultrasound transmitting plate and a reflector, and examined on an ultrasound transducer using the echo technique

technique, which has been proposed by some of the authors, was named the ultrasound transmission technique [1] (Fig. 1).

In the present report, phantom experiments were conducted to obtain good results. The idea was developed from clinical findings using ultrasound computed tomography that the velocity of sound in a malignant tumor is greater by 49 to 90 m/s than in the normal tissue of the same patient [2]. The attenuation coefficient of a malignant tumor and normal tissue are approximately the same. The sound velocity in normal tissue is 1350 to 1500 m/s depending on the tissue, being greater in parenchyma and less in fat [2].

Materials and Methods

Phantom experiments were conducted to verify the validity of the technique. The Toshiba Ultrasound Diagnostic System SSA-390A with a linear transducer of 9 MHz was employed for the experiment. First, the sound velocity of plexiglas to be used in the phantom experiment was measured by the echo technique. The echogram of plexiglas of 30.2 mm thickness was taken in degassed water, and the apparent thickness was compared. The result was analyzed using the published datum of sound velocity in water (1500 m/s), yielding the velocity of sound in the plexiglas to be 2670 m/s, compared to the published datum of 2720 m/s.

Second, plexiglas (PMMA) plates 3 mm, 2 mm, or 1 mm thick were put in degassed water in a cubic container ($86 \times 86 \times 86$ mm). Apparent protrusion of the container wall behind each PMMA plate was eminent, which is due to higher sound velocity in PMMA than in water.

Next, pork slices were sandwiched between PMMA plates 4 mm thick, and examined from above with the ultrasound transducer. A PMMA plate of 2 mm or 1 mm was inserted between 4 mm PMMA plates. Approximately the same result was achieved with no PMMA plate inserted.

Third, the forearm of a human volunteer was sandwiched between PMMA plates 4 mm thick, and examined in approximately the same manner as the pork slices (Fig. 2).

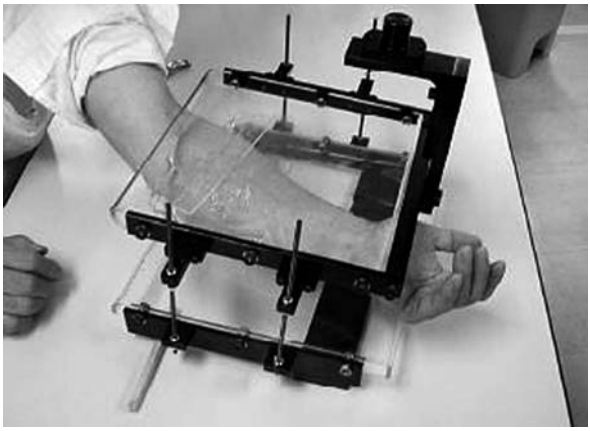

Fig. 2. Experimental setup of volunteer human forearm with plexiglas (PMMA) plate inserted

Results

Experiment with Pork Slices

Protrusion of the lower PMMA plate, which serves as a reflector, was apparent behind the 2-mm and 1-mm PMMA plate insertion, mocking a tumor. No such protrusion was observed without the PMMA plate insertion (Fig. 3).

Experiment with Human Forearm

Two kinds of experiments were achieved using different thickness of forearm (46 mm and 65 mm). Protrusion of the lower PMMA plate, which serves as a reflector, was apparent behind the 2-mm PMMA plate insertion, mocking a tumor. No such protrusion was observed without the PMMA plate insertion (Fig. 4). In the case of the 1-mm PMMA plate insertion, the protrusion was not so apparent. B-mode images of forearm with the sound velocity of 1600 m/s of muscle and with PMMA plate of 1 mm (or 2 mm), corresponds approximately to 11 mm (or 22 mm) of tumor thickness in the case of the sound velocity difference of 49 m/s and corresponds approximately to 6 mm (or 12 mm) of tumor thickness in the case of the sound velocity difference of 90 m/s. This relationship is derived from the equation

$$Y(1/1600 - 1/2720) = X(1/\mathrm{v} - 1/(\mathrm{v} + d\mathrm{v}))$$

where Y is the thickness of PMMA, X is the corresponding tumor thickness, v is the sound velocity of normal tissue, and dv is the difference of sound velocity of 49 m/s or 90 m/s.

Discussion

The present work shows that the proposed method may be used for mass screening of breast cancer for young females. The PMMA plate mocking the tumor seems to be useful to represent a tumor on a patient's breast to check the operation of the

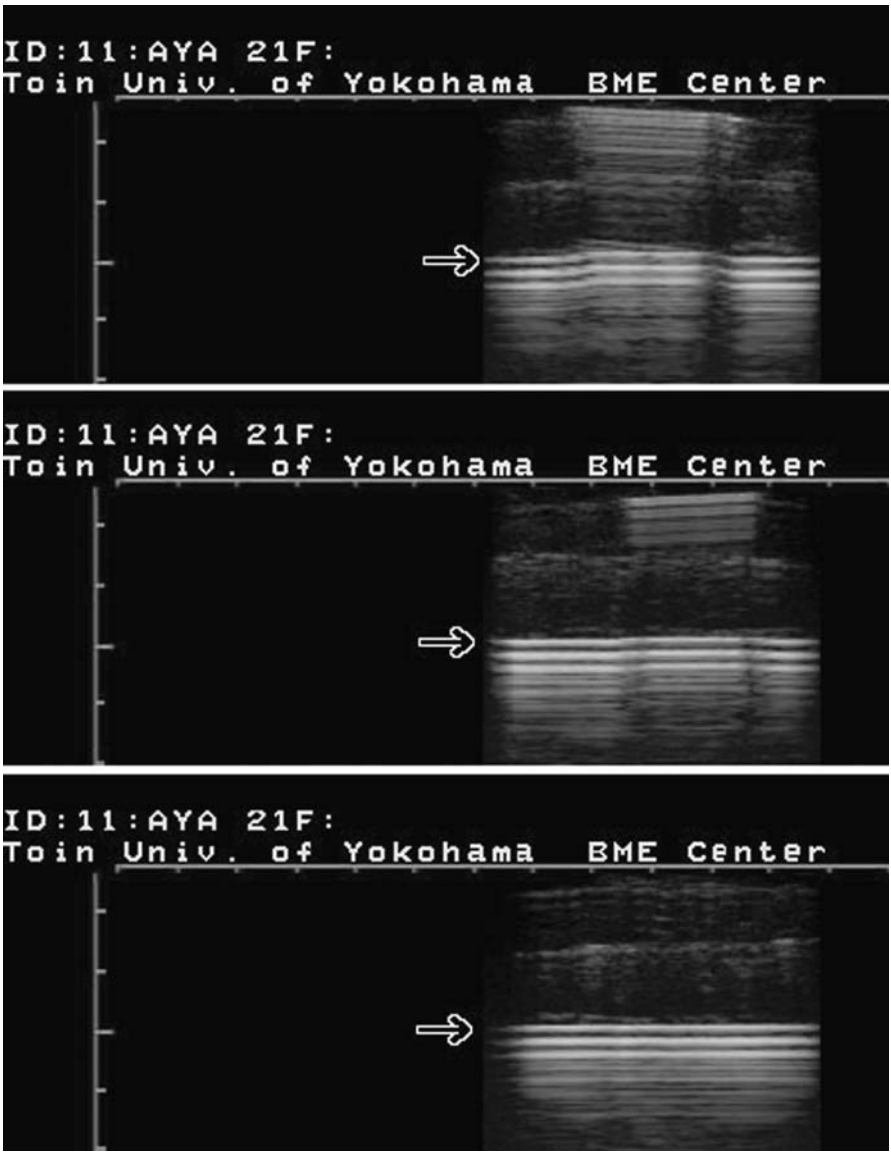

FIG. 3. **a** Pork slices of thickness of 49 mm with 2-mm-thick PMMA plate. **b** Pork slices of thickness of 49 mm with 1-mm-thick PMMA plate. **c** Pork slices of thickness of 49 mm without PMMA plate. All the B-mode image is zoomed to enlarge the apparent protrusion. Apparently three-layered echo signals are due to multiple scattering in the upper and lower PMMA plates. Uppermost reflection is indicated by an *arrow*

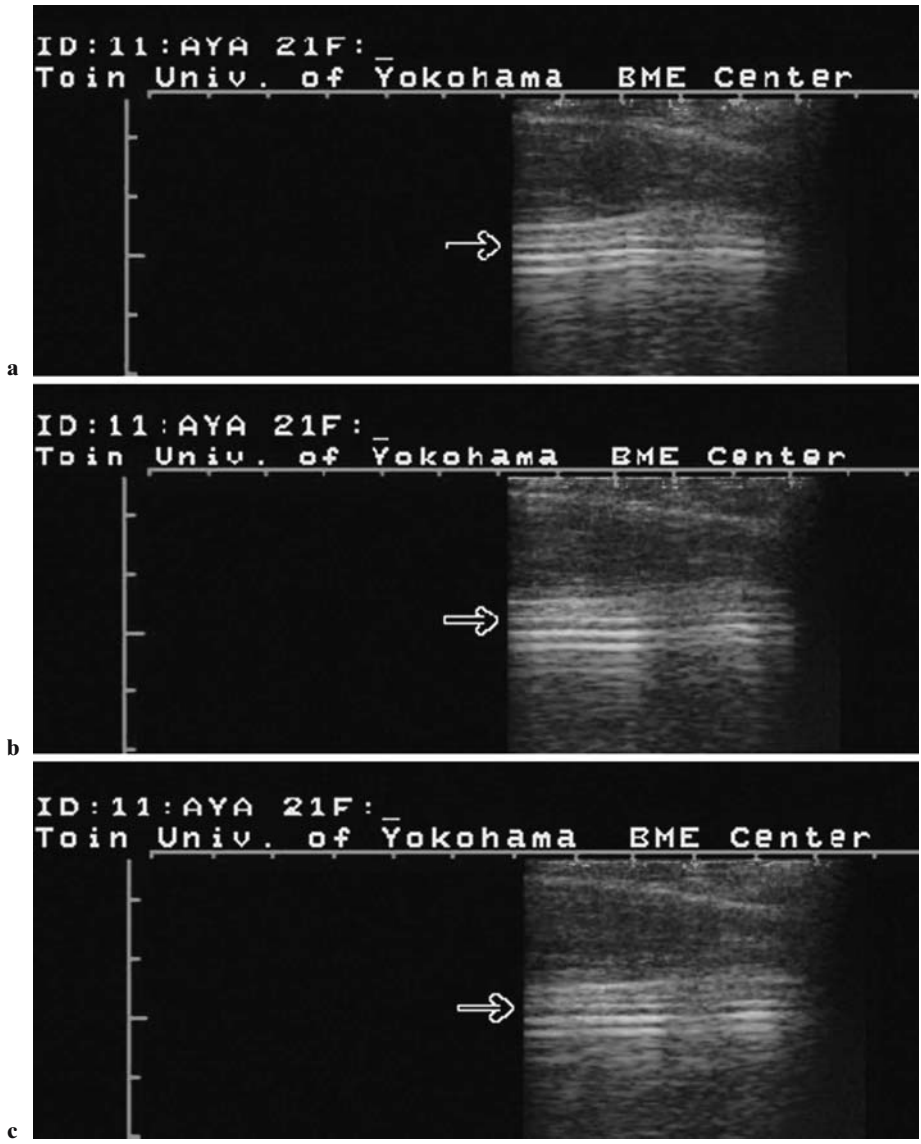

FIG. 4. **a** Forearm of thickness of 46 mm with 2-mm-thick PMMA plate. **b** Forearm of thickness of 46 mm with 1-mm-thick PMMA plate. **c** Forearm of thickness of 46 mm without PMMA plate. All the B-mode image is zoomed to enlarge the apparent protrusion. Apparently three-layered echo signals are due to multiple scattering in the upper and lower PMMA plates. Uppermost reflection is indicated by an *arrow*

transducer. Echo images may also be useful to observe the reflector position, which may be apparently protruding due to the higher sound velocity of the tumor. The echoic volume may be useful to estimate the sound velocity of the region. The reason we have examined a forearm instead of an actual breast is the lack of volunteers. The examination of the forearm, however, does not seem to be so inadequate because the present method seems to be most suitable for examination of dense breasts of young females less than 40 years of age with scirrhous cancer, and the velocity of sound is greater compared to older, fatty breasts [3].

References

1. Hayakawa Y, Inada T, Ueno E, et al (1984) Mass screening of breast cancer by ultrasound transmission technique: theoretical considerations. Jpn J Appl Phys 24(suppl 24-1):82–83
2. Carson PL, Scherzinger AL, Brand PH, et al (1983) Ultrasonic computed tomography instrumentation and human studies. In: Ultrasonic examination of the breast. Wiley, Chichester, pp 187–199, Fig. 4
3. Bamber JC (1983) Ultrasonic propagation profiles of the breast. In: Ultrasonic examination of the breast. Wiley, Chichester, pp 37–44, Fig. 2

Breast Cancer Ablation: Imaging and Early Experience

Hernan I. Vargas

Summary. The goal of minimally invasive therapy for breast cancer is to eradicate cancer cells with minimal damage to the underlying normal breast parenchyma or skin. Tumor ablation is seen as a means of obtaining local control of breast cancer without surgery. Breast imaging is a critical component of therapy to (1) detect the primary tumor, (2) demonstrate the anatomical extent of the tumor, (3) Guide the tumor-ablative device, (4) monitor tissue effects during treatment, and (5) Monitor the long-term effects of treatment. Current protocols of minimally invasive ablation of primary breast cancer use physical means for tumor ablation. Preliminary data exist for the use of percutaneous excision and thermal energy (cryotherapy, interstitial laser photocoagulation, radiofrequency, and microwaves).

Key words. Breast, Cancer, Ablation, Ultrasound, Magnetic resonance

Introduction

The principles of breast cancer surgery underscoring removal of the breast and regional lymphatics originated in the late nineteenth century in Europe. Subsequently, Halsted proposed that breast cancer dissemination occurs sequentially involving the breast first, followed by involvement of lymphatics and regional progression that subsequently leads to systemic disease. This paradigm has served as a premise for surgical management of breast cancer during the past century [1].

Investigators from the NSABBP (National Study for Breast and Bowel Project) have questioned the validity of this concept with a series of prospective studies [2]. Current understanding of cancer biology suggests that systemic progression of breast cancer occurs early and independently from lymph node involvement.

As our understanding of the natural history and biology of breast cancer has evolved, the surgical treatment of breast cancer and local regional disease have also changed. Respect of patient autonomy in the decision-making process and the development of effective screening with mammography have contributed to a demonstrable change in breast cancer survival and clinical presentation. Cady et al. have

Division of Surgical Oncology, Harbor-UCLA Medical Center, 1000 W. Carson Street, Torrance, CA 90509, USA

documented a progressive decrease in the average size of breast cancer [3]. Subclinical breast cancer is currently a common presentation. This stage is defined as the detection of breast cancer before the development of any symptoms. Therefore, the management of breast cancer has evolved toward less invasive surgical treatment [2, 4]. The possibility of treating the primary tumor without surgery is currently the subject of several clinical trials [5].

Minimal Invasive Treatment of Breast Cancer (MITBC)

Definition

The effectiveness of breast-conservation therapy has been documented in multiple prospective clinical trials [2, 6]. Similarly, less invasive procedures of axillary staging are used commonly today [4]. Minimally invasive treatment is the next step in the evolution of management of breast cancer [5]. MITBC refers to local therapy without surgery and is the subject of ongoing investigation.

Principles

The ideal local therapy for breast cancer should eradicate cancer cells with minimal damage to the underlying normal breast parenchyma. Current local management of breast cancer requires wide local excision with negative margins [7]. Achieving pathologically negative margins may be challenging and may lead to repeat surgery and undesirable poor cosmetic outcomes. In spite of obtaining negative margins, adjuvant therapy (radiation) is required because the local recurrence rate is high with surgery alone [2, 6, 7]. Methods for percutaneous excision and breast cancer ablation seek to achieve the goal of targeted local cancer eradication without significant damage to surrounding tissues. Imaging guidance is essential to outline the diseased areas of the breast and direct the therapy.

Breast Imaging

The role of imaging in breast cancer minimally invasive treatment includes the following:

1. Tumor detection: magnetic resonance imaging (MRI) is the single most sensitive technique for diagnosis of breast cancer [8, 9]. However, MRI may not be superior to a combination of sonography and mammography [10]. The main limitation of MRI is its relatively low specificity and the difficulty in detection of in situ breast cancer [9, 10].
2. Determination of the anatomical pattern of spread is useful in patient selection and in planning ablative therapy. MRI is more accurate than sonography and mammography in the detection of a multifocal pattern of spread and multicentricity [11]. MRI is valuable in establishing the extent of disease, even in difficult scenarios such as lobular carcinoma [12] or intraductal cancer spread [13]. Breast sonography is less sensitive than MRI but is better than mammography.
3. Breast imaging is used as a guide to the percutaneous excision/ablative tool. Ablation devices have been guided with MRI [14], sonographic [15], and stereotactic

techniques [16]. Limitations to the use of MRI are the need of nonferromagnetic equipment and the cost and availability of the equipment. Sonography is widely available at a reasonable price and is highly accurate in the localization of tumors.

4. Real-time imaging for treatment monitoring is ideal. Real-time imaging enables adjustments of treatment parameters and targeting of multiple irregular areas in the breast. MRI is cumbersome because of the need of MRI coils for best imaging and the need of nonferromagnetic equipment. Ultrasound affords the highest versatility in targeting and monitoring. The use of ultrasound contrast agents may be helpful in the evaluation of tumor blood flow, which may be a primary endpoint of ablative techniques.
5. A combination of clinical assessment, breast imaging, and pathology may be important in the long-term monitoring of success or failure. A combination of these techniques seems more promising than the use of imaging alone. MRI may be able to distinguish necrotic, avascular tissue from viable tumor. Further experience is required in this field.

A combination of imaging techniques may provide the best outcome. Clinical examination, mammography, and sonography are useful for diagnosis of breast cancer. A combination of mammography, sonography, and MRI are needed for best assessment of the extent of disease. Patient selection is critical because cases of multicentric disease, extensive local or focal disease with Pagetoid spread, and those with large areas of ductal carcinoma in situ (DCIS) may be impossible to treat with focal ablative techniques. Sonographic guidance of the therapy is reliable, widely available, and affordable. Sonography may also be useful in the monitoring of therapy as a measure of blood flow. Long-term monitoring may prove to be difficult and may require tissue diagnosis of the residual abnormalities. Complete biopsy of the abnormality under ultrasound guidance may afford the only means of measuring the success of therapy.

Investigational Methods of Minimally Invasive Therapy

MITBC may be accomplished through percutaneous excision or tumor ablation with physical energy, generally extreme temperatures.

Percutaneous Excision

Advanced breast biopsy instrument (ABBI) is a procedure that mimics needle localized excisional biopsy but is performed under image guidance. In this procedure, the patient is placed prone on the stereotactic table and under compression; the location of the lesion is established by obtaining two stereo views on mammography. Using the Cartesian theorem, the location of the lesion is determined. A needle is then introduced into the target and a wire is deployed. A skin incision in the breast is required to advance the cutting mechanism of a cannula. A cylindrical specimen with a 2-cm diameter and of variable length can be removed. Assessment of the margins is possible. The major caveat is that the lesion is often located eccentrically and margins are involved in 60% of cancers excised with ABBI [17].

Vacuum-assisted core biopsy (VACB) is commonly used for diagnosis of breast lesions. Using stereotactic or ultrasound guidance, the vacuum-assisted core device

can be guided to the breast abnormality allowing for extensive tissue sampling. Lieberman et al. [18] reported that calcific lesions were completely removed in 51% of cases. Gajdos et al. [19] reported that no cancer was found on the reexcision specimen in 17% of cases who underwent VACB for diagnosis. More recently, Fine et al. [20] have reported that benign palpable masses can be removed with a success rate of 99%. This result raises a possibility of its use directed at the treatment of breast cancer. With the vacuum-assisted core biopsy, a tumor can be removed in pieces, retrieving tissue samples of approximately 100 to 150 mg per sample. The success of this approach in the management of breast cancer has not yet been reported.

Tumor Ablation

Cryotherapy with liquid nitrogen as developed for the treatment of nonresectable liver has reported on the treatment of 16 patients by generating an iceball with a diameter of 28 mm. Complete tumor ablation was achieved in 5 tumors less than 16 mm in size. However, there was residual in situ carcinoma. Tumors larger than 16 mm had evidence of incomplete necrosis [21]. The freeze ball is highly anechoic on sonography, but assessment of the tissues deep to the freeze ball is impossible. Animal studies have documented the presence of residual cells in the frozen tissue.

Interstitial laser photocoagulation (ILP) uses a fiberoptic probe to conduct laser energy. The energy delivered causes hyperthermic ablation. Dowlatshahi et al. [16] have reported complete ablation in 70% of cases treated with ILP. A tissue temperature of 60°C and energy of 2500 joules/ml of tumor are predictors of successful ablation.

Radiofrequency ablation (RFA) was also developed for the treatment of nonresectable liver metastases. Cell death is secondary to dessication, denaturing of cytoskeletal proteins, and destruction of nuclear structure in the treated area. The size of the ablation field is determined by physics of resistive heat generation, requiring an array of conductors to deliver the thermal energy to a broad area. Izzo et al. [22] have reported on the results of a phase I study of 27 patients with a mean tumor diameter of 1.8 cm. Complete tumor ablation was seen in 96% of patients.

Focused microwave phased array ablation (FMPA) uses two opposing microwave applicators to generate microwave energy that produce deep tissue heating when properly focused. In a multicenter phase I study [15], we reported variable degrees of tumor necrosis in 68% of patients. Tumor necrosis was seen in 87% of patients receiving the highest dose in this dose escalation trial. However, patients with complete tumor ablation had residual DCIS.

References

1. Haagensen C (1986) Diseases of the breast. Saunders, Philadelphia
2. Fisher B, Anderson S, Bryant J, et al (2002) Twenty-year follow-up of a randomized trial comparing total mastectomy, lumpectomy, and lumpectomy plus irradiation for the treatment of invasive breast cancer. N Engl J Med 347:1233–1241
3. Cady B, Stone MD, Schuler JG, et al (1996) The new era in breast cancer: invasion, size, and nodal involvement dramatically decreasing as a result of mammographic screening. Arch Surg 131:301–308

4. Giuliano AE (2001) Current status of sentinel lymphadenectomy in breast cancer. Ann Surg Oncol 8:52–55
5. Singletary ES (2001) Minimally invasive techniques in breast cancer treatment. Semin Surg Oncol 20:246–250
6. Veronesi U, Cascinelli C, Mariani L, et al (2003) Twenty-year follow-up of a randomized study comparing breast-conserving surgery with radical mastectomy for early breast cancer. Cancer (Phila) 347:1227–1232
7. Singletary SE (2002) Surgical margins in patients with early-stage breast cancer treated with breast conservation therapy. Am J Surg 184(5):383–393
8. Warner E, Plewes DB, Shumak RS, et al (2001) Comparison of breast magnetic resonance imaging, mammography, and ultrasound for surveillance of women at high risk for hereditary breast cancer. J Clin Oncol 19:3524–3531
9. Malur S, Wurdinger S, Moritz A, et al (2001) Comparison of written reports of mammography, sonography and magnetic resonance mammography for preoperative evaluation of breast lesions, with special emphasis on magnetic resonance mammography. Breast Cancer Res 3:55–60
10. Blohmer JU, Oellinger H, Schmidt C, et al (1999) Comparison of various imaging methods with particular evaluation of color Doppler sonography for planning surgery for breast tumors. Arch Gynecol Obstet 262:159–171
11. Rizzato G (2001) Towards a more sophisticated use of breast ultrasound. Eur Radiol 11:2425–2435
12. Munot K, Dall B, Achuthan R, et al (2002) Role of magnetic resonance imaging in the diagnosis and single-stage surgical resection of invasive lobular carcinoma of the breast. Br J Surg 89:1296–1301
13. Hlawatsh A, Teifke A, Schmidt M, Thelen M (2002) Preoperative assessment of breast cancer: sonography versus MR imaging. AJR (Am J Roentgenol) 179:1493–1501
14. Halls-Craggs MA (2000) Interventional MRI of the breast: minimally invasive therapy. Eur Radiol 19:59–62
15. Vargas HI, Dooley WC, Gardner RA, et al (2003) Results of thermal dose escalation of focused microwave phased array (FMPA) thermotherapy for early-stage breast cancer. Ann Surg Oncol 10:S32
16. Dowlatshahi K, Francescatti DS, Bloom KJ, et al (2001) Image-guided surgery of small breast cancers. Am J Surg 182:419–425
17. Vargas HI, Kakuda J, Klein SR, Khalkhali IJ (1999) Stereotactic excisional biopsy of the breast. Presented at the annual meeting of the Pacific Coast Surgical Association (abstract)
18. Liberman L, Smolkin JH, Dershaw DD, et al (1998) Calcification retrieval at stereotactic, 11-gauge, directional, vacuum-assisted breast biopsy. Radiology 208:251–260
19. Gajdos C, Levy M, Herman Z, et al (1999) Complete removal of nonpalpable breast malignancies with a stereotactic percutaneous vacuum-assisted biopsy instrument. J Am Coll Surg 189:237–240
20. Fine RE, Boyd BA, Whitworth PW, et al (2002) Percutaneous removal of benign breast masses using a vacuum-assisted hand-held device with ultrasound guidance. Am J Surg 184:332–336
21. Pfeiderer SO, Freesmayer MG, Marx C, et al (2002) Cryotherapy of breast cancer under ultrasound guidance: initial results and limitations. Eur Radiol 12:3009–3014
22. Izzo F, Thomas R, Delrio P, et al (2001) Radiofrequency ablation in patients with primary breast carcinoma. A pilot study of 26 patients. Cancer (Phila) 92:2036–2044

US-Guided Mammotome Biopsy of Breast Masses in Comparison with US-Guided Aspiration Biopsy Cytology

N. Tohnosu[1], Y. Kobayashi[1], T. Natsume[1], T. Kato[2], and T. Uehara[2]

Summary. Ultrasound (US)-guided fine-needle aspiration biopsy cytology is useful for diagnosing hard-to-palpate tumors or small-sized tumors. However, it is sometimes difficult to establish diagnosis of masses with insufficient samples or to manage the diagnosis of questionable features. The purpose of this study was to evaluate US-guided Mammotome biopsy for the diagnosis of breast masses in comparison with US-guided fine-needle aspiration biopsy cytology. Fifty-eight histologically proven breast masses on US-guided fine-needle biopsy cytology and US-guided Mammotome biopsy were analyzed during January 1999–March 2003. US guidance was performed with a 7.5-MHz linear array ultrasonic transducer (Aloka SSD 5500); US-guided aspiration biopsy cytology was performed using a 21-gauge needle. Needle biopsy was performed using a Biopsis Mammotome with an 11-gauge needle with a freehand technique. Sensitivity, specificity and accuracy of aspiration biopsy cytology were 92.7%, 76.9%, and 88.9%, respectively. Duct cells were not obtained in 4 of 58 patients (6.9%). The sensitivity, specificity, and accuracy of Mammotome biopsy were 94.1%, 100%, and 97.1%, respectively. Mammotome biopsy is useful for the accurate diagnosis of masses with insufficient materials on aspiration biopsy cytology, sonographic-cytologic discordance, and radiotherapy after breast-conserving surgery.

Key words. Breast masses, Breast cancer, Mammotome biopsy, Fine-needle aspiration biopsy cytology, Ultrasonography

Introduction

Fine-needle aspiration biopsy cytology (FNAC) is frequently performed and is accepted as a reliable tool for the diagnosis of breast masses. However, FNAC using palpation alone has the limitations of lesion sampling specifically in nonpalpable masses, and hence ultrasound (US)-guided FNAC has come to be preferred to diagnose hard-to-palpate tumors or small-sized tumors. Nevertheless, it is sometimes difficult to establish accurate diagnosis due to sampling errors or questionable features.

[1] Department of Surgery, [2] Laboratory Division of Pathology, Funabashi Municipal Medical Center, 1-21-1 Funabashi, Chiba 273-8588, Japan

The purpose of this study was to evaluate US-guided vacuum-assisted Mammotome biopsy for the diagnosis of breast masses in comparison with US-guided FNAC.

Materials and Methods

Fifty-eight histologically proven breast masses on US-guided FNAC or Mammotome biopsy were retrospectively reviewed between January 1999 and March 2003. There were 55 palpable masses (94.8%) and 3 nonpalpable masses (5.2%). The masses ranged in sonographic size from 6 to 88 mm (mean, 20.3 mm). Sonographic guidance was performed with a 7.5-MHz linear array ultrasonic transducer (Aloka SSD 5500); US-guided FNAC was performed two times per lesion using a 21-gauge needle. Needle biopsy was performed using a Biopsis Mammotome with an 11-gauge needle, and a mean of five specimens were obtained per lesion under a freehand technique. Color Doppler sonography was always combined before this procedure to confirm vascular locations in and around the masses for avoiding bioptic bleeding.

Results

On US-guided FNAC, there were 4 of 58 masses (6.9%) in which duct cells were not obtained, and 1 of the lesions was found to be malignant. Three false negatives were invasive ductal carcinoma, papillary carcinoma, and mucinous carcinoma. Sensitivity, specificity, and accuracy were 92.7%, 76.9%, and 88.9%, respectively (Table 1). Although the sensitivity of US-guided FNAC was most favorable, it is necessary to reduce the number of poor samplings and false negatives. For this purpose, we consider that the indication for Mammotome biopsy is masses with no diagnosis due to inadequate materials on US-guided FNAC, masses showing sonographic-cytologic discordance and masses detected after breast conserving surgery followed by radiotherapy (Fig. 1). The respective sensitivity, specificity, and accuracy of Mammotome biopsy were 94.1%, 100%, and 97.1% (Table 2). One (5.6%) of 18 benign masses evaluated by this procedure was correctly diagnosed on surgical excision to be malignant (Table 3).

Table 1. Accuracy of US-guided aspiration biopsy cytology

	Pathology	
Cytology	Malignant	Benign
No duct cells	1	3
Malignant	38	3
Benign	3[a]	10

Sensitivity, 38/41 (92.7%); specificity, 10/13 (76.9%); accuracy, 48/54 (88.9%)

[a]Invasive ductal cancer, papillary cancer, mucinous cancer

1. Masses with no diagnosis due to insufficient samples on US-guided aspiration biopsy cytology
2. Masses showing sonographic-cytological discordance
3. Masses detected after breast-conservation surgery followed by radiotherapy

Fig. 1. Indication of Mammotome biopsy

Table 2. Accuracy of Mammotome biopsy

	Pathology	
Mammotome biopsy	Malignant	Benign
Malignant	16	0
Benign	1	17

Sensitivity, 16/17 (94.1%); specificity, 17/17 (100%); accuracy, 33/34 (97.1%)

Table 3. Pathologic findings on US-guided Mammotome biopsy

Lesion	No. of masses
Benign ($n = 18$)	
Fibrocystic change	7 (1 carcinoma)
Benign breast tissue	2
Fibroadenoma	1
Ductal hyperplasia	1
Papilloma	1
Others	6
Malignant ($n = 16$)	
Invasive ductal carcinoma	14
Invasive lobular carcinoma	1
Intraductal carcinoma	1

Discussion

Sonographically guided, continuous, and reliable visualization of the needle allows for accurate material sampling. Consequently, US-guided FNAC and Mammotome biopsy are minimally invasive tools for the accurate diagnosis of breast masses to avoid unnecessary surgical excision. For US-guided FNAC, sensitivities, specificities, and accuracy ranges are 86.9%–98.9%, 45.6%–95.3%, and 74.7%–89% [1–3], respectively. More than 50% of samples by FNAC are insufficient [4], and a lower yield is reported in tumor types producing a desmoplastic stroma (tubular carcinoma, invasive lobular carcinoma) or in noncomedonic in situ ductal carcinoma [2]. Sampling errors by FNAC using palpation alone were as high as 43%, and tumor types resulting in insufficient samples were small-sized, invasive ductal carcinoma rich in scirrhous component or invasive lobular carcinoma in our series also. In contrast, 6.9% of samples

obtained on US-guided FNAC were inadequate. Therefore, we prefer to perform US-guided FNAC first if the masses sonographically show the aforementioned findings.

US-guided core-needle biopsy significantly improved the specificity and accuracy of inadequate biopsy, by US-guided FNAC [3]. Although other authors [5–7] stress the usefulness of core-needle biopsy, Simon et al. [7] mentioned vacuum-assisted core-needle biopsy, stating that sensitivity, specificity, and accuracy were 94.7%, 98%, and 98.6%, respectively, similar to our series. The vacuum-assisted core needle is superior to a spring-loaded needle in sampling volume, thus leading to more accurate diagnosis. Considering their report of bioptic massive bleeding in 7%, color Doppler sonography before biopsy is strongly recommended to avoid the complication, as in our series.

Conclusions

Mammotome biopsy is an accurate method for evaluating breast masses with insufficient samples on US-guided FNAC, sonographic-cytologic discordance, and breast-conserving surgery followed by radiotherapy.

References

1. Thibault F, Meunier M, Klijanienko J, et al (2000) Diagnostic accuracy of sonography and combined sonographic assessment and sonographically guided cytology in non-palpable solid breast lesions. J Clin Ultrasound 28:387–398
2. Zanconati F, Bonifacio D, Falconieri G, et al (2000) Role of fine-needle aspiration cytology in nonpalpable mammary lesions: a comparative cytohistologic study based on 308 cases. Diagn Cytopathol 23:87–91
3. Hatada T, Ishi H, Ichii S, et al (2000) Diagnostic value of ultrasound-guided fine-needle aspiration biopsy, core-needle biopsy, and evaluation of combined use in the diagnosis of breast lesions. J Am Coll Surg 190:299–303.
4. Joelle M, Schoonjans, Rachel F, et al (2001) Fourteen-gauge ultrasonographically guided large-core needle biopsy of breast masses. J Ultrasound 20:967–972
5. Rubin E, Mennemeyer ST, Desmond RA, et al (2001) Reducing the cost of diagnosis of breast carcinoma: impact of ultrasound and imaging-guided biopsies on a clinical breast practice. Cancer (Phila) 91:324–332
6. Liberman L (2000) Clinical management issues in percutaneous core breast biopsy. Radiol Clin N Am 38:791–807
7. Simon JR, Kalbhen CL, Cooper RA, et al (2000) Accuracy and complication rates of US-guided vacuum-assisted core breast biopsy: initial results. Radiology 215:694–697

Ultrasonographic Appearance and Clinical Implication of Bilateral Breast Infiltration with Leukemia Cells

Satomi Asai[1], Hayato Miyachi[1], Mitsuhiro Kubota[2], Noriko Koyanagi[3], Yoshiaki Ogawa[4], Tomomitsu Hotta[4], and Yasuhiko Ando[1]

Summary. We assessed the ultrasonographic appearance and clinical implication of bilateral breast involvement in three cases of acute leukemia: L1, L3, and M1 of the FAB subtype. Breast involvement was observed in one case at the initial presentation and in two cases at relapse after bone marrow transplantation. Common findings of ultrasonograms of the cases were hypoechoic masses with diffusely mixed internal echogenicity, including a mottled appearance in the case with L3. The ultrasonographic appearance was nonspecific to leukemia. In each case, both sides of breast involvement were identical to each other in appearance at the diagnosis and during the course of treatment. When breasts were found to be involved by leukemia cells, all three cases had another extramedullary lesion: meninx in two cases at relapse and ovary in one case at the initial presentation. These findings suggested the bilateral breast involvement occurred as a part of the diffuse and generalized leukemia process and as extramedullary lesions at sanctuary areas of antileukemia agents.

Key words. Leukemia cell, Infiltration, Breast, Ultrasonography

Introduction

One frequent cause of morbidity in acute leukemia is extramedullary leukemia cell infiltration. Leukemia cell infiltration of the breast is rarely seen as an extramedullary lesion [1–4]. Both unilateral and, less frequently, bilateral breast involvement with leukemia cells has been reported [4–7]. We experienced bilateral breast involvement in three women with acute leukemia. This study attempted to assess the ultrasonographic appearance of these and to clarify the clinical implication of bilateral breast infiltration with leukemia cells.

[1] Department of Laboratory Medicine, Tokai University School of Medicine, Bohseidai, Isehara, Kanagawa 259-1193, Japan
[2] Department of Surgery, Tokai University School of Medicine, Isehara, Kanagawa, Japan
[3] Clinical Laboratory Center, Tokai University Hospital, Isehara, Kanagawa, Japan
[4] Department of Internal Medicine, Tokai University School of Medicine, Isehara, Kanagawa, Japan

Patients and Methods

Three women with acute leukemia were diagnosed having bilateral breast involvement from 1990 to 2001 at Tokai University Hospital. Case 1 was a 47-year-old woman with acute lymphoblastic leukemia (ALL L3 of the FAB subtype) at the initial diagnosis. She presented with bilateral breast masses and a lower abdominal mass. Ultrasonographic examination of the pelvis revealed a large ovarian solid mass with internal echogenicity accompanying small cystic areas, which was suspected to be leukemic involvement of the ovary. Case 2 was a 16-year-old girl with pre-B ALL (L1 of the FAB subtype). She underwent bone marrow transplantation (BMT) during the first complete remission, and then had painless bilateral breast masses and headache at the second relapse. Cerebrospinal fluid examination revealed meningeal leukemia. Case 3 was a 35-year-old woman with acute myeloblastic leukemia (AML, M1 of the FAB subtype). She underwent BMT at the first relapse. After engraftment, she had painless bilateral breast masses and headache. Cerebrospinal fluid examination revealed meningeal leukemia.

Ultrasonographic examination of the breast mass was carried out with real-time linear scanners (SSD 650, Aloka; LOGIQ500, GE Yokogawa) using a 7.5-MHz probe. Breast involvement with leukemia cells was diagnosed with histopathological examination of needle aspiration biopsy of the breast or bone marrow. Ultrasonographic findings of the breast lesions in each patient were assessed in association with clinical course.

Results

Ultrasonographic appearance of bilateral breast involvement was assessed in three female cases with acute leukemia. Common findings of their ultrasonograms were large hypoechoic masses with internal echogenicity. The shape of these masses was oval or long on the side. The margin was irregular but the border was clear, not involving the fat and muscle elements of the surrounding tissues. The posterior echo of the masses was enhanced. The parenchyma echo of these lesions was a heterogeneous or diffuse mixed echo texture. The parenchyma echo of the masses in the case with L1 of the FAB subtype showed a hypoechoic mass with small hyperechoic area (Fig. 1) [7]. The parenchyma echo of the masses in the case with M1 was hypoechoic solid masses with slight internal echogenicity (Fig. 2). The parenchyma echo of the masses in the case with L3 showed characteristically a mottled pattern. The finding was mimicking mastopathy [8].

In each case, the ultrasonographic appearance of both sides of breast involvement was identical at the diagnosis and during the course of treatment. With induction chemotherapy, both sides of breast involvement and ovary tumor in the case of L3 reduced in size and disappeared concomitant with attainment of bone marrow remission. By contrast, both sides of breast involvements as well as bone marrow disease in L1 and M1 were nonresponsive to chemotherapeutic treatment of leukemia.

The ultrasonographic appearance and clinical course of breast involvement are summarized in Table 1.

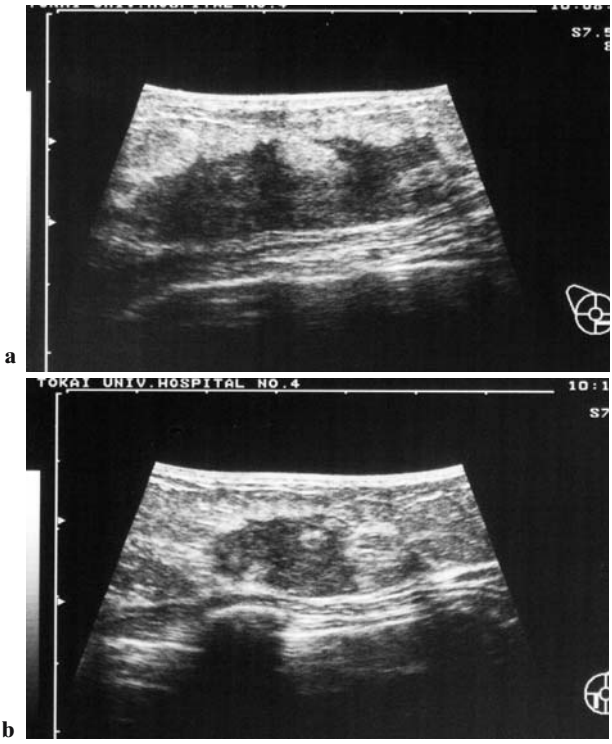

Fig. 1. Ultrasonogram of the right (**a**) and left (**b**) sides of breast with L1 of the FAB subtype after 1 year and 6 months of bone marrow transplantation. There were hypoechoic solid masses with hyperechoic area. The posterior echo enhancement is demonstrated

Discussion

Leukemic infiltration may occur in any tissue in the body, and breast involvement is rarely seen as extramedullary lesions [1,2]. We assessed the ultrasonic and clinical features of bilateral breast involvement in three Japanese females with acute leukemia. FAB types of the three patients were various, namely, L1, L3, and M1, which was consistent with the previous reports describing breast involvement in all ranges of acute leukemia subtype [2,4]. Leukemia cell infiltration of the breast was observed not only as manifestation of advanced disease at relapse but also as the initial presentation.

On ultrasonography, a lesion of the breast usually appears as a solid hypoechoic lesion with an ill-defined and irregular margin [9–11]. Normal breast tissue was bilaterally replaced by a mass of leukemic cells, the parenchyma echo resulting in heterogeneous or diffuse mixed echo texture. These ultrasonographic appearances were nonspecific to leukemia. The parenchyma echo of L3 showed characteristically a mastopathy-mimicking mottled pattern [8]. In each case, the ultrasonographic appearance of both sides of breast involvement was identical at the diagnosis and during the course of chemotherapy.

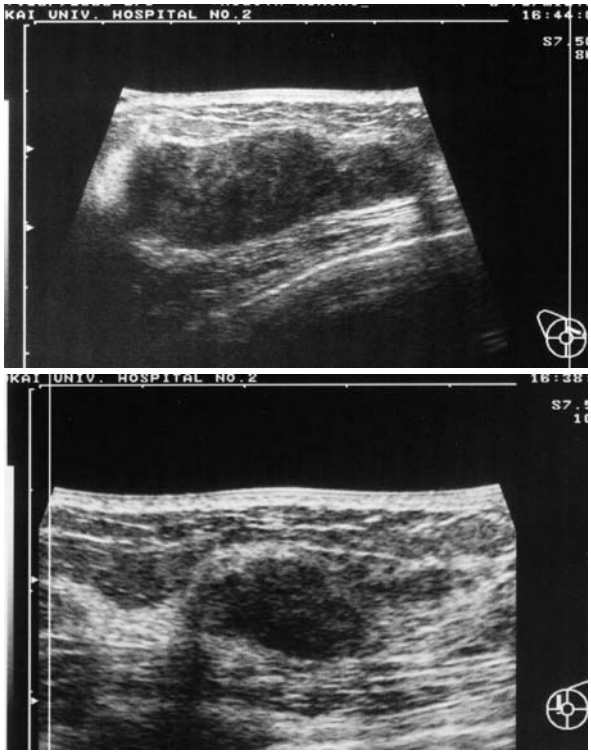

FIG. 2. Ultrasonogram of the right (**a**) and left (**b**) side of breast with M1 of the FAB subtype after 8 months of bone marrow transplantation. There were bilaterally hypoechoic solid masses with slight internal echogenicity. The posterior echo enhancement is demonstrated

TABLE 1. Ultrasonographic appearance and clinical course of bilateral breast involvement

FAB subtypes	Internal echo of the mass	Treatment responsiveness		Other extramedullary lesion
		Breast	BM disease	
L1	Bilateral hyperechoic area	Bilateral nonresponsive	Nonresponsive	CNS
L3	Bilateral mottled pattern	Bilateral responsive	Responsive	Ovary
M1	Bilateral heterogeneous	Bilateral nonresponsive	nonresponsive	CNS

BM, bone marrow; CNS, central nervous system

When the breast involvement was diagnosed, all three cases had another extramedullary lesion, meninx and ovary. These organs are known as sanctuary areas of antileukemic agents. Both sides of breast involvement showed the same responsiveness to chemotherapy as the bone marrow disease. Bilateral breast involvement at relapse was suggested to be an indication of poor prognosis, because the patients had concomitant meningeal leukemia as well as unresponsiveness to chemotherapy, prob-

ably due to resistant leukemic cells in the sanctuary areas. Bilateral breast involvement was suggested to be a part of a diffuse and generalized leukemic process because they had identical clinical course and ultrasonographic appearance and concomitant involvement of other sanctuary organs such as central nervous system (CNS) or ovary. It was also suggested that one may consider exploring for other extramedullary lesions when bilateral breast involvement is observed in leukemia patients.

References

1. Bohman LG, Bassett LW, Gold RH, et al (1982) Breast metastases from extramammary malignancies. Radiology 144:309–312
2. McCrea ES, Johnston C, Haney PJ (1983) Metastases to the breast. AJR (Am J Roentgenol) 141:685–690
3. Monteleone PM, Steele DA, King AK, et al (2001) Bilateral breast relapse in acute myelogenous leukemia. J Pediatr Hematol/Oncol 23:126–129
4. Memis A, Killi R, Orguc S, et al (1995) Bilateral breast involvement in acute lymphoblastic leukemia: color Doppler sonography findings. AJR (Am J Roentgenol) 165:1011
5. Chim CS, Shek TWH, Liang R (2000) Isolated relapse of acute lymphoblastic leukemia in the breast masquerading as gynecomastia. Am J Med 108:677–679
6. Fitoz S, Atasoy Ç, Yavuz K, et al (2002) Granulocytic sarcoma: cranial and breast involvement. Clin Imaging 26:166–169
7. Okumura A, Kubota M, Okamoto Y, et al (2000) Acute lymphoblastic leukemia with breast involvement suggested by ultrasonography: A case report. J Med Ultrasonics 27:805–809
8. Asai S, Miyachi H, Ochiai N, et al (2001) Mastopathy-mimicking appearance in Burkitt's lymphoma in breasts. J Clin Imaging 25:309–311
9. Yang WT, Metrewel I (1999) Sonography of nonmammary malignancies of the breast. AJR (Am J Roentgenol) 172:343–348
10. Khoury NJ, Al-Kass FMH, Jaafar HN, et al (2000) Bilateral breast involvement in acute myelogeneous leukemia. Eur Radiol 10:1031
11. Son HJ, Oh KK (1998) Multicentric granulocytic sarcoma of the breast: mammographic and sonographic findings. AJR (Am J Roentgenol) 171:274–275

Analysis of Ultrasonographic Findings of Breast Masses by the Nagasawa Computer-Aided Diagnosis System

Setsuko Kaoku[1], Yasuyuki Kato[2,3], Tsutomu Takashima[3], Yoshinari Ogawa[3], Yasuhisa Fujimoto[4], Toru Nagasawa[5], and Kosei Hirakawa[3]

Summary. The Computer-Aided Diagnosis (CAD) software Nagasawa ver. 7.2 was developed by Professor Toru Nagasawa. The purpose of this study was to evaluate our decisions on ultrasonographic (US) findings using the CAD system. We analyzed 29 ultrasonograms (14 breast cancers and 15 fibroadenomas, diagnosed in Osaka City University Hospital). We categorized the US findings of the masses by the features of their shapes and borders (shape: regular, relatively irregular, irregular; border: smooth, relatively rough, rough). Then, we analyzed these ultrasonic categories with the CAD system. Each feature was compared with CAD parameters [shape: deformity index (DI), irregularity (Irr), marginal area index (MAI); border: entropy (Ent), fractal dimension (Fd), surface–length index (SL)]. The CAD parameters of DI, Irr (respectively, $P = 0.0059$), Ent ($P = 0.0039$), Fd ($P = 0.0214$), and SL ($P = 0.0054$) were significantly correlated with US categories. According to multiple comparisons, categories of "regular" and "relatively irregular," and "smooth" and "relatively rough," were in the same group. The CAD parameters indicated almost identical results with conventional US findings in breast masses. "Relatively irregular" and "relatively rough" can include "regular" and "smooth," respectively.

Key words. Ultrasonography, Computer-aided diagnosis, Breast cancer, Fibroadenoma

[1] Department of Clinical Laboratory, Minami Osaka Hospital, 1-18-18 Higashikagaya, Suminoe-ku, Osaka 559-0012, Japan
[2] Department of Surgery, Osaka Medical Prison, Osaka, Japan
[3] Department of Surgical Oncology, Osaka City University Graduate School of Medicine, Medical School, Osaka, Japan
[4] Department of Surgery, Osaka City Sumiyoshi Hospital, Osaka, Japan
[5] Department of Healthcare Informatics, Takasaki University of Health and Welfare, Gunma, Japan

Background

Recently, a computer-aided diagnosis (CAD) system for mammography has been in practical use even though research into CAD for ultrasonography (US) has just started. Herein, we evaluate the usefulness of the CAD system in ultrasonographic (US) diagnosis.

The CAD software Nagasawa ver. 7.2 was developed for objective US diagnosis for breast tumors by T. Nagasawa. The purpose of this study was to evaluate our decision on US findings by the CAD system.

How to Use the Nagasawa System

The system is semiautomatic, and works on Microsoft Windows (Fig. 1). Only about 1 min is necessary for the diagnosis of each image of a breast mass.

We use the Nagasawa system as follows:

1. Setting of region of interest (ROI).
2. Detection of mass.
3. Detection of position. (Users click the mouse at the positions of surface of skin, upper border of mammary gland, and fascia of major pectoral muscle.)
4. Features analysis.
5. Results of calculation.
6. Decision.

Materials and Methods

We analyzed 29 ultrasonograms [14 breast cancers (CA) and 15 fibroadenomas (FA), diagnosed pathologically in the Department of Surgical Oncology, Osaka City University Graduate School of Medicine]. Patient mean age was 58.8 (31–80) years for CA and 44.0 (20–72) years for FA. Tumor mean diameter was 21.7 (10–35) mm for CA and 22.9 (10–31) mm for FA. We used an Aloka SSD-2000, SSD-650CL with a 10-MHz mechanical sector scanner. The CAD diagnosis was performed using US images of long axial dimension of breast masses stored in JPEG format. The US images were categorized by four sonographers and four medical doctors who are experts in breast ultrasonography. We categorized the US findings of the masses by the features of their shapes and borders (shape: regular, relatively irregular, irregular; border: smooth, relatively rough, rough). The US images were classified by agreement of more than five experts. The group of "shape" were categorized as regular ($n = 3$), relatively irregular ($n = 8$), or irregular ($n = 15$); the group of "border" were categorized as smooth ($n = 6$), relatively rough ($n = 7$), or rough ($n = 10$). Then, we analyzed these ultrasonic categories with the CAD system. Each feature was compared with CAD parameters [shape: deformity Index (DI), irregularity (Irr), marginal area index (MAI); border: entropy (Ent), fractal dimension (Fd), surface–length index (SL)].

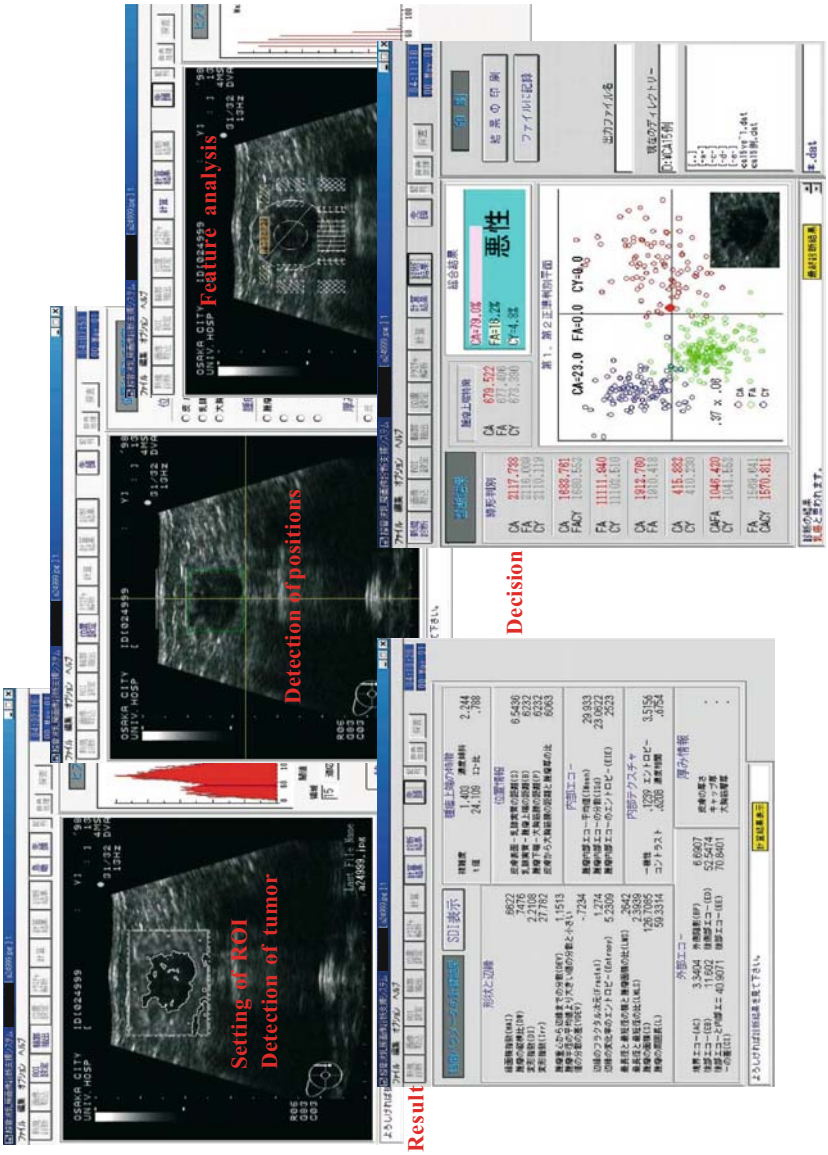

FIG. 1. Diagram of the CAD of ultrasonic image analysis for breast tumors

Table 1. Results (median ± variance): shapes

	DI	Irr	MAI
Regular	1.80 ± 0.52	22.65 ± 82.52	0.55 ± 0.25
Relatively irregular	1.62 ± 0.19	20.32 ± 30.30	0.69 ± 0.05
Irregular	2.75 ± 0.91	34.59 ± 143.12	0.55 ± 0.04
P value	0.0059	0.0059	0.6348

Kruskal-Wallis test
DI, deformity index; Irr, irregularity; MAI, marginal area index

Table 2. Results (median ± variance): borders

	Ent	Fd	SL
Smooth	4.039 ± 0.447	1.229 ± 0.002	1.278 ± 0.043
Relatively rough	4.233 ± 1.002	1.254 ± 3.890	1.400 ± 0.018
Rough	5.964 ± 0.895	1.288 ± 0.002	1.673 ± 0.079
P value	0.0039	0.0214	0.0054

Kruskal-Wallis test
Ent, entropy; Fd, fractal dimension; SL, surface–length index

Results

The CAD parameters of DI, Irr (respectively, $P = 0.0059$), Ent ($P = 0.0039$), Fd ($P = 0.0214$), and SL ($P = 0.0054$) significantly correlated with US categories (Kruskal–Wallis test) (Tables 1, 2). According to multiple comparisons (Bonferroni correction, Mann–Whitney *U* test), each parameter significantly correlated with categories of "regular" and "relatively irregular"; "smooth" and "relatively rough" were in the same group (Figs. 2–6).

Discussion

In general, many Japanese sonographers and medical doctors tend to categorize into "relatively irregular" or "relatively rough" when US images of "regular" and "smooth" are not so clear. In this study, experts had categorized in the same way. In other words, the group of relatively irregular and relatively rough should be categorized into regular and smooth. In the near future, prospective and consecutive studies are necessary to evaluate discrimination of ultrasonic image analysis of CAD for breast tumors.

Conclusion

The CAD parameters indicated almost identical results with conventional US findings in breast masses. Relatively irregular and relatively rough can be included in regular and smooth, respectively.

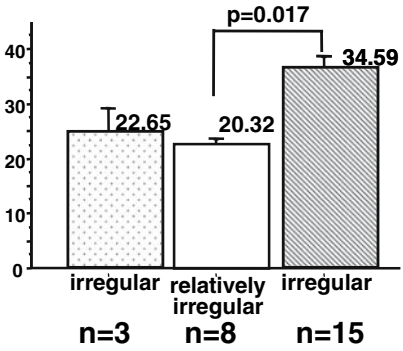

Fig. 2. Irregularity

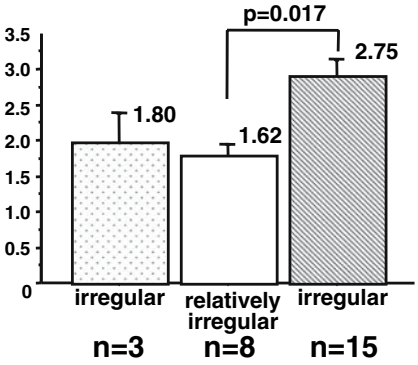

Fig. 3. Deformity index

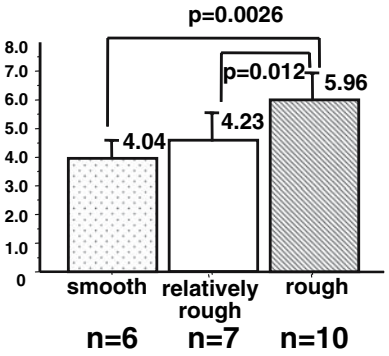

Fig. 4. Entropy

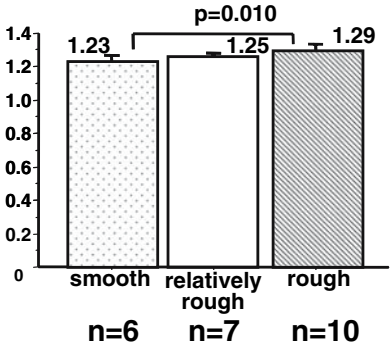

Fig. 5. Fractal dimension

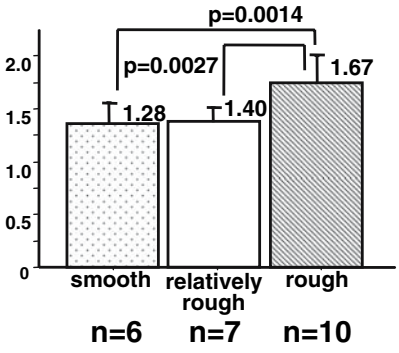

Fig. 6. Surface–length index

References

1. Nagasawa T, et al (2000) Quantitative diagnosis in ultrasonic image of breast tumor using image analysis: evaluation of feature parameters (in Japanese). Jpn J Med Ultrasonics 27:682
2. Kaoku S, Kato Y, Ogawa Y, et al (2000) Nyubou no chouonpashindan (in Japanese). Iyaku J: 64–68

Dorsal Growth of Breast Cancer May Correlate with the Prognosis

Hiroshi Yoshibayashi, Satoru Nishimura, and Satoru Matusue

Summary. We studied whether the growth of breast cancer as shown by ultrasonography (US) relates to prognosis. A total of 193 patients who had a single mass on US and had undergone radical operation between January 1992 and December 1997 were studied. The tumors on US were classified the direction of backward or forward growth. Internal type was defined as the tumors within the mammary glands; ventral type was tumors that grew upward toward the subcutaneous tissue; dorsal type was masses that grew downward toward the retromammary space; and mixed type was masses that grew in both subcutaneous tissues and retromammary spaces. The ventral type was seen in 106 cases, mixed type in 66 cases, internal type in 12 cases, and backward type in 9 cases. Disease-free survival rate (DFS) and overall survival rate (OS) (10 years) of these types were 100%/100% (internal type), 79%/86% (ventral type), 68%/76% (mixed type), and 39%/67% (dorsal type). We concluded that breast cancer tends to grow ventrally rather than dorsally and that the dorsal type showed poorer prognosis than the other types.

Key words. Breast cancer, Growth pattern, Prognosis, Ultrasonography

Introduction

The invasion of breast cancer differs between the areas of tumor. For example, all lymph node metastases are different. We usually evaluate horizontal growth of breast cancer and classify five areas of A, B, C, D, and E. However, we do not yet know classification by growing of backward or forward. Therefore, the purpose of this study was to evaluate breast cancer on ultrasonography (US), to classify the direction of backward or forward growth, and to demonstrate whether this classification correlate with the prognosis (Fig. 1).

Department of Abdominal and General Surgery, Tenri Hospital, 200 Mishima, Tenri, Nara 632-8552, Japan

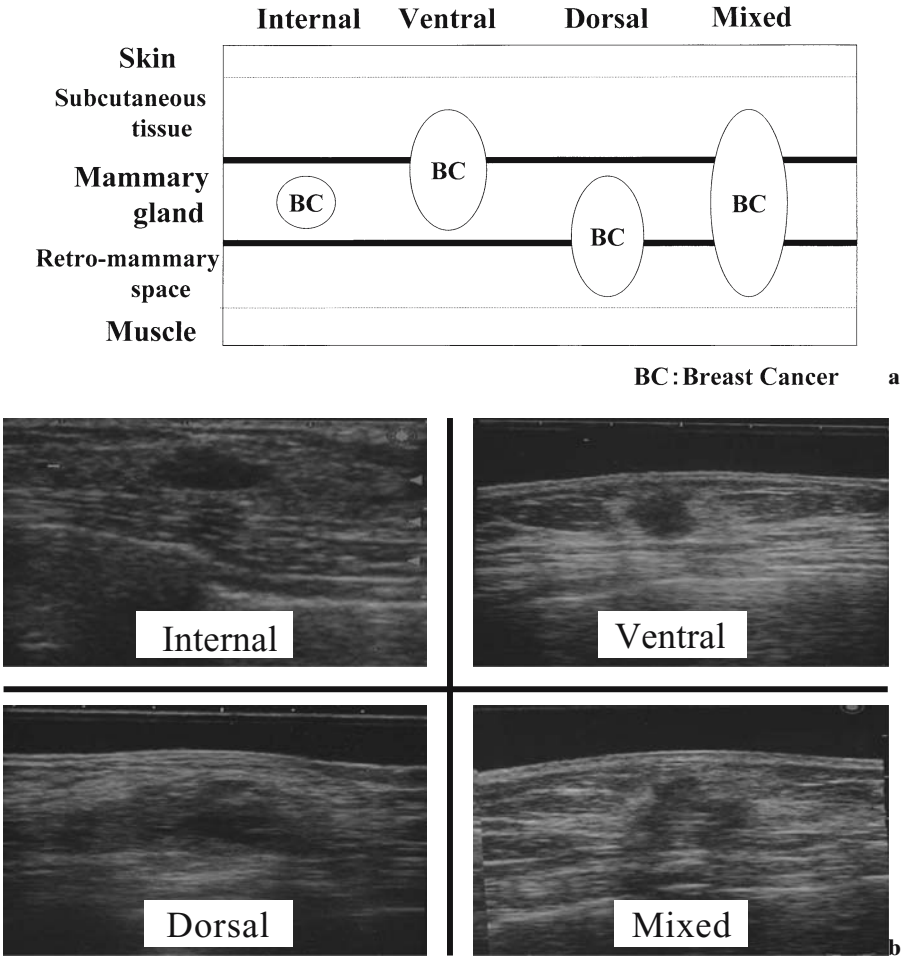

Fig. 1. The four categories of breast cancer by ultrasonography (US)

Results

All patients were Japanese women. A summary of the 193 cases is shown in Table 1. The mean tumor size of mixed type was 28.1 mm, 25.5 mm in dorsal type, 20.5 mm in ventral type, and 18.8 mm in internal type. The mixed type was significantly larger than the other three categories ($P < 0.01$, χ^2 test).

The frequency of the four categories is shown in Fig. 2. The ventral type (55%) was found in more than half of the 193 cases studied, followed by mixed type, which occurred in 34% of the cases. Internal type and dorsal type were found in 6% and 5% of the cases, respectively.

Table 1. Summary of the 193 cases

	Internal	Ventral	Dorsal	Mixed	Totals
Area of tumor					
A	2	26	4	23	55 cases
B	0	7	1	2	10 cases
C	9	54	3	27	93 cases
D	1	16	1	12	30 cases
E	0	3	0	2	5 cases
Mean tumor size	18.8	20.5	25.5	28.1	23.2 mm
Pathological stage					
Stage I	6	45	3	18	72 cases
Stage II	6	58	5	42	111 cases
Stage III	0	3	1	6	10 cases

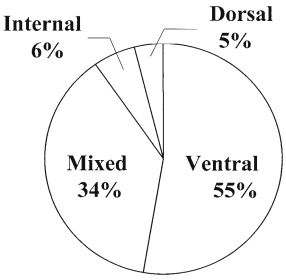

Fig. 2. The frequency of the four categories

Table 2. The rate of lymph node metastases, only T1 and T2 ($n = 187$)

	T		
Category	T1	T2	Total
Internal	25%	0%	17%
Ventral	25%	40%	31%
Dorsal	0%	33%	22%
Mixed	31%	46%	39%

Two patients of no dissection of lymph node and four patients of T3 excluded

Table 2 shows the rate of lymph node metastases. Among the four categories, mixed type, at 24 of 61 cases (39%), showed the most metastases, followed by ventral type at 33 of 105 cases (31%), dorsal type at 2 of 9 cases (22%), and internal type at 2 of 12 cases (17%). As the size of the tumor increases, the density of the lymph node metastases also increases.

The cumulative 10-year disease-free survival rate is shown in Fig. 3. Internal type had 10 years disease-free survival rate at 100%, ventral type at 79.9%, mixed type at 67.7%, and dorsal type at 39.5%. The greatest difference was between ventral type and dorsal type ($P < 0.05$). The cumulative 10-year overall survival rates are shown in

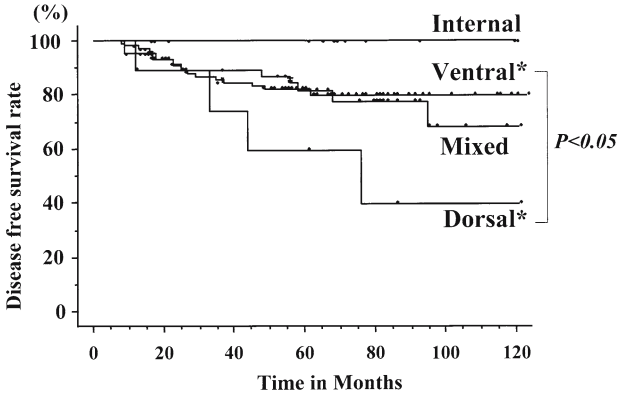

Fig. 3. The 10-year disease-free survival rate for the four types

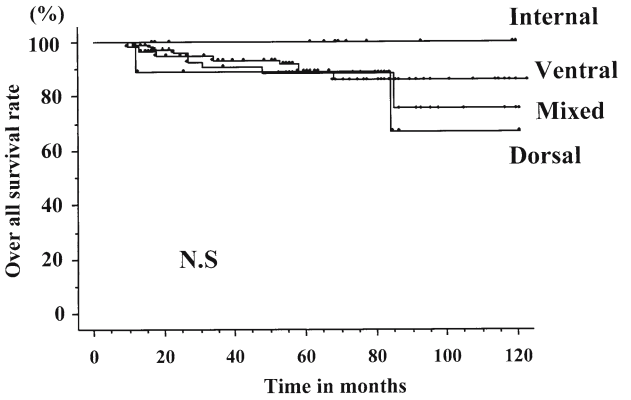

Fig. 4. The 10-year overall survival rate

Fig. 4. At the time of the present study, there was no significant difference among these.

The other data were statistically analyzed by the χ^2 test, using the Stat View software package (SAS Institute, Cary, NC, USA). All results were considered statistically significant at a *P* value less than 0.05.

Discussion

We usually evaluate horizontal growth of breast cancer and classify five areas as A, B, C, D, and E. However, we do not know how to classify by the direction of growth. Therefore, the purpose of this study was to evaluate breast cancer on US, to classify the direction of backward or forward growth, and to demonstrate whether this classification correlates with the prognosis. Breast cancer tends to grow ventrally rather

than dorsally. The reason for growth was considered as into the cancer itself or the surrounding stroma. The invasion of breast cancer accompanies reactive changes in the surrounding stroma [1, 2]. These stromal changes are best known as desmoplasia. Breast cancer lumps include these reactive changes. Histological studies have revealed that these reactive changes are composed of a proliferation of myofibroblasts [3, 4], collagen synthesis (type 3 and 5), and angiogenesis [1, 2, 5]. These growth patterns may differ as to the point that these changes turn to the ventral or dorsal direction.

The mean size of the mixed type was 28.1 mm, and the mixed type was significantly larger than the other three categories ($P < 0.01$, χ^2 test). If breast cancer grew above a definite size, ventral type or dorsal type might become mixed type.

Next, we studied the reference between the classification of the four categories and prognosis. Dorsal type had 10 years disease-free survival rate at 39.5% and ventral type at 79.9%. The biggest difference was between ventral type and dorsal type ($P < 0.05$).

We studied the relationship with lymph node metastases for that reason. Among the four categories, however, mixed type at 39% showed the most metastases, followed by ventral type at (31%), dorsal type at (22%), and internal type at (17%). The lymph node metastases of dorsal type tended to occur less often than the others (N.S., χ^2 test). Therefore, this study did not show the relationship between the poor prognosis of dorsal type and lymph node metastases. We consider that the other reason for the poor prognosis of dorsal type may be metastasis by blood, because there are many blood vessels from the pectoral major to mammary glands.

Nakano et al. [6] reported the importance of the retromammary space. The retromammary space is a collection of very loose connective tissue. If dye is placed in the retromammary space, the dye immediately spreads in all directions by capillary action and reaches the lymph nodes. They reported that the relationship between lymph node involvement and retromammary space was statistically significant. The dorsal type grew in the retromammary space and had a poorer prognosis than the ventral type. However, the role of the anatomy, pathology, and function of the retromammary space is not known.

Conclusion

This study showed that breast cancer tends to grow ventrally rather than dorsally. Also, there is a tendency that the dorsal type showed a poorer prognosis than the others. The cause for poorer prognosis of dorsal type should be resolved.

References

1. Barsky SH, Rao CN, Grotendorst HR, et al (1982) Increased collagen content of type V collagen in desmoplasia in human breast cancer. Am J Pathol 108:276–383
2. Liotta RA, Rai CN, Barsky SH, et al (1983) Tumor invasion and extracellular matrix. Lab Invest 49:636–649
3. Seemayer TA, Lagace R, Schurch W, et al (1979) Myofibroblast in the stroma of invasive and metastatic carcinoma. Am J Surg Pathol 3:525–533

4. Lagace R, Grimaud JA, Scurch W, et al (1985) Myofibroblastic stromal reaction in carcinoma of the breast: variation of collagenous matrix and structural glycoprotein. Virchows Arch 408:49–59
5. Matrotta M, Martino G, D'Armiento FP, et al (1985) Collagen in human breast cancer. Appl Pathol 3:170–178
6. Nakano Y, Monden T, Tamaki Y, et al (2002) Importance of the retromammary space as a route of breast cancer metastases. Breast Cancer 9:203–207

Index